COPY

N-47628

NATIONAL ADVISORY COMMITTEE
FOR AERONAUTICS

RESEARCH - AIRPLANE - COMMITTEE REPORT

ON CONFERENCE ON THE

PROGRESS OF THE X - 15 PROJECT
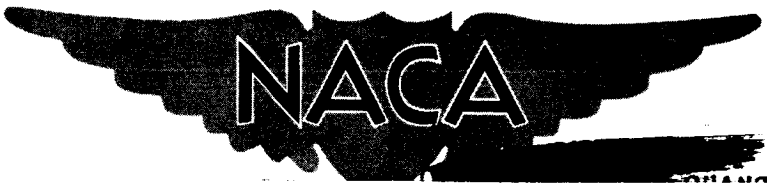
A COMPILATION OF THE PAPERS PRESENTED

Langley Aeronautical Laboratory

Langley Field, Va.

OCTOBER 25-26, 1956

NACA

N65-24101

(ACCESSION NUMBER) | (THRU)

(PAGES) | (CODE)

02

(NASA CR OR TMX OR AD NUMBER) | (CATEGORY)

RESEARCH-AIRPLANE-COMMITTEE REPORT

ON CONFERENCE ON THE

PROGRESS OF THE X-15 PROJECT

A Compilation of the Papers Presented

Langley Aeronautical Laboratory
Langley Field, Va.

Oct. 25 and 26, 1956

TABLE OF CONTENTS

DECLASSIFIED

INTRODUCTION

This document is a compilation of the papers presented at the
Conference on the Progress of the X-15 Project held at the Langley
Aeronautical Laboratory October 25 and 26, 1956. This conference was
held by the Research Airplane Committee of the U. S. Air Force, the
U. S. Navy, and the National Advisory Committee for Aeronautics to
report on the technical status of this research airplane. The papers
were presented by members of the staffs of North American Aviation, Inc.,
Reaction Motors, Inc., and the NACA.

DECLASSIFIED

LIST OF CONFEREES

The following were registered at the Conference on the Research-Airplane-Committee Report on the Progress of the X-15 Project, Langley Aeronautical Laboratory, Langley Field, Va., October 25 and 26, 1956.

ABBOTT, Ira H.	NACA Headquarters
ALBERI, A.	Republic Aviation Corporation
AMBROSE, James Richard	Aeronutronic Systems, Inc.
AMES, Milton B.	NACA Headquarters
AMICK, James L.	Aeronautical Engineering Labs., University of Michigan
ANDERSON, Lt. Col. Richard C.	Air Research and Development Command, Baltimore
ARCIDIACONO, Thomas	Fairchild Engine and Airplane Corp.
ATKINSON, Allen S.	Bureau of Aeronautics
AULD, Charles B.	Naval Ordnance Laboratory, White Oak
BAGBY, Frederick L., Jr.	Battelle Memorial Institute
BANNER, Richard D.	NACA High-Speed Flight Station
BARCUS, Ronald	Bendix Aviation Corporation
BEACH, William C.	North American Aviation, Inc.
BECHBERGER, Paul Franklin	Bendix Aviation Corporation
BECK, N. John	Douglas Aircraft Company, Inc.
BECKER, John V.	NACA - Langley Laboratory
BECKETT, Lt. Col. Walter R.	Air Research and Development Command, Baltimore
BEELER, De E.	NACA High-Speed Flight Station
BELL, E. Barton	Wright Air Development Center
BELLMAN, Donald R.	NACA High-Speed Flight Station
BERINATI, Vincent J.	Bureau of Aeronautics
BITNER, John D.	Glenn L. Martin Company
BLAKE, Charles L.	Convair
BOHLING, Raymond F.	Bureau of Aeronautics
BONNEY, E. A.	Subcommittee on Aerodynamic Stability and Control
BOZAJIAN, John M.	Hughes Aircraft Company
BRADSHAW, Harold Roger	General Electric Company
BREWER, Thomas Larche	Curtiss Wright Corporation
BROWN, Charles Goodwin	Douglas Aircraft Company, Inc.
BROWN, Clinton E.	NACA - Langley Laboratory
BROWNE, Thomas Peter	Douglas Aircraft Company, Inc.
BRUNOW, Charles L.	Temco Aircraft Corporation
BUCKLEY, Edmond C.	NACA - Langley Laboratory
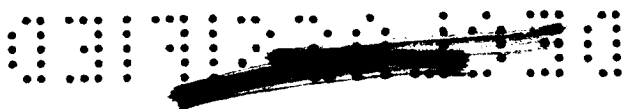
CAMPBELL, Gordon W. — North American Aviation, Inc.
CARTER, Maj. David L. — Air Research and Development Command, Inglewood

CARTER, Jack Warren — Glenn L. Martin Company
CASH, George M. — Cornell Aeronautical Laboratory, Inc.
CASPAR, William C. — Bureau of Aeronautics
CESARO, Richard S. — NACA Headquarters
CHAPMAN, Charles Edward — Convair
CLARK, Edward E. — Glenn L. Martin Company
CLARKSON, Mark Hall — Chance Vought Aircraft, Inc.
CLOUSING, L. A. — NACA - Ames Laboratory
COGSWELL, W. P. — Stromberg-Carlson Company
CRAWFORD, James Edgar — Northrop Aircraft, Inc.
CREEL, Ralph L. — Subcommittee on Aircraft Structures
CRICHLOW, Walter Jack — Lockheed Aircraft Corporation
CROSSFIELD, A. Scott — North American Aviation, Inc.
CROWLEY, John W. — NACA Headquarters
CZARNECKI, Edwin G. — Boeing Airplane Company

DAY, Richard E. — NACA High-Speed Flight Station
DECREVEL, Roland — Bell Aircraft Corporation
DICKINSON, R. L. — Lockheed Aircraft Corporation
DIEHL, Capt. Walter S. (USN Ret.) — Committee on Aerodynamics
DILWORTH, John A., III — Subcommittee on Aircraft Loads
DIMEFF, J. — NACA - Ames Laboratory
DONELY, Philip — NACA - Langley Laboratory
DONLAN, Charles J. — NACA - Langley Laboratory
DOVER, Jerome J. — Air Force Flight Test Center, Edwards Air Force Base

DOW, Norris Fitz — General Electric Company
DRAKE, Hubert M. — NACA High-Speed Flight Station
DRAKE, James Frederic — Marquardt Aircraft Company
DRALEY, Eugene C. — NACA - Langley Laboratory
DRYDEN, Dr. Hugh L. — NACA Headquarters
DUNHOLTER, Howard F. — Subcommittee on Rocket Engines
DUNNING, Robert W. — NACA - Langley Laboratory

EDELMAN, Gilbert M. — Republic Aviation Corporation
EDMONDS, Lt. George P. — Air Research and Development Command, Baltimore

EDWARDS, Lawrence K. — Lockheed Aircraft Corporation
EIMER, Dr. Manfred — Jet Propulsion Laboratory, C.I.T.
ELDER, Donald Lee — Douglas Aircraft Company, Inc.
EPSTEIN, Albert — Republic Aviation Corporation
EVERETT, Maj. Phillip E. — AF Development Field Representative, NACA, Langley Laboratory
EVERETT, Willard F. — Fairchild Engine and Airplane Corp.

FABER, Stanley	NACA - Langley Laboratory
FEDZIUK, Henry A.	NACA - Langley Laboratory
FELLER, William V.	NACA - Langley Laboratory
FELTZ, Charles H.	North American Aviation, Inc.
FIORE, A. W.	Wright Air Development Center
FISCHEL, Jack	NACA High-Speed Flight Station
FORMHALS, Edwin J.	Bureau of Aeronautics
FORREST, Clarence Lyman	Bell Aircraft Corporation
FRICK, Charles W., Jr.	Convair
FRIEND, Carl Frederick	Lockheed Aircraft Corporation
FROST, Maj. Jack W.	Air Research and Development Command, Baltimore
FUHRMAN, Robert Alexander	Ryan Aeronautical Company
GARDNER, Frederick H.	North American Aviation, Inc.
GARNER, William Gerald	Redstone Arsenal
GASICH, Welko Elton	Northrop Aircraft, Inc.
GAYNOR, Frank A.	Subcommittee on Automatic Stabilization and Control
GENIESSE, Maj. Eugene	Subcommittee on High-Speed Aerodynamics
GEORGE, James	Bureau of Aeronautics
GILBERT, Lt. Loran	Wright Air Development Center
GILRUTH, Robert R.	NACA - Langley Laboratory
GODET, Sidney	Reeves Instrument Corporation
GONZALEZ, Jose I.	Convair
GOODRICH, Capt. John W.	Wright Air Development Center
GOODWIN, Philip M.	Bureau of Aeronautics
GORANSON, R. Fabian	NACA Headquarters
GOUGH, Melvin N.	NACA - Langley Laboratory
GOUGH, William V.	NACA - Lewis Laboratory
GRAFF, George Stephen	Subcommittee on Aerodynamic Stability and Control
GRAY, Edward Z.	Subcommittee on Aircraft Loads
GREEN, George Garner	Convair
GREENE, Lawrence P.	Subcommittee on High-Speed Aerodynamics
GREENLEES, William D.	Bureau of Aeronautics
GRIFFIN, E. J.	Bureau of Aeronautics
GROGAN, George C., Jr.	Convair
GUNIA, Russell B.	United States Steel Corporation
GUNKEL, Robert J.	Douglas Aircraft Company, Inc.
GUSTAFSON, Robert L.	Subcommittee on High-Speed Aerodynamics
HARKNESS, John Loomis	Defense Research Laboratory, University of Texas
HARRINGTON, Joseph H.	Subcommittee on Aircraft Loads
HARRIS, Thomas A.	NACA - Langley Laboratory
HARSHMAN, Jack D.	Boeing Airplane Company
HAYES, Lt. Richard J.	Wright Air Development Center
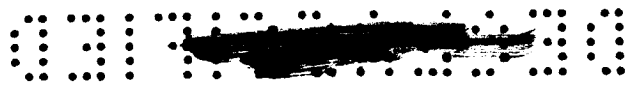
HEDRICK, Ira Grant	Grumman Aircraft Engineering Corp.
HELDENFELS, Richard R.	NACA - Langley Laboratory
HEMSLEY, Lt. Col. Richard T.	Subcommittee on Rocket Engines
HENDERSON, James Henry	Redstone Arsenal
HENDERSON, Maj. William J.	Air Research and Development Command, Baltimore
HERMANN, Dr. Rudolf	Rosemount Aeronautical Laboratory, University of Minnesota
HESSE, Walter John	Chance Vought Aircraft, Inc.
HICKERSON, Frederick J.	U. S. Naval Air Rocket Test Station
HIGGINS, H. C.	Boeing Airplane Company
HILL, Col. Otis R.	Air Research and Development Command, Baltimore
HOEKSTRA, Harold D.	Committee on Aerodynamics
HOLDEN, Frederick Raymond	Naval Air Development Center, Johnsville
HOLMQUIST, Comdr. C.·O.	Naval Air Test Center, Patuxent River
HOWELLS, Fred W.	North American Aviation, Inc.
HYATT, Abraham	Bureau of Aeronautics
JAEGER, B. F.	Naval Ordnance Test Station, Inyokern
JAKOSKY, Milton	Subcommittee on Aircraft Structures
JOHNSON, J. A.	Subcommittee on Aircraft Loads
JOHNSTON, Robert B.	The RAND Corporation
KARTVELI, Dr. A.	Committee on Aerodynamics
KATKOV, R. B.	Subcommittee on Aerodynamic Stability and Control
KAUFMAN, Harold	Naval Air Development Center, Johnsville
KEARNS, Thomas F.	Bureau of Aeronautics
KINCHELOE, Capt. Iven Carl, Jr.	Air Force Flight Test Center, Edwards Air Force Base
KING, William B.	Boeing Airplane Company
KINSEY, Robert S.	Reaction Motors, Inc.
KLEINKNECHT, Kenneth S.	NACA High-Speed Flight Station
KNEMEYER, Franklin H.	Naval Ordnance Test Station, Inyokern
KOCH, Charles J.	Subcommittee on High-Speed Aerodynamics
KOTCHER, Ezra	Wright Air Development Center
KOVEN, William	Subcommittee on Automatic Stabilization and Control
KRUG, Edwin H.	Lear, Inc.
KUGEL, E.	Wright Air Development Center
KULLAS, Albert John	Glenn L. Martin Company
LACEY, Capt. Robert J.	Wright Air Development Center
LALLI, John O.	Sperry Gyroscope Company
LAMPROS, Alexander Ferdinand	Naval Air Missile Test Center, Pt. Mugu
LAROE, Comdr. E. T.	Bureau of Aeronautics
LEE, John G.	Subcommittee on High-Speed Aerodynamics
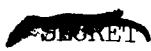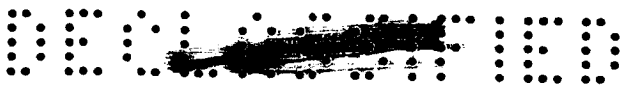
LEFLER, E. Dale	Wright Air Development Center
LICCINI, Luke L.	Subcommittee on Aerodynamic Stability and Control
LINDELL, Lt. Col. Keith Gordon	Directorate of Research and Development Office, USAF
LINDEN, J. E.	Bureau of Aeronautics
LINDSTROM, Fred A.	Convair
LOCKE, F. W. S., Jr.	Bureau of Aeronautics
LOMBARD, Dr. A. E., Jr.	Committee on Aerodynamics
LONGFELDER, Harlowe J.	Subcommittee on High-Speed Aerodynamics
LOUDEN, F. A.	Committee on Aerodynamics
LOW, George M.	NACA - Lewis Laboratory
LU, H.	Republic Aviation Corporation
LUCK, D. G. C.	Radio Corporation of America
LUNDIN, Bruce T.	NACA - Lewis Laboratory
LUSKIN, Harold T.	Douglas Aircraft Company, Inc.
MacDONALD, Donald Lloyd	North American Aviation, Inc.
McBREARTY, J. F.	Committee on Aircraft Construction
McCARTY, Lt. John L.	Wright Air Development Center
McCOLLOUGH, Capt. Chester E., Jr.	Air Research and Development Command, Wright-Patterson Air Force Base
McGINNESS, Capt. William T.	Subcommittee on Aircraft Structures
McKAY, John B.	NACA High-Speed Flight Station
McLELLAN, Charles H.	NACA - Langley Laboratory
MACK, Charles Edward, Jr.	Grumman Aircraft Engineering Corp.
MAGGIN, Bernard	NACA Headquarters
MALVESTUTO, Frank S., Jr.	NACA High-Speed Flight Station
MARCUM, Arnold	North American Field Representative, Hampton
MARKS, Clifford Dunham	McDonnell Aircraft Corporation
MASAKI, Mamoru	Convair
MATTHEWS, Howard F.	NACA - Ames Laboratory
MAY, Ralph W.	NACA Headquarters
MEIRS, John	Grumman Aircraft Engineering Corp.
MEULLEN, Norman Franklin	Bell Aircraft Corporation
MICHEL, Douglas	Bureau of Aeronautics
MILLIKEN, W. F., Jr.	Subcommittee on Aerodynamic Stability and Control
MISKAM, Frederick Charles	Douglas Aircraft Company, Inc.
MOECKEL, Wolfgang E.	NACA - Lewis Laboratory
MOUL, Martin T.	NACA - Langley Laboratory
MULHOLLAND, Frank J.	Subcommittee on Aerodynamic Stability and Control
MULTHOPP, Hans	Glenn L. Martin Company
MUNGER, William P.	Subcommittee on Rocket Engines
MUNIER, Alfred E.	Grumman Aircraft Engineering Corp.
MUNSON, Lloyd Emery	Convair
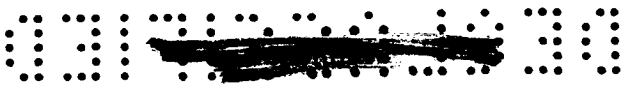
MURPHY, John A.   North American Aviation, Inc.
MUSE, Thomas C.   Office of the Assistant Secretary of
                                           Defense for Research and Development
MUSIL, Jay Louis   Cook Research Laboratories

NAVOY, Anthony Joseph   Institute for Defense Analyses, The
                                           Pentagon
NAY, Col. Paul F.   Air Research and Development Command,
                                           Baltimore
NEEL, C. B.   NACA - Ames Laboratory
NEWBY, Clinton T.   Subcommittee on Aircraft Loads
NIEHAUS, James J.   Wright Air Development Center
NORTH, Warren   NACA - Lewis Laboratory
NOVOTNY, Raymond J.   U. S. Naval Air Rocket Test Station

O'DONNELL, Dr. William J.   Committee on Aerodynamics
OLIVER, Raymond B.   North American Aviation, Inc.
OLSON, Gordon Axel   North American Aviation, Inc.
ORR, William A.   Convair

PAGLIANETE, Francis J.   Bureau of Aeronautics
PAPPAS, C.   Republic Aviation Corporation
PAPPAS, C. C.   NACA - Ames Laboratory
PARKER, Maurice E.   Reaction Motors, Inc.
PARKINSON, John B.   NACA - Langley Laboratory
PARSONS, Thomas Richard   Aerophysics Research Group, M.I.T.
PATTILLO, Lt. Col. Leslie G., Jr.   AF Development Field Representative,
                                           NACA, Lewis Laboratory
PAULSON, John W.   NACA - Langley Laboratory
PEARSON, Ernest O.   NACA Headquarters
PENN, Maj. William W., Jr.   AF Development Field Representative,
                                           NACA, Ames Laboratory

PHILLIPS, Franklyn W.   NACA Headquarters
PHILLIPS, William H.   NACA - Langley Laboratory
PIERCE, Ernest William   Douglas Aircraft Company, Inc.
PIPITONE, S. J.   Goodyear Aircraft Corporation
POOR, C. L., 3d   Subcommittee on High-Speed Aerodynamics
PRUDDEN, T. M.   Aerojet-General Corporation
PURCELL, George H.   Wright Air Development Center

RAMEY, Madison Lewis   McDonnell Aircraft Corporation
REDDING, Arnold H.   Subcommittee on Engine Performance
                                           and Operation
REID, Dr. Henry J. E.   NACA - Langley Laboratory
RIDYARD, Herbert W.   NACA - Langley Laboratory
ROBINSON, Robert F.   Air Research and Development Command,
                                           Baltimore
ROCHÉ, Jean A.   AF Development Field Office, NACA,
                                           Langley Laboratory

xiv

ROSCHE, Melvin G.	NACA Headquarters
ROSS, Paul Kenneth	North American Aviation, Inc.
RYAN, Edwin M.	Bureau of Aeronautics
SAVAGE, Hugh J.	Wright Air Development Center
SAVET, Paul H.	American Bosch Arma Corporation
SCHERBERG, Dr. Max G.	Wright Air Development Center
SCHLEICHER, Richard L.	Committee on Aircraft Construction
SCHNEIDER, William C.	Bureau of Aeronautics
SCHNITT, Arthur	Bell Aircraft Corporation
SCHUELLER, Carl	NACA - Lewis Laboratory
SCHULDENFREI, Marvin	Subcommittee on Automatic Stabilization and Control
SCHULTZ, Frederick E.	Subcommittee on Rocket Engines
SEACORD, Charles L.	Convair
SEARS, Richard I.	Raytheon Manufacturing Company
SEIDMAN, Oscar	Subcommittee on High-Speed Aerodynamics
SHERMAN, Windsor L.	NACA - Langley Laboratory
SHORR, Melvin	Subcommittee on Aerodynamic Stability and Control
SHORTAL, Joseph A.	NACA - Langley Laboratory
SJOBERG, S. A.	NACA - Langley Laboratory
SLOOP, John L.	Subcommittee on Rocket Engines
SMITH, C. Branson	United Aircraft Corporation
SMITH, Stanley Wilson	Bell Aircraft Corporation
SMITH, William Mage	Bell Aircraft Corporation
SOULE, Hartley A.	NACA - Langley Laboratory
SPEAKER, Robert F.	Bureau of Aeronautics
SPICER, Kenneth M.	International Nickel Company, Inc.
SPIELBERG, Irvin N.	Ramo-Wooldridge Corporation
STACK, John	NACA - Langley Laboratory
STALDER, J. R.	NACA - Ames Laboratory
STANLEY, Max Richard	Northrop Aircraft, Inc.
STANLEY, Robert M.	Stanley Aviation Corporation
STEIN, Hyman	Republic Aviation Corporation
STERNFIELD, Leonard	NACA - Langley Laboratory
STEVENS, John Erwin	Chance Vought Aircraft, Inc.
STILLWELL, Wendell H.	NACA High-Speed Flight Station
STOOLMAN, Dr. Leo	Hughes Aircraft Company
STUBER, B. V.	Naval Air Test Center, Patuxent River
SULLIVAN, Edward J.	Boeing Airplane Company
SUMMERS, Allan Joseph	McDonnell Aircraft Corporation
SYVERTSON, C. A.	NACA - Ames Laboratory
TABACK, I.	NACA - Langley Laboratory
TALBOT, Curtis Garwood	General Electric Company
TANCZOS, Frank I.	Subcommittee on Rocket Engines
TAYLOR, Harlan D.	United Aircraft Corporation

GENERAL BACKGROUND OF THE X-15 RESEARCH-AIRPLANE PROJECT

By Dr. Hugh L. Dryden

Chairman of Research Airplane Committee

During the spring of 1952, a resolution was passed by the NACA Committee on Aerodynamics and ratified by the NACA Executive Committee directing the Laboratories to initiate studies of the problems likely to be encountered in space flight and of the methods of exploring them. Laboratory techniques, missiles, and manned airplanes were considered. By the spring of 1954 the NACA had a team at work to determine the characteristics of an airplane suitable for exploratory flight studies of the aerodynamic heating, stability, control, and physiological problems of hypersonic and space flight and to determine the technical feasibility of designing and building such an airplane. This work led to an NACA proposal for the construction of an airplane capable of a speed of 6,600 feet per second and an altitude of 250,000 feet, both not necessarily to be attained simultaneously. The performance that would have to be built into an airplane that would meet these two requirements would permit the desired exploration. It was suggested that a heat-sink type of structure of Inconel X would require the least development and would give a reasonable factor of safety, when the assumptions that had to be made in the light of the knowledge then available were considered.

When, on July 9, 1954, NACA representatives met with members of the Air Force and Bureau of Aeronautics research and development groups to present the proposal as an extension of the cooperative research airplane program, it was discovered that the Air Force Scientific Advisory Board had been making similar proposals to the Air Force Headquarters and that the Office of Naval Research had an active contract to determine the feasibility of constructing a manned aircraft capable of climbing to an altitude of 1,000,000 feet. These independent actions on the part of the Air Force and the Navy made for early acceptance of the NACA proposal for a joint effort and eventually led to the X-15 project.

On October 5, 1954, the NACA Committee on Aerodynamics adopted the following resolution:

WHEREAS, The necessity of maintaining supremacy in the air continues to place great urgency on solving the problems of flight with man-carrying aircraft at greater speeds and extreme altitudes, and

WHEREAS, Propulsion systems are now capable of propelling such aircraft to speeds and altitudes that impose entirely new and unexplored aircraft design problems, and

WHEREAS, It now appears feasible to construct a research airplane capable of initial exploration of these problems,

BE IT HEREBY RESOLVED, That the Committee on Aerodynamics endorses the proposal of the immediate initiation of a project to design and construct a research airplane capable of achieving speeds of the order of Mach number 7 and altitudes of several hundred thousand feet for the exploration of the problems of stability and control of manned aircraft and aerodynamic heating in the severe form associated with flight at extreme speeds and altitudes.

Because of the magnitude of the anticipated cost of the project, which would require support from Defense Department emergency funds as well as Air Force and Navy research and development funds, a relatively formal memorandum of understanding based on the resolution was prepared and signed in December 1954 by the Special Assistant, Research and Development of the Air Force, the Assistant Secretary of the Navy for Air, and the Director of the NACA. The memorandum provided that technical direction of the project would be the responsibility of the Director of the NACA acting with the advice and assistance of a "Research Airplane Committee" composed of one representative each from the Air Force, the Navy, and the NACA. Administration of the design and construction phases of the project was assigned to the Air Force. The NACA was given the task of conducting the flight tests after acceptance of the airplane as an airworthy article. The Director of the NACA and the Research Airplane Committee were charged with the responsibility of informing the military services and the aircraft industry of the progress and results of the project. The concluding statement of the memorandum was: "Accomplishment of this project is a matter of national urgency." The full text of the memorandum is appended to this paper.

After the Department of Defense approval was obtained, the Air Force was authorized in December 1955 to issue invitations to contractors having experience in the design of fighter-type airplanes to participate in the design competition for the X-15 airplane. A formal briefing on the specifications was presented in January 1955 to representatives of the 10 companies that exhibited an interest in the competition. Bids were received from four of the companies and evaluated during the summer and fall of 1955. The go-ahead signal was finally given to North American Aviation, Inc., the winner of the competition in early December 1955. The detail design and development, therefore, have been under way for not quite a year at this time.

The memorandum of understanding provides for the dissemination of technical information regarding the progress and results of the project to the military services and the aircraft industry. This conference will be a report on the progress of the project to this time. It is the first

such meeting and others will follow in due course. It should not be expected that these meetings will be held frequently because it takes time to accumulate sufficient significant data to warrant taking such a large group of this type away from its work.

Because this is the first of these meetings, some of the technical background for the original NACA proposal and the status of the current research-airplane flying experience in addition to reports on the progress of the X-15 project will be given.

Two final points should be noted relative to the X-15 project and this current progress report. First, in line with the urgency expressed in the memorandum of understanding, the project is proceeding on an expedited basis with the intent of realizing flights of a man-carrying aircraft at hypersonic speeds and high altitudes as soon as possible for explorations to separate the real from the imagined problems and to make known the overlooked and the unexpected problems. For this reason, no attempt has been made to optimize the configuration or, generally speaking, to use unconventional methods of approach to the problems expected. The second point is that the research and development connected with the project are not completed at the time of this conference. In the papers presented in this conference, it may be noted that the airplane configurations discussed and their stated weights vary from paper to paper. This apparent inconsistency results from the fact that the airplane configuration is still not completely firm and the figures represent those current at the time the particular studies were started. It should be borne in mind that some of the tentative conclusions for certain of the problems may be discarded in the future as new data are obtained.

MEMORANDUM OF UNDERSTANDING

SUBJECT: Principles for the Conduct by the NACA, Navy, and Air Force of a Joint Project for a New High-Speed Research Airplane

A. A project for a high-speed research airplane shall be conducted jointly by the NACA, the Navy, and the Air Force to implement the recommendations of the NACA Committee on Aerodynamics, as adopted on 5 October 1954.

B. Technical direction of the project will be the responsibility of the Director, NACA, acting with the advice and assistance of a "Research Airplane Committee" composed of one representative each from the NACA, Navy, and Air Force.

C. Financing of the design and construction phases of the project shall be determined jointly by the Navy and Air Force.

D. Administration of the design and construction phases of the project shall be performed by the Air Force in accordance with the technical direction as prescribed in paragraph B.

E. The design and construction of the project shall be conducted through a negotiated contract (with supplemental prime or sub-contracts) obtained after evaluating competitive proposals invited from competent industry sources. The basis for soliciting proposals will be the characteristics determined by the configuration on which the NACA has already done much preliminary design work.

F. Upon acceptance of the airplane and its related equipment from the contractor, it will be turned over to the NACA, who shall conduct the flight tests and report the results of same.

G. The Director, NACA, acting with the advice and assistance of the Research Airplane Committee, will be responsible for making periodic progress reports, calling conferences, and disseminating technical information regarding the progress and results of the

XX

project by other appropriate media subject to the applicable laws and executive orders for the safeguarding of classified security information.

H.   Accomplishment of this project is a matter of national urgency.

1 Incl   Hugh L. Dryden
   Resolution Adopted by   Director, NACA
   NACA Committee on
   Aerodynamics, October 5, 1954

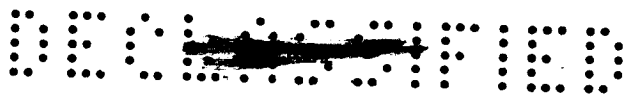
                                                          J. H. Smith, Jr.
                                        Assistant Secretary of the Navy (Air)

                                                          Trevor Gardner
                                        Special Assistant (R & D) Air Force

Signing of this document was completed on December 23, 1954.

REVIEW OF TECHNOLOGY RELATING TO THE X-15 PROJECT

By John V. Becker

Langley Aeronautical Laboratory

INTRODUCTION

From recent studies of the possibilities of flight at very high supersonic speeds there has developed a general consensus that we are on the threshold of an era in which the speed of manned aircraft is likely to increase by an order of magnitude, ultimately exceeding the velocity required for an earth satellite. A primary factor influencing these studies has been the achievement of rocket engines capable of large thrusts in the range needed for boosting long-range manned aircraft.

These appraisals of hypersonic flight have clearly established the urgent need for research on high-temperature structures, hypersonic aerodynamics, stability and control, and piloting problems. Because of the inadequacy of existing facilities for research in many of the problem areas, the National Advisory Committee for Aeronautics initiated a study in February of 1954 to determine the extent to which a manned research airplane could contribute toward solution of these problems. An important requirement specified at the outset of the study was that a period of only about 3 years be allowed for design and construction in order to provide the maximum possible time lead for application of the research results. This requirement, of course, allowed little or no time for the development of new materials, radical new methods of construction, or new techniques for launching. Also, it was obviously impossible that the proposed aircraft be in any sense an optimum hypersonic configuration.

The purpose of this paper is to review the considerations that established in a general way the main features, the performance, and the research missions which appeared feasible in an airplane to be constructed within the specified time limitation.

PERFORMANCE

The National Advisory Committee for Aeronautics performance study indicated that a maximum speed of about 6,800 feet per second could be achieved, if launching from the B-36 airplane was assumed. The altitude-speed performance envelope which appeared feasible is shown in figure 1 in relation to those of typical previous research airplanes and possible future manned aircraft. The maximum speed, which is more than double

that achieved by the X-2, places this airplane in a region where heating is the primary problem of structural design, and where little background information exists for aerodynamic design.

Winged aircraft capable of carrying human beings at hypersonic speeds are referred to in figure 1 as "rocket gliders." The upper limit of the zone in which they are likely to operate corresponds to lightly loaded aircraft with high optimum C_L, while the lower limit corresponds in general to low optimum C_L and high wing loadings. As the speed increases, an increasingly large proportion of the weight is borne by centrifugal force until, at satellite velocity, no aerodynamic lift is needed and the aircraft may be operated completely out of the atmosphere. At these speeds the pilot must function for long periods in a weightless condition, which is of considerable concern from the aeromedical standpoint. Attitude control of the aircraft for this condition is an additional problem. The proposed research airplane, although its speed is far below the satellite value, can be used to investigate both of these problems. By employing a high-altitude trajectory extending to about 250,000 feet, the aircraft at low angles of attack will operate in an essentially weightless condition for about 2 minutes. The dynamic pressure during this period is less than 10 pounds per square foot and reaches a minimum of less than 1 pound per square foot, so that the use of small auxiliary rockets for attitude control can be investigated under conditions approximating those of space flight.

Broadly speaking, rocket gliders operating within the atmosphere at sub-satellite speeds have two additional major problems: first, aerodynamic heating, and second, the problem of achieving as high a lift-drag ratio as possible. The wind tunnel is better suited than flight for configuration studies bearing on the L/D problem. However, the research airplane can contribute to one important phase of L/D research by providing information on the extent to which laminar boundary layers can exist in a realistic aerodynamic environment and for typical surface conditions which are generally impossible to simulate properly in wind tunnels. This question of the extent of laminar flow becomes, of course, even more critical as it affects the heating problem. In addition to these transition studies, determination of aerodynamic heating rates for both laminar and turbulent boundary layers over a wide range of flight conditions - in many cases far beyond those which can currently be duplicated in wind tunnels - will be another major research area for this airplane.

CONFIGURATION

Considerations of stability and control problems throughout the whole speed range, including low-speed launching and landing, led to selection

of a more-or-less conventional arrangement (fig. 2). The configuration
shown is not the X-15, but rather one which embodies all of the features
indicated to be desirable in the NACA study.

It was found that inordinately large tail areas were required at the
highest speeds if thin sections were used, because of the rapid loss in
lift-curve slope of thin sections as the Mach number increased. The
variable-wedge tail section was proposed as a means of restoring the lift-
curve slope at high speeds, thus permitting the conventional tail areas
shown. These wedge surfaces also act as dive brakes to reduce the Mach
number and heating during reentry. Both the braking effect and the sta-
bility derivatives can be varied through wide ranges by variable deflec-
tion of the wedge surfaces. The flexibility made possible by variable
wedge deflection was thought to be of great value because a primary use
of the airplane will be in studies of stability, control, and handling
characteristics through extreme ranges of speed and altitude.

Preliminary hypersonic wind-tunnel studies revealed the need for a
ventral tail to provide directional stability and control at high angles
of attack where the upper tail becomes immersed in the low-pressure flow
fields from the wing and body. These studies also revealed that the
horizontal-tail location should lie in a narrow range close to the wing
chord plane.

It was recommended that the airplane be statically stable for all
flight conditions and that artificial damping be incorporated in view of
the many uncertainties in the area of dynamic stability at the extreme
flight conditions of this airplane.

For operation at high altitudes where the aerodynamic controls
become ineffective, hydrogen-peroxide rockets were proposed for attitude
control.

Studies of the heating problems of this airplane pointed toward an
Inconel X heat-sink structure with blunt leading edges.

The size of the airplane was chosen as approximately the largest
that could be conveniently accommodated in a B-36 mother airplane. Weight
estimates indicated that such an airplane would have a gross weight of
about 30,000 pounds and a weight of 12,000 pounds without fuel. The
resultant weight ratio of 2.5, together with an initial thrust-weight
ratio of 1.8, provided a maximum burnout velocity of about 6,800 feet per
second with the B-36 launching technique. This thrust level is much higher
than in any previous manned aircraft. It results in a final longitudinal
acceleration at burnout of about 4.5g, which approaches the maximum value
currently believed to be acceptable by pilots. This velocity of 6,800 feet
per second thus represents about the maximum performance achievable with
this technique of launching from the B-36 airplane.

STRUCTURAL CONSIDERATIONS

Because of the paramount importance of the heating considerations in the design and uses of this airplane, the rest of this paper is devoted to a discussion of the structural and heating problems. An idea of the air-temperature environment of this airplane as a function of Mach number can be obtained from figure 3. The temperature shown is the recovery temperature of the air at the surface of an insulated flat plate in the absence of radiation, based on the assumption of a recovery factor of 0.9 for the turbulent boundary layer. Air temperatures of about 3,500° F are encountered. At this temperature appreciable imperfect-gas effects exist as a result of vibrational excitation of the molecules. Dissociation, however, starts to occur at a Mach number beyond the reach of this airplane. For the assumed range of skin temperatures a large temperature potential exists for heat flow into the skin at $M = 7$ (vertical line in figure 3), the ratio of air to wall temperatures ranging from about 3 to about 10. These large temperature ratios are characteristic of the hypersonic regime and provide a stabilizing influence on the boundary layer which is the principal basis for the hope that long runs of laminar boundary layer may exist at high speeds. An airplane with a Mach number capability of, say, only 3 or 4 would be unable to achieve a significantly wide range of values of this parameter.

During a typical flight the recovery temperature of course varies with changes in Mach number, Reynolds number, and angle of attack (fig. 4). The flight assumed here is one in which burnout occurs in climb at an altitude of about 130,000 feet, where the first peak value in the air temperature on the upper curve of figure 4 occurs. The airplane then coasts along a zero-lift path to a peak altitude of 250,000 feet and then reenters, encountering a second peak in speed and temperature. Because of the beneficial effect of radiation of heat away from the surface, the actual skin temperature is much lower than the boundary-layer recovery temperature during most of the flight. The dashed curve applies to a structure in which no heat is absorbed by the skin - either an insulated structure or one having a very thin skin of negligible heat capacity. A relatively high radiation coefficient ($\epsilon = 0.8$) was used in this case, corresponding to a darkened surface condition. The temperatures shown thus represent about the lowest that could be achieved in practice for the insulated type of structure. A peak temperature of about 1,850° F is reached on reentry, presenting very difficult material and fabrication problems for this type of structure.

If a metal skin of appreciable thickness is used, much of the imposed heat will be absorbed by the skin under the transient conditions of this type of flight and the resulting temperatures are thus reduced to more tractable levels, as shown by the lowest curve in figure 4. This type of construction is usually called a "heat-sink" structure.

For the contemplated flight conditions any one of several metal alloys might have been used in a heat-sink design, provided the skin gage was sufficiently thick to permit absorption of the heat load without exceeding the design temperature of the material. The principal considerations which pointed toward Inconel X as the most suitable material for this research airplane are indicated in figure 5. At a design temperature of 1,200° F, Inconel X has suffered only a negligible deterioration of its strength and stiffness properties. All of the other materials shown in this figure have significantly lower design temperatures - 300° for aluminum alloy, 500° to 600° for certain magnesium alloys, and perhaps 850° for stainless steel. The high design point for Inconel X permits complete freedom of operation up to nearly 4,000 feet per second, at which speed the recovery temperature is of the order of 1,200° F. Up to this speed, therefore, there need be no heat or temperature restrictions on operating altitude, angle of attack, or duration of flight. By contrast, if an aluminum alloy had been used the corresponding limiting speed would be less than 2,000 feet per second, and full-throttle, full-fuel flights would generally be impossible below an altitude of about 100,000 feet with a skin designed for the specified high-speed and high-altitude missions of this airplane.

A second advantage of the high design temperature of Inconel X stems from the significant amount of heat which can be radiated rather than absorbed by the skin. The dashed curve of figure 5 indicates that over three times as much radiation occurs at 1,200° F as at 850° F, the design temperature selected for stainless steel. No radiation benefit occurs for aluminum or magnesium alloys. The total amount of heat radiated from Inconel X in a typical flight is indicated in figure 6. The dashed curve indicates the heat absorbed by the skin as the skin temperature rises. A temperature of 1,350° F would be required to absorb the design heat load in the absence of radiation, in contrast to 1,200° F with the benefit of radiation.

As is well known, there are at present many uncertainties in the estimation of heat-transfer coefficients for a project of this kind. In addition, deviations from design flight trajectories, both intentional and accidental, will probably occur. It is imperative, therefore, that the structure be designed with the capability of absorbing excess heat loads. If a 50-percent excess heat load is assumed in a typical flight, it is found that the temperature increases by only 25 percent to 1,500° F. Thus about half the excess heat is radiated from the structure. At 1,500° F the material still retains about 60 percent of its design strength. The other structural materials, under similar circumstances, would lose a much larger fraction of their strength and stiffness.

A question of considerable interest in a heat-sink structure is "How much otherwise useless metal is carried solely for heat-sink purposes?" Figure 7 indicates the situation for this airplane at 6,600 feet
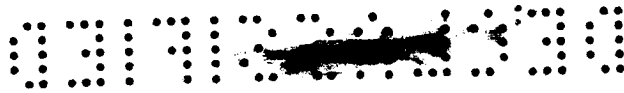
per second with an Inconel X skin; the solid line shows the metal
required for a uniform maximum temperature of 1,200° F along the wing
chord, and the dashed line is the approximate skin thickness required
for strength and stiffness near the wing root. Over much of the wing,
more than enough skin is seen to be available, and thus the maximum
temperatures in this area will be less than 1,200° F. Over the foremost
portions of wing and fuselage, however, and near the wing tips some extra
material is required.

If a higher speed had been chosen, say 12,000 feet per second, two
or three times as much material would be required for a heat sink, and a
heavy penalty in skin weight would then be involved.

The leading edge itself develops the highest heating rates found on
the aircraft, although over a relatively small area. It appeared from
the NACA study that either a heat-sink design or a non-load-carrying
very-high-temperature material such as one of the carbides would be fea-
sible for the leading edge.

Under the rapidly changing heating environment of this airplane
thermal stresses present a major problem for all types of structure. The
NACA study of the heat-sink type indicated that a number of modifications
could be made to a conventional structure which would reduce the thermal
stresses to tolerable levels. It was thought that such schemes could be
incorporated without an extended period of development.

There were two final important research considerations favoring the
proposed heat-sink structure:

(1) The heat-sink structure offered a reasonable possibility for
maintaining the smooth external surface necessary in heat-transfer and
boundary-layer-transition research.

(2) Accurate heat-transfer measurements can be obtained readily
from the temperature time histories of an Inconel X heat-sink structure.

FLIGHT TRAJECTORIES AND HEATING RATES

With the proposed structure this airplane was found to be capable
of widely varying research missions, some of which are shown in figure 8.
The design altitude mission extending to 250,000 feet followed by a reentry
pull-up in which the dive brakes are not used produces the maximum heating
rate of about 20 BTU/sq ft/sec on the lower surface of the wing when a
turbulent boundary layer is assumed. Maximum speed is achieved at a lower
altitude which produces a maximum heating rate of about 15 BTU/sq ft/sec.
If the airplane is operated at best L/D for maximum range, the initial

heating rate is about 6.5 BTU/sq ft/sec but the time of appreciable heating is much greater than in the previous cases.

In all the flights shown in figure 8 the upper surface of the wing was subject to much lower heating rates, with the result that temperature differentials of the order of 500° F developed between upper and lower surfaces. This differential and the high local heat rate combine to produce the condition of maximum thermal stress in the design altitude flight. Less extreme heating conditions with maximum heating rates of about 5 BTU/sq ft/sec can be achieved in low-angle-of-attack reentries in which deceleration is accomplished mainly by use of the dive brakes. It is evident that a wide variation in heating conditions can be achieved by varying the angle-of-attack schedule and flight trajectories. Conversely, careful adherence to planned schedules is essential if excessive heating is to be avoided.

In figure 9 it is of interest to compare the range of heating rates encountered in trajectories of this kind with typical rates likely to occur at higher speeds in rocket gliders operating near their best L/D. For the same wing loading, 60 pounds per square foot, and the optimum angle of attack, 12°, of the airplane assumed in the NACA study, the rocket gliders operate at ever-increasing altitude as the speed increases. The heating rate does not increase indefinitely but reaches a maximum of roughly 20 BTU/sq ft/sec. This maximum is a consequence primarily of the effect of centrifugal force in nullifying an increasing fraction of the weight and thereby permitting operation at lower dynamic pressures and higher altitudes.

The heating rate for the airplane at 6,600 feet per second and at the angle of attack for best L/D is about one-third of the maximum; however, in a reentry pull-up a maximum rate of the same order as for the rocket glider at $M \approx 15$ can be obtained.

In conclusion, none of the figures are meant to imply that this first hypersonic airplane will solve all the problems of the future. The conclusion was reached from this study that a significant first step toward the era of long-range rocket-propelled man-carrying aircraft was feasible and desirable, and that the proposed airplane would be capable of research in many areas which could not be adequately explored in any other way.
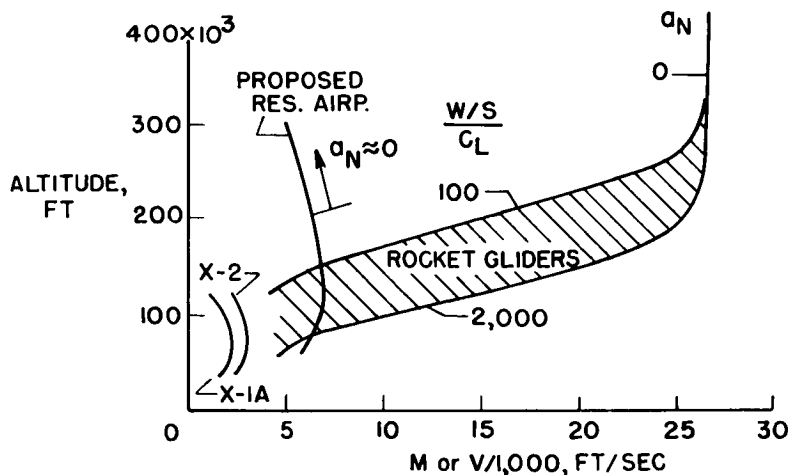
FLIGHT REGIMES

400×10³
ALTITUDE, FT

PROPOSED
RES. AIRP.
$\alpha_N \approx 0$
$\frac{W/S}{C_L}$
α_N
0
300
200
100
100
ROCKET GLIDERS
2,000
X-2
X-1A
0   5   10   15   20   25   30
M or V/1,000, FT/SEC

Figure 1

PRINCIPAL FEATURES OF PROPOSED RESEARCH AIRPLANE

3/4" RADIUS
.05c
A-A
A   A
5' DIAM.
B   B
B-B
B   B
27.4'
47.5'
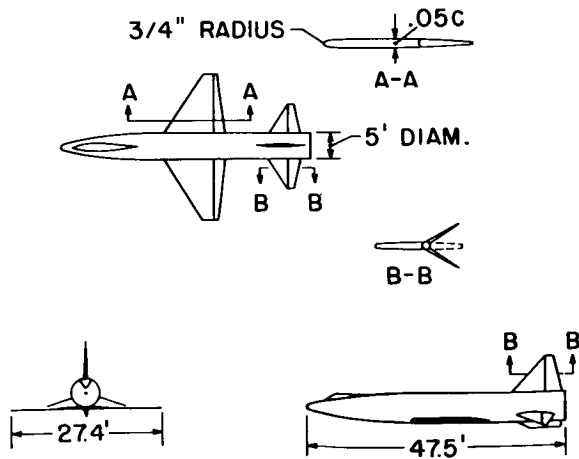
$\dfrac{\text{WGT. AT LAUNCH}}{\text{WGT. AT BURNOUT}} = \dfrac{30,000\ \text{LB}}{12,000\ \text{LB}} = 2.5$
$\dfrac{\text{THRUST}}{\text{WGT. AT LAUNCH}} = \dfrac{54,000\ \text{LB}}{30,000\ \text{LB}} = 1.8$

Figure 2

RECOVERY TEMPERATURE FOR FLAT PLATE
ALTITUDE, 150,000 FT
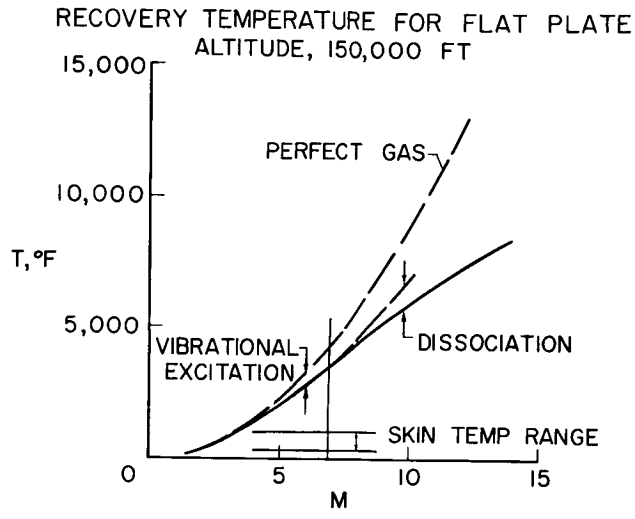
Figure 3

TYPICAL TEMPERATURE HISTORY
DESIGN ALTITUDE FLIGHT

LOWER SURFACE, x = I FT

Figure 4

COMPARISON OF INCONEL X WITH OTHER ALLOYS

TENSILE YIELD STRESS,
KSI

DESIGN TEMP.

HEAT RADIATED,
BTU/SQ FT/SEC

100

TITANIUM

STAINLESS
STEEL

INCONEL X

10

50

ALUMINUM

5

MAGNESIUM

HEAT RADIATED

0

0   500   1000   1500   0

T, °F

Figure 5

EFFECT OF RADIATION ON SKIN TEMP.
INCONEL X, t=.082"

HEAT INPUT,
BTU/SQ FT

1000

TOTAL HEAT INPUT

RADIATION
EFFECT

150% DESIGN

DESIGN

HEAT ABSORBED
BY SKIN

500

0   500   1000   1500   2000

T, °F
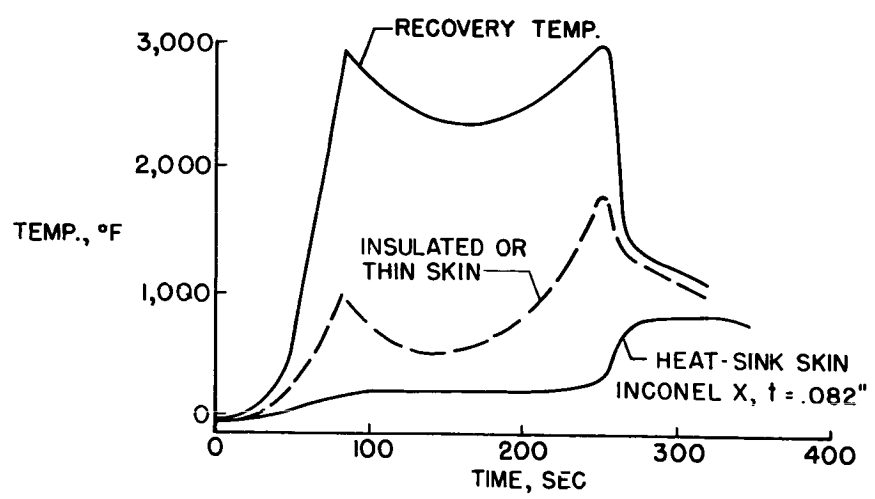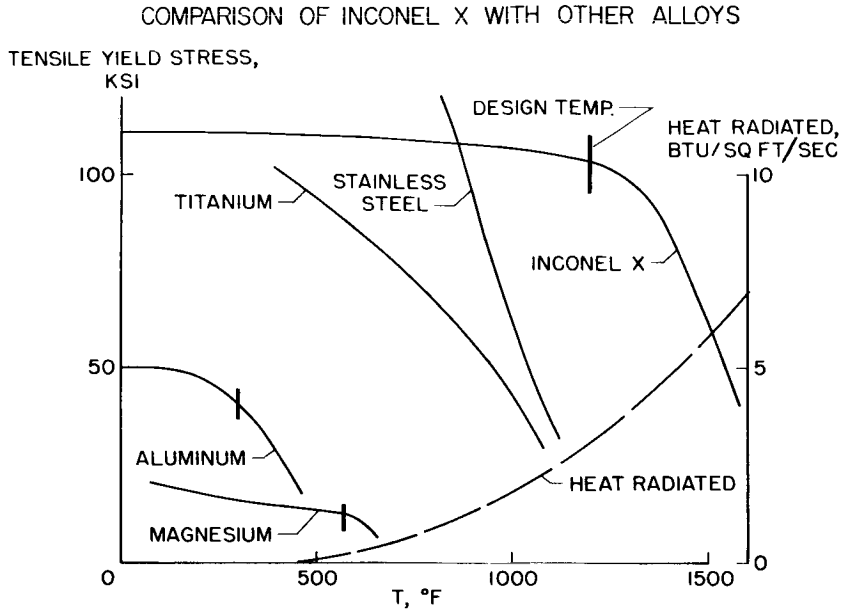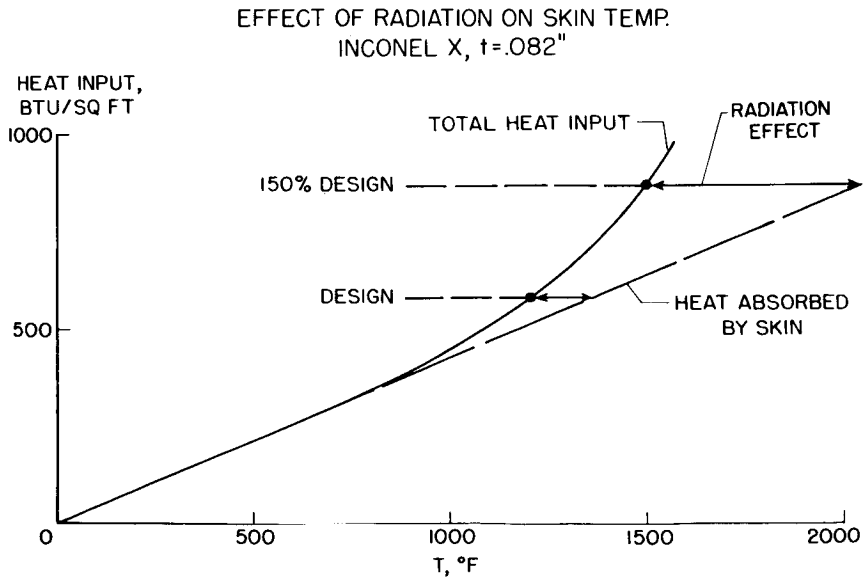
Figure 6

WING SKIN THICKNESS REQ'D FOR HEAT SKIN

SKIN THICKNESS, INCHES

.2

INCONEL X
$T_{DES} = 1200\ °F$

V, FT/SEC

6600

.1

REQ'D FOR LOAD

0

.5

1.0

X/C
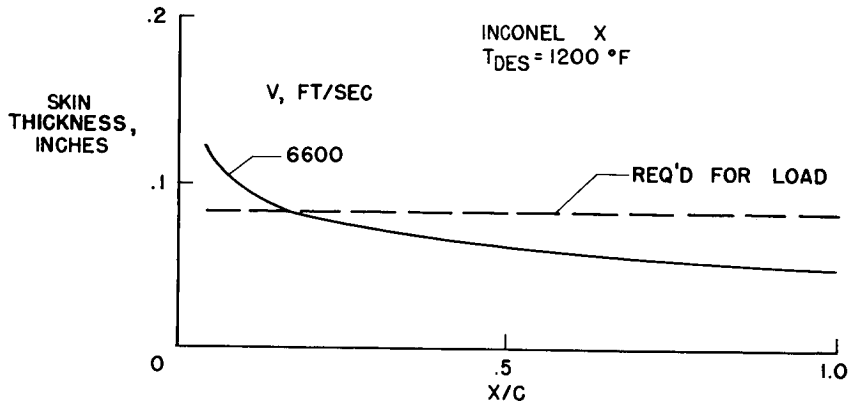
Figure 7

TYPICAL FLIGHT PATHS AND HEATING RATES

$V_{BURNOUT}$, FPS
6,500
6,600
6,500

MAX. HEAT RATES
ON WING, x = 1 FT
$BTU/FT^2/SEC$

ALTITUDE, FT
300×10^3

200

100

20

15

6.5 $BTU/FT^2/SEC$

0   50   100   150   200   250
MILES

Figure 8

ROCKET-GLIDER HEATING RATES

Figure 9

FLIGHT EXPERIENCE WITH PRESENT RESEARCH AIRPLANES
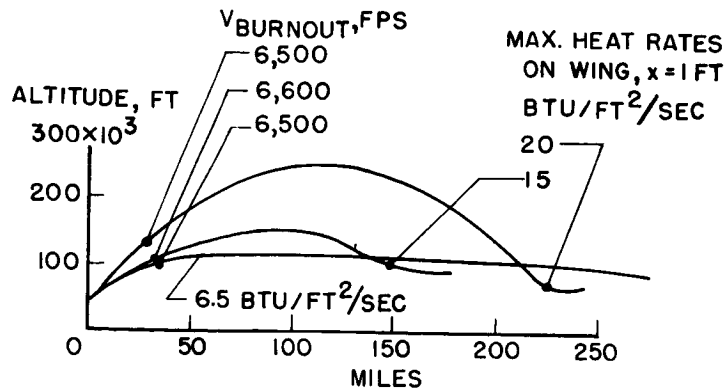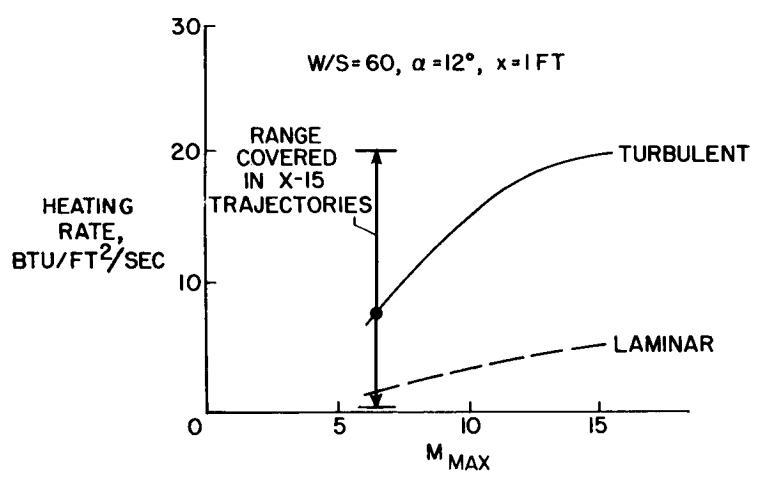
By Hubert M. Drake

NACA High-Speed Flight Station

INTRODUCTION

The North American X-15 airplane is being designed for speeds and altitudes considerably greater than those presently being encountered by airplanes. In this regard, it might be well to consider the status of flight research with the current research airplanes and see what experience and planned research are pertinent to the X-15 project.

DISCUSSION

Figures 1 and 2 show the regions of Mach number and altitude to be discussed in reference to these present research airplanes. Figure 1 illustrates the envelope of combinations of pressure altitude and Mach number that has been explored to date with the airplanes indicated therein. No one airplane has covered the entire range; for example, the highest altitude and Mach number points were obtained with the Bell X-2 airplane, but the low-speed point at an altitude of 83,000 feet was obtained with the Douglas D-558-II airplane. Figure 2 shows the region of altitude and Mach number which is possible with the X-1 airplanes. Although the recent loss of the X-2 will prevent the investigation of Mach numbers above 3, the X-1E will be able to reach Mach numbers near 2.8. The amount of ballistic flight possible with these airplanes is indicated by the region above the line for q = 10 pounds per square foot. The actual amount of this possible region that will be explored cannot be determined at present. Some of the problems that may prevent attaining the entire envelope will be discussed in this report.

Within the envelope already explored, these research airplanes have experienced a number of the problems that are being considered for the much higher performance of the X-15 airplane. Some of the problems encountered with these airplanes are as follows: longitudinal-control effectiveness, high-altitude dynamic stability, thrust misalinement, control at low dynamic pressure, roll coupling, and supersonic directional stability. This listing is not necessarily in the order of the importance of the individual problem.

Several of these problems are illustrated in figure 3 which shows time histories of a flight to the highest altitude yet attained. Low

longitudinal-control effectiveness prevented the attainment of a higher altitude by limiting the climb angle. Although all available control was used in the pull-up to climb attitude, only about 1.2g was obtained. Similarly, in the reentry and recovery phase, almost constant full-up control was used, but level flight was not attained until an altitude of nearly 40,000 feet was reached. The pilot was of the opinion that the control was much too weak, the pullout being completed at an uncomfortably low altitude.

This flight resulted in a considerable period of semiballistic flight. Although zero g was not actually reached, a value of normal acceleration of less than 0.1g was maintained for about 50 seconds. The minimum dynamic pressure for this flight was 18.8 pounds per square foot at a pressure altitude of 120,000 feet. In this condition the airplane indicated very poor dynamic stability as shown by the angle-of-attack trace. When the airplane was disturbed by a control application, a pitching oscillation with a period of about 6 seconds and a maximum total angle-of-attack amplitude of about 6° was excited. Although the damping of this motion was extremely low, the oscillation did not annoy the pilot because it produced no appreciable change in normal acceleration and the attitude was still too steep for the pilot to see the horizon. When the peak of the trajectory was attained and the horizon was in view, the pilot was too busy initiating the recovery to bother with attempting to control the longitudinal oscillation. The shortening of the period of increased damping with increasing dynamic pressure is shown in figure 3.

Another problem that has been encountered with current research airplanes and which is of considerable interest in the X-15 project is the matter of thrust misalinement. Figure 4 shows the motions resulting from about a 1/4° (or 0.7 inch) thrust misalinement for the X-2. Two conditions are shown; one at high-speed medium altitude, the other at the high-altitude and moderate-speed condition shown in figure 3. When the power goes off, the misalinement produces a disturbance in sideslip. The pilot did not object to the disturbance at high Mach number and quickly damped it out. At high altitude, however, he objected to the increased magnitude of the disturbance and the large resulting motions. This condition was considerably more difficult to control; however, the pilot was able to damp the motion and restrict the sideslip motions to small amplitude.

On two occasions with the X-1A airplane, under conditions of low directional stability or extremely high altitude, the disturbance caused by thrust misalinement resulted in loss of control. These occurrences have been reported in reference 1. Figure 4 indicates that engine misalinement can be determined at noncritical conditions and may then be corrected by adjusting the engine in its mount. Misalinement would then result only from the small changes within the engine from flight to flight.

The problem of control at low dynamic pressure when aerodynamic controls are used is being investigated. The lowest dynamic pressure at which flight has so far been performed in the current research program is the 18.8 pounds per square foot previously mentioned. For this condition, the pilot was able to control lateral motions, although the airplane was very unsteady. Plans are to continue this program, utilizing the X-1B and X-1E, to lower dynamic pressure. Analog investigations have indicated that the aerodynamic controls should retain a degree of effectiveness down to a dynamic pressure below 10 pounds per square foot.

Another problem of flight at high altitude is, of course, inertial coupling. The critical average roll rate for divergence is very low at high altitudes as a consequence of the very low magnitude of the aerodynamic restoring moments. The X-2, for example, in the previously cited condition of a Mach number of 1.7 and an altitude of 120,000 feet would experience roll divergence at an average roll rate of 45° per second. Analog studies indicate that the rate of divergence is slow but the low control effectiveness may make it very difficult for the pilot to control the motion. Severe roll coupling has been encountered on the X-1A airplane at an altitude of 90,000 feet and a Mach number of about 2 (ref. 1). In this case the critical roll velocity of about 65° per second was exceeded because of a disturbance produced by thrust misalinement and use of the rudder. Extremely large motions were developed, and control was not regained for about 50 seconds. This occurrence indicates that roll coupling can be of extreme importance, even though the divergence rates are low and high accelerations are not developed.

One of the most important problems of high Mach number flight is the familiar reduction of directional stability as the Mach number is increased supersonically. Figure 5 shows the variation of C_{n_β} at an angle of attack of 0° for some of the current research airplanes. These data were obtained from wind-tunnel investigations and from flight tests. All these configurations would have greatly reduced C_{n_β} at positive angles of attack. The ticks indicate the maximum speeds attained by the various airplanes. All these airplanes except the X-1E have encountered lateral-stability difficulties at supersonic speeds, and the X-1E can be expected to have similar difficulties at high angles of attack. The difficulties ranged from the unstable Dutch roll exhibited by the D-558-II at low angles of attack to the actual directional divergence encountered by the X-1A and the X-2.

The only one of these occurrences which will be discussed in detail is the maneuver that resulted in the loss of the X-2 and the death of Captain Milburn G. Apt, the pilot. Figures 6 and 7 present time histories of various recorded quantities obtained from NACA instruments recovered from the wreckage. Because of light leakage there are gaps in some of

the data, as indicated by the dashed lines. Some of the motions were sufficiently large to be off the scale. The data are divided between the two figures in order to avoid confusion. Only a general description of the maneuver was given, and no attempt is made to discuss all the curves.
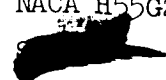
As the X-2 accelerated to the maximum Mach number, the angle of attack was maintained at less than 1° and had a value of 1° at the maximum Mach number of 3.2. The rudder was locked for supersonic flight. At maximum speed a left turn was initiated by aileron- and stabilizer-control motion that produced a longitudinal disturbance. The pilot had some trouble with this motion but finally was able to control it. In this period the increasing angle of attack decreased the directional stability. Aileron control was gradually moved to neutral, but this movement did not stop the increase of left roll because sideslip had now become positive and the dihedral effect maintained the left rolling moment. The right aileron was then applied to stop the rolling, but aileron yaw caused development of more sideslip. This process continued until finally the airplane diverged sufficiently to develop roll coupling, and the pilot completely lost control.

SUMMARY

In summary, it has been shown that several of the problems of direct pertinence to the X-15 project have been experienced on current research airplanes. The future investigations of the handling qualities of the X-1B and X-1E will furnish additional information. The experiences with the X-1A and the X-2 airplanes are indicative of the extreme caution that is required in this type of flight research. Critical conditions with the X-1B and X-1E will be approached with great care. The X-1B is to be used in investigations of handling qualities at high altitudes and low dynamic pressure. The flights with this airplane will probably not involve Mach numbers much above 2 because of the loss of directional stability. The investigation of control at very low dynamic pressure will be extended to include rocket reaction controls.

Initially, the X-1E program will be to investigate the stability and control characteristics in the Mach number range above 2 and will include means of improving directional stability and handling at high angles of attack. At a later date, the X-1E will be used to extend the low-dynamic-pressure investigation of the X-1A.

REFERENCE

1. Drake, Hubert M., and Stillwell, Wendell H.: Behavior of the Bell X-1A Research Airplane During Exploratory Flights at Mach Numbers Near 2.0 and at Extreme Altitudes. NACA H55G25, 1955.
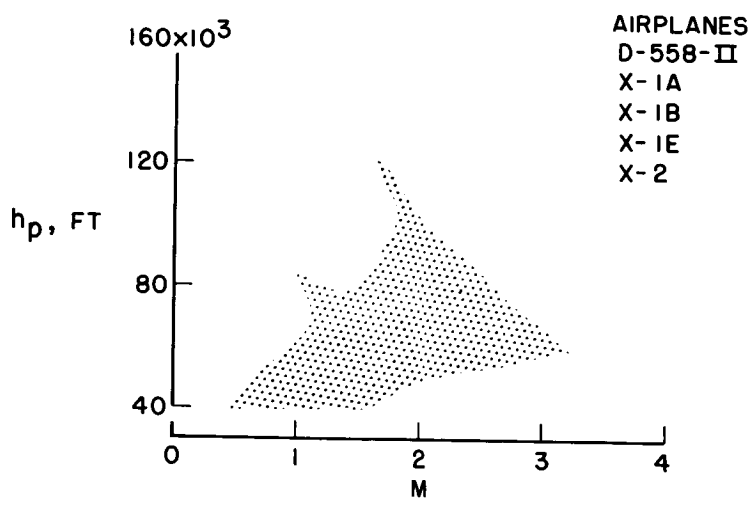
PERFORMANCE RANGE ATTAINED
BY RESEARCH AIRPLANES

AIRPLANES
D-558-II
X-1A
X-1B
X-1E
X-2

h_p, FT

Figure 1

PLANNED RANGE OF FLIGHT RESEARCH
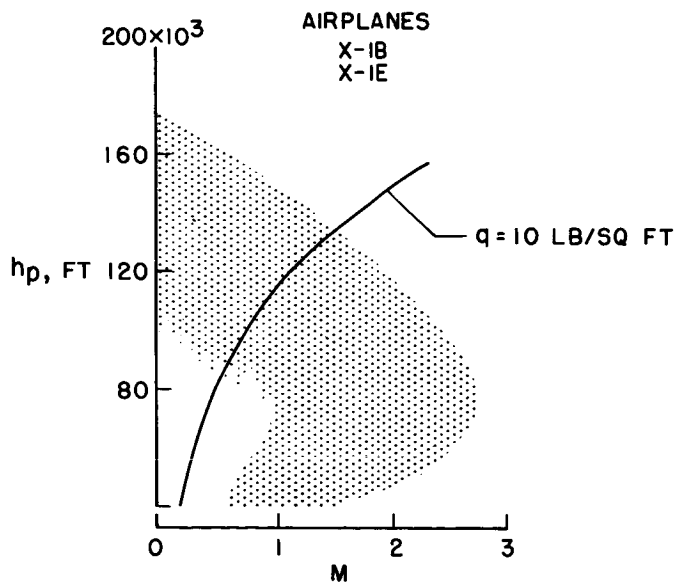
AIRPLANES
X-1B
X-1E

$q = 10$ LB/SQ FT

h_p, FT

Figure 2

TIME HISTORY OF HIGH-ALTITUDE X-2 FLIGHT
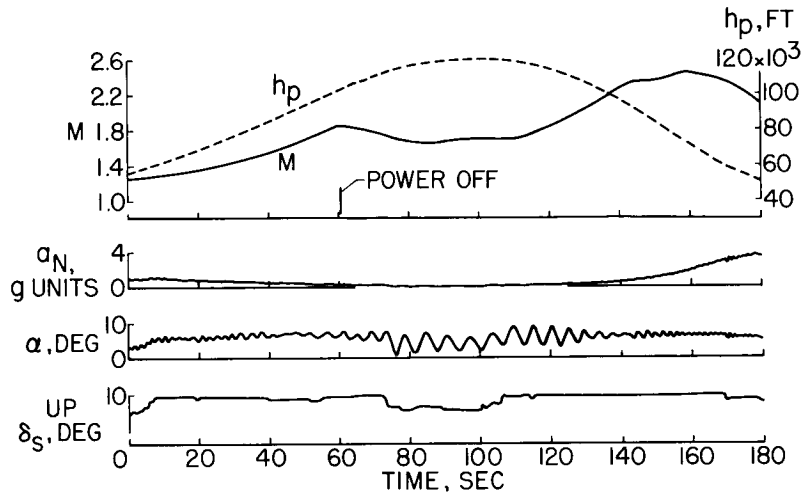
Figure 3

EFFECTS OF THRUST MISALINEMENT
X - 2 AIRPLANE

Figure 4

VARIATION OF DIRECTIONAL STABILITY
$\alpha = 0$

C_{n_β}
PER DEG

.004

.003 — D-558-II

.002 — X-IE
X-2

.001
X-IA, X-IB

0

-.001

1.0   1.8   2.6   3.4
M
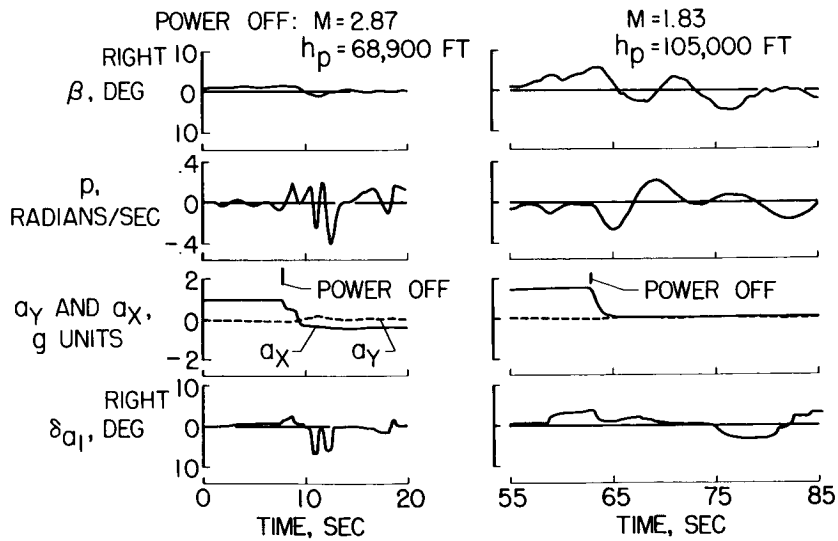
Figure 5

HIGH MACH NUMBER BEHAVIOR OF X-2

3.2
2.8   M
M 2.4   hp
2.0
1.6   ⌐POWER OFF
1.2

70×10³
60
50   hp, FT
40
30

δ_a

20
10   RT. ROLL
0   δ_a, DEG
10

UP -10
0
i_t, DEG 10 i_t a_z

a_x, a_y, a_z 2
g UNITS 0 a_y a_x
-2

260   265   270   275   280   285   290   295   300
TIME, SEC

Figure 6

HIGH MACH NUMBER BEHAVIOR OF X-2

Figure 7

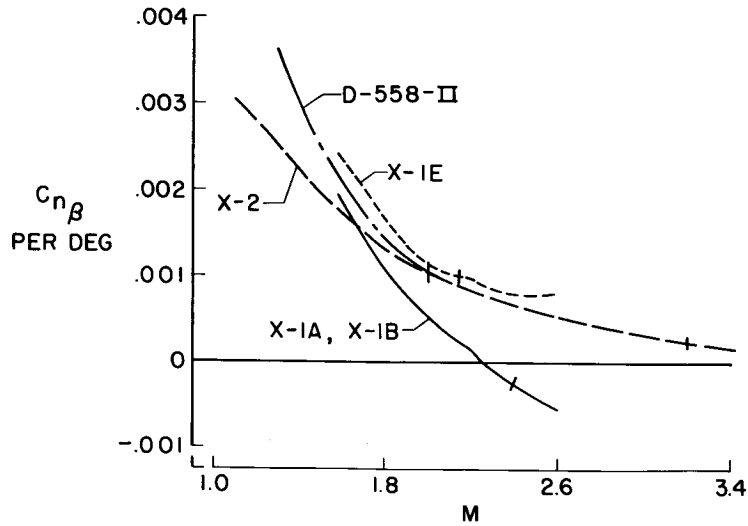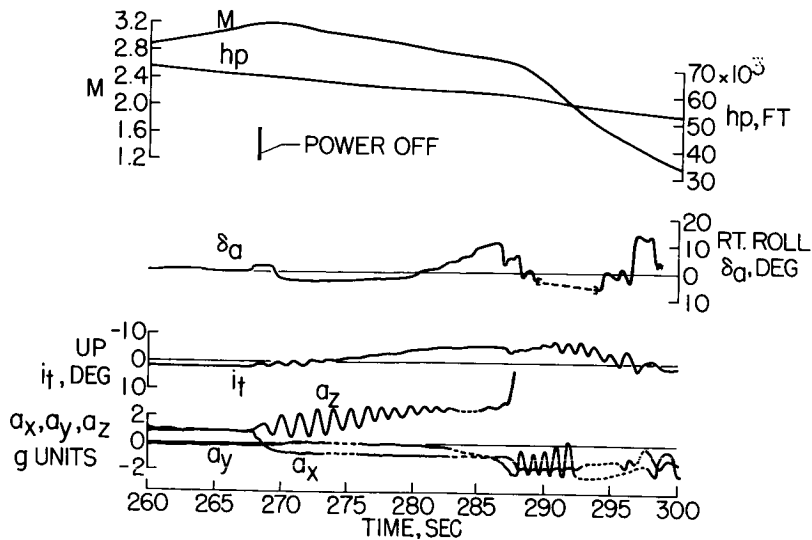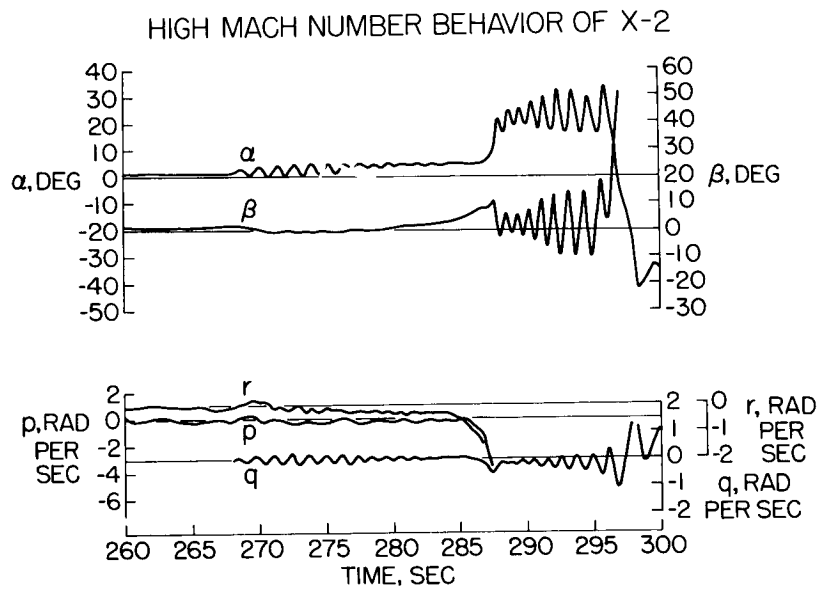# DESCRIPTION OF THE X-15 AIRPLANE, PERFORMANCE,

AND DESIGN MISSIONS

By Charles H. Feltz

North American Aviation, Inc.

This presentation introduces the X-15 airplane, its design missions, and its performance capabilities. The X-15 is a single-place, rocket-propelled, research aircraft that is to be air-launched from a B-36 carrier airplane. The structure is designed for high aerodynamic heating rates and temperatures. A suitable environment is provided for the pilot and equipment for all the varied flight conditions which will be encountered with this airplane.

The X-15 will be fabricated from Inconel X in all areas where aerodynamic or internal heating is severe. Other materials such as Inconel, titanium, and duralumin are to be used where their application is more suitable.

Figure 1 presents the X-15 configuration essentially as it was proposed. Almost all the basic aerodynamic data, aerodynamic heating, and structural analyses have been conducted for this configuration.

The airplane has the general physical shape, performance, weight characteristics, and engine data as are shown on the 3-view drawing. (See fig. 2.) The required velocity of 6,600 feet per second and a design altitude of 250,000 feet can be attained. The Reaction Motors, Inc., rocket engine installed in the X-15 has a maximum thrust rating of 57,000 pounds at 40,000 feet with a specific impulse of 276 seconds. Burning time at maximum thrust is about 88 seconds, and it may be throttled to as low as 17,000 pounds of thrust. The body, wing, and tail configurations are fairly conventional. The landing gear consists of a conventional nose gear and two ski-type main gears located at the far rearward end of the fuselage. Side fairings are provided which run the length of the fuselage and which are used as enclosures for routing of plumbing, wiring, and controls. The airplane has a wing area of 200 square feet with a five-percent thickness, an aspect ratio of 2.5, and a sweep of the quarter chord of 25°. Launching weight is 31,275 pounds which includes 18,304 pounds of usable fuel.

In addition to the upper vertical tail, a lower vertical tail has been incorporated. The upper tail is of the all-movable type and provides adequate directional stability and control at all lift coefficients in the subsonic Mach number range. At supersonic Mach numbers the double-wedge airfoil section of the vertical tails is changed by

deflecting the double split flaps located on the rearward of the 50-percent chord line of the vertical tails. In this manner, improved directional stability has been provided in the supersonic and hypersonic speed range. The lower vertical was designed to compensate for the loss of directional stability of the upper tail at high angles of attack and at high Mach numbers. The double split flaps are also utilized as speed brakes by increasing the brake deflection.

The horizontal tail is all movable for pitch control and is deflected differentially for roll control. Calculations of dynamic pressure and downwash at supersonic speeds indicated that placing the horizontal tail slightly below the wing reference plane would be a favorable location. Considerations of tail buffet in the transonic speed range also indicated the use of a low tail. The negative dihedral of the horizontal tail places the mean aerodynamic chord at the correct elevation.

Characteristics of the wing as shown in figure 2 were selected upon the basis of aerodynamic and structural efficiency, as compromised by weight and thermal problems. The sweep of the wing leading edge of 37° was selected to reduce aerodynamic heating. The leading-edge radius was chosen to provide adequate heat sink. The thickness ratio and the taper ratio are selected to give the best balance of structural and aerodynamic parameters and to provide satisfactory flying qualities over the speed range. A blunt trailing edge was incorporated to avoid thin sharp-edge sections and associated aerodynamic heating problems. Conventional trailing-edge flaps are used to reduce the touchdown angle of attack for landing-gear structural reasons and to provide improved pilot vision.

The wing area selected was the result of the several effects of wing loading during launch, recovery, and landing. The wing area of 200 square feet with a wing loading of about 150 pounds per square foot was selected to provide approximately 1.0 g launchings at angles of attack where satisfactory stability and control existed. For reentry considerations, a wing of 200 square feet serves adequately to accomplish recovery without exceeding temperature and dynamic-pressure limitations. For landings, the minimum speed is determined by the maximum allowable airplane attitude for the design sink speed of 9 feet per second for landing-gear load. With the wing of 200 square feet, the speed is 164 knots requiring only 50 percent of the available lift coefficient with flaps down.

The fuselage, as is shown in figure 3, was determined as follows: First, the cross-sectional area was governed by the working space required by the pilot. Second, a circular cross section the length of the fuselage was used for structural efficiency. And third, the length of the body is that required to contain the propellants, instruments, equipment, and powerplant. The ogive forebody is the minimum required to house the nose wheel and the hypersonic airspeed system. Attempts to define a fuselage shape having curvilinear lines for optimum hypersonic drag characteristics

were dropped in the interests of the long cylindrical sections with minimum structural cutouts and minimum fuselage weight. The control system, fuel lines, and hydraulic equipment then had to be carried outside the basic fuselage lines to avoid any structural cutouts in the integral tanks.

The arrangement of major airplane components and equipment items can be seen in the inboard profile shown in figure 4. The extreme nose of the airplane consists of a removable section containing the NACA angle-of-attack and angle-of-yaw sensor. Immediately rearward of the airspeed system nose, eight monopropellant rockets are mounted in pairs in cruciform arrangement to provide airplane pitch and yaw attitude control when the flight dynamic pressure is essentially zero. The airspeed-altitude recorder is installed just rearward of these rockets. The nose gear occupies the fuselage space to the forward cockpit bulkhead.

The cockpit and equipment compartment is a double-walled compartment insulated against outer surface heating and pressurized with nitrogen gas to maintain a minimum pressure of 3.5 pounds per square inch absolute. At the extreme rearward end of this compartment, isolated from the equipment compartment, are the two auxiliary power units which supply power for the airplane dual hydraulic and electric systems. The auxiliary power units are powered by hydrogen peroxide turbines.

Rearward of the equipment compartment bulkhead are the tanks containing the liquid nitrogen used for cockpit cooling and pressurization, and the two tanks containing hydrogen peroxide for the auxiliary power units and the previously mentioned space control rockets. Next is the integral liquid-oxygen tank. Stored in the center tube through the tank is a bottle containing helium for pressurizing and purging of both propellant tanks. Between the liquid-oxygen (designated LOX herein) tank and the integral fuel (ammonia) tank is a small equipment compartment and a helium tank used for engine purging and engine-pump hydrogen peroxide pressurization. A hydrogen peroxide tank for the engine pump is located rearward of the ammonia tank and is separated from the engine compartment by means of a fire wall.

The dynamic stability about all three axes will reduce to zero as the flight dynamic pressure and the damping forces reduce to zero at high altitudes. In this region of flight, the space attitude controls have been designed to provide the pilot with attitude control after leaving the atmosphere and in preparation for the reentry maneuver.

As shown in figure 5, the attitude control is achieved from forces of the hydrogen peroxide rockets exhausting at the nose for pitch and yaw control and in the wing for roll control. Two independent systems have been provided.

In a study on the analog-computer dynamic simulator, the values of required acceleration were determined where airplane response and the fuel required were prime considerations. As shown in figure 5, the rotational accelerations per system for pitch and yaw are 2.5 deg/sec^2 and for roll, 5 deg/sec^2.

A typical complete mission as shown in figure 6 represents the attainment of an altitude requirement of 250,000 feet. If it is assumed that the X-15 was launched above Salt Lake City, it would take approximately 25 minutes to travel the 475 nautical miles to the Edwards Air Force Base. During this time the X-15 would have used up its fuel in $1\frac{1}{2}$ minutes in accelerating to speeds of approximately Mach 6 while covering a distance of 30 miles. It would have achieved an altitude of 250,000 feet and reentered the atmosphere while covering a distance of less than 200 miles. It would then decelerate and glide more than 275 miles to its home base.

The X-15 design-mission exit phases are defined in figure 7 and were analyzed through the use of a high-speed digital computer. In the interests of simplicity in the initial investigations, instantaneous changes to the airplane angle of attack were programmed. Also, the refining details of the launch maneuvers were eliminated. The light weight B-36 series of airplanes has the capability of achieving an altitude of 38,000 feet and a Mach number 0.65. The X-15 missions, however, were started in level flight at 30,000 feet and Mach number 0.60; these conditions allow considerable margin for the launch maneuver. It is planned that refined study of the entire mission will be investigated through use of analog computers where the cockpit and the controls will be included in the simulation. Six degrees of freedom of airplane motion will be programmed.

The details of the exit phase of the design missions which have been chosen for the primary evaluation of airplane dynamics, aerodynamic heating, and structural analyses are as follows: First, ignite rocket engine at 30,000 feet and Mach number 0.6 in level flight. Second, accelerate at 30,000 feet to approximately Mach number 0.65. Third, pull-up at limit lift coefficient until desired flight-path angle is achieved. Fourth, reduce the lift to zero during burning phase of mission. Fifth, make a zero-lift ballistic-type coast-to-peak altitude, and sixth, recover in a variety of manners.

The zero-lift ascent conditions were defined to retain the maximum amount of energy in the airplane for reentry conditions. This mission definition is only one of many which could have been selected. It does represent an optimum to achieve the design speed with the minimum fuel load. Missions using lift during burning and coasting are entirely feasible.

Figure 8 shows the exit phase of the maximum speed mission. In accomplishing the speed of 6,600 feet per second, the pull-up is made to an initial climb angle of 55° at approximately an altitude of 35,000 feet. The design speed of 6,600 feet per second or Mach number 6.5 is achieved at 120,000 feet.

The coast at zero-lift results in a peak altitude of 143,000 feet. It is to be noted that a maximum dynamic pressure of only 600 pounds per square foot is obtained during burning; at burnout the dynamic pressure is only about 200 pounds per square foot.

The exit phase of the altitude mission is shown in figure 9 and is accomplished in the same manner as the speed mission, with the pull-up achieved at 36,000 feet but at an initial climb angle of 62°. Burnout is achieved at an altitude of 156,000 feet at which time 6,340 feet per second or Mach number 5.9 is achieved. The flight-path angle at this point has reduced in the ballistic type of flight to 22.5°.

The effect of the initial climb angle on the speed at burnout and the subsequent peak altitude is shown in figure 10. It is to be noted that the maximum speed is influenced to some degree by the initial climb angle; however, the resultant peak altitude is markedly influenced. For example, an initial climb angle of 55° would result in an altitude of 143,000 feet and a speed of 6,600 feet per second; however, an initial climb angle of 90° would result in a peak altitude of 700,000 feet.

Two types of recovery are used in the analysis of both the speed and the altitude missions; however, the altitude mission is used herein as the example while defining each type of reentry. Figure 11 depicts the maximum dynamic-pressure reentry from the altitude mission.

First, the speed brakes are opened to maximum deflection at the peak altitude. This then results in slowing down during the descent while still maintaining zero lift which, it should be noted, has been maintained throughout the trajectory from the initial pull-up. Maximum desired longitudinal decelerations are maintained during this reentry by allowing the speed brakes to "blow back" as necessary. Recovery is then attained by a 7.33g pullout at a maximum dynamic pressure of 2,500 pounds per square foot and without exceeding 1,200° F skin temperature. To accomplish this, the 7.33g pullout is initiated at 64,000 feet and recovery is completed at 48,000 feet.

It is expected that designing to this condition will result in a rugged airplane because of the requirement of 7.33g at a dynamic pressure of 2,500 pounds per square foot. Symmetrical heating of the wings and fuselage is expected to exist at temperatures somewhat lower than 1,200° F.

Figure 12 shows the maximum angle of attack reentry. When the peak altitude is reached, the speed brakes are opened only to the position required for lateral directional stability. A zero-lift dive is continued from peak altitude until a 7.33g pullout can be accomplished. This results in initiating the pullout at 117,000 feet with the recovery complete at 96,000 feet. A maximum dynamic pressure of about 500 pounds per square foot and a maximum angle of attack of about 30° is experienced during this pullout.

This condition was chosen to investigate the effects of differential heating of the wings and fuselage. Thermal stresses and distortions are expected to be a severe problem.

These recoveries are typical also of the recoveries from the speed mission. The dynamic pressures, angles of attack, and pullout altitudes are of the same general order of magnitude.

Early in the proposal stage, it was determined that the drag of the airplane would not be as important as that normally experienced on conventional jet-propelled fighter aircraft. Weight was of prime importance.

Figure 13 presents the variation with time of drag, drag plus the weight component in the flight-path direction, and the thrust available for accelerating the airplane. The time is defined as the period from launch to burnout of a typical mission.

Integrating these data shows that approximately 10 percent of the energy is used to overcome the drag and 20 percent to overcome the weight component. The remainder of the energy, 70 percent, is used to accelerate the airplane to a nominal Mach number 6.5 at burnout. It is seen that drag is relatively unimportant, whereas weight and thrust for acceleration are of prime importance.

In conclusion, North American Aviation, Inc., is designing the X-15 to accomplish the design requirements of speed and altitude with an airplane that is as simple and light as possible.

SYS-447L **NORTH AMERICAN X-15 RESEARCH AIRPLANE**

Figure 1

SYS-447L **THREE VIEW**

49 FT

22 FT

14 FT

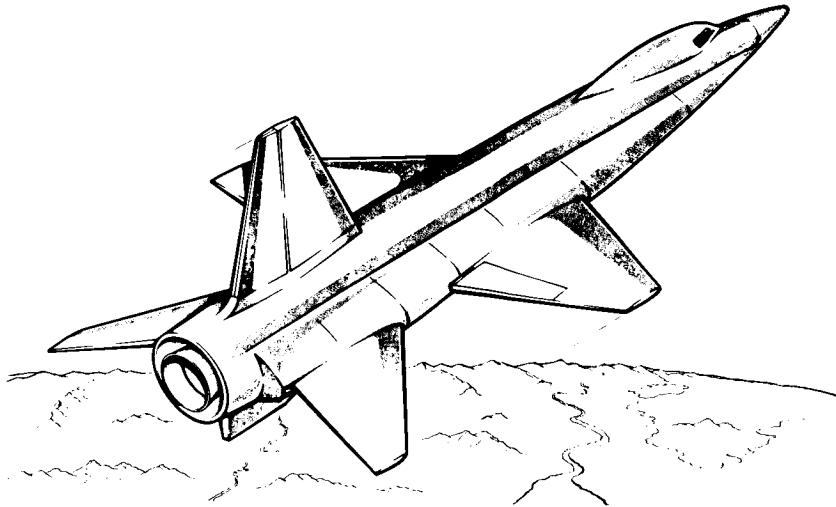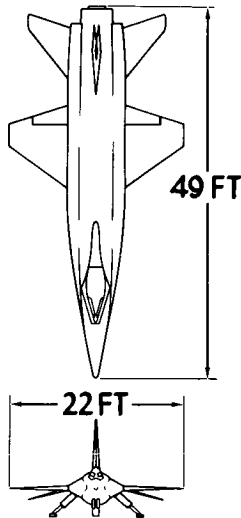PERFORMANCE
   VELOCITY   6600 FT PER SEC
   DESIGN ALTITUDE   250,000 FT
   LANDING SPEED   164 KN

POWER PLANT - RM1
   MAX THRUST (40,000 FT)   57,000 LB
   MIN THRUST (40,000 FT)   17,000 LB

WING
   AREA   200 SQ FT
   SWEEP ¢/4   25 DEGREES
   THICKNESS   5 PERCENT
   ASPECT RATIO   2.5

WEIGHT
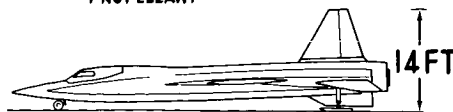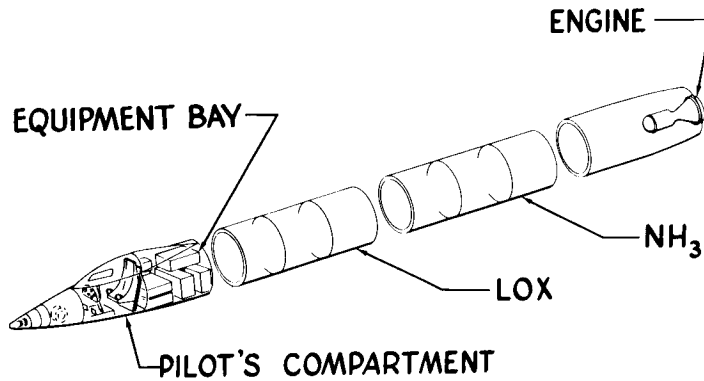   LAUNCHING   31,275 LB
   BURN-OUT   12,971 LB
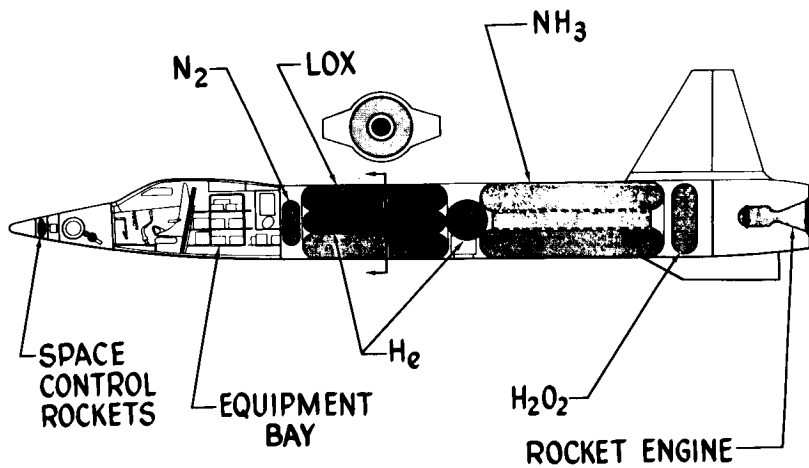   PROPELLANT   18,304 LB

Figure 2

SYS-447L FUSELAGE CONFIGURATION DESIGN

ENGINE

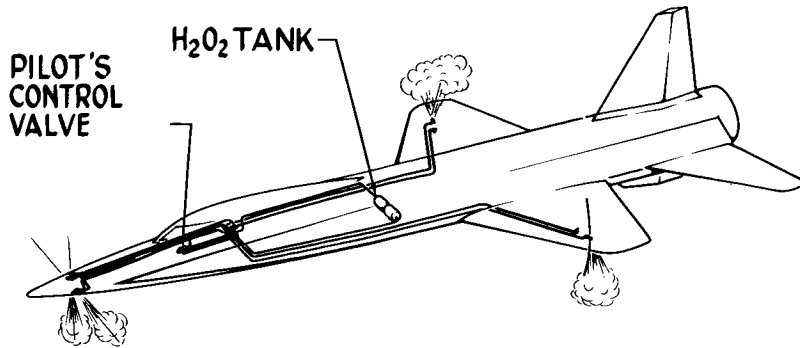EQUIPMENT BAY

NH₃

LOX

PILOT'S COMPARTMENT

Figure 3

SYS-447L INBOARD PROFILE

NH₃

N₂ LOX

SPACE CONTROL ROCKETS

He

EQUIPMENT BAY

H₂O₂

ROCKET ENGINE

Figure 4

SYS-447L **SPACE-ATTITUDE CONTROLS**

PILOT'S CONTROL VALVE

H_2O_2 TANK

EACH SYSTEM	ACCELERATION	THRUST
PITCH	$2\frac{1}{2}°/SEC^2$	113 LB
YAW	$2\frac{1}{2}°/SEC^2$	113 LB
ROLL	$5°/SEC^2$	50 LB

Figure 5

SYS-447L **COMPLETE ALTITUDE MISSION**

COAST

THRUST ON

PULL-OUT

GLIDE TO BASE

DECELERATE

ALT 1000 FT

280

240

160 BURN-OUT

120

80

40

0

25 MINUTES

0   80   160   240   320   N MI   480
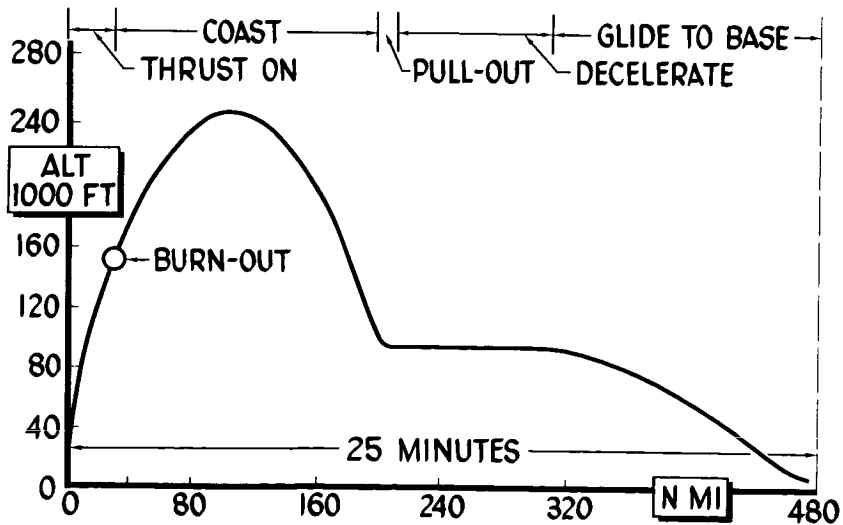
Figure 6

SYS-447L

DESIGN MISSION DEFINITION
EXIT

ALT 1000FT

LIGHT UP
PULL-UP

BURNOUT

30

ZERO LIFT CLIMB

ZERO LIFT COAST

TIME
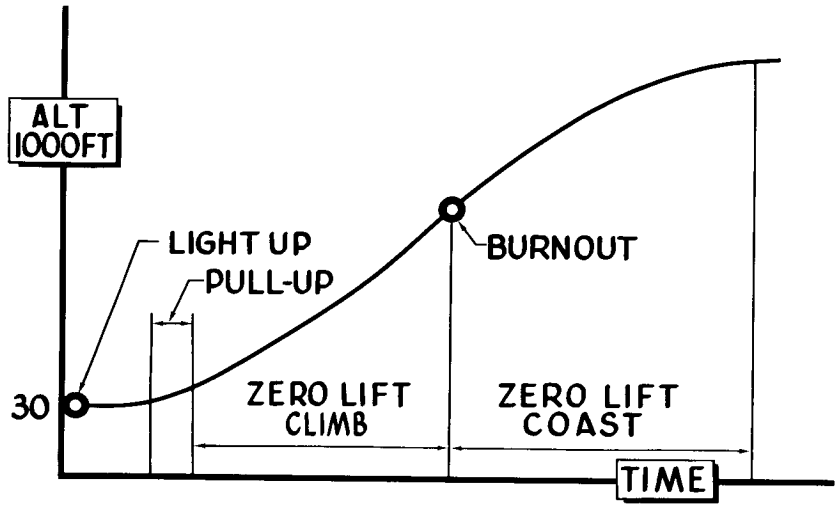
Figure 7

SYS-447L

SPEED MISSION

ALTITUDE

BURN-OUT
V = 6600 FPS
M = 6.5

ALT 1000 FT

q-LB/FT²

800

400

q

TIME SEC

0   20   60   80   100   120   140

Figure 8

ALTITUDE MISSION

SYS-447L

Figure 9

EFFECT OF INITIAL CLIMB ANGLE

SYS-447L

Figure 10

SYS-447L **ALTITUDE MISSION DESIGN RECOVERY**
MAXIMUM-g

Figure 11

SYS-447L **DESIGN RECOVERY FROM ALTITUDE MISSION**
MAX ANGLE OF ATTACK

7.33g PULL-OUT AT 117,000 FT
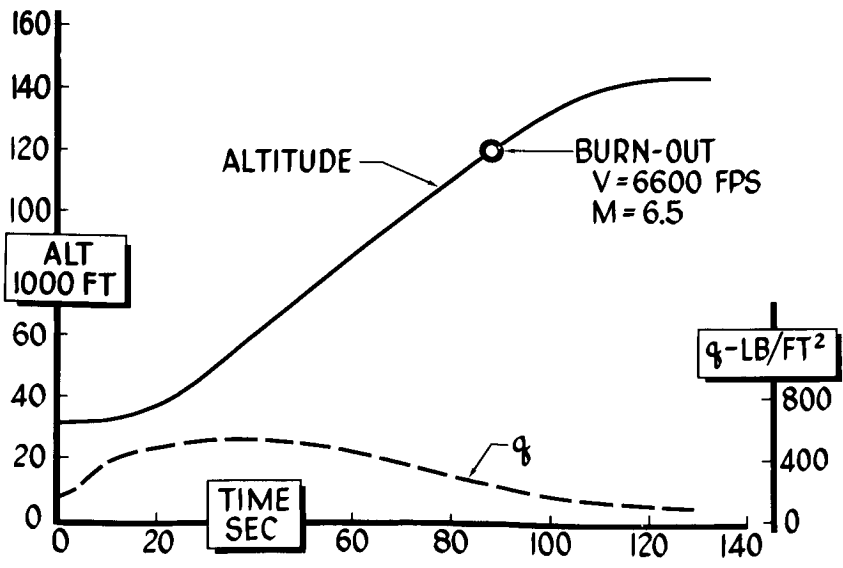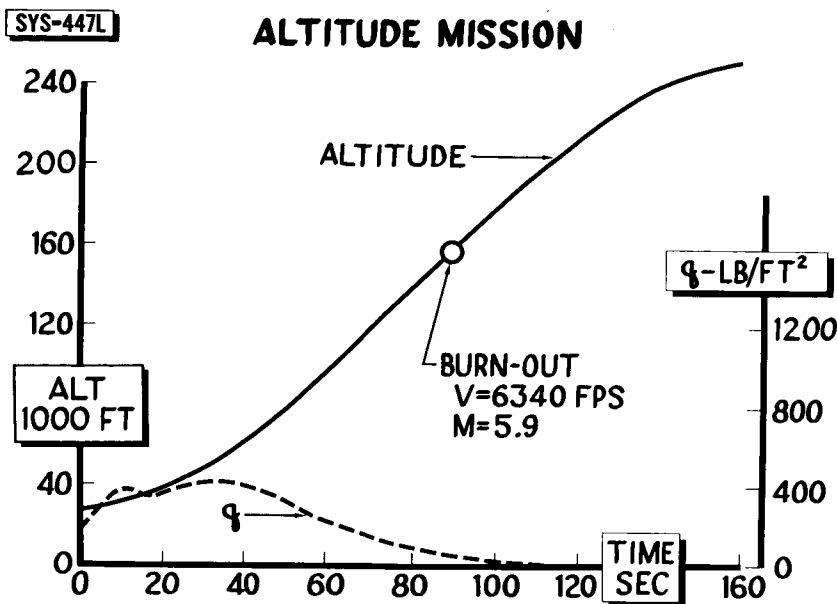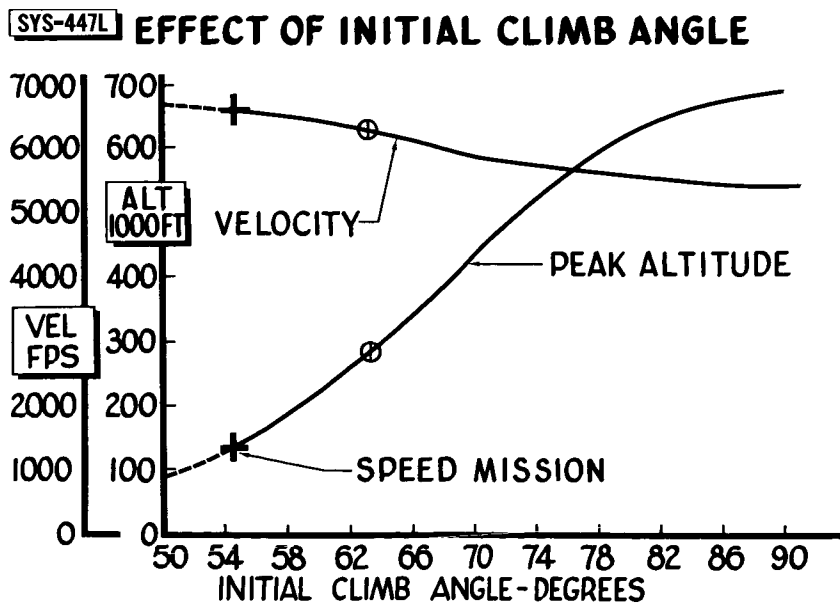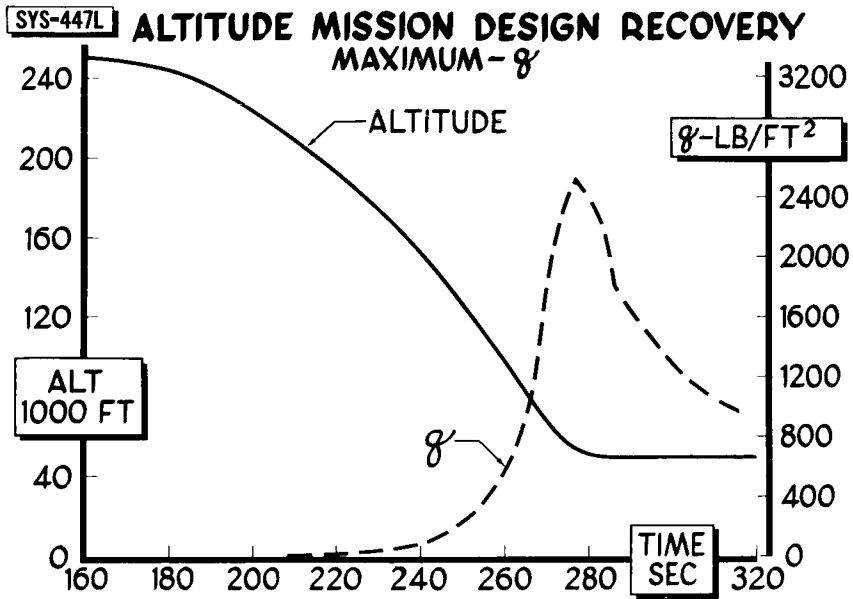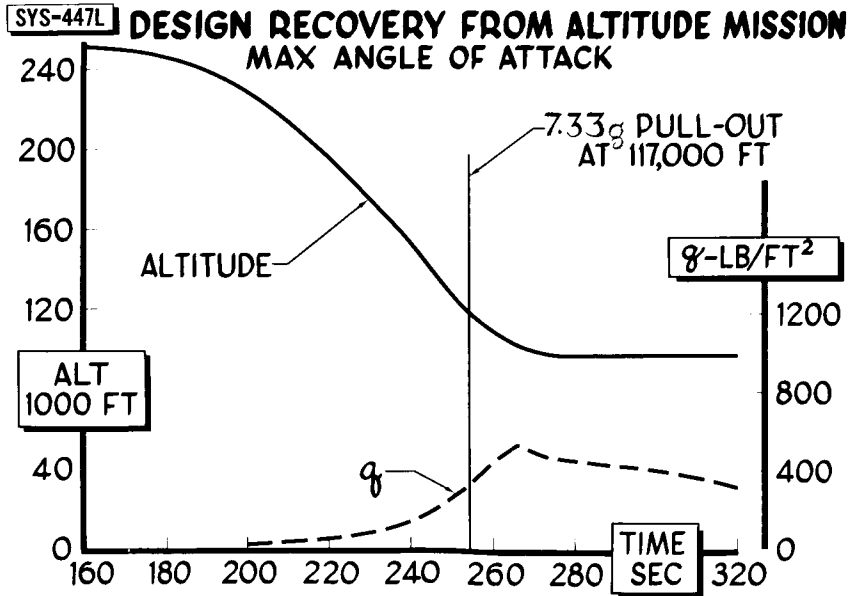
Figure 12

INFLUENCE OF WEIGHT AND DRAG
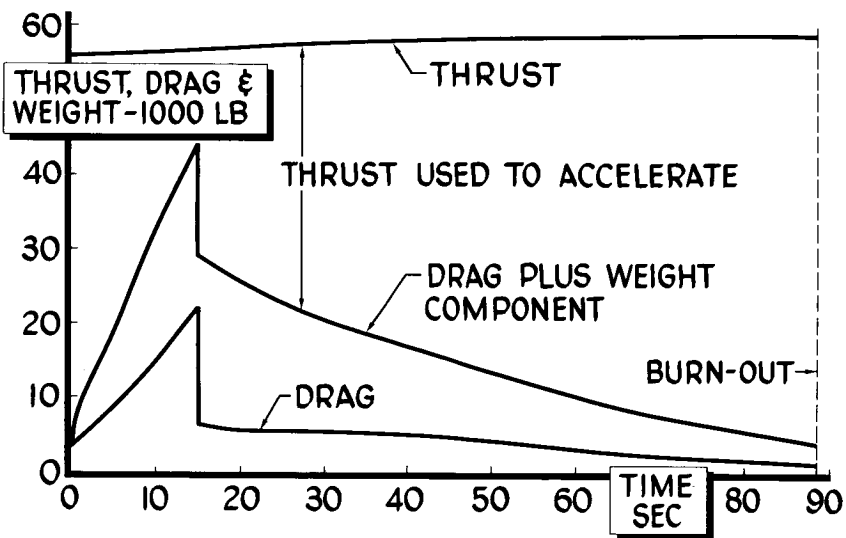
Figure 13

AERODYNAMICS AND STABILITY
AND HANDLING CHARACTERISTICS

AERODYNAMIC CHARACTERISTICS FROM WIND-TUNNEL

STUDIES OF THE X-15 CONFIGURATION

By Herbert W. Ridyard and Robert W. Dunning
Langley Aeronautical Laboratory

and E. W. Johnston
North American Aviation, Inc.

INTRODUCTION

In order to investigate the aerodynamic characteristics of the X-15 research airplane, an exploratory wind-tunnel test program was initiated in January of 1956. Since that time, X-15 models have been tested in eight different facilities through a Mach number range from less than 0.1 to about 6.9. Several variations of the original configuration have been tested. The aerodynamic characteristics of two of the configurations are presented in this paper.

DISCUSSION

A three-view sketch of these two configurations with speed brakes deflected 45° is shown in figure 1. Some of the differences between the two configurations are indicated by the solid and dashed lines. Configuration 1, which is indicated by the solid lines, represents the original proposed design by the North American Aviation, Inc. (See ref. 1 for description.) Configuration 2, as indicated by the dashed lines, is a revised configuration and is the configuration described in the preceding paper by Charles H. Feltz and in reference 2.

The primary difference between the configurations is that the nose of configuration 2 is considerably more blunt than that of configuration 1. This increase in bluntness was necessary to provide an increase in fuel capacity. The diameter of the basic body of revolution was increased about 6 percent for the same reason. The wing was moved rearward about 2.5 percent of the mean aerodynamic chord in an attempt to balance aero-dynamically the change in nose shape. It should be noted that the center of gravity was moved also so that it would be located at 25 percent of the mean aerodynamic chord for either configuration.

In addition to these differences, the rear portions of the side fairings were enlarged for configuration 2 as shown in figure 1. The landing skids (shown in the retracted position in fig. 1) were moved rearward from beneath the wing on configuration 1 to a position beneath

the horizontal tail. Finally, the leading-edge radii of the wing and tail surfaces and the radius at the tip of the body nose were increased to satisfy the aerodynamic-heating requirements.

Figure 2 presents the wind-tunnel program for these two configurations. The facilities utilized in this program are the North American 8.75- by 11-foot tunnel, the Langley 8-foot transonic tunnel, the North American 16-inch tunnel, the Massachusetts Institute of Technology supersonic tunnel, the Langley 9- by 9-inch Mach number 4 blowdown jet, the Ames 10- × 14-inch tunnel, and the Langley 11-inch hypersonic tunnel. The data presented in this paper are unpublished preliminary results obtained from these facilities. The test Mach number range is illustrated by the bar graph at the right of figure 2. Note that configuration 1 has been tested in each facility whereas configuration 2 has been tested only in three facilities.

The drag characteristics of the X-15 are shown in figure 3. This figure presents the effect of speed-brake deflection on the drag coefficient at an angle of attack of 0° over the test Mach number range. The results presented in this figure are for brakes closed and deflected 20°, 30°, and 45°. Note that the open symbols refer to configuration 1 and the shaded symbols to configuration 2. This method of identification of the results for the two configurations will be used throughout the paper.

As noted in the previous paper by Feltz, the drag of the configuration with the speed brakes closed is not of major importance in the design performance of the airplane. For the configurations with the speed brakes deflected, high values of drag coefficient are important for speed control during reentry, and these high values are seen to be available; in fact, the values presented in figure 3 for the speed brake deflected 45° are so high that the speed brakes require a blow-back feature such as that discussed by Charles H. Feltz.

Another point of interest is that the variation of drag coefficient with speed-brake deflection is considerably more nonlinear at a Mach number of 6.86 than at a Mach number of 3 or 4.

The effect of lift coefficient on drag coefficient is shown in figure 4. These results are for Mach numbers of 1.43 and 6.86 and for configuration 1 with speed brakes closed and deflected 45°. It is apparent from figure 4 that the drag due to lift increases greatly with Mach number; however, even for the higher Mach number, in order to obtain the same drag coefficient, it is necessary to go to a much higher lift coefficient with the speed brakes closed than with speed brakes deflected to 45°.

Figure 5 presents the variation of lift-curve slope at an angle of attack of $0°$ with Mach number. These data, as indicated by the front-view sketches, are for the following configurations: the complete airplane; the body, wing, and side fairing; the body and side fairing; and the basic body of revolution. It is shown that the lift-curve slopes for the complete and the body-wing configurations decrease with Mach number in the supersonic speed range. This decrease is primarily due to the loss in lifting effectiveness of the wing. On the other hand, for the body configurations the lift-curve slope remains relatively constant with Mach number. The end result is that at a Mach number of 6.86 almost one-half of the total lift of the complete airplane is derived from the body—side-fairing configuration. Further inspection of figure 5 indicates that about one-fourth of the lift of the airplane is derived from the side fairings at this same Mach number (6.86). Although not shown in figure 5, speed-brake deflection had little effect on the lift-curve slope of the complete airplane throughout the Mach number range.

Figure 6 presents the variation of lift coefficient with angle of attack for configuration 1 at several Mach numbers. The data show that nonlinearities are small up to a Mach number of 3; however, at a Mach number of 6.86 the curve is somewhat nonlinear. Although it is not readily apparent from figure 6, the value of C_L at $\alpha = 20°$, obtained by extrapolation by use of the lift-curve slope at an angle of attack of $0°$, is about 50 percent lower than the experimental value of C_L at $\alpha = 20°$. Attempts to estimate the data for a Mach number of 6.86 have not been entirely successful up to the present time, primarily because of the nonsymmetrical cross section of the fuselage. However, estimates obtained by a summation of experimental lift coefficients for the body and theoretical coefficients for the wing and tail surfaces, calculated by use of shock-expansion theory, are in excellent agreement with the data at a Mach number of 6.86.

Figure 7 depicts the variation of the longitudinal-stability parameter dC_m/dC_L at $C_L = 0$ with Mach number for the following configurations: the body and side fairing; the body, wing, and side fairing; and the complete airplane. The data for configuration 1 (open symbols) show that the configuration of body and side fairing is unstable throughout the Mach number range; however, this instability decreases with Mach number because of a rearward movement of the center of pressure. The configuration of body, wing, and side fairing, which is unstable at subsonic Mach numbers, the center of gravity being located at one-quarter of the mean aerodynamic chord, becomes stable at low supersonic Mach numbers as the wing center of pressure moves rearward. This configuration then decreases in stability at higher Mach numbers as the wing effectiveness decreases.
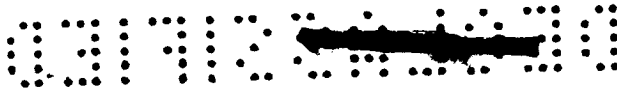
The complete configuration 1 is stable throughout the Mach number range as a result of the large tail input; however, there are two regions of marginal stability, one at subsonic speeds and one at hypersonic speeds. As a matter of fact, there is a dip to almost neutral stability at a Mach number of 0.95. These regions of marginal stability are restricted to small lift coefficients as is shown in figure 8 which presents the variation of the pitching-moment coefficient with lift coefficient for configuration 1 with the speed brakes closed for several Mach numbers. The results for configuration 2 are also included for comparison in figure 8 for a Mach number of 6.86. For configuration 1 the longitudinal stability is marginal at small values of lift coefficient for Mach numbers of 0.95 and 6.86; however, the slopes of these curves at high values of lift coefficient are nearly as great as that for a Mach number of 1.43. Therefore, the problem of longitudinal stability is not as serious for high values of lift coefficients as for low values of lift coefficient.

The longitudinal stability of configuration 2 is indicated by the shaded symbols in figures 7 and 8. It is obvious that all the results for zero-lift coefficient show less stability at supersonic Mach numbers. At a Mach number of 6.86 the complete configuration is shown to be unstable, the center of gravity being located at one-quarter of the mean aerodynamic chord. This decrease in stability can apparently be traced to the increased bluntness of the fuselage of configuration 2 as shown by the shift in all three sets of data points at a Mach number of 6.86 in the destabilizing direction. (See fig. 7.)

As a possible means of improving the longitudinal stability of the complete configuration, the body and side fairing of configuration 1 was modified by removing part of the side fairing in the vicinity of the nose. Additional tests (not presented herein) obtained with this modified configuration in the Langley 11-inch hypersonic tunnel have indicated large gains in stability. It is therefore plausible to assume that a similar removal of the side fairing from configuration 2 would restore a large part of this decrease in stability. Further considerations of possible means of improving the longitudinal stability are discussed in a subsequent paper by Lawrence P. Greene.

Figure 9 presents the effect of speed-brake deflection on the longitudinal stability at zero-lift coefficient. The experimental results are for complete configurations 1 and 2 with speed brakes closed or deflected 45° as indicated by the sketches of the vertical-tail sections. It is evident that the longitudinal stability increases with speed-brake deflection, and in the higher Mach number range the stability due to the speed brakes increases greatly with Mach number.

The explanation for this effect at a particular Mach number can probably be found by considering the variations with angle of attack of the dynamic pressure in the flow fields above and below the airplane. The effect of these variations in dynamic pressure with angle of attack is to decrease the pitching-moment contribution of the upper speed brake and to increase the pitching-moment contribution of the lower speed brake; the net effect of both speed brakes is to increase the stability of the airplane. At the higher Mach numbers these variations in dynamic pressure with angle of attack are known to become more pronounced; therefore, the speed-brake effect on stability increases greatly with Mach number in the hypersonic Mach number range.

Another means of increasing the longitudinal stability of the complete configuration at high Mach numbers is described in figure 10 where the effect of horizontal-tail section on the longitudinal stability of configuration 2 is given. Pitching-moment coefficient is plotted against lift coefficient for the complete configuration with an NACA 66-series modified symmetrical horizontal-tail section and for the complete configuration with a 10° wedge horizontal-tail section. These results are compared for Mach numbers of 1.51, 3.50, and 6.86. At a Mach number of 1.51, there is no effect on the stability due to airfoil section; however, at the higher Mach numbers, the stability is greater for the wedge section. This result is particularly apparent at a Mach number of 6.86 at small values of lift coefficient where, in fact, an increase in stability is very much needed.

This increase in stability at small values of lift coefficient for a Mach number of 6.86 could have been obtained with a speed-brake deflection of about 30°; however, a higher drag penalty would have been incurred. For example, the minimum drag for the complete configuration would double with the use of a 30° speed-brake deflection; whereas the minimum drag would increase by only 10 percent with the use of a 10° wedge horizontal-tail section.

The longitudinal-control results for configuration 2 are given in figure 11. Shown in this figure are the variations in pitching-moment coefficient with lift coefficient for several horizontal-tail deflections for Mach numbers of 2 and 6.86. At a Mach number of 2 the increment in pitching moment between tail deflections is relatively constant; however, at a Mach number of 6.86, at small negative values of lift coefficient, longitudinal control is very small compared with the control at high lift coefficients.

The reason for the loss in control in the region of small negative lift coefficients is apparent in figure 12. The effect of the wing on the incremental pitching moment of the horizontal tail due to a tail deflection of -20° is shown in figure 12. These results are plotted for wing on and off through the test angle-of-attack range. At small, particularly negative, angles of attack there is a large effect of the wing

on the horizontal-tail pitching moment as indicated by the sketch at the left of the figure where the tail is deflected into the wing wake. At high angles of attack there is little effect of the wing on the horizontal-tail pitching moment since the low-dynamic-pressure flow from the wing passes over the tail as indicated by the sketch at the right.

Figure 13 presents the effect of speed-brake deflection on the longitudinal control of configuration 2 at a Mach number of 6.86. Pitching moment is plotted against lift coefficient for horizontal-tail deflections of 0°, -10°, and -20° for three speed-brake deflections. The first is a combination of deflections, 5° for the upper speed brakes and 7.5° for the lower speed brakes. These deflections transform the basic double-wedge section of the vertical tails into a single-wedge airfoil section. The other two speed-brake deflections are 20° and 45°.

All three sets of results in figure 13 show less control power at small lift coefficients than for high lift coefficients as shown in figure 12. Furthermore, there are only small differences in longitudinal control between the full-wedge speed-brake-deflection results and the 20° speed-brake-deflection results; however, for the 45° case the conditions for trim are considerably different and should be taken into account in dynamic studies of the configuration.

Since the horizontal tail provides lateral as well as longitudinal control, it is appropriate to consider the lateral-control results in figure 14. The rolling-moment and yawing-moment coefficients per degree of differential tail deflection $C_{l_{\delta_h}}{}'$ and $C_{n_{\delta_h}}{}'$ are plotted against Mach number. These data were obtained for the complete configuration with a differential tail deflection of $\pm 5^\circ$ and are presented for angles of attack of 0°, 10°, and 20°. As noted, some of the data are for the single-wedge vertical-tail section indicated by the 5°, 7.5° combination of speed-brake deflections and some, for the 20° speed-brake deflection.

The rolling-moment-parameter data show that, for an angle of attack of 0°, lateral control decreases with Mach number at supersonic speeds. At the higher Mach numbers, lateral control increases with angle of attack. These trends are similar to those discussed for the longitudinal-control results (fig. 11), as might have been expected.

In figure 14 $C_{n_{\delta_h}}{}'$ is seen to decrease with Mach number, but in the higher Mach number range this parameter does not vary greatly with angle of attack.

It should be noted that the coupling parameter $C_{n_{\delta_h}}{}'$, as defined herein, represents a favorable yawing moment; that is, the airplane will tend to yaw in the direction that it is being rolled.
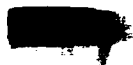
Figure 15 gives the variation with Mach number of the static directional stability derivative C_{n_β} at an angle of attack of 0° for the complete configuration with speed brakes closed and deflected, as indicated by the sketches of the vertical-tail sections, and also for the vertical-tail-off configuration.

These results show that, for the speed-brakes-closed configuration, static directional stability decreases with Mach number and becomes unstable at Mach numbers above about 4.3. This loss in stability is due to the decrease in effectiveness of the double-wedge section as the Mach number is increased. The use of a full-wedge vertical section (that is, $\delta_b = 5^\circ$, 7.5°) provides about neutral stability at the higher Mach numbers. The use of 45° speed brakes, however, provides large values of directional stability throughout the Mach number range.

In figure 16 is a similar presentation for the effective-dihedral parameter C_{l_β} at an angle of attack of 0°. The results for the complete configuration with speed brakes closed show that C_{l_β} decreases with Mach number. These results also show that C_{l_β} increases with speed-brake deflection in much the same way as C_{n_β}, but it should be remembered that these large negative values of C_{l_β} are primarily due to the lack of symmetry of the vertical tail.

Figure 17 presents the variation of C_{n_β} and C_{l_β} with angle of attack for configuration 2 with speed brakes deflected 20° at Mach numbers of 2.98 and 6.86. As indicated by the sketches, these results are for the complete airplane with both vertical tails, with the upper vertical tail off, and with both vertical tails off.

At a Mach number of 2.98 the directional-stability derivative C_{n_β} decreases to zero at an angle of attack of about 20° whereas for a Mach number of 6.86 C_{n_β} is fairly constant with α. At both Mach numbers the upper vertical tail loses its effectiveness with angle of attack as shown by the decrease in the increment between the curves, for the configuration with both vertical tails on and with the upper vertical tail off; whereas the lower vertical tail increases in effectiveness as shown by the increment between the curves for the configuration with the upper vertical tail off and with both vertical tails off. The main difference between the results is that at a Mach number of 6.86 the lower vertical tail increases its effectiveness by several times and thus maintains positive values of C_{n_β} at high angles of attack which are about as high as those for an angle of attack of 0°.

Although these results are only for a speed-brake deflection of 20°, they are representative of the trends for other speed-brake deflections; for example, at a Mach number of 2.98 for a smaller speed-brake deflection than 20°, the C_{n_β} curve would drop to zero at a smaller angle of attack; likewise, for a larger speed-brake angle C_{n_β} would go to zero at a higher angle of attack. For a Mach number of 6.86 the curve for the complete airplane also would shift roughly parallel to itself for other speed-brake deflections and would become more stable as the speed-brake deflection increased.

It is significant to note from these results that, if the speed brakes are used for improving directional stability, the directional-stability problem could be more critical at a Mach number of 2.98.

In figure 17 C_{l_β} for the complete airplane is seen to increase with angle of attack at a Mach number of 2.98 and to decrease with angle of attack at a Mach number of 6.86. At an angle of attack of 0° the rolling moments are negative at both Mach numbers because they are derived primarily from the upper vertical tail. At high angles of attack, at a Mach number of 2.98, C_{l_β} for the configuration with both tails off agrees closely with C_{l_β} for the complete airplane; thus, the upper and lower tail contributions to the rolling moments have about canceled each other. At high angles of attack for a Mach number of 6.86, however, C_{l_β} is less negative than the value for the configuration with both vertical tails off because the difference in rolling moments are primarily due to the lower vertical tail.

Figure 18 depicts the directional-control results for configuration 2 throughout the Mach number range. The parameters are the yawing- and rolling-moment coefficients per degree of vertical-tail deflection. These results show that, for either the full-wedge vertical tail or the 20° speed-brake deflection at an angle of attack of 0° or 20°, $C_{n_{\delta_v}}$ and $C_{l_{\delta_v}}$ decrease with Mach number and also with angle of attack. At high Mach numbers and angles of attack these parameters are approaching zero. Note that only the upper tail is movable and therefore this decrease in directional control could have been anticipated from the discussion of directional stability (fig. 17). As is discussed further by Lawrence P. Greene in a subsequent paper, the lower vertical tail will be movable on future configurations so that a considerable amount of the loss in control with angle of attack will be restored.

Finally, it is interesting to note that the magnitude of the coupling parameter $C_{l_{\delta_v}}$ at a Mach number of 6.86 is higher for an angle of attack of 0° where, as noted in figure 14, the roll-control parameter $C_{l_{\delta_h}}$ is at its lowest.

REFERENCES

1. Johnston, E. W.: Test and Model Information for Wind Tunnel Tests of a Full Span .02-Scale Weapon System 447L (X-15 Research Airplane, NA-240) Sting Mounted Force Model at the Langley 11" Hypersonic and 9" Supersonic Blowdown Jet Wind Tunnels. Rep. No. NA-56-170, North American Aviation, Inc., Feb. 8, 1956.
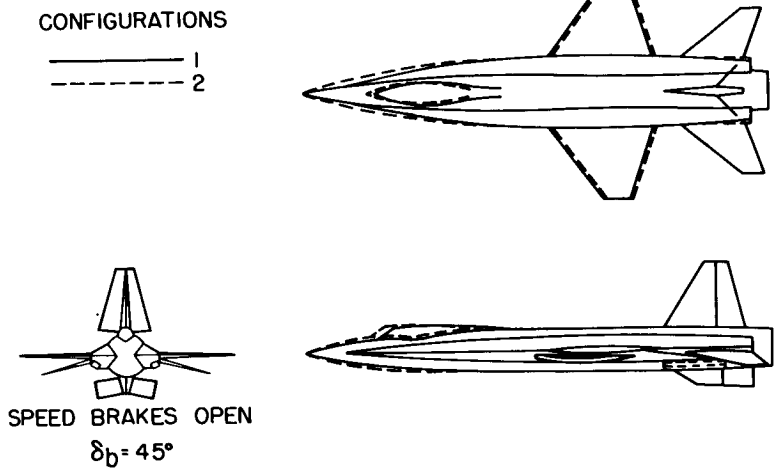
2. Winfrey, J. T.: Test and Model Information for Wind Tunnel Tests of a Revised Full Span .02-Scale Weapon System 447L (X-15 Research Airplane, NA-240) Sting Mounted Force Model at the Langley 11" Hypersonic and 9" Supersonic Blowdown Jet Wind Tunnels. Rep. No. NA-56-694, North American Aviation, Inc., May 31, 1956.

X-15

CONFIGURATIONS
——————— 1
— — — — — 2

SPEED BRAKES OPEN
$\delta_b = 45°$

Figure 1

WIND-TUNNEL PROGRAM

CONFIGURATIONS
▭ 1
▨ 2

NAA 8.75×11-FT
LAL 8-FT TRANS.
NAA SAL 16-IN.
MIT NSL
LAL HIGH M JET
AAL 10×14-IN.
LAL 11-IN. HYP.

0   1   2   3   4   5   6   7
M
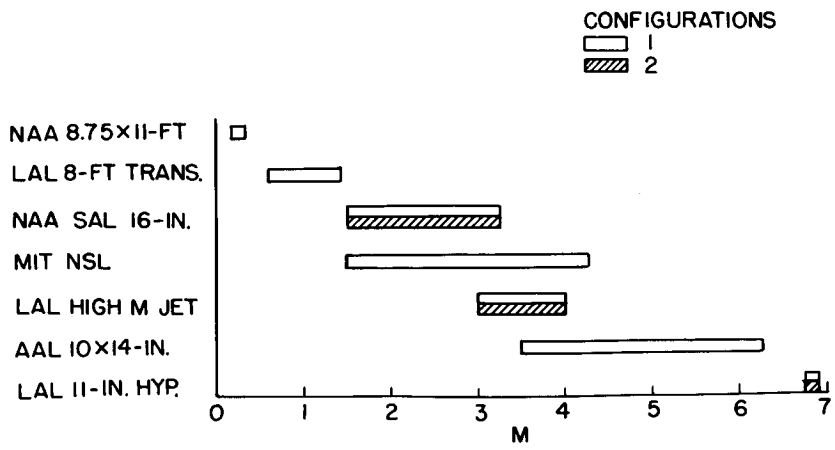
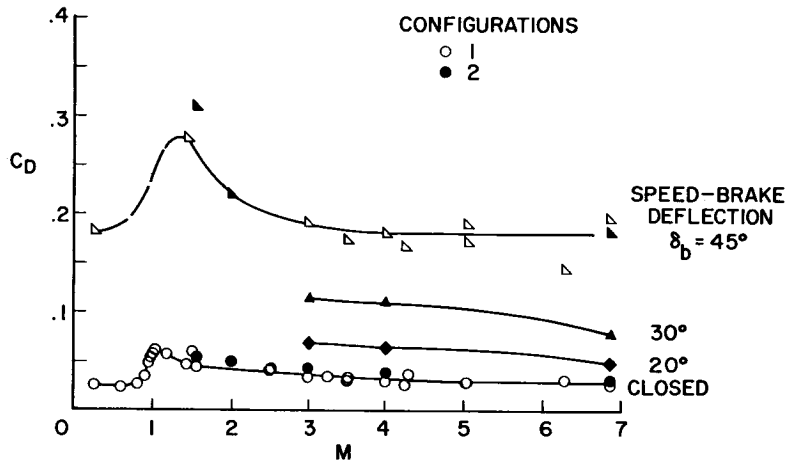Figure 2

EFFECT OF SPEED-BRAKE DEFLECTION
ON C_D AT $\alpha = 0°$
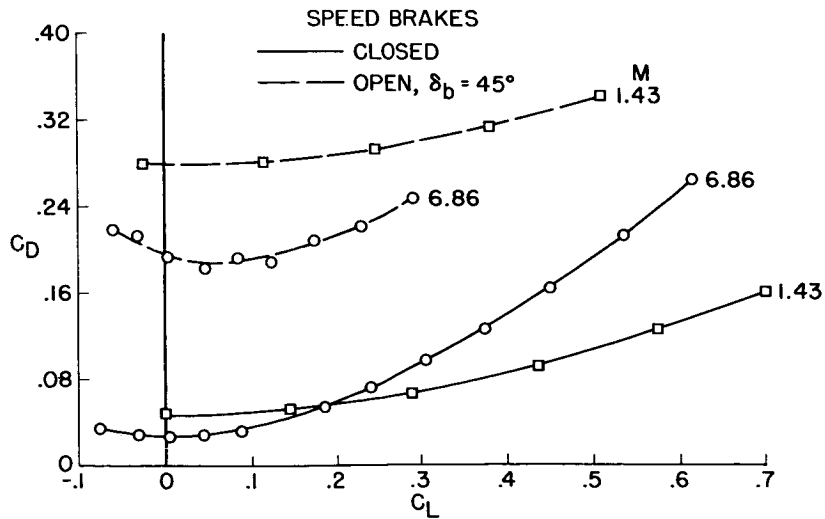

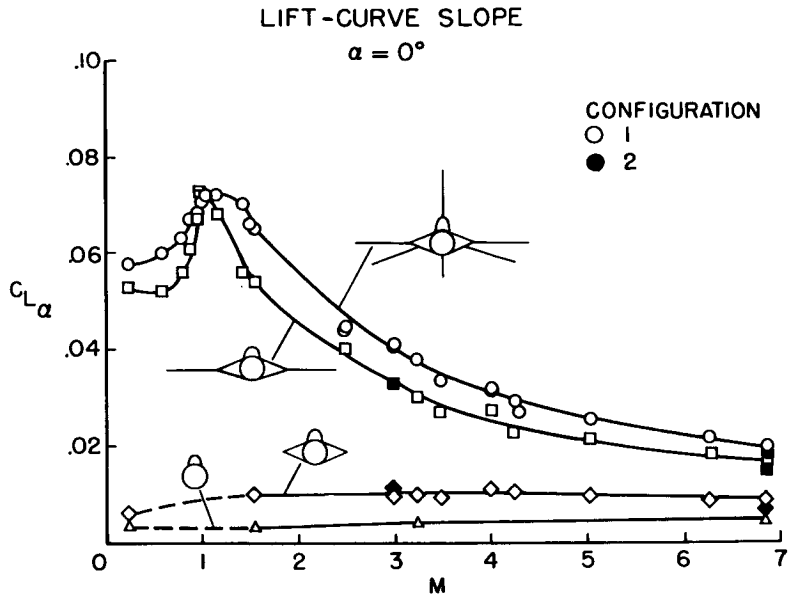Figure 3

EFFECT OF C_L ON C_D
CONFIGURATION I

Figure 4

LIFT-CURVE SLOPE
$\alpha = 0°$

Figure 5

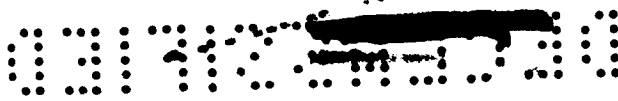## VARIATION OF C_L WITH α
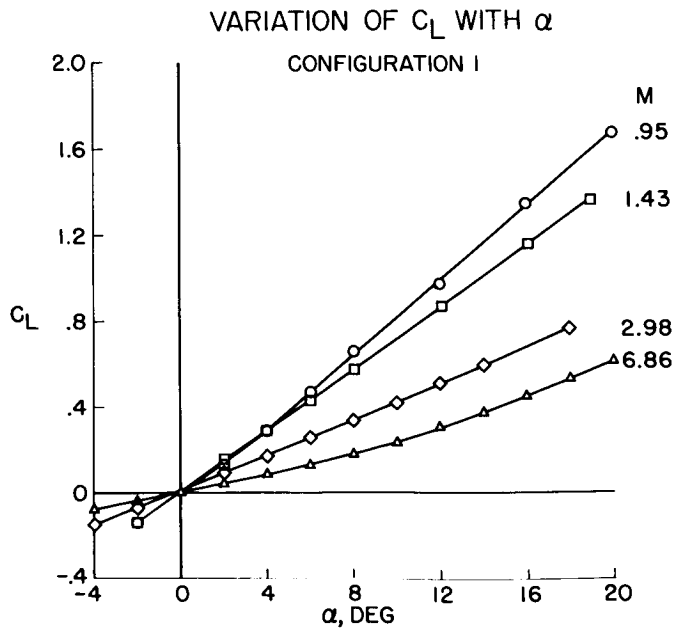### CONFIGURATION I

Figure 6

LONGITUDINAL STABILITY AT $C_L = 0$
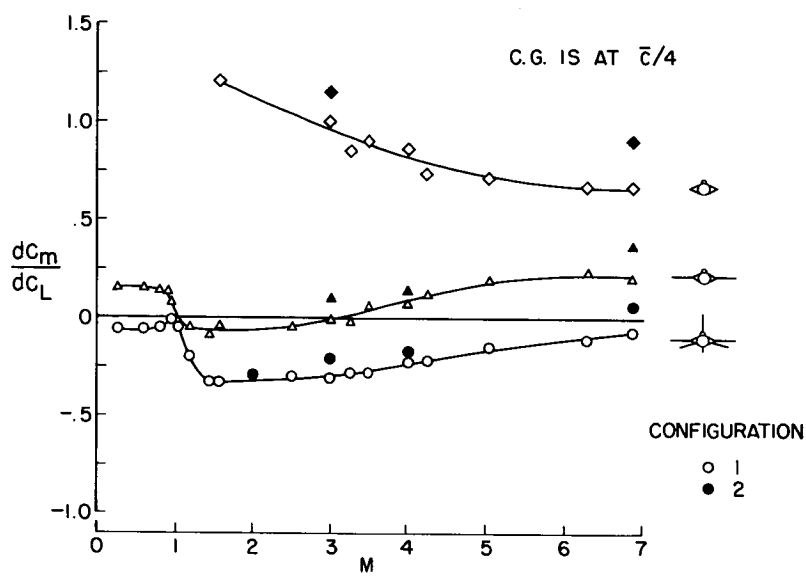

Figure 7

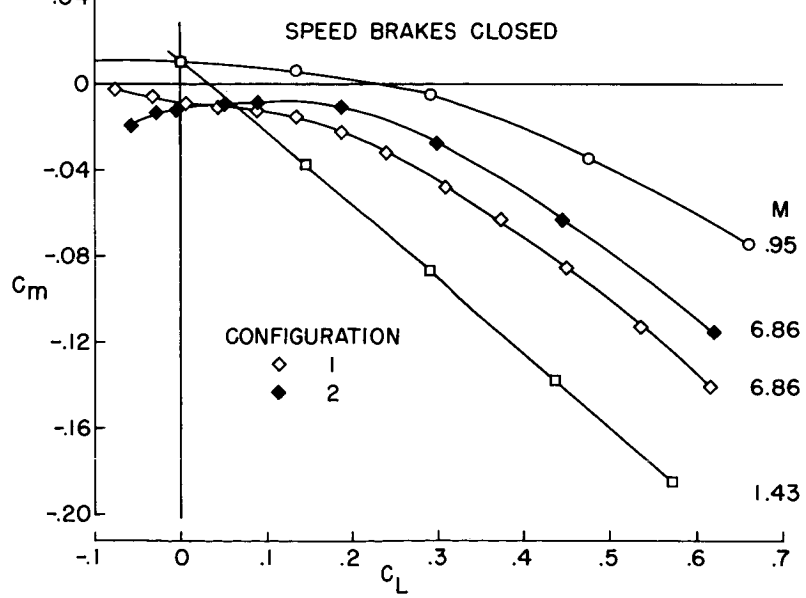## VARIATION OF C_m WITH C_L

Figure 8

EFFECT OF SPEED-BRAKE DEFLECTION
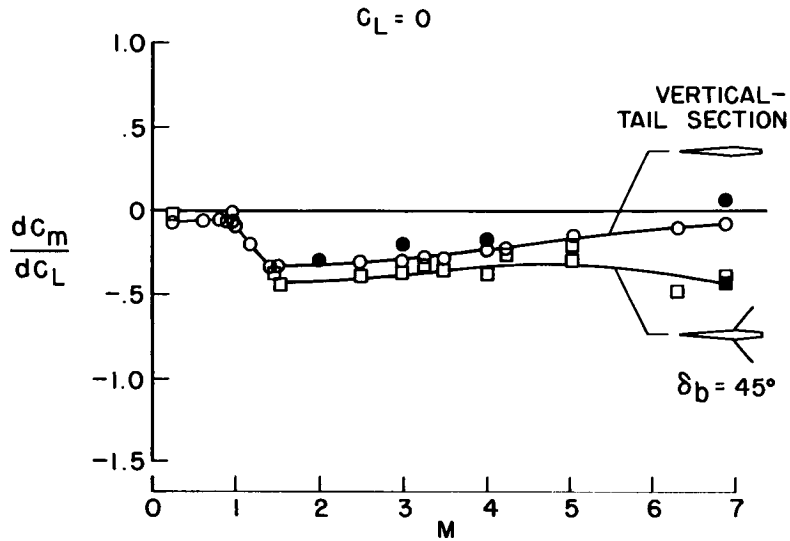## ON LONGITUDINAL STABILITY

Figure 9

EFFECT OF HORIZONTAL-TAIL SECTION ON
LONGITUDINAL STABILITY

Figure 10

LONGITUDINAL CONTROL
CONFIGURATION 2

Figure 11

EFFECT OF WING ON TAIL PITCHING MOMENT
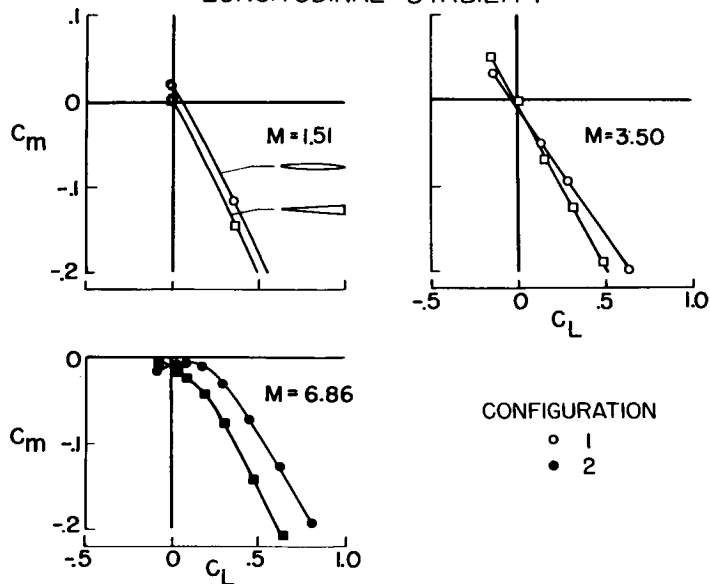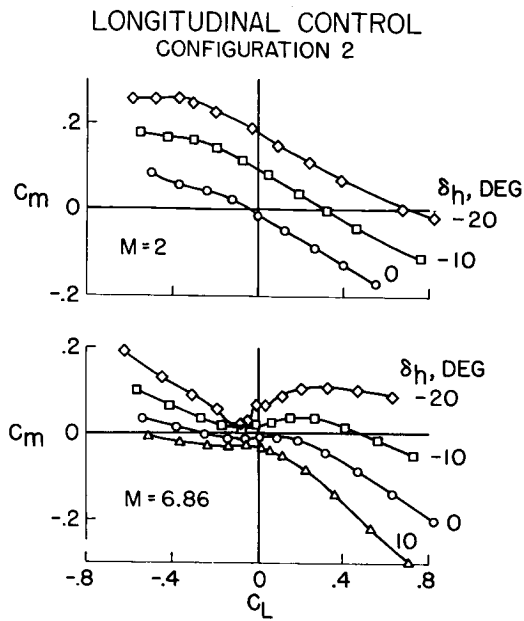### CONFIGURATION 2; $\delta_b = 20°$; M = 6.86

Figure 12

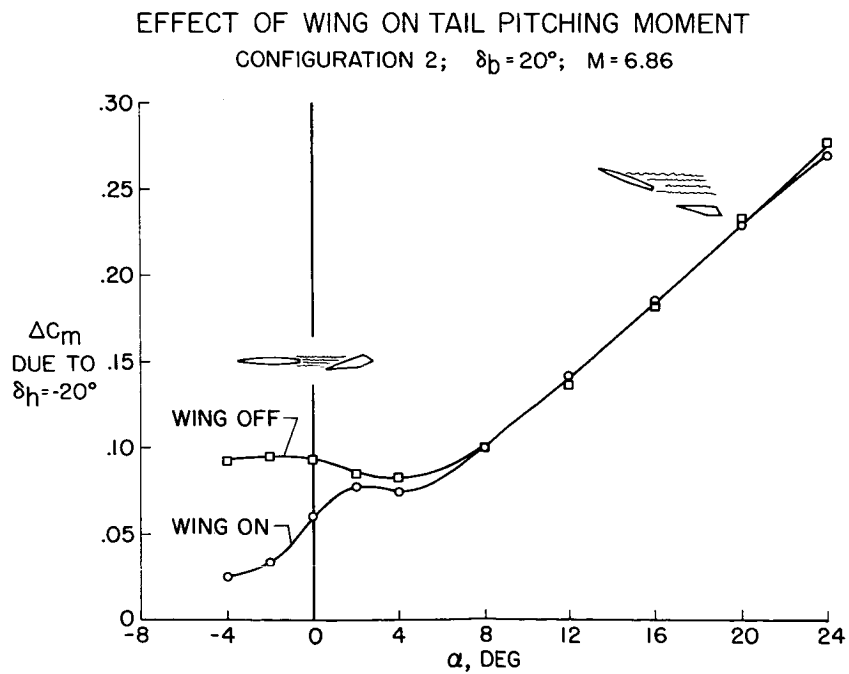# EFFECT OF SPEED BRAKES ON LONGITUDINAL CONTROL
CONFIGURATION 2; M = 6.86
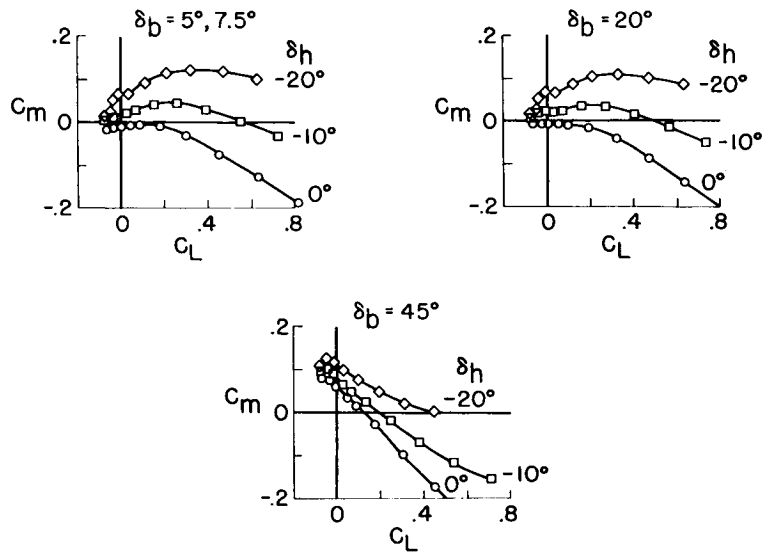

Figure 13

LATERAL CONTROL
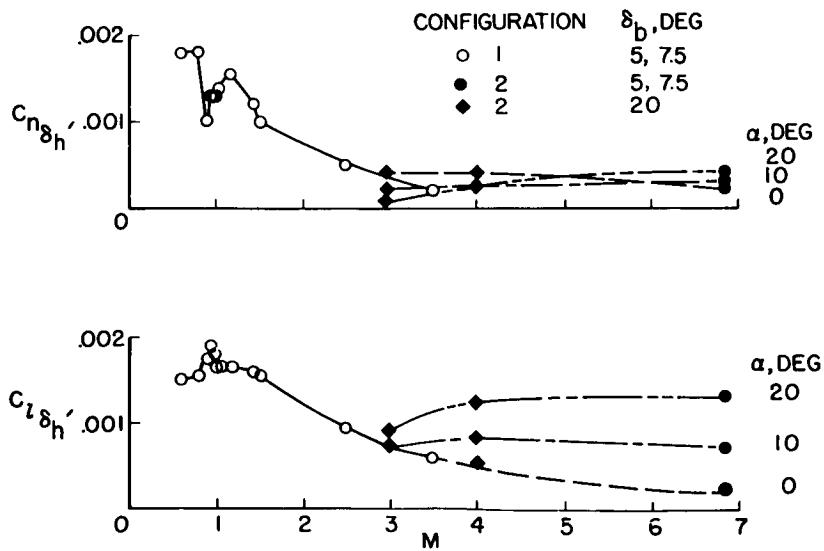

Figure 14

DIRECTIONAL STABILITY

$\alpha = 0°$
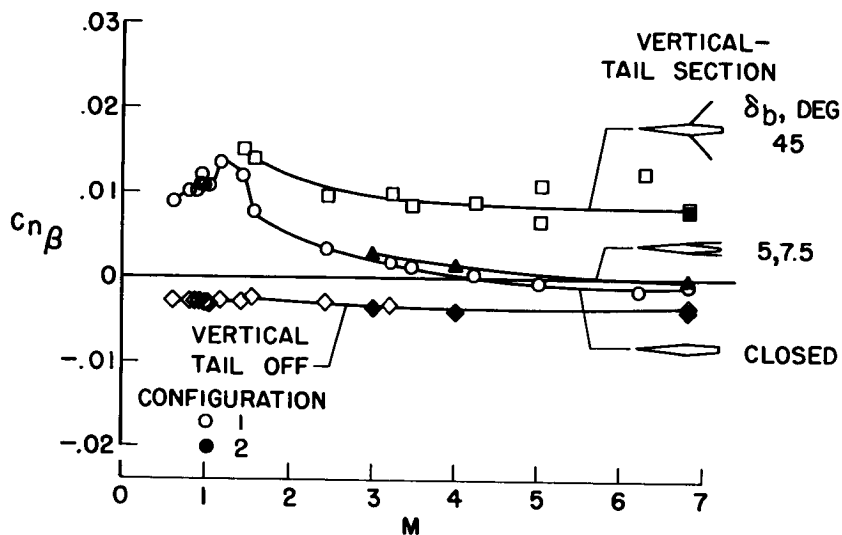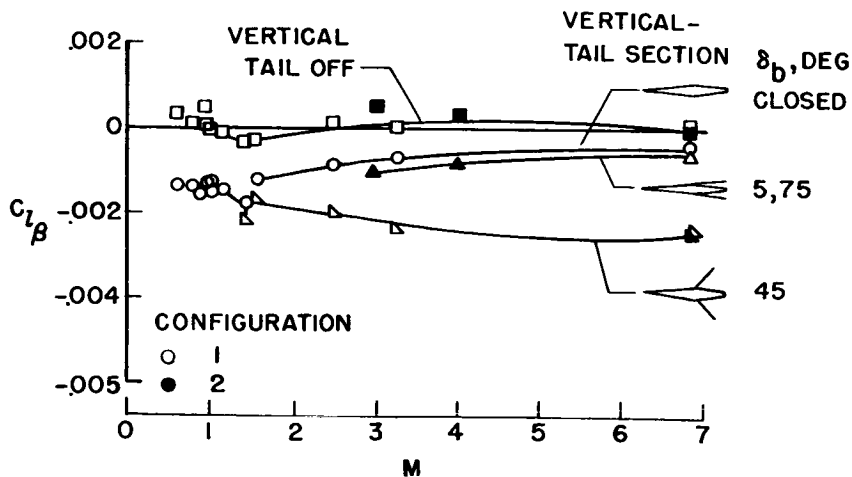

Figure 15

DIHEDRAL EFFECT
$\alpha = 0°$

Figure 16

VARIATION OF C_{n_β} AND C_{l_β} WITH α
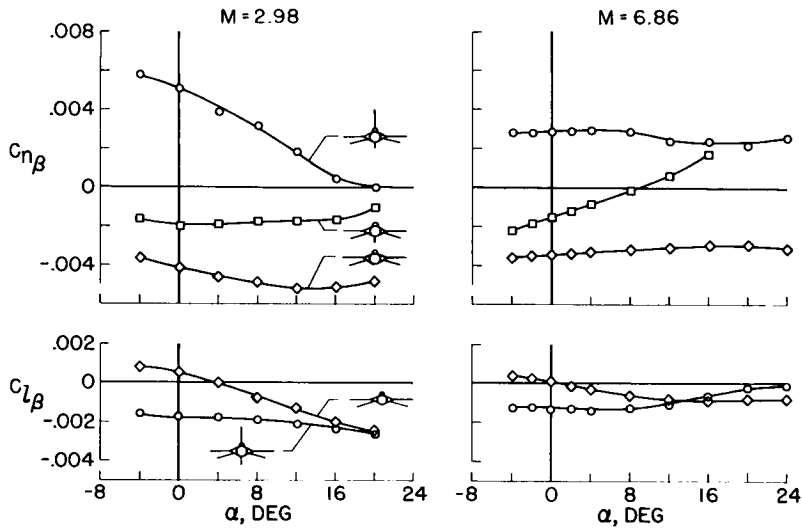
CONFIGURATION 2; $\delta_b = 20°$

Figure 17

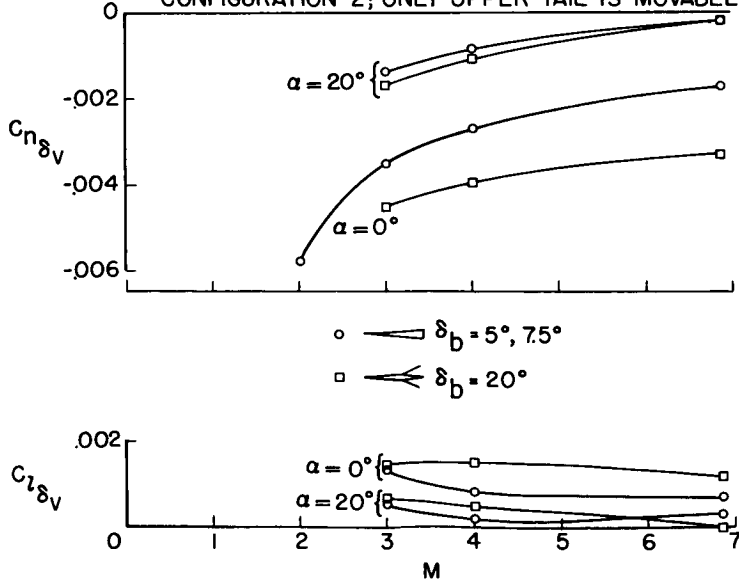DIRECTIONAL CONTROL

CONFIGURATION 2; ONLY UPPER TAIL IS MOVABLE

Figure 18

SOME CALCULATIONS OF THE LATERAL DYNAMIC

STABILITY CHARACTERISTICS

By Martin T. Moul

Langley Aeronautical Laboratory

Utilizing the results of the wind-tunnel tests of an X-15 configuration reported in the previous paper by Herbert W. Ridyard, Robert W. Dunning, and E. W. Johnston, analytical investigations of the airplane dynamic lateral behavior are being conducted for high altitudes where aerodynamic damping is low, and difficulty in controlling the airplane can be expected. The purpose of this study is to show some calculated lateral response characteristics of a configuration without dampers for two speed-brake conditions. Stability augmentation was not considered since it would be desirable to have the airplane flyable in the event of failure of dampers. Results will be presented of Dutch roll characteristics and lateral response to small yawing- and rolling-moment inputs for a Mach number of 6.86 and altitude of 100,000 feet. The rotary derivatives have been neglected in this study because they have insignificant effects at the speed and attitude considered.

The following table shows the burnout weight and moments of inertia used in this investigation:

Weight, lb 10,443
Moment of inertia about principal X-axis, slug-ft^2 2,800
Moment of inertia about principal Y-axis, slug-ft^2 50,000
Moment of inertia about principal Z-axis, slug-ft^2 52,000

These values were obtained from early estimates and are somewhat smaller than current weight and inertias. It should be noted that the roll moment of inertia is only about 1/20 the pitch and yaw inertias and follows the trend of other high-speed aircraft.

In addition to inertias, the aerodynamic sideslip derivatives are important in determining airplane lateral motions. For this analysis the experimental results presented in the previous paper by Ridyard, Dunning, and Johnston for configuration 2 were used. In figure 1 the static lateral stability derivatives C_{Y_β}, directional stability C_{n_β}, and effective dihedral C_{l_β} for this configuration are presented for two speed-brake positions, one in which the brakes are deflected to form a wedge and the other in which the brakes are fully open $45°$. In the present paper these brake positions are identified by the notation "wedge" and "open." The wedge configuration has about zero directional stability

and small effective dihedral for all angles of attack, whereas the brakes-open configuration has large directional stability and an effective dihedral which is large at $\alpha = 0^\circ$ and decreases with angle of attack. Stability results will be shown for the extreme angles of attack, 0° and 24°.

These inertia and aerodynamic data then were used to determine the characteristics of Dutch roll, the oscillatory mode of lateral motion. Past experience showed that the Dutch roll characteristics which have the most effect on airplane lateral motions and pilots' opinions of the airplane are period, damping, and roll-to-sideslip ratio. In figure 2, results are presented of period and roll-to-sideslip ratio for an angle of attack of 0° as a function of directional stability and effective dihedral. No damping results are shown as the airplane has poor damping for any combination of C_{n_β} amd C_{l_β}. The constant-period lines are horizontal since period is a function only of directional stability for an angle of attack of 0°. These small periods, 1.5 and 3 seconds, coupled with poor damping, produce a Dutch roll oscillation which has been found to be objectionable to pilots in the past.

The radial lines shown are curves of constant roll-to-sideslip ratios, $|\varphi/\beta| = 4$ and $|\varphi/\beta| = 15$. From flight tests at low altitudes, it has been reported that pilots prefer airplanes having small roll-to-sideslip ratios. In fact, roll-to-sideslip ratios greater than 4, on the cross-hatched side of the curve, were intolerable regardless of the airplane damping.

The labeled points in figure 2 indicate the period and $|\varphi/\beta|$ characteristics for the wedge and fully opened speed-brake conditions. The wedge configuration is directionally unstable and hence divergent at this angle of attack. The brakes-open configuration has a large amount of directional stability and effective dihedral, a period of about 1 second, and a roll-to-sideslip ratio of about 5. From this figure it can be seen that an airplane configuration which lies in the region of moderate C_{n_β} and small C_{l_β} is desirable.

These results were for an angle of attack of 0° but flight at high angles of attack is also contemplated on some flight plans. For 24° angle of attack figure 3 shows the Dutch roll characteristics. The period curves, which were horizontal in the previous figure, now have a large slope due to the effect of principal axis inclination. Both the brakes-open and wedge configurations have a small period at this angle of attack, the wedge obtaining its small value from the contribution of effective dihedral and principal axis inclination. In fact, even for some negative values of C_{n_β}, the response is oscillatory and the periods small.

The roll-to-sideslip curves remain radial lines but the curve for 4 has shifted around into the lower quadrant. The smaller $|\phi/\beta|$ values at $\alpha = 24^\circ$ indicate that the lateral-control problem would be considerably eased at higher angles of attack.

After investigating the Dutch roll characteristics, calculations were made of the airplane motion in response to step yawing and rolling moments. An immediate consideration for high-altitude flight was the possibility of roll coupling occurring even for small rolling velocities. Five-degree-of-freedom calculations of airplane motions showed coupling effects for large rolling maneuvers, rolls of 180° or 360°, but motions in bank up to 90° were free of inertia coupling. For the purpose of controlling the airplane over a high-altitude trajectory, it was assumed that most maneuvers would not exceed bank angles of 90° and hence the motions were computed from three-degree-of-freedom linear equations.

The following three figures (figs. 4, 5, and 6) will show the effect of configuration on airplane lateral motions. Figure 4 presents the airplane bank and sideslip motions in response to a step yawing moment $(C_n = -0.0017)$. Results are for angles of attack of 0° and 24°.

The responses for $\alpha = 0^\circ$ are rapidly divergent for the wedge configuration because of its directional instability. With the brakes open 45°, the sideslip motion is small due to the large value of directional stability and one might expect the roll motion due to dihedral effect to be small. However, the bank motion is severe (80° in less than 3 seconds) as a result of the large effective dihedral of this configuration and the small rolling inertia. Equivalent rudder deflection for this configuration was 0.4° or about 7 percent of available rudder, assuming no rolling moments are produced by rudder deflection, and indicates a large rolling sensitivity to yaw controls for this Mach number and altitude.

For an angle of attack of 24°, the rolling sensitivity to yaw control is reduced for both brake-position configurations. For the wedge the reduction in bank angle results from the stabililizing effect of angle of attack in reducing the sideslip response. The sideslip motion for the brakes-open configuration is unchanged but the roll motion is much smaller due to the variation of dihedral effect with angle of attack. Hence, the response of both configurations to a yawing-moment input is improved by increasing angle of attack.

The other lateral control is the roll control (obtained by differential deflection of horizontal tail), and figure 5 shows the airplane response to a rolling-moment input $(C_l = -0.00036$ or about 2° of control deflection, which is 8 percent of the available control).

At an angle of attack of 0° both tail configurations roll because of the rolling-moment input but the wedge configuration is unstable and is divergent in sideslip.

For $\alpha = 24°$ the rolling motion of the wedge configuration is slow, since dihedral effect is bucking the control rolling moment. In fact, at low angles of attack, where the wedge configuration was shown to be directionally unstable but the response periodic, the final roll motion is in the positive direction, or opposite to the way the pilot is attempting to bank the airplane. Hence, to insure rolling performance of the airplane at high angles of attack, a moderate amount of directional stability, as well as small effective dihedral, is required.

The results discussed in figures 4 and 5 were motions due to pure yawing- or rolling-moment inputs. Generally, airplane lateral controls produce both rolling and yawing moments, that is, ailerons produce a yawing moment and rudders produce a rolling moment in addition to the primary control moments. The actual response due to horizontal-tail differential deflection or rudder deflection can be determined by superimposing the results of figures 4 and 5 in accordance with the control effectiveness derivatives. The actual aileron response is little different from these results in that differential deflection of the horizontal tail for roll produces a small favorable yawing moment which increases rolling performance by a small amount.

The response to rudder deflection for the brakes-open configuration is presented in figure 6. For this configuration the entire upper vertical fin was used as a rudder and was shown in the previous paper by Ridyard, Dunning, and Johnston to produce a large rolling moment. Notice that the resulting roll is positive or opposite to the roll direction that the pilot expects from dihedral effect. The positive roll results because the contribution of rolling moment due to rudder deflection exceeds that of dihedral effect.

Also, in applying rudder to reduce an initial sideslip angle to zero, a positive rolling moment produced by rudder deflection would require the pilot to apply additional aileron to prevent rolling, which he might interpret as a loss of aileron power. This is particularly critical for this brakes-open configuration for $\alpha = 0°$, for which $1°$ of rudder produces about 10 times as much rolling moment as $1°$ of aileron. Hence a configuration for which the rolling moment produced by rudder deflection is small and favorable is desirable.

The following comments regarding the lateral stability and control of configuration 2 can be made for a Mach number of 6.86 and altitude of 100,000 feet:

1. Roll-to-sideslip ratios are large at an angle of attack of $0°$ as a result of high effective dihedral.

2. Lateral response of the wedge configuration is unsatisfactory for all angles of attack as a result of insufficient directional stability.

3. The airplane is very sensitive in roll to yawing-moment inputs at an angle of attack of 0°.

4. Rolling moment due to rudder deflection is large and can have adverse effects on roll control.

At this time other vertical tail and rudder configurations are being investigated in an attempt to improve directional stability and reduce the effective dihedral and adverse roll of the rudder.

STATIC LATERAL STABILITY DERIVATIVES OF
CONFIGURATION 2

M = 6.86
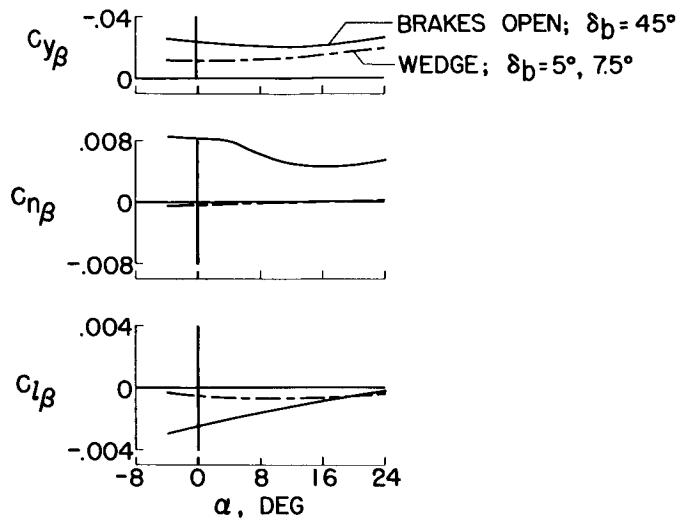
Figure 1

DUTCH ROLL CHARACTERISTICS
M = 6.86; h = 100,000 FT
α = 0°
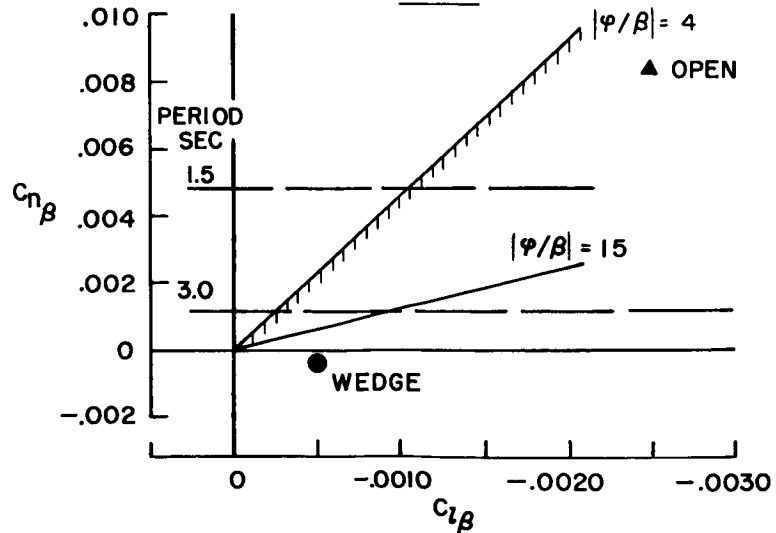
Figure 2

DUTCH ROLL CHARACTERISTICS
M = 6.86; h = 100,000 FT
α = 24°

Figure 3

RESPONSE TO STEP INPUT OF YAWING MOMENT
$C_n = -0.0017$; M = 6.86; h = 100,000 FT

Figure 4

64

RESPONSE TO STEP INPUT OF ROLLING MOMENT
$C_l = -0.00036$; $M = 6.86$; $h = 100,000$ FT

Figure 5

RESPONSE TO STEP INPUT OF RUDDER
$\delta_v = 0.2°$; $\alpha = 0°$;
$M = 6.86$; $h = 100,000$ FT; 45° BRAKE DEFLECTION

Figure 6

65

EFFECTS OF AERODYNAMIC CHARACTERISTICS ON

THE PILOT'S CONTROL OF THE EXIT PHASE

By Windsor L. Sherman, Stanley Faber,
and James B. Whitten
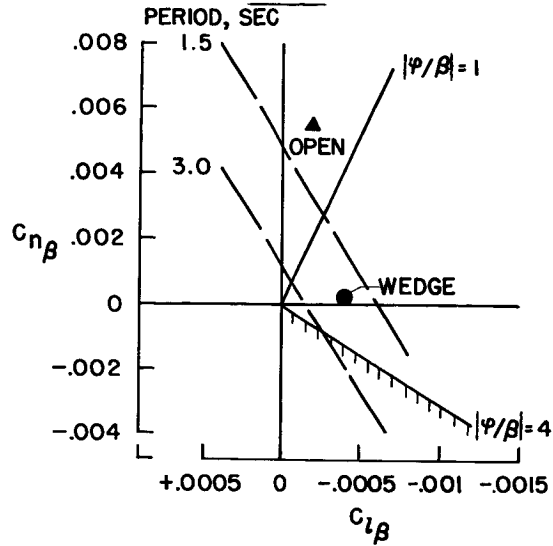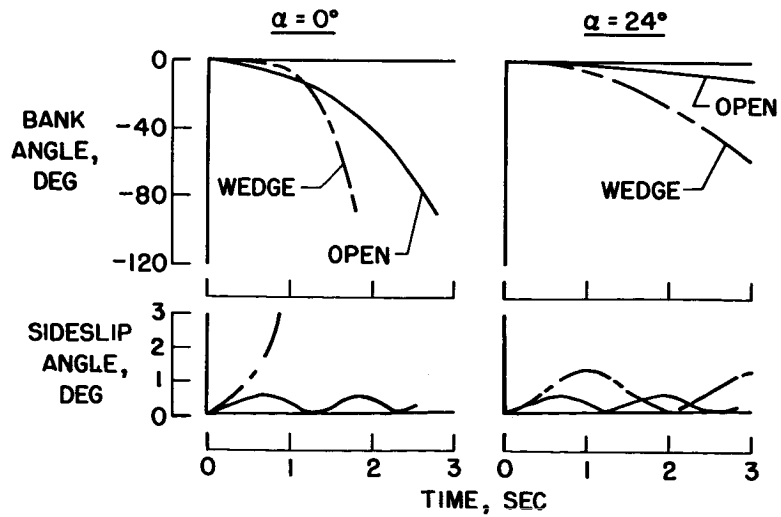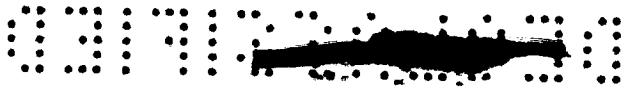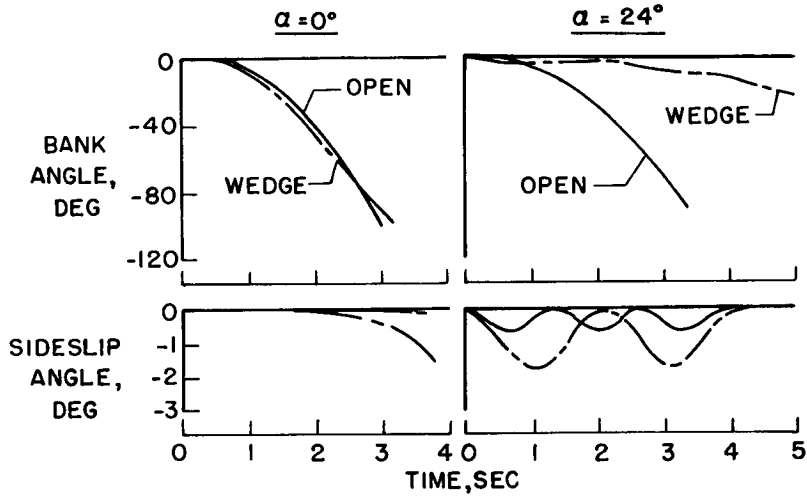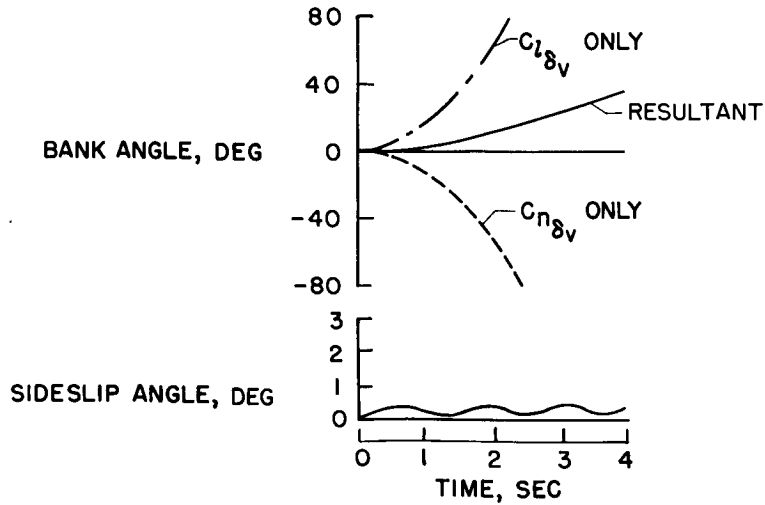
Langley Aeronautical Laboratory

INTRODUCTION

The purpose of the X-15 project is to develop an airplane capable of flight at very high altitude and at hypersonic speeds. The lack of flight experience with this type of airplane created a void in the understanding and meaning of wind-tunnel data with respect to flight characteristics. Therefore, a pilot-controlled simulation of the original design proposed by North American Aviation, Inc., flying the exit phase of a typical mission was made on an analog computer. (This original design was referred to as "configuration 1" in a previous paper by Herbert W. Ridyard, Robert W. Dunning, and E. W. Johnston, and is so designated hereinafter.) As a pilot was included in the control loop, pilots' opinion was relied on to a large extent to evaluate the results. In addition to pilots' opinion, selected time histories of airplane parameters are used to illustrate the results.

STATEMENT OF PROBLEM AND ANALOG-COMPUTER SETUP

The primary object of this study was to evaluate qualitatively the aerodynamic characteristics of the airplane with respect to the ability of the pilot to control the airplane. In order to realize this objective it was necessary to use a proposed X-15 flight plan and to represent the airplane as completely as possible.

Figure 1 shows the time histories of Mach number, altitude, and dynamic pressure for the first 160 seconds of a high-altitude flight plan. The unshaded area of this figure is the portion of the flight plan over which these studies were made. This region was selected because burnout occurs approximately halfway through the flight and may introduce violent trim changes. In addition, the variations in Mach number from 3.2 to 5.5, in altitude from 84,000 to 180,000 feet, and in dynamic pressure from 350 lb/sq ft to 20 lb/sq ft provided a wide range of flight conditions over which the pilot must control the airplane.

In this investigation it was assumed that the airplane in flight would follow the variations of dynamic pressure and Mach number of the
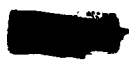
flight plan. This assumption permitted Mach number and dynamic pressure to be programed as functions of time. Thus, the airplane could be represented by the five-degree-of-freedom equations of rigid-body motion. The aerodynamic data were obtained from the wind-tunnel tests of configuration 1 reported in the paper by Ridyard, Dunning, and Johnston. The section of the high-altitude trajectory selected calls for the airplane to fly at zero angles of attack and sideslip. Therefore, the static stability derivatives were expressed as functions of Mach number for $\alpha = \beta = 0$. As there was a lack of control-surface-effectiveness-coefficient data as a function of Mach number at the time of programing, these parameters were assumed to be constant. The values of these constants were obtained from wind-tunnel tests made at a Mach number of 3.5.

Burnout was accounted for by adding a thrust misalinement of 1 inch, which is the maximum misalinement permitted by the engine specifications, to the pitching- and yawing-moment equations. This 1-inch misalinement corresponds to an out-of-trim moment of approximately 5,000 ft-lb. Figure 2 shows the mass and inertia data obtained from preliminary design reports on the airplane's physical characteristics. These data permitted the mass and inertias to be programed as functions of flight time during burning period. After burnout these parameters remain constant at the lower values.

Figure 3 shows the control setup used. As can be seen, the control setup consisted of a pilot's seat, center control stick and rudder pedals, and a display that replaced the standard flight instruments with cathode ray tubes. While the simulator was operating, the control station was enclosed with canvas screens. The control-stick and rudder-pedal forces were supplied by simple springs and were independent of Mach number and dynamic pressure.

The control-stick and rudder-pedal movement and forces and the corresponding control-surface deflection used in this study are shown in the following table:

Control	Movement, in.	Force, lb	Surface deflection, deg
Horizontal tail	2.5	10	45
Horizontal-tail roll control	4	10	24 total
Vertical tail	1	50	6

Mechanical or electrical stops limited all control-surface deflections at the values shown in the table. The forces and deflections used do not, in the opinion of the pilot, represent good control harmony; however, they were not considered too objectionable. The movie camera shown in figure 3 was used to photograph the pilot's display during the simulated flights. Standard recording instruments were also used to obtain time histories of the significant parameters of the airplane motion from the analog equipment.

Information was displayed to the pilot on three closely grouped cathode ray tubes. The variables displayed were the angles of attack, sideslip, bank, heading, and pitch attitude. These five variables could be arranged as desired, three on the center cathode ray tube and one each on the two auxiliary cathode ray tubes. The first type of display considered presented attitude angles on the center scope and the angles of attack and sideslip on the auxiliary scopes. The pilots found it impossible to fly configuration 1 with this display. A preliminary study of presentation showed that simultaneous presentation of β and ϕ on the same scope was necessary to control the directionally unstable case.

This result led to the display shown in figure 4, the β-ϕ display, which was used throughout most of the study so as to give a more quantitative comparison of the directionally stable and unstable cases. The center scope presents roll attitude and the angles of attack and sideslip by the motion of the inverted T. This marker may be thought of as the rear view of the airplane. The inverted T rotates to present roll attitude and shows the angles of attack and sideslip by vertical and horizontal displacements, respectively. The scales for the angles of attack and sideslip are 6° per inch; negative sideslip is shown to the right. The auxiliary scope at the top of the center scope presents heading and the one on the left presents pitch attitude. The scales for these scopes were 20° per inch. After operating this simulator, the test pilots stated that it constituted a reasonable representation of the task of flying an airplane.

The pilots' task was to maintain the angles of attack, sideslip, and roll to zero. Because of the programing of Mach number and dynamic pressure, this assigned task, if perfectly executed, caused the airplane to fly the programed portion of the flight plan. Each flight was divided into two parts. The first part consisted of a constant Mach number flight at 84,000 feet to trim the airplane at the correct climb angle. When trim conditions had been established the flight over the programed part of the trajectory was made.

Pilots' opinion was used to evaluate the effect of changes in airplane characteristics on the flyability of configuration 1. In general, the opinion of two experienced engineering test pilots was obtained for major changes in airplane characteristics.

68

PRESENTATION OF RESULTS

Wind-tunnel data indicated that the directional stability parameter C_{n_β} (see fig. 5) might be critical. The value of C_{n_β} for configuration 1, shown by the solid line, changes sign at a Mach number of 4.5, making the airplane directionally unstable. The dashed curve shows the upper limit of C_{n_β} used which gives directional stability throughout the Mach number range considered. Other values of the directional stability parameter between these two limits were tried, including one that approximated the full-wedge vertical tail. Results are presented herein for the two curves shown in this figure.

As the pilot's task was to control the airplane so that α, β, and ϕ were held to zero, these quantities were of primary interest. The results of this study are illustrated by the recorded time histories of α, β, and ϕ.

Figure 6 shows the time history of configuration 1 flying the programed part of the trajectory. The airplane becomes directionally unstable during this run and there are no damping and no disturbance moments. Even though the airplane is rolling, sideslipping, and oscillating in angle of attack, the motions appear small and are not representative of the difficulty encountered by the pilot in controlling the airplane. This successful flight was obtained only after several unsuccessful practice flights had been made. The pilot stated that he had to exercise extreme concentration and mental effort to control the airplane and considered it unflyable. In order to illustrate the critical attention required to control the airplane, this flight was repeated and the pilot's view of the display was obscured for 2 seconds to simulate distraction of other tasks. Figure 7 shows this flight. The time of the coverup is indicated by the solid bar in the figure. As can be seen, shortly after being distracted the pilot loses control of the airplane; that is, all three quantities diverge. In order to show the effect of increased directional stability, C_{n_β} for configuration 1 was increased as shown by the dashed line in figure 5. A flight was made during which the pilot was again distracted. This flight is shown in figure 8. The distraction is again indicated by the bar in the figure. As shown, the distraction caused the pilot to have a little more trouble controlling the airplane than previously, but did not cause him to lose control of the airplane. The pilot felt that with the increase of directional stability the task of controlling the airplane was easier but that damping should be added to the airplane.

No damping derivatives were available for this airplane when the problem was programed; therefore, estimates of the rotary damping derivatives

in pitch, roll, and yaw were made and added to the simulation. The damping supplied by these rotary damping derivatives proved completely inadequate, the pilot noting only negligible improvement in the control task. Three-axis auxiliary damping was added to the simulator by feeding the angular velocities back to drive the control surfaces. These feedback gains were gradually increased so as to provide increasing damping, until the pilot felt the necessary minimum damping requirements had been provided.

The next two time histories (figs. 9 and 10) compare the airplane motions with and without three-axis auxiliary damping. In both flights the airplane has increased C_{n_β} so that it is directionally stable at all times. The engine thrust misalinements in the pitching- and yawing-moment equations are included for the first time. A warning as to when burnout was to occur was given the pilot by a signal lamp. At 2 seconds before burnout the lamp was lit and at burnout the lamp was turned off. The marker bar in figures 9 and 10 shows the operation of this lamp.

In the first of these time histories (fig. 9) there was no auxiliary damping. It can be noted that the pilot had considerable difficulty in maintaining control when burnout trim changes take place. It is of interest to note the effect of altitude on the records. At the start of the climb the periods of the motions are very short, while toward the end of the flight the period lengthens considerably. This lengthening of the periods eases the pilot's control task.

Figure 10 shows this same run except that three-axis auxiliary damping has been added to the simulation of the airplane. This damping gives times to damp to half-amplitude of 0.9 and 0.5 second in the Dutch roll and damping-in-roll modes and 0.75 second in the longitudinal mode. While the oscillations are still discernible, the motions are much smoother and the pilot has less trouble holding the angles of attack and sideslip at zero. As shown, the pilot has little difficulty in controlling the airplane when the burnout disturbance occurs. The pilot stated that both the increased directional stability and added damping provided the necessary minimum stability requirements to fly the part of the trajectory simulated.

In order to determine which damper was critical, various combinations of pitch, roll, and yaw damping were studied. The pilot stated that pitch damping appeared more critical than damping about the other axes.

During this simulation, the effect of variations in the rolling moment due to the vertical-tail deflection and the yawing moment due to differential horizontal-tail deflection on the control task were investigated. In the case of rolling caused by vertical-tail deflection, the pilot found this rolling objectionable and he thought it should be kept as small as possible. The effect of yawing due to the differential deflection of the horizontal tail was not as obvious, the pilot noticing
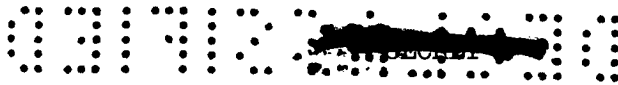
little difference between favorable and unfavorable yaw caused by use of the roll control. The pilot felt that both of these parameters had a secondary effect on the control task.

Figure 11 shows the variations in the effective-dihedral parameter C_{l_β} considered in this simulation study. The solid line is the basic effective dihedral for configuration 1 and the dotted and dashed lines show the limits of positive and negative dihedral considered. Small effective dihedral (that is, near zero) was the preferred value; as the effective dihedral increased either positively or negatively, the pilot noted a gradual deterioration of the control problem. The pilot was able to control the airplane for all values of effective dihedral between the limits shown in figure 11. He considered effective dihedral to have a secondary effect in the control task.

In order to obtain some appreciation as to the effect of display on the pilots' opinions of flying qualities and the control task, some simulator runs were made with a more conventional display that presented the attitude angles on the center scope and the angles of attack and sideslip on the auxiliary scopes. In each of the cases shown in the time histories, the pilot felt the control task was more difficult for the display with the attitude angles on the center scope. In order to illustrate the effects of information arrangement, the time histories of figures 12 and 13 have been included. Figure 12 is the time history of a flight with the $\beta-\phi$ display, and figure 13, a flight with the attitude display. The airplane configuration in both flights was the same, having directional stability and a high ϕ/β ratio. The figures show that with the $\beta-\phi$ display the pilot has little trouble completing the flight; however, for the attitude display the pilot loses the airplane at approximately the time of burnout. In addition, it was found that the effective-dihedral parameter, which was of secondary importance for the $\beta-\phi$ display, became critically important to the control task when the attitude display was used. These results, which are of a preliminary nature, indicate that those quantities which are of primary importance to the control task should be presented to the pilot so that the scanning requirement and data assimilation time are a minimum.

CONCLUDING REMARKS

Configuration 1 is considered by the test pilots to be unflyable because of the extreme concentration and mental effort required to control it. The test pilots considered directional stability and three-axis damping very desirable and with both of these added considered the airplane to possess the necessary minimum stability requirements to fly the programed part of the flight plan. The investigation of effective dihedral

showed that it had a secondary influence on the control task when the β-⌀ display was used, whereas it had a primary influence on the control task when the attitude display was used. These simulation studies are being extended to other regions of the flight plan.

A HIGH ALTITUDE FLIGHT PLAN
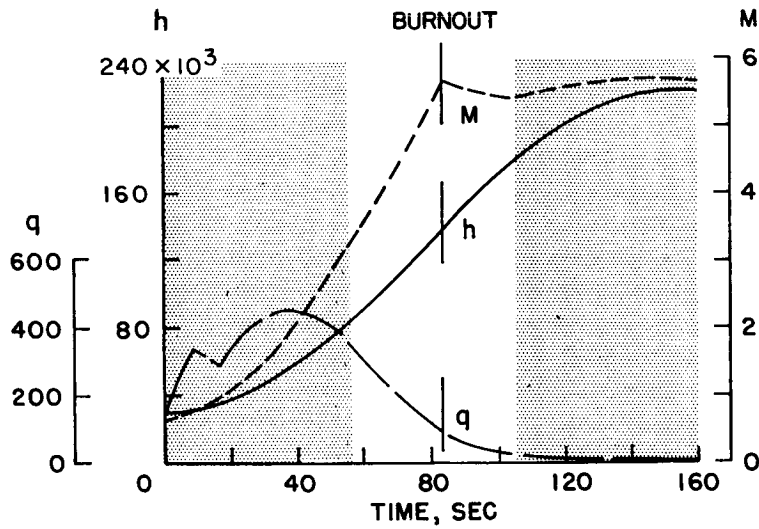
Figure 1

VARIATION OF MASS AND INERTIAS WITH FLIGHT TIME

Figure 2

DECLASSIFIED

CONTROL SET-UP
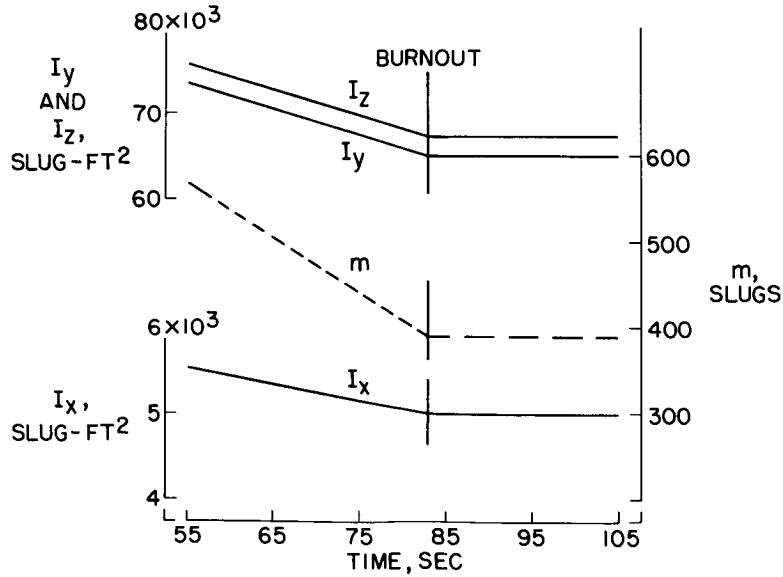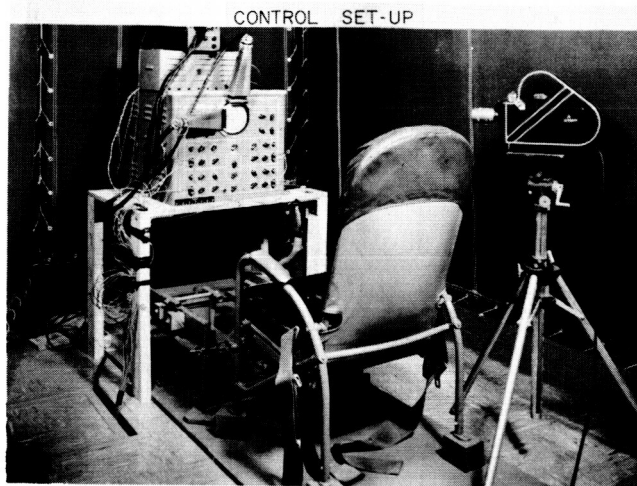
Figure 3

SKETCH OF SCOPE PRESENTATION TO PILOT

HEADING

-20° 0 20°

PITCH ATTITUDE

20°

0

6°

6°

ANGLE OF ATTACK

BANK ANGLE

ANGLE OF SIDESLIP
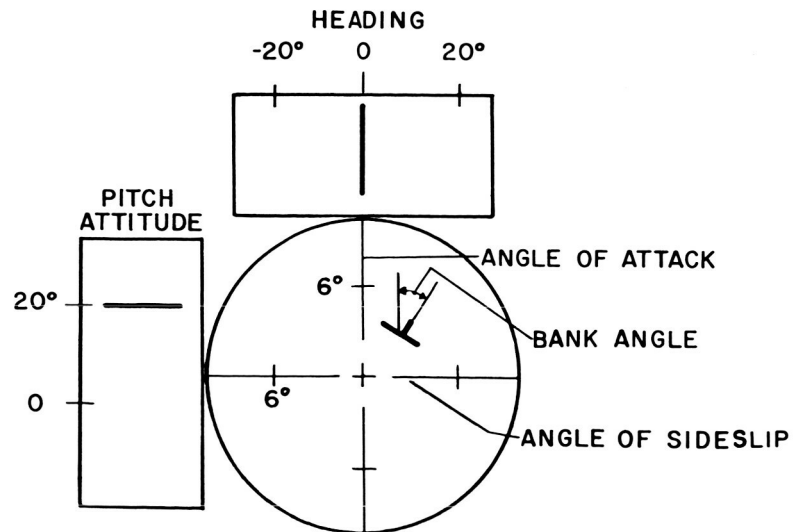
Figure 4

VARIATION OF C_{l_β} WITH MACH NUMBER

$\alpha = 0°$
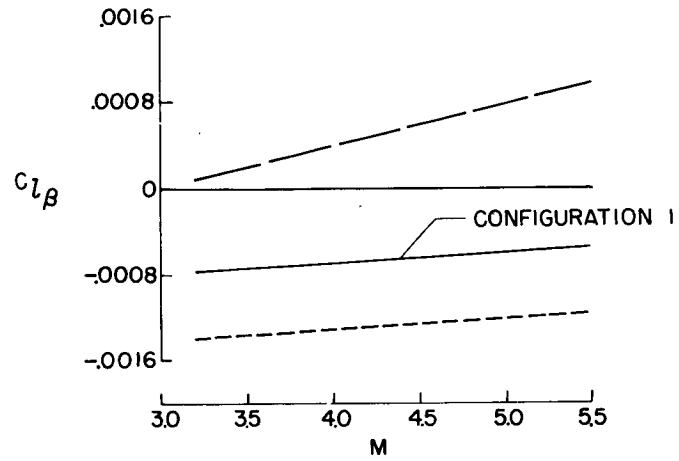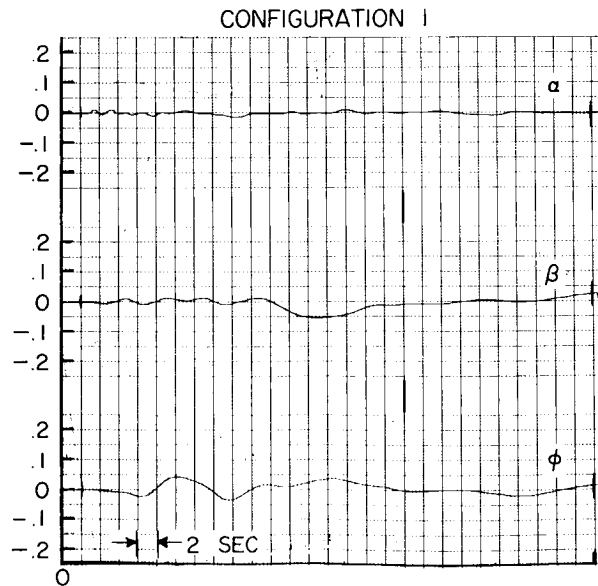
Figure 5

Figure 6

CONFIGURATION I   PILOT DISTRACTION
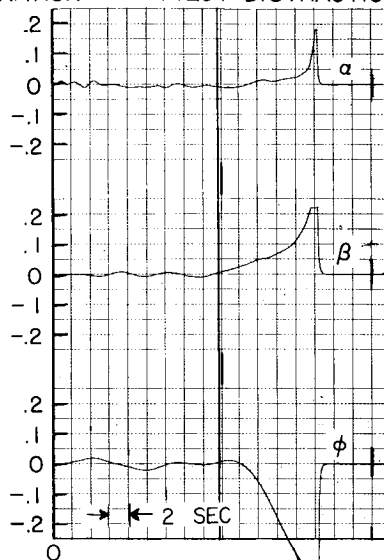
Figure 7

CONFIGURATION I + ΔC_{n_β} PILOT DISTRACTION

Figure 8

CONFIGURATION I + Δc_{n_β}
ENGINE THRUST MISALINEMENT

Figure 9

CONFIGURATION I + Δc_{n_β} + DAMPING
ENGINE THRUST MISALINEMENT
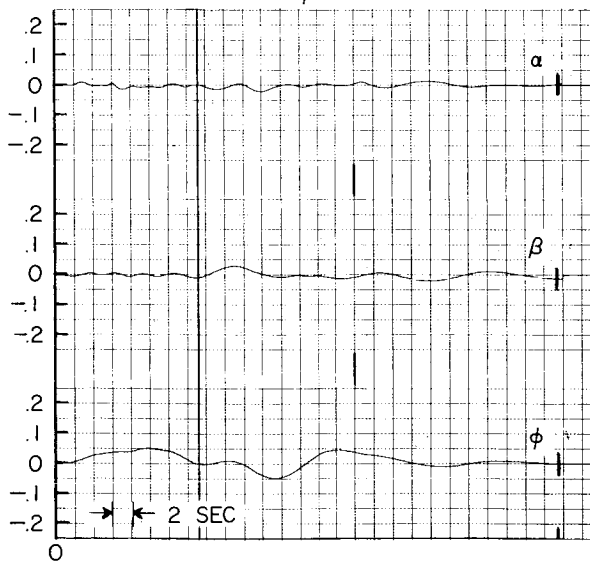
Figure 10

VARIATION OF C_{n_β} WITH MACH NUMBER

$\alpha = 0°$

Figure 11

CONFIGURATION I + ΔC_{n_β} + ROTARY DERIVATIVES $\beta - \phi$ DISPLAY

ENGINE THRUST MISALINEMENT
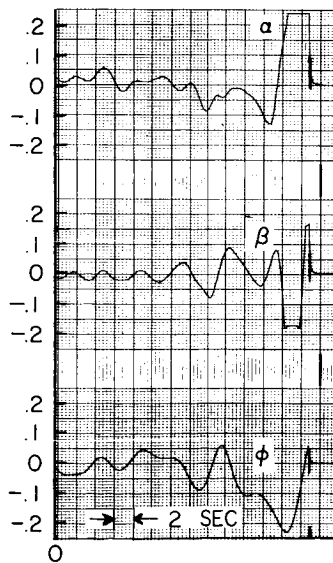
Figure 12
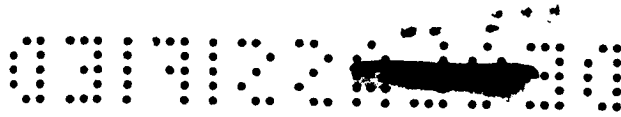
CONFIGURATION I + ΔC_{n_β} + ROTARY DERIVATIVES,
ATTITUDE DISPLAY ENGINE THRUST MISALINEMENT
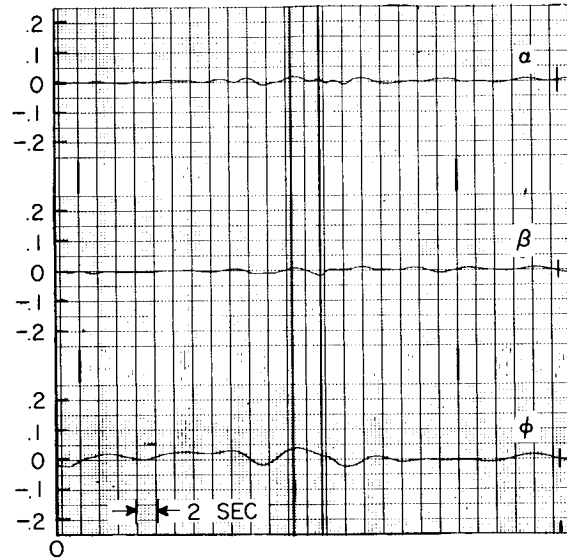
Figure 13

SIMULATION STUDIES OF ENTRY STABILITY AND CONTROL

By Howard F. Matthews
Ames Aeronautical Laboratory

and George B. Merrick
North American Aviation, Inc.

INTRODUCTION

Considerable interest in the problems associated with entry of the X-15 airplane into the atmosphere prompted the early initiation of several simulator programs. Two of these investigations, one by the Ames Laboratory of the NACA (see ref. 1) and the other by North American Aviation (see ref. 2), were for the longitudinal mode only. Primarily the objectives of these two studies were to investigate the longitudinal flying qualities during rapid changes in dynamic pressure, with particular emphasis on the need and requirements of the control system for auxiliary pitch damping, and to investigate the pilot's ability to execute various entry techniques. Thes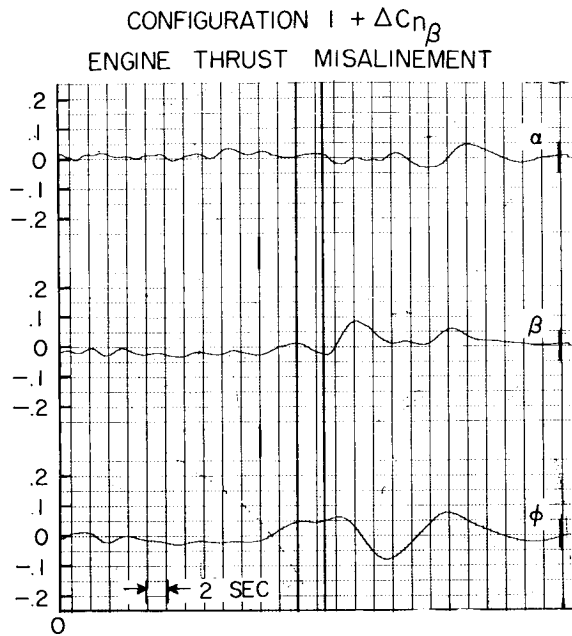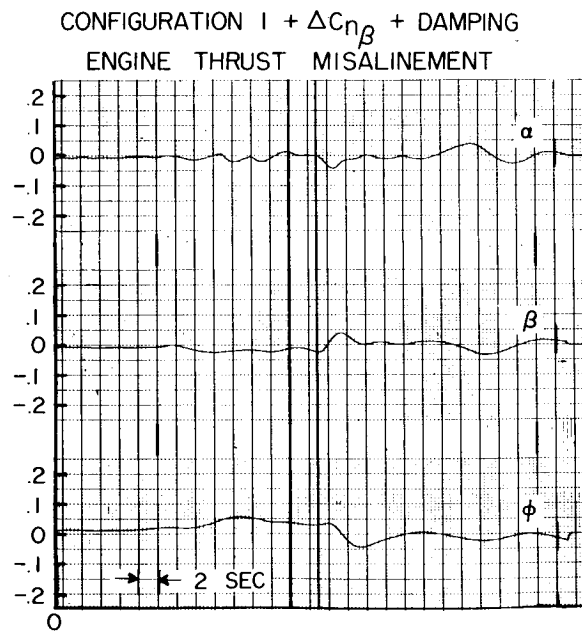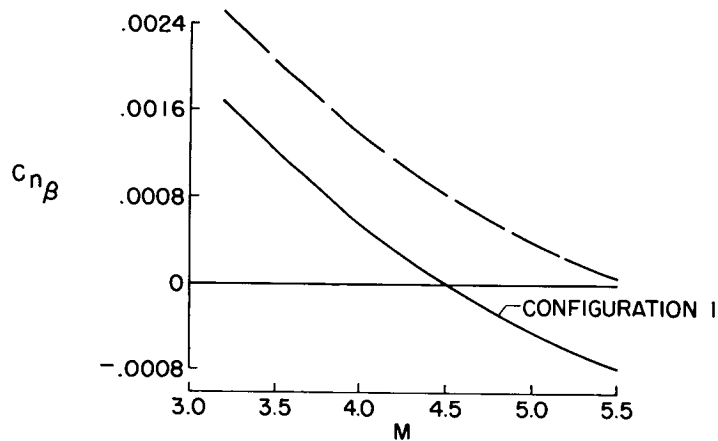e programs were followed by a North American modified five-degree-of-freedom study (see ref. 3), which was undertaken with the objective of obtaining initial conditions near an altitude of 200,000 feet for an investigation of reaction controls. However, some interesting results of entry down to the beginning of pullout were obtained also and will be included herein.

RESULTS AND DISCUSSION

Before presenting the results of these three studies, it is desired to make a few remarks about the simulators. Of perhaps the most interest in the details of the simulators are the flight instruments used and the type of cockpit control. Shown in figure 1 are the pitch-control formation stick and the instrument panel used in the Ames studies. Figure 2 is a photograph of the cockpit of the North American simulator. Both instrument panels, in general, indicated the same quantities with the exception that North American added a sideslip indicator and gyro horizon for their five-degree-of-freedom investigation.

The results of the two studies on the longitudinal mode only will be considered first. Shown in figure 3 are time histories of significant quantities for the design mission of a zero-lift-coefficient entry from 250,000 feet with a 7.33g pullout beginning at an altitude of 117,000 feet.

The aerodynamics used were those of the original X-15 configuration. A number of interesting points can be noted from the data shown in this figure. First, the damping ratio of the unaugmented airplane is low and reaches a peak value of only about 0.03. A second point to be noted is the considerable change in period and the effectiveness of the control in producing normal acceleration during the entry. These changes are due primarily to differences in dynamic pressure q and static stability of the aircraft. For example, the decrease in the period and the increase in the control sensitivity between the altitudes of 180,000 feet to the beginning of pullout at 117,000 feet is principally the effect of increasing q. The decrease in control sensitivity and the decreased period which follow reflect the increased static stability at the high angles of attack encountered during the 7.33g pullout. The remainder of these two curves also change in accordance with the decreased stability as the angle of attack is reduced at the end of the recovery to level flight. A third point to be noted is the relatively rapid rate at which the period and control sensitivity change with time. For instance, in just 20 seconds the period reduces from 15 to 6 seconds, while the g's per degree of stabilizer incidence $(g/\delta_h{}^o)$ change from 0.05 to 0.30. In addition, during the next 15 seconds the period reduces further to 1.4 and back to 2.8 seconds while the sensitivity reduces to 0.15 and then rises quickly to 0.67. Thus, three dynamic characteristics have been shown to occur during entry which may be troublesome to a pilot: those of low damping and large and rapid changes in period and control sensitivity.

Shown in figure 4 are time histories of normal acceleration and stabilizer incidence of an entry in which the pilot's task was to hold an angle of attack of 20° until the normal accelerometer indicated 3.5g, maintain this acceleration until level flight was achieved, and then reduce the normal acceleration to 1 g. The change to monitoring the normal accelerometer occurs at about 100,000 feet. The upper curves are representative of those records when the pilot made no attempt to damp out an oscillation resulting from inadvertant control motions. As is seen from the acceleration record, the pilot was able to maintain the acceleration to approximately 3.5g by ignoring the oscillations of about ±1 g. These oscillations, of course, would not compromise the structural integrity of the aircraft but the flying qualities were considered to be unsatisfactory by the pilot. At the center of figure 4 are similar time histories which resulted occasionally when the pilot attempted to damp out any oscillations but instead, as is shown by the stabilizer incidence record, reinforced the motions of the aircraft. The curves shown at the bottom of figure 4 are those with the pitch damper operative. The gain of the pitch damper used here was such as to result in an average damping ratio of 0.3 during the constant g portion of the pullout. Also, since the maximum stabilizer deflection due to the damper was only slightly over 1°, the control motion is essentially that put in by the pilot. These time histories effectively show that if the pilot is given some artificial damping he has relatively little difficulty controlling the normal acceleration and can easily make a satisfactory entry to level flight.

Shown in figure 5 are some results obtained when various constant gains of the damping feedback loop were tried. For orientation purposes, the present damping requirements of the longitudinal flying qualities specification is shown as the vertical line. For dampers inoperative, this line would move to the left to a damping ratio of approximately 0.1. The dynamic characteristics shown in the figure are those for the angle of attack α to normal acceleration n_z type of entry and begin at an altitude of 150,000 feet with the constant 3.5g portion of the entry indicated by the solid line. The curve at the far left is, of course, that of the unaugmented airplane whose dynamic characteristics were considered unsatisfactory by the pilots. The other three curves are for different values of the constant gain of the damping feedback loop which were tried, the first one on the left being that of the augmented damping entry shown in figure 4. Note particularly the wide range of damping ratio during an entry which is the result of holding the gain constant. Now, in general, the pilots would accept the damping given by the lowest gain other than zero, but considered the gain which gave a damping ratio of about 0.6 at the middle of pullout as the best of the three. However, there is some evidence that the pilots would accept much less damping if it were constant during entry. For example, the feedback gain was programmed as a function of altitude so as to give substantially the constant damping ratio of 0.2 with no unfavorable comments by the pilots.

Entry techniques other than the design mission and the constant angle of attack to normal acceleration were tried with dampers operative, such as a constant angle of attack, a constant attitude, or attitude to normal acceleration. Although there was no strong preference for any one type of entry, the pilots did express a mild opinion that it was easiest to monitor attitude. The constant-attitude entry is quite interesting for several reasons. First, attitude information, in contrast to angle of attack, is free from instrument errors due to the low density of the air at high altitudes; in fact, it can be judged reasonably accurately by eye if the horizon is visible. Second, a constant-attitude entry, through its relationship with flight-path angle and angle of attack, automatically programs the angle of attack in such a manner as to result in peak normal accelerations which are not excessive. In order to illustrate this point, in figure 6 are shown three nonpiloted or programmed entries for a zero constant attitude, the differences being due to changes in the initial altitude and velocity. Plotted as the ordinate is the altitude in thousands of feet and plotted as the abscissa is the angle of attack; or, since attitude is zero, the abscissa is also the negative of the flight-path angle. The three entries are: one starting from the design altitude mission of 250,000 feet; one from 142,000 feet, which is comparable to that achieved in the high-speed mission; and one from 428,000 feet. The latter is included since the X-15 is potentially capable of exceeding this altitude. On the three trajectories are marked the peak normal acceleration; the maximum for the design high-altitude mission being only 3.9g whereas that for the extreme altitude is 5.7g,

a value which is well below the limit load factor of 7.33. All these zero-attitude entries will end in mild dives since the flight-path angles are small at the termination of the curves where the normal acceleration is about 1.5g.

As mentioned previously, entry results are to be presented of a modified five-degree-of-freedom study. Since the five degrees of freedom include the lateral mode, the relationship of the dynamic characteristics of an X-15 entry to the lateral-directional damping requirements of the flying qualities specification are shown in figure 7. For comparison purposes, the characteristics of the F-100 airplane flying at 30,000 to 40,000 feet and Mach numbers of 0.6 to 1.3, and those of the X-1B and X-1E airplanes at Mach numbers of 1.26 to 1.58 at 56,000 feet are indicated by the shaded areas. The characteristics of the X-15 below 150,000 feet for the high-altitude, normal-load-factor pullout, design mission are given by the solid curved line. As can be seen, the X-15 exhibits negative to poor damping during the entry, and, at altitudes somewhat above that for initiation of the pullout (which begins at $|\phi| / |v_e| \approx 0.3$), the values of the roll coupling parameter $|\phi| / |v_e|$ are high. These large values of the coupling parameter are primarily due to the sizeable magnitude of the effective-dihedral parameter C_{l_β}.

Since the objective of this study was to investigate control characteristics at extreme altitudes, certain simplifications in the simulation were made. Among the most important of these were that entry was limited to altitudes above pullout, that entry was constrained to a fixed trajectory by programming dynamic pressure and altitude as a function of time, and that all the aerodynamic derivatives were constant throughout the entire entry with the speed brakes open 20° so as to increase the directional-stability derivative C_{n_β}. For this condition, the magnitudes of certain of the derivatives were such that 6° of sideslip or 5° of vertical-stabilizer deflection would give about the same rolling moment as full deflection of the rolling tail, and the roll-to-sideslip ratio was near 6. In addition, as shown in figure 2, the pilots used an instrument display similar in many respects to that identified in the previous paper by Windsor L. Sherman, Stanley Faber, and James B. Whitten as the attitude or more conventional display.

Shown in figure 8 is a time history of a piloted entry from a peak altitude of 250,000 feet, but beginning at 200,000 feet, with initial conditions of a positive rolling velocity of 10 deg/sec and a value of α and β of -10°. Plotted as solid curves are the instrument readings of inertial roll angle Φ, α, and β and plotted as dashed curves are the deflections of the rolling tail and the horizontal and vertical stabilizers. Note that in each instance the instrument record and the corresponding time history of the control that the pilot normally deflects

to obtain a change in the reading are placed together. Now the objective of the pilot was to cancel out the initial conditions and then keep the wings level and α and β zero. The record of this entry shows, however, that the angles of attack and sideslip were small for only a short period of the time, and that the aircraft rolled past vertical to the right and then made more than one revolution to the left. On the record, note how often an angle of sideslip of 6°, which gives the same rolling power as full deflection of the rolling tail, was exceeded. The inability to keep angles of attack, sideslip, and roll small is traceable primarily to this overpowering of the roll control by sideslip. This in turn couples α and β and makes it extremely difficult for the pilot to control the motions of the aircraft. A secondary effect of the strong coupling also may appear to the pilot as changes in control effectiveness although the aerodynamic derivatives are constant. For example, note that the positive deflection of the horizontal stabilizer at an altitude of about 180,000 feet would appear to the pilot as having an immediate effect in reducing the angle of attack; although, $3\frac{1}{2}$ seconds later, a similar deflection apparently has no effect. The best technique found in coping with the effect of the large magnitude of C_{l_β} was to try to stop the roll first and then reduce β to zero. Some successful flights have been made in this manner, but extremely close attention to the instruments and rapid, precise use of the controls were required.

Shown in figure 9 are two time histories of entry with the same initial conditions as before, but differing in that one is for one-half the normal value of C_{l_β} and the other for zero C_{l_β}. A comparison of these results with those of figure 8 shows that a reduction in C_{l_β} by one-half eased the pilot's task and he was able to keep the rolling and the values of α and β within reasonable magnitudes until near an altitude of 130,000 feet. As indicated by the solid curves, a further decrease in C_{l_β} to zero essentially eliminated the problems of controllability during this portion of the descent. These results have been reflected by the initiation of a North American study of means to reduce substantially C_{l_β}. The ease of control with zero C_{l_β} and dampers off as exhibited in figure 9, however, does not reflect the difficulties in longitudinal control at the shorter periods and higher dynamic pressures encountered during the pullout.

A comparison of figures 8 and 10 demonstrates the effect of adding dampers about all three axis. The dampers used here gave a damping ratio of about 0.4 in pitch and 0.3 in yaw at 150,000 feet, but since the gain settings were constant their effect varied with altitude. The roll damper provided a similar improvement in the roll characteristics. The primary
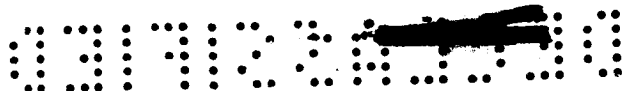
advantage of the dampers is that they limit the rates of motion, particularly that of roll, which, as can be seen, gave the pilot adequate control.

The use of dampers raises the question of the authority necessary to accomplish the damping action by the controls. The values used in this study are $\pm 10^\circ$ for each side of the rolling tail and $\pm 3^\circ$ for the vertical stabilizer. Since one of the design missions of the X-15 attains a dynamic pressure of 2,500 pounds per square foot, increased importance of the design of the fail-safe features of the dampers is evident.

CONCLUDING REMARKS

It has been shown that the original X-15 had the unsatisfactory longitudinal flying qualities of low damping, which is characteristic of aircraft flying at high Mach numbers and high altitudes, and large and rapid changes in period and control sensitivity during pullout, which also adversely affect control. In addition, the X-15 was shown to be difficult to control at altitudes above that of pullout because of the strong coupling between yaw and roll. The reduction of C_{l_β} was shown to minimize the coupling, but the favorable simulator results are not completely conclusive since they do not include the pullout. The use of dampers has heretofore been considered somewhat of a luxury for high-speed aircraft, but, in this instance, the addition of damping about all three axes has been demonstrated as almost a necessity to insure consistent and successful entries.

REFERENCES

1. Matthews, Howard F., and Merrick, Robert B.: A Simulator Study of Some Longitudinal Stability and Control Problems of a Piloted Aircraft in Flights to Extreme Altitude and High Speed. NACA RM A56F07, 1956.

2. Cooper, N., and Zumbrunnen, D.: Analog Simulation Studies of the X-15 Longitudinal Stability and Control Characteristics. Rep. No. NA-56-759, North American Aviation, Inc., July 25, 1956.

3. Cooper, N., and Zumbrunnen, D.: Analog Simulator Studies of the High Altitude Control Characteristics During the Design Altitude Mission of the X-15 Airplane. Rep. No. NA-56-973, North American Aviation, Inc., Sept. 26, 1956.

AMES
PILOT CONTROL STICK AND INSTRUMENT PANEL

Figure 1

NORTH AMERICAN SIMULATOR COCKPIT
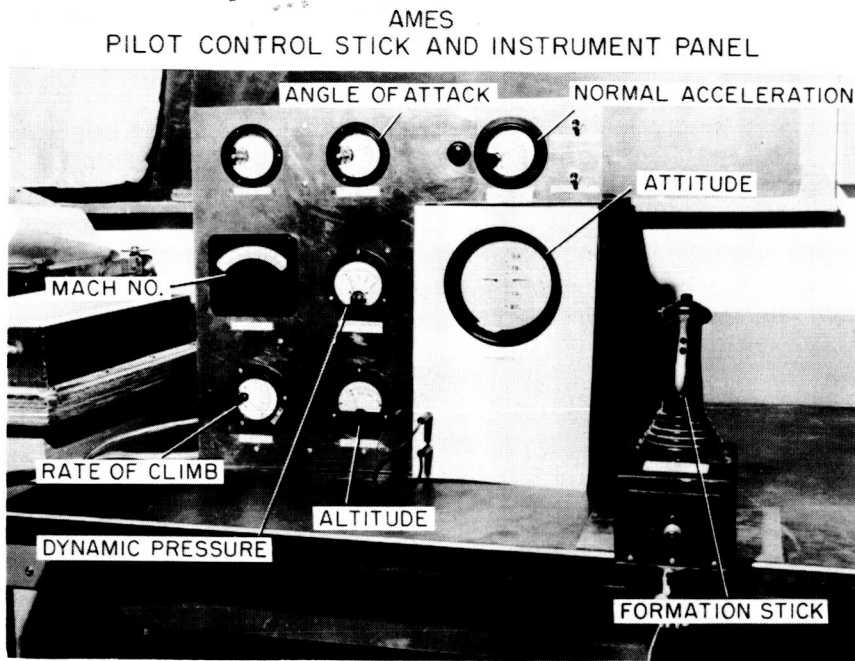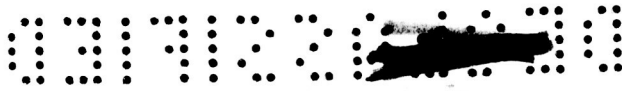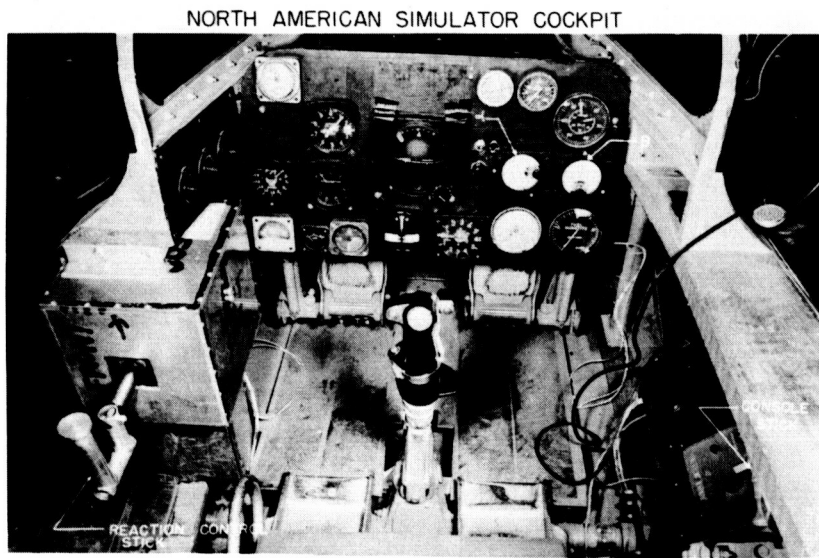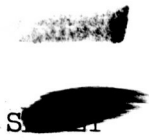
Figure 2

CHARACTERISTICS OF LONGITUDINAL MODE:
DESIGN MISSION-BRAKES CLOSED, $C_L=0$ ENTRY FROM
250,000 FT, 7.33g PULL-OUT INITIATED AT 117,000 FT
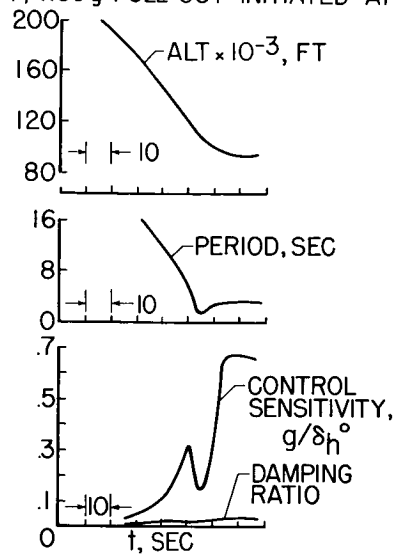
Figure 3

LONGITUDINAL OSCILLATIONS DURING ENTRY
$\alpha=20°$ TO $n_z=3.5g$ ENTRY
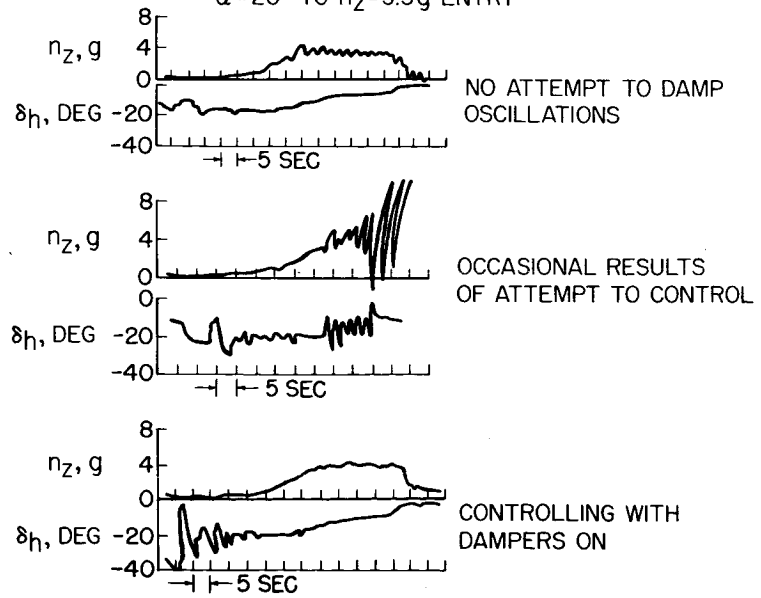
Figure 4

SCOPE OF DAMPER INVESTIGATION
$\alpha = 20°$ TO $n_Z = 3.5$ g ENTRY

SATISFACTORY BY FLYING
QUALITIES SPECIFICATION

DAMPER δ_{h_s}/θ
GAIN

0   $-.25$ $-.60$ -1.00

UNDAMPED SHORT-PERIOD FREQUENCY, CPS

DAMPING RATIO, ζ
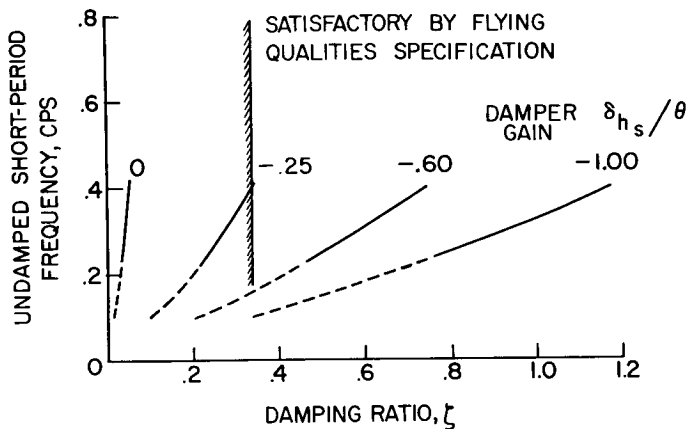
Figure 5

CHARACTERISTICS OF PROGRAMMED
ZERO θ ENTRIES; BRAKES CLOSED

$V_0 = 4506$ FPS

$V_0 = 5750$

$V_0 = 6450$

$n_Z = 2.6$ $n_Z = 3.9$

$n_Z = 5.7$

ALTITUDE x 10^{-3}, FT

α, DEG

Figure 6

COMPARISON OF LATERAL-DIRECTIONAL DAMPING
CHARACTERISTICS WITH FLYING
QUALITIES SPECIFICATIONS
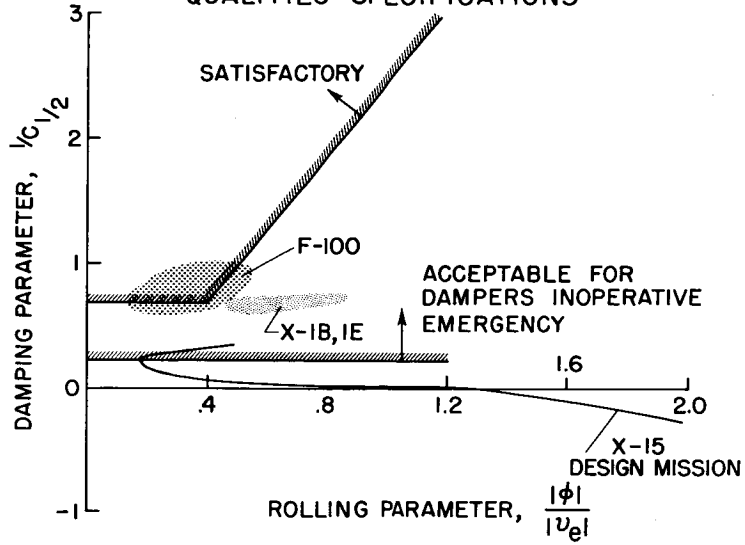
Figure 7

ENTRY WITH DAMPERS OFF, NORMAL C_{l_β}

Figure 8

ENTRY WITH DAMPERS OFF,
HALF NORMAL AND ZERO C_{l_β}
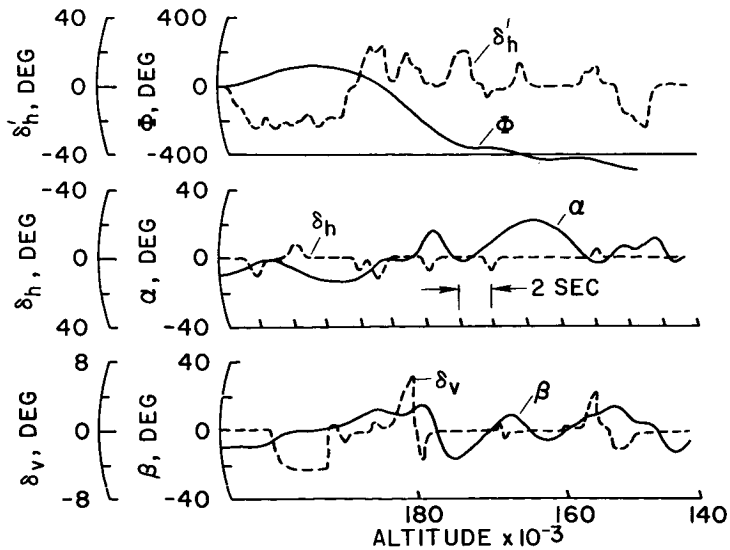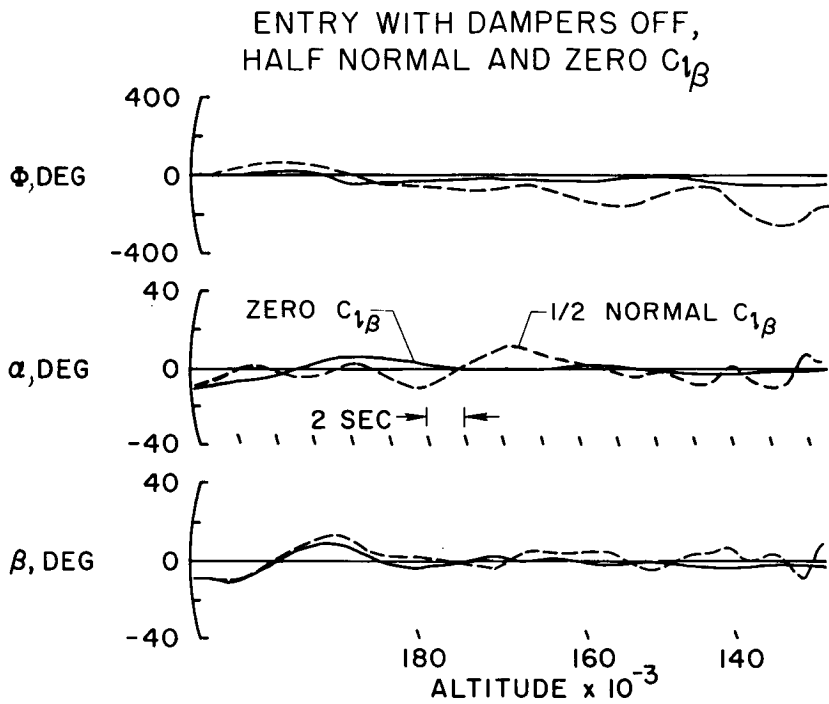
Figure 9

ENTRY WITH DAMPERS OPERATIVE, NORMAL C_{l_β}
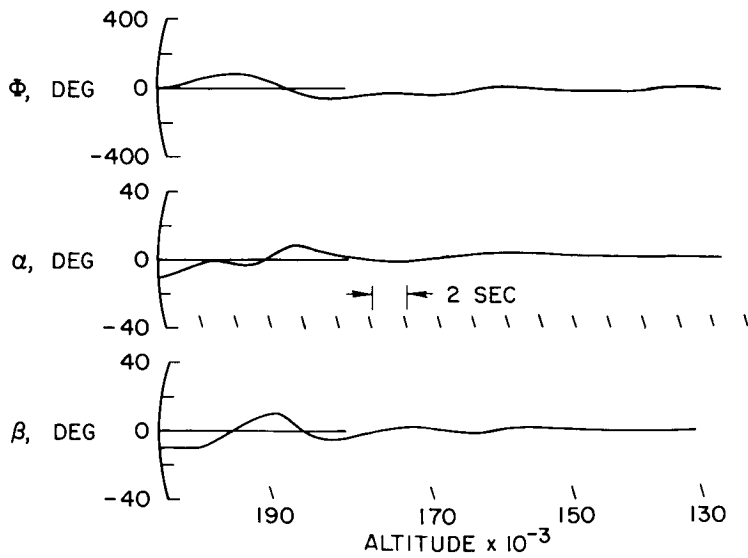
Figure 10
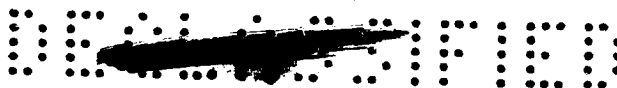
FLIGHT CHARACTERISTICS OF AN X-15 MODEL AT LOW SPEEDS

By John W. Paulson

Langley Aeronautical Laboratory

INTRODUCTION

A low-speed stability and control investigation has been made with a 1/7-scale free-flying model representing configuration number one of the X-15 airplane. The primary purpose of this investigation was to aid in the evaluation of one of the unique features of this airplane - the use of the horizontal tail for roll control. This type of roll control has appeared to be quite promising on the basis of various force-test investigations in the past. One of the questions that has arisen regarding the use of such a control is the effect of its large favorable yawing moments on dynamic lateral control characteristics. In this model-flight investigation, therefore, the lateral control characteristics of the X-15 configuration were studied with particular attention being given to the effect of the large favorable yawing moments.

DISCUSSION

As an introduction to the stability and control data to be presented, figure 1 shows the lift characteristics of the model which are quite unusual because of the large fairings. These data were obtained from low-speed force tests. The lift curve for the wing-body combination (without fairing) breaks at a fairly low angle of attack where the wing stalls. The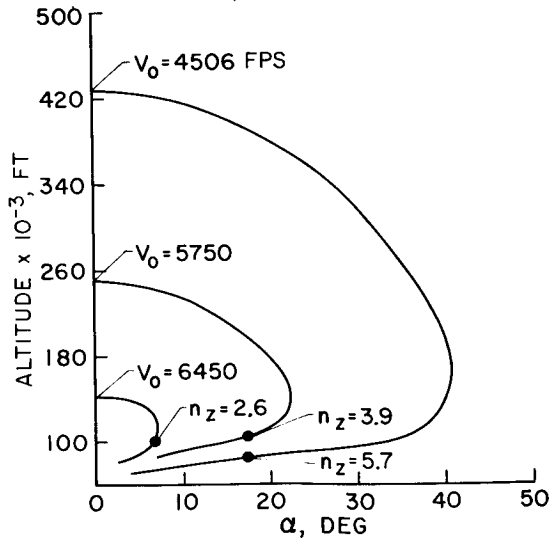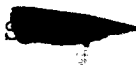 addition of the fairing delays the break to a much higher angle of attack and nearly doubles the maximum lift coefficient. The addition of the horizontal tail causes a further increase in the maximum lift and delays the stall so that the lift of the complete model is still increasing at an angle of attack of 40°. At the higher angles of attack, the wing is producing only about one-half the total lift.

It should be pointed out that, although data are shown up to an angle of attack of 40° in this and subsequent figures, the maximum angle of attack at which the airplane is expected to be operated in low-speed flight is less than 20°.

Shown in figure 2 are the roll control characteristics of the model determined from low-speed force tests. These data are for horizontal-tail deflections of ±9°. The rolling effectiveness decreases with angle of attack, but some effectiveness is maintained even up to 40°. This

8

characteristic has been found in other investigations to be typical of
the horizontal-tail roll control. It was found during the flight tests
that the horizontal tail provided good roll control up to the highest
angle of attack at which the model could be flown ($\alpha = 30^\circ$).

Shown in the lower part of the figure is the parameter C_n/C_l, the
ratio of the yawing moment to the rolling moment produced by the roll
control. These data show that the differentially deflected horizontal
tail produces a favorable yawing moment that is about 0.7 as great as the
rolling moment at low and moderate angles of attack. As the angle of
of attack increases, the yawing moment decreases and finally becomes
unfavorable at about 32°. Most of the large yawing moment results from
the fact that the horizontal tail has 15° negative dihedral so that when
the tail is deflected differentially a rather large side force is pro-
duced. In other airplane configurations in which the horizontal tail
has been used for roll control, most of the large favorable yawing moment
has been produced by the loads induced on the vertical tail by the hori-
zontal tail, but for the X-15 configuration this effect was quite small
because of its particular tail arrangement.

It should be pointed out that the yawing-moment parameter C_n/C_l
is only one of several factors that affect the yawing motions during
rolling maneuvers. For example, at moderate and high angles of attack,
large adverse yawing moments might be produced by the yawing moment due
to rolling velocity C_{n_p} and by the product-of-inertia effect. Thus,
the resultant yawing moment might actually be small or adverse even when
the value of C_n/C_l is highly positive. It would be expected that the
most critical condition for excessive favorable yawing moments would be
the low-angle-of-attack range. The lowest angle of attack reached in
the model flight tests was 8° and no objectionable yawing motions were
produced by roll control at this angle of attack. In fact, the roll
control appeared to be very good over the angle-of-attack range from 8°
to 30° except that at the high angles of attack some adverse yawing was
obtained. At angles of attack lower than 8°, the values of C_{n_p} and
the product-of-inertia effect are likely to be quite small so that the
resultant yawing moment would approximately correspond to the value of
C_n/C_l shown in figure 2 at low angles of attack. In this event the
large favorable yawing moment might well prove to be objectionable.

Figure 3 shows the test setup used to fly the model in the Langley
full-scale tunnel. In this setup there is an overhead safety cable to
prevent crashes of the model. Combined with this cable is another cable
composed of plastic hoses which provide compressed air to nozzles in the
model for thrust and wires which provide power for the control actuators.
The thrust controller remotely controls the flow of air to the model by
adjusting a valve located at the top of the entrance cone. The thrust

controller and the pitch pilot must coordinate their efforts in order to maintain steady flight. Another operator adjusts the safety cable so as to keep it slack during flight and takes up the slack to prevent the model from crashing if it goes out of control. A second pilot who controls the rolling and yawing motions of the model is located near the bottom of the exit cone. Motion-picture records of the flights are obtained with cameras located at the side of the test section and at the top and bottom of the exit cone.

Figure 4 shows the pitching-moment characteristics of the model with horizontal tail off and on. The pitching moment about the quarter chord of the mean aerodynamic chord is plotted against angle of attack. These data show that the model is longitudinally stable up to about an angle of attack of 30° and it then becomes unstable. The break in the curve is usually associated with pitch-up and occurs at about the maximum angle of attack at which the model could be flown. In the flight tests the model had a definite pitch-up tendency at angles of attack of about 30° which resulted in the model reaching very high angles of attack beyond the stall if no control was applied to prevent it. However, the pilot could usually prevent a pitch-up by proper use of control, since the pitching motion was fairly slow and the longitudinal control was powerful.

Shown in figure 5 are the lateral stability characteristics as given by the directional-stability parameter C_{n_β} and the effective-dihedral parameter C_{l_β} plotted against angle of attack for the complete model and for the model with upper vertical tail off. The directional stability of the complete model is high through the lower angle-of-attack range and then falls off rapidly to become negative at an angle of attack of about 30°. This can be attributed to both an increase in the destabilizing moment of the wing-fuselage combination and to a decrease in the contribution of the upper vertical tail. It is shown on the lower part of the figure that C_{l_β} also becomes zero at an angle of attack of about 30°. Static characteristics such as these in which C_{n_β} and C_{l_β} both become zero usually give rise to a directional divergence. As the model approached an angle of attack of 30° in the flight tests, there was some evidence of the decreasing directional stability and the model finally diverged despite attempts by the pilot to prevent it.

Figure 6 shows the damping in roll and the damping in yaw about the body axes obtained from rotary-oscillation tests. The variations of these derivatives with angle of attack are shown for two values of the reduced-frequency parameter ($k = 0.06$ and 0.16). The data show that the values of damping in roll and yaw are both essentially constant up to an angle of attack of about 20° and then the values of both derivatives increase negatively with increasing angle of attack. At the lower angles of attack there is very little effect of frequency, but at the higher

angles more damping is obtained with the lower frequencies. Large values of damping in roll and yaw such as these are considered very desirable for damping of the Dutch roll oscillation. The influence of these large values of the damping derivatives was evident in the flight tests where damping of the Dutch roll oscillation following a disturbance appeared to be almost deadbeat.

CONCLUDING REMARKS

In conclusion, it may be stated that on the basis of previous correlations of model and full-scale flight results the airplane will have generally good low-speed stability and control characteristics. The airplane should experience the pitch-up and directional divergence at an angle of attack somewhat higher than the 30° indicated by the model tests.

LIFT CHARACTERISTICS

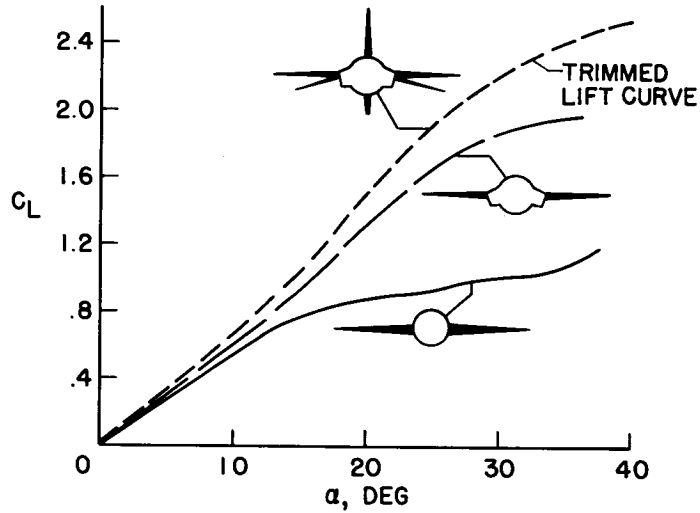Figure 1

EFFECT OF ANGLE OF ATTACK ON ROLL CONTROL

Figure 2

FLIGHT-TEST SETUP
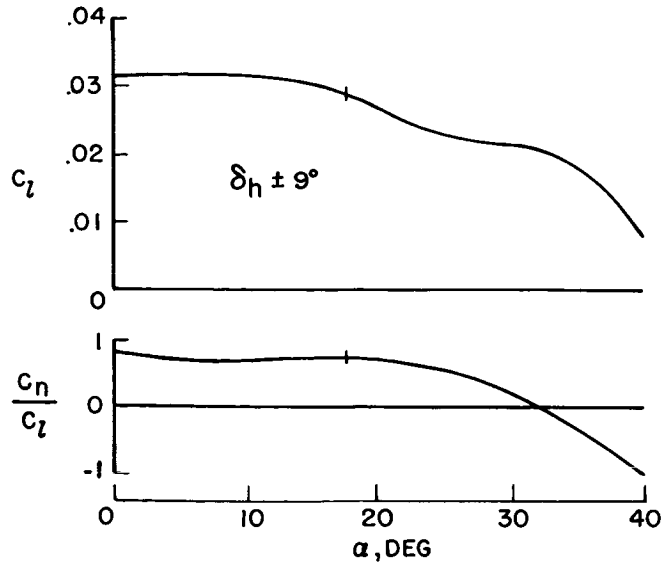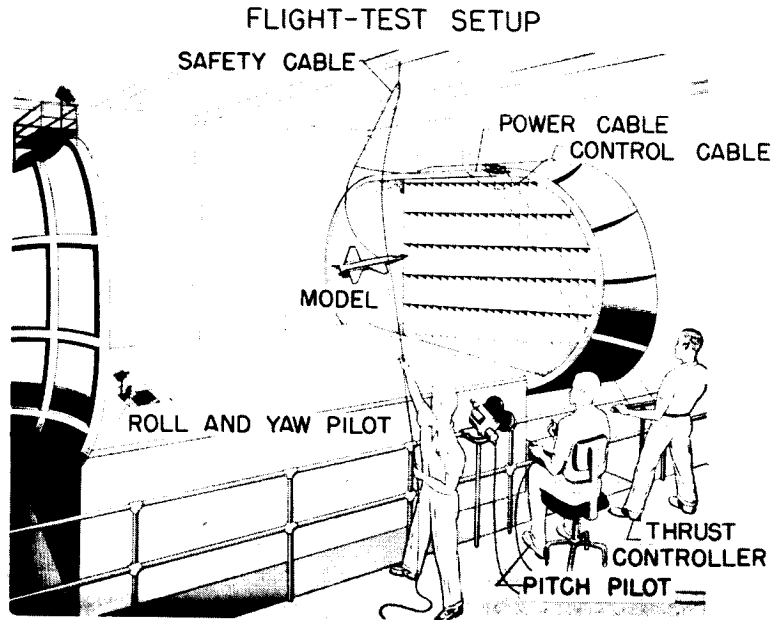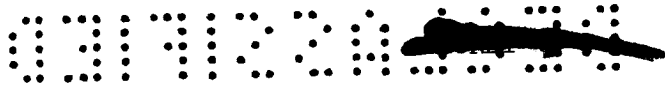
Figure 3

PITCHING-MOMENT CHARACTERISTICS

Figure 4

LATERAL STABILITY CHARACTERISTICS

Figure 5

DAMPING IN ROLL AND YAW
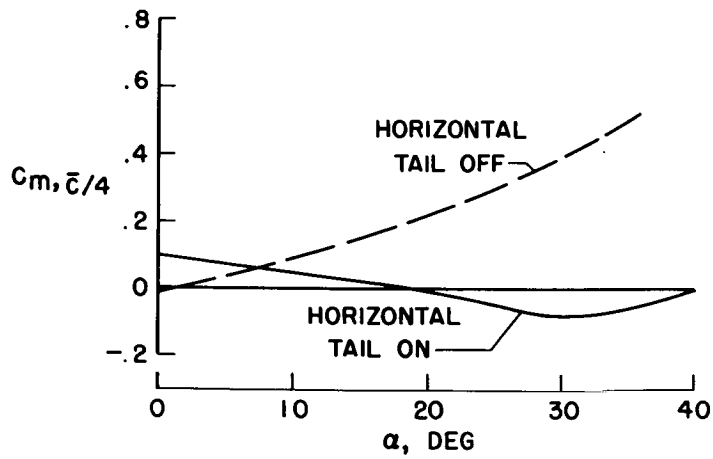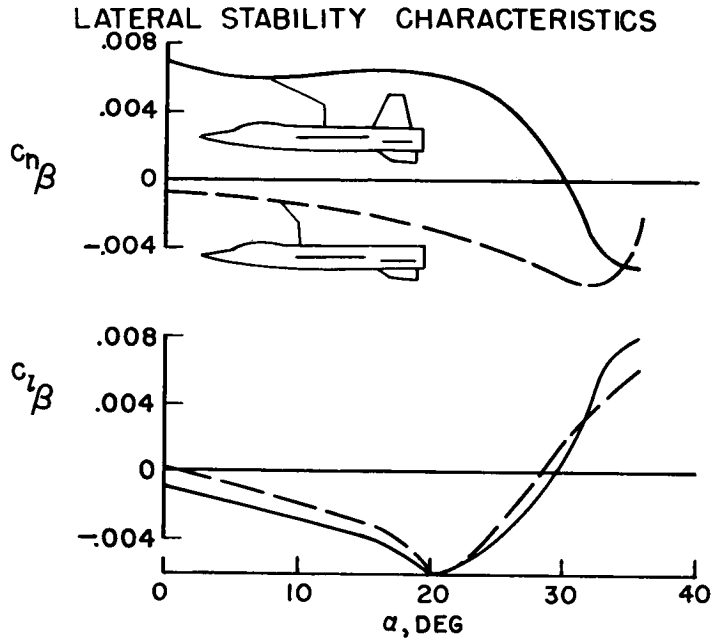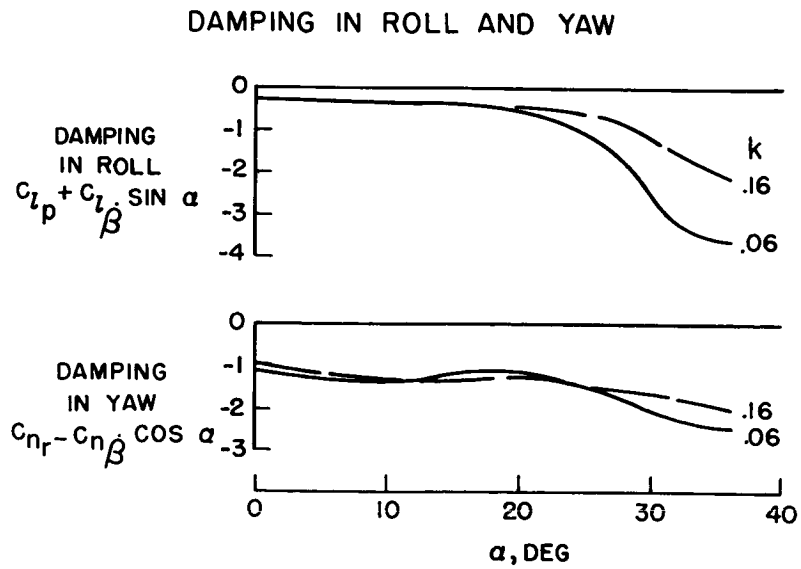
Figure 6

AERODYNAMIC HEATING
AND STRUCTURES

SKIN AND STRUCTURAL TEMPERATURE MEASUREMENTS ON

RESEARCH AIRPLANES AT SUPERSONIC SPEEDS

By Richard D. Banner and Frank S. Malvestuto, Jr.

NACA High-Speed Flight Station

INTRODUCTION

The NACA High-Speed Flight Station is presently engaged in a comprehensive program to investigate and analyze the aerodynamic heating of airplanes in flight at supersonic speeds. Skin and structural temperatures have been determined in flight by use of thermocouples and temperature resistance gages installed on various research airplanes. Such data have recently been obtained on two research airplanes, the Bell X-2 and the Bell X-1B. The object of this paper is to show some of the actual magnitudes and trends in the structural temperatures that exist in an airplane experiencing the effects of aerodynamic heating. Although time has not permitted an analysis of much of these temperature data, the information presented herein is a cross section of the work that is presently being done. The data presented do not cover the speed and altitude range anticipated for the proposed North American X-15; however, they provide actual full-scale, experimental, structural temperature information for comparison with present analytical and wind-tunnel studies.

Shown in figure 1 is a sketch of the two airplanes. The X-2 airplane is constructed primarily of steel. Nose-cone skin temperatures have been obtained on this airplane at supersonic speeds up to a Mach number of 3.2. The X-1B airplane is constructed primarily of aluminum. The maximum speed capability of the X-1B is less than that of the X-2. Very extensive temperature measurements are being made throughout the structure of the airplane. To date, data have been obtained in flight to a Mach number of 1.8 at about 300 locations throughout the airplane.

DATA OBTAINED ON THE BELL X-2 AIRPLANE

Data were obtained on the Bell X-2 nose cone at flight conditions shown in figure 2. The Mach number is shown for only the supersonic portion of the flight. The maximum Mach number of 3.2 was reached at an altitude of 62,000 feet about 160 seconds after drop. The air temperature at this altitude and down to the altitude for drop was approximately -90° F. The structure prior to drop was only slightly warmer. The angles of attack for the flight conditions shown were small.

As mentioned previously, only nose-cone skin temperatures were measured on the X-2. Figure 3 shows, in time-history form, the measured skin temperatures at stations 9.5 and 35.25 inches back of the nose-cone apex. Maximum temperatures on the order of 420° to 430° F were measured at the two stations shown. (It should be pointed out here that all the skin temperatures were measured on the inside surface of the skin.) The theoretical stagnation temperature, which is shown as the upper curve, reads a maximum of 700° F at a Mach number of 3.2. The turbulent adiabatic, or insulated, wall temperature was estimated by using a recovery factor of 0.9 and is shown as the second curve from the top. The maximum adiabatic wall temperature was 630° F. The difference between the adiabatic wall temperature and the skin temperature shown here is due, of course, to the conductivity of the skin. The temperature of the nose-cone compartment was measured during the flight and is shown as the lower curve. The measuring point for the compartment temperature was $1\frac{1}{2}$ inches from the skin. A maximum nose-cone-compartment temperature of about 60° F was measured. A spot check indicated that this temperature was due primarily to the effects of the skin's internal radiation.

Time-history data at several points along the nose cone are briefly summarized in figure 4 which shows the longitudinal temperature distribution at three times during the flight. The data are shown at Mach numbers of 1.4, 3.20 (the maximum Mach number), and 9 seconds later at a Mach number of 3.00. At a Mach number of 1.4, the temperatures were constant along the cone at a little above 0°. At the higher speeds and higher temperatures, there are some inflections in the curves shown. These inflections are associated with the heat sinks in the regions of the internal bulkheads. It should be pointed out that the skin thicknesses at the locations shown in this figure were constant at 0.019 inch. Some effects of material thickness can be seen in figure 5, which shows time histories of the temperatures measured on the top and bottom of the nose cone. The stations for which these temperature data are shown are 9.5 and 18.44 inches back of the nose-cone apex. The temperatures measured on top are shown by the solid lines. The material thickness on the top is 0.019 inch. The dashed lines are the bottom temperatures, measured on the inside of a splice plate. The total thickness on the bottom, including splice, is 0.038 inch. The skin temperatures on top of the nose cone, at both stations, reached a maximum of about 400° F at approximately the same time. The bottom temperatures, measured on the splice plate, lagged the top, as might be expected from the conductivity effect of the increased thickness. Also, the effectiveness of the welded splice joint no doubt affects the temperatures indicated on the bottom.

Measured data have been presented for various conditions on the X-2 nose cone during flight at angles of attack near zero. It was noticed that only small differences in the maximum skin temperatures existed

at the locations where conduction effects to the internal structure were negligible. It is of interest to compare these measured temperatures with those calculated by theory. Figure 6 shows a time-history comparison of the measured and calculated temperatures at two locations on the side of the X-2 nose cone. The measured data are shown by the solid curves. The calculations, which are based on the Colburn relationship for a turbulent boundary layer on a flat plate and modified to a cone, are shown as dashed lines. As can be seen, the calculations give a 20- to 25-percent conservative estimate of the skin temperatures. A check at several points indicated that use of Van Driest's turbulent theory would have given estimates of the skin temperatures about 10 to 15 percent lower than the calculations used here. The local Reynolds numbers used in the calculations were based on the distance rearward of station 0, as shown in the sketch. It should be pointed out that the X-2 has a nose boom (which is not shown completely in figure 6) that protrudes about 3 feet ahead of the nose cone. Wind-tunnel studies have indicated that such protuberances are very effective in producing turbulent flow. The existence of a turbulent boundary layer at these stations can be seen in the comparison of the calculated and measured-skin-temperature data.

DATA OBTAINED ON THE BELL X-1B AIRPLANE

As pointed out previously, very extensive temperature measurements are being obtained on the Bell X-1B airplane. These measurements include not only the skin temperatures on the wing and tail surfaces but also the temperatures on the spars and supporting structure where the internal heat conduction effects are greatest. Fuselage skin temperatures are also being measured and an attempt is being made to assess the effects on the structural temperatures of the internal heat sinks and sources, such as the fuel and liquid-oxygen tanks and the rocket engine.

Presented in figure 7 are the supersonic flight conditions for the X-1B airplane. The altitude varied between 50 and 58,000 feet and the ambient air temperature was approximately -90° F at the altitudes shown. The angles of attack during flight were small and varied between 0° and 4°.

The ambient air temperature is shown in figure 7 in order to give an indication of the temperature of the X-1B prior to drop. The structure of the airplane was approximately 10° to 20° warmer than the ambient air temperature. In the region near the liquid-oxygen tank, however, the temperatures were considerably colder.

Figure 8 shows the longitudinal variation of temperatures measured on the fuselage at a Mach number of 1.6, during the accelerating portion of the flight, and at a Mach number of 1.8, the maximum Mach number for

the flight. The temperatures are given for the locations shown by the black dots along the fuselage. The skin thicknesses at these locations are indicated above. The theoretical stagnation temperature at a Mach number of 1.8 is 150° F.

In the stagnation region of the nose, temperatures on the order of 110° to 115° were measured. The temperatures decrease slightly at positions rearward along the fuselage to a point on the side of the cockpit. The skin thicknesses in this region differ only slightly. The next point shown, however, is in the region of the liquid-oxygen tank, where the skin thickness is increased considerably. The temperature in this region drops rapidly to about -25° F.

In the fuselage region just above the wing, the material thickness increases slightly and the temperatures decrease to about 50°. At the next location shown, where the thickness is 0.072 inch, the skin temperature is also about 50° F. The temperatures increase at positions rearward along the fuselage to about 75° in the very rear portion. It can be seen that in this region the skin thicknesses have decreased and are of the same order as those near the nose. Heat sources, such as the rocket engine, and heat sinks, such as the liquid-oxygen and fuel tanks, affect the skin temperatures shown; however, it is felt that these variations in the fuselage skin temperatures are typical of those that would be encountered on research airplanes.

Temperature distributions for two fuselage cross sections and along the chord of the vertical tail at a midspan station are shown in figure 9. The data are again shown for the following flight conditions: a Mach number of 1.8, a stagnation temperature of 150° F, and an ambient air temperature of -90° F.

On the nose station of the fuselage the temperatures measured around the periphery are about constant at 90° F. The material thickness here is also constant.

At the aft fuselage station, the temperatures gradually decrease from about 80° F on the side of the vertical tail down to about 60° F near the bottom of the fuselage. There is a small inflection in the temperatures near the intersection of the vertical tail and the horizontal tail. This decrease in temperature is partly due to the increased material thickness in this particular area.

The chordwise variations of the vertical-tail skin temperatures are shown at the bottom of figure 9. The temperatures decrease with increasing distance along the chord, from a value of about 100° F at the leading edge. The slight increase in the temperature near the trailing edge is due to the decreased skin thickness on the rudder.

The temperatures shown by the black squares were measured on the center line of the vertical-tail spars. The difference between these temperatures and the skin temperatures is seen to be about 30° F.

In figure 10 are shown the chordwise temperature variations measured on the wing at the 54-percent semispan station and the 95-percent semispan station (or a tip station). The thermocouple locations are indicated by the black dots. The skin thicknesses vary from front to rear at both span stations. For the upper surface of the inboard station, these thicknesses are 0.081 inch at the leading edge, 0.270 inch in the wing box section, and 0.064 inch on the flap. For the lower surface of the inboard station they are 0.081 inch, 0.230 inch, and 0.064 inch. Skin thicknesses at the tip station along the upper and lower surfaces vary from 0.064 inch to 0.072 inch and again to 0.064 inch on the aileron. The wing is of multiple-spar construction, the spars serving as internal heat sinks. For this reason, the data are not faired continuously along the chord.

The chordwise temperatures at the 54-percent-semispan station may be seen to decrease from the leading edge back along the chord to the forward end of the flap and then increase near the trailing edge. Theoretical estimates of these temperature variations have not been completed; however, the variations are understandable. The decrease in the aerodynamic heat input with increasing distance from the leading edge results in lower temperatures. Of course, the change in skin thickness along the chord has a considerable influence on the temperatures; for example, the thinner skin in the trailing-edge region accounts for the increase of skin temperature in this region. Also, the temperatures in the center section are, relatively speaking, very low due to the increased skin thickness in this region. The general level of the temperatures at the tip region is higher than at the inboard station. Apparently, the increased level is associated with the thinner skins at this span station. It is realized, however, that aerodynamic input in the tip region is not the same as the input at the midsemispan station.

In order to give some indication of the internal-conduction effects in the wings of research airplanes, time histories of the temperatures that were measured on and near the spars at the 54-percent semispan station are shown in figure 11. The left sketch shows the temperatures measured in the leading-edge region. The temperature of the leading edge, as shown in figure 10, is a maximum of about 90° F. The internal temperatures on the relatively thick spar and the spar flanges are seen to be considerably lower.

The data for all the spar locations show, as would be expected, that the temperatures at the spar center line are lower than the temperatures of the upper and lower skins. This trend seems to be true also at the leading edge of the flap where not only conduction but also convection effects influence the temperature.

The spanwise variation of the wing skin temperatures is shown in figure 12. Shown above the wing are the temperatures that were experienced on the leading edge, and also on the upper skin at the 66-percent-chord station. As can be seen, the leading-edge temperatures vary from about 90° F near the root to a little above 100° F near the tip. The skin temperatures at the 66-percent-chord station are lower, particularly at the root where the wing skin thickness is 0.5 inch. The spanwise variation in the skin thickness is shown below for both the 66-percent-chord station and the leading edge. It is interesting to note that the temperature variations over the span are roughly proportional to the inverse of the skin thickness. The existence of these trends at higher temperature levels may result in important thermoelastic effects, particularly in the wing-tip region.

RESEARCH AIRPLANES UTILIZED FOR TEMPERATURE STUDIES

X-2
(Steel constr.)

X-IB
(Alum. constr.)
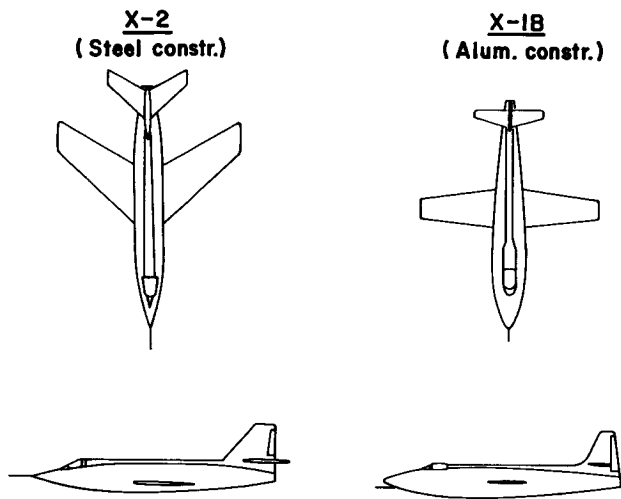
Figure 1

X-2 AIRPLANE—FLIGHT CONDITIONS

Time, seconds (from drop)

Figure 2

TIME HISTORY OF SKIN TEMPERATURES —
X-2 NOSE CONE

STAGNATION TEMPERATURE

T_{aw} (Turb.)

Sta. 0   Sta. 9.5   Sta. 35.25

T,°F

COMPARTMENT

Time, sec.(from drop)
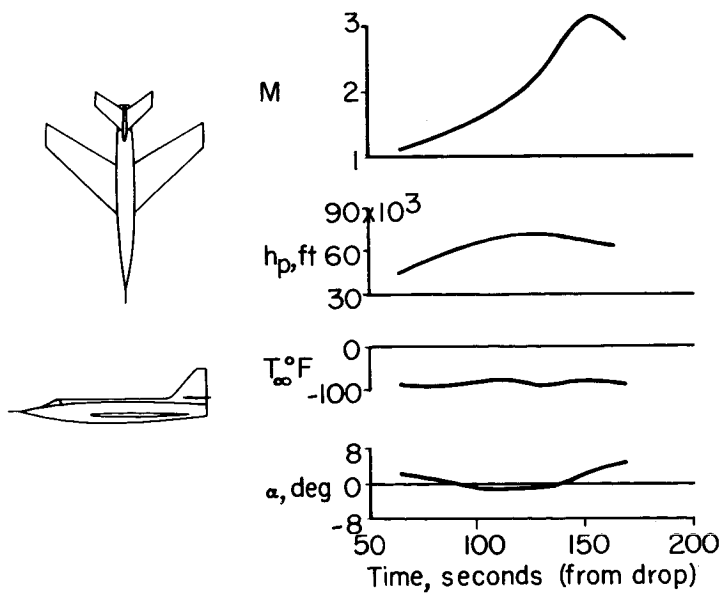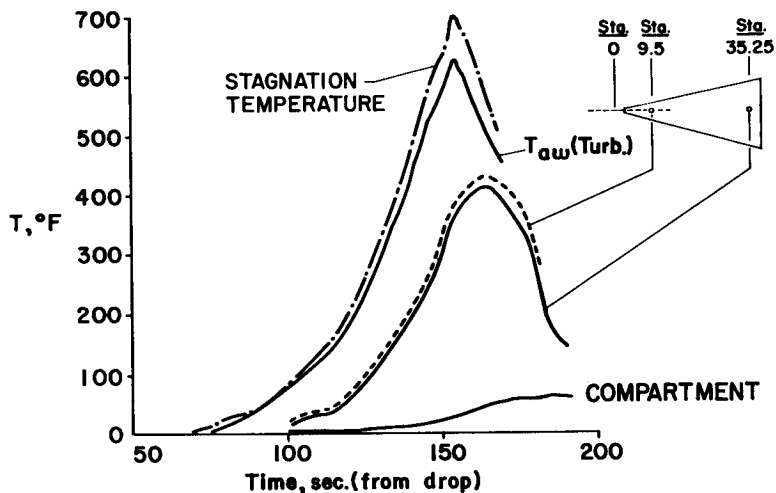
Figure 3

LONGITUDINAL SKIN TEMPERATURE DISTRIBUTIONS
X-2 NOSE CONE

K MONEL
(T = .019)

T, F°

$M = 1.4$
$t = 95$ sec.

$M = 3.20$ (max.)
$t = 154$ sec.

$M = 3.00$
$t = 163$ sec.
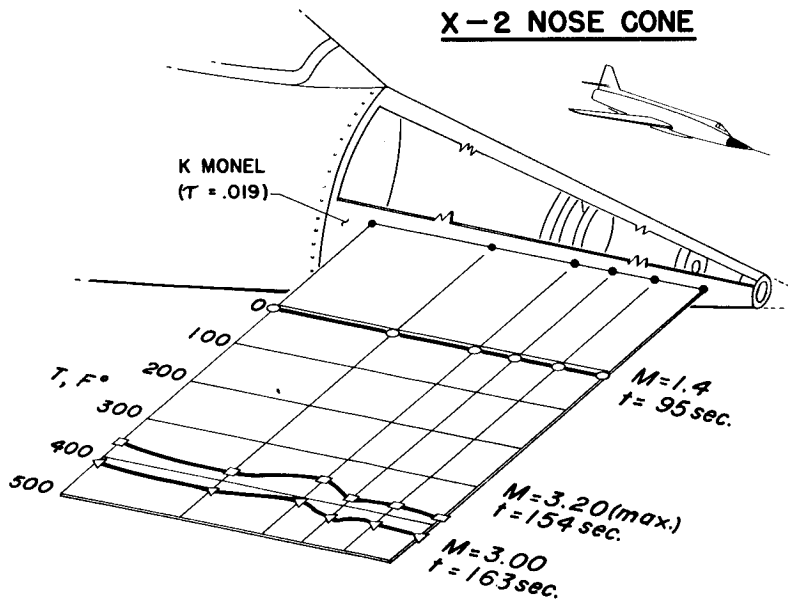
Figure 4

TIME HISTORY OF SKIN TEMPERATURES —
TOP AND BOTTOM OF X-2 NOSE CONE
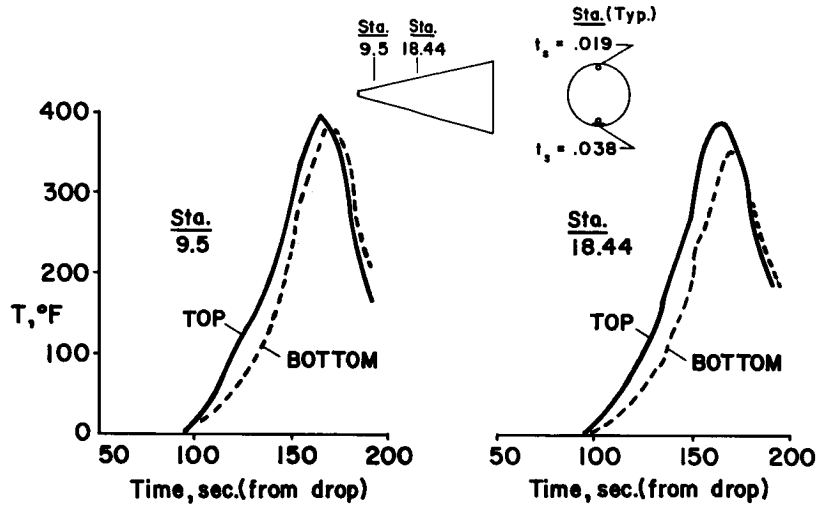
Figure 5

MEASURED AND CALCULATED SKIN
TEMPERATURES—X-2 NOSE CONE
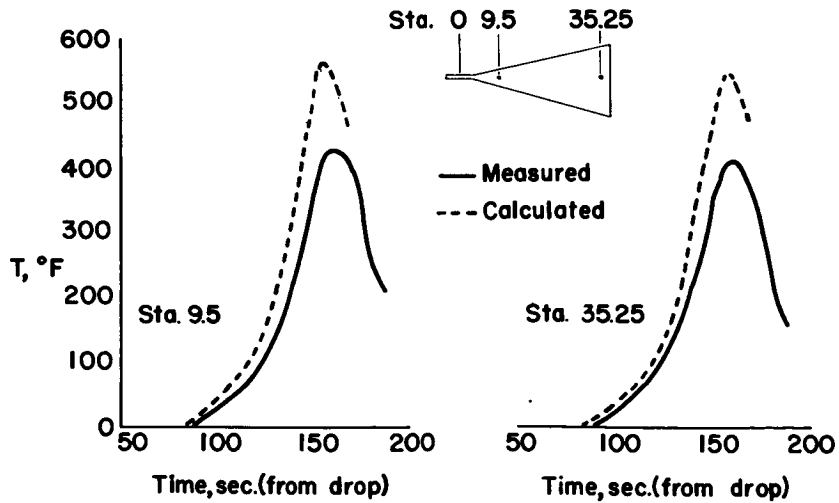
Figure 6
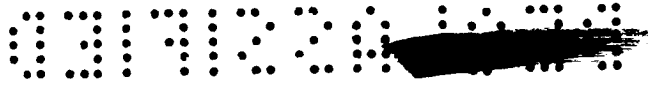
X-IB AIRPLANE—FLIGHT CONDITIONS
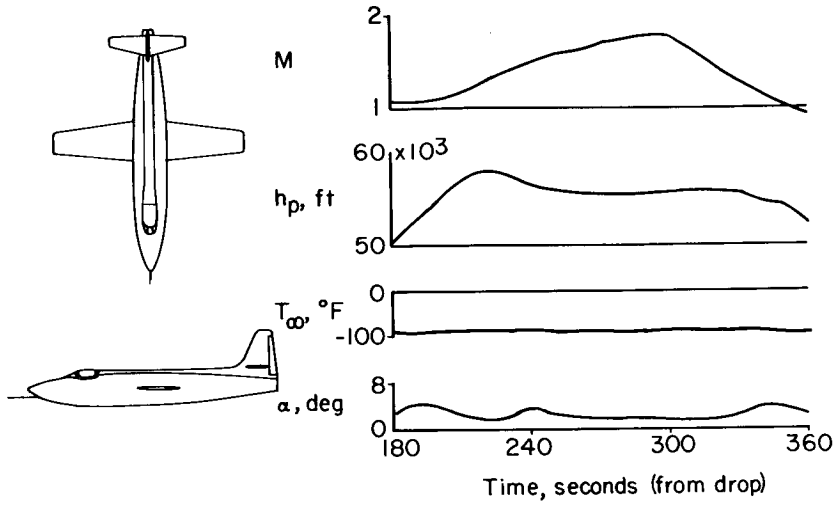
Figure 7

LONGITUDINAL SKIN TEMPERATURE DISTRIBUTIONS
X-IB FUSELAGE
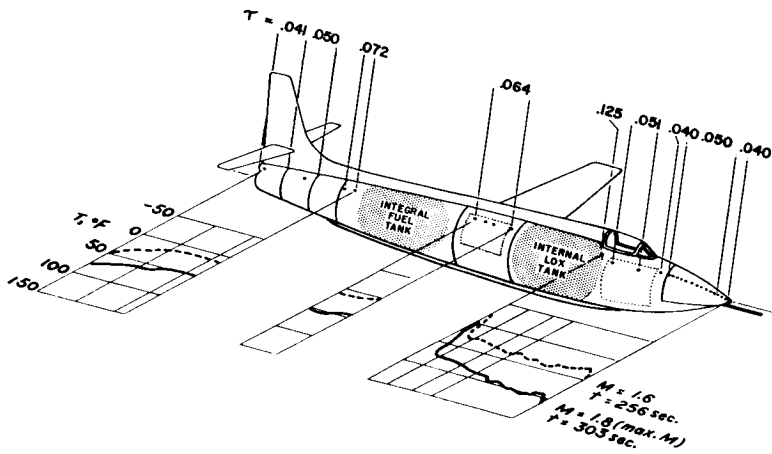
Figure 8

MEASURED TEMPERATURES AT DIFFERENT STATIONS
X-IB AIRPLANE

SKIN TEMP.(M ≈ 1.8)
SPAR TEMP.(M ≈ 1.8)
$T_s = 150\,°F$
$T_\infty = -90\,°F$

NOSE STATION

$T,\,°F$

AFT FUS. STATION

VERTICAL TAIL STATION
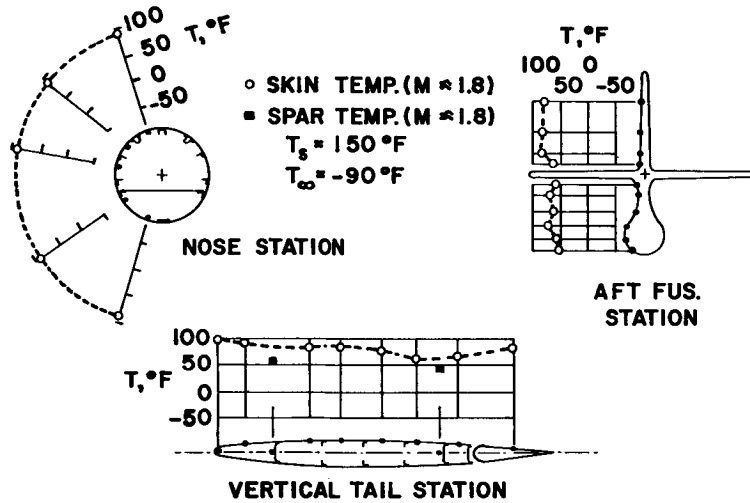
Figure 9

CHORDWISE SKIN TEMPERATURES, X-IB WING

$M_\infty = 1.8,\quad T_s = 150\,°F,\quad T_\infty = -90\,°F$

$54\%\frac{b}{2}$

$95\%\frac{b}{2}$

Upper

$\tau = .081$ | .270 | .064

$\tau = .081$ | .230 | .064

.064 | .072 | .064

.064 | .072 | .064

Lower
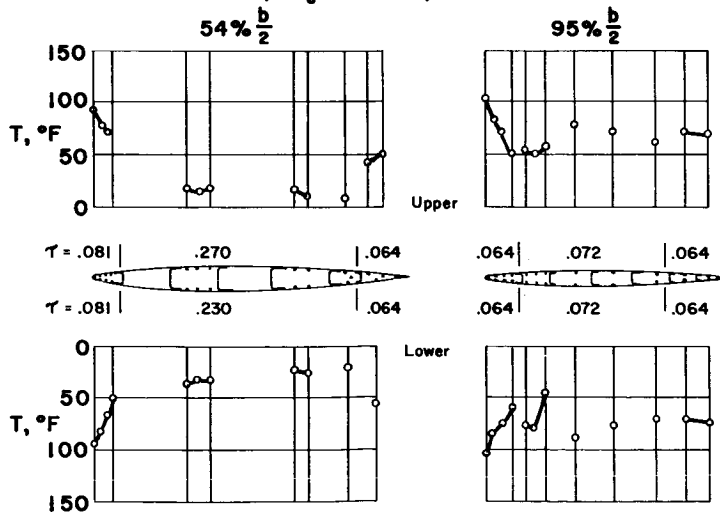
Figure 10

X-IB WING CHORD TEMPERATURES—54% b/2
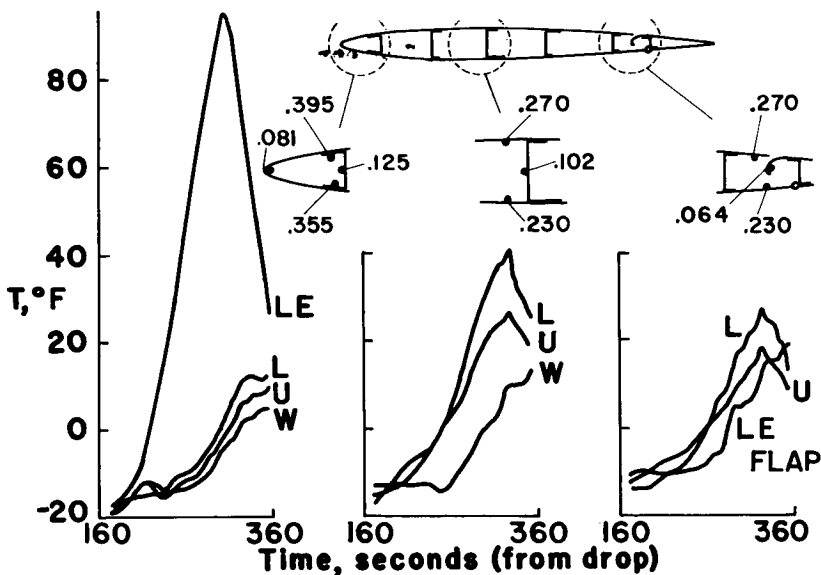
Figure 11

SPANWISE SKIN TEMPERATURE DISTRIBUTIONS
X-IB WING

$M_\infty = 1.8$, $T_S = 150°F$, $T_\infty = -90°F$
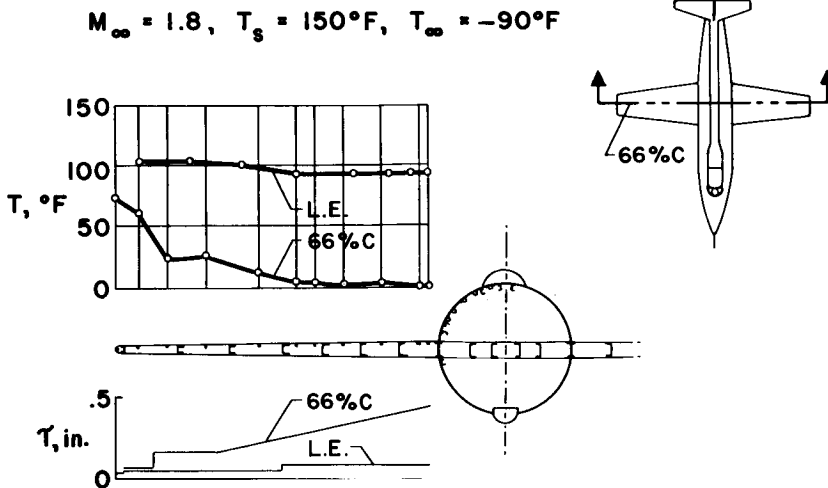
Figure 12

METHOD OF CALCULATION OF HEAT-TRANSFER COEFFICIENTS

FOR THE X-15 AIRPLANE

By William V. Feller

Langley Aeronautical Laboratory

One of the principal missions of the X-15 airplane is to investigate the high aerodynamic heating rates which are expected in hypersonic flight. However, in order to design the airplane to perform this mission safely and effectively, the designer must have some idea of the magnitude of the heating rates to which the airplane will be exposed.

One of the major unknowns in the design of the airplane is how much of the boundary layer will be laminar. Available theoretical and experimental studies indicate the possibility of extensive areas of laminar flow at the conditions under which the airplane will fly. However, the surface of the airplane probably will not be as fair and polished as those on laboratory models, so the prediction of the extent of laminar flow on the basis of model tests cannot be relied on. Conservative design would require that nearly all of the airplane be assumed to have a turbulent boundary layer. If, in flight, the airplane is found to have long runs of laminar boundary layer, it will be desirable to trip transition artificially in some flights in order to study turbulent heating rates.

The flow field around the complete airplane configuration is far too complex to permit calculation of the heat transfer including interference or interaction between the parts of the airplane. Therefore, it is necessary to consider isolated parts of the airplane, and in some cases approximate those by bodies of simpler shapes for which theoretical or experimental studies are available.

Figure 1 shows a breakdown of the airplane into the parts which will be discussed in this paper. The wing (and tail surfaces) can be divided into two elements: the swept-cylinder leading edge, and the rest of the wing, which is so slightly curved that it can be considered a flat plate. In the combination, however, there is the additional consideration of how the shock wave from the cylinder affects the heat transfer over the plate portion. The dive brakes will be treated as flat plates at angle of attack. The fuselage nose is actually a part of a sphere. The fuselage, omitting the side tunnels and canopy, is a body of revolution. Calculations can be made for this shape at zero angle of attack in laminar flow, and in turbulent flow it can be approximated by considering the surface locally a flat plate but using the varying local flow conditions. At small angles of attack, the flow pattern over the body can be considered similar to that at zero angle and the same procedures can be applied, with modifications of the local flow conditions because of the angle of attack. At

high angles of attack, however, the flow around the fuselage will more nearly resemble that on a swept cylinder.

Consider first the wing, which is thin (about 0.05 chord) and has a semicircular-section leading edge with a 3/4-inch diameter. Except for the regions influenced by the tip and by the fuselage (neglecting for the moment the effect of the bow shock from the fuselage nose) the wing can be approximated by a flat plate with a swept-circular-cylinder leading edge.

The X-15 project has stimulated work on swept cylinders, both theoretical and experimental (refs. 1 to 5), so that the heat transfer to the cylindrical part of the leading edge can be calculated with confidence. At some distance back from the leading edge the heat transfer should be nearly that for a flat plate which has also been extensively studied (refs. 6 to 8). The question is how the two calculations should be joined.

Figure 2 shows some wind-tunnel test results which, while not for the same configuration as the X-15 wing, give some idea of the trend to be expected. The model tested was a slab wing with a semicircular leading edge swept 60°. Tests were made in the Langley 11-inch hypersonic tunnel at zero angle of attack, $M = 6.86$, and a Reynolds number of 0.214×10^{6} based on cylinder diameter and free-stream conditions. The ordinate in figure 2 (on a logarithmic scale) is the dimensionless heat-transfer parameter $N_{St}\sqrt{R_D}$ which is used to correlate laminar heat-transfer results at different Reynolds numbers, and the abscissa is X/D, the distance from the stagnation point (measured in the streamwise direction) divided by the leading-edge diameter.

Over the cylinder the experimental values of the heat-transfer parameter $N_{St}\sqrt{R_D}$ agree well with the theory of Goodwin, Creager, and Winkler for swept cylinders (ref. 1). This kind of agreement has been found at several Mach numbers and over a wide range of Reynolds numbers, so that the theory can be considered well established.

For the flat-plate portion of the wing, two curves are shown for both laminar and turbulent flow, which were calculated from the laminar and turbulent theories of Van Driest (refs. 6 and 7). The upper curve in each case (dashed) is for a flat plate at the free-stream conditions, neglecting the effect of the shock from the blunt leading edge. This can be expected to be valid a long distance downstream, where the effect of the strong shock due to the cylinder has been dissipated. The lower curve for each type of boundary layer is calculated by using the total pressure behind the bow shock and then expanding to free-stream pressure to determine the conditions for the flat-plate calculation of heat transfer. The validity of this procedure has been verified experimentally in reference 9 and elsewhere for distances of several nose diameters along the flat plate.

At 60° sweep as in these tests, the heat-transfer coefficients calculated with and without the leading-edge shock are not very different. This is due to a compensating effect - although the local Mach number is lower over the surface affected by the leading-edge shock, the local temperatures are higher and the net result is to bring the curves for the heat-transfer coefficients nearly together. The experimental-data points in figure 2 indicate that the heat-transfer coefficients fall from the value on the cylinder fairly quickly, and in about two leading-edge diameters are close to the values calculated for the flat plate. The data then rise, indicating transition, and approach the turbulent curves.

These data give no indication of how far back on the plate the effect of the shock from the cylinder might be felt. There has been some study of the effect of a blunt leading edge on the pressures over a plate (ref. 10) which indicates that the pressure is still 10 percent higher than free-stream pressure at a distance of 70 leading-edge diameters downstream.

For a given wing profile, a more accurate approach would be to calculate the local pressures over the profile and use these to determine the local flow properties, which are then inserted into the flat-plate theory to determine the local heat-transfer coefficients. There are also more exact theories which can be applied for a given profile if the local velocity outside the boundary layer can be approximated by a power-law variation with distance from the stagnation point. For very thin wings, however, the simpler flat-plate calculation can be expected to give good engineering accuracy in the heat-transfer calculations.

Figure 3 shows a sample of the application of the simple cylinder and flat-plate theories to the X-15 airplane wing at an angle of attack. The conditions assumed are $M = 6.0$, an altitude of 102,000 feet, and an angle of attack of 26°, for which the local Reynolds numbers near the nose are small enough to assure laminar flow.

Values of the heat-transfer coefficient on the nose were calculated from the laminar swept-cylinder theory for an effective sweep angle of 32.75°, which includes the effect of angle of attack in reducing the sweep angle. Two curves are shown for the lower surface behind the cylinder. The dashed line is the heat-transfer coefficient calculated by using the flow conditions behind the shock wave appropriate to a sharp-edge plate at an angle of attack of 26°. The solid line was calculated by using the total pressure at the stagnation point of the cylinder with 32.75° sweep and expanding isentropically to the pressure determined by the plane shock for an angle of attack of 26°, the same pressure as was used for the sharp-edge-plate calculation. For design purposes, transition was arbitrarily assumed to occur 4 inches from the leading edge, and for both laminar and turbulent flow in each of the calculations the flat-plate leading edge was assumed to coincide with the actual wing leading edge.

Near the leading edge, the effect of bluntness should be predominant, and the heat-transfer values should be close to the solid curve in the laminar regions and some distance back in the turbulent regions. However, farther back on the wing the flow affected by the small region of the curved shock at the leading edge must eventually become submerged in the boundary layer, after which the heat-transfer coefficients will approach the dashed line, their values being determined by the conditions behind the plane shock.

The difference between the two calculations in the turbulent region is appreciable. However, it is not yet clear how far back the effect of bluntness can be expected to continue, particularly at an angle of attack.

On the upper surface, behind the nose, the heat-transfer coefficients are computed with the assumption that the flow separates from the leading edge of the flat plate. In the method used, which is based on results from a limited number of wind-tunnel tests, the separated-flow heat-transfer coefficients were assumed to be half those for a flat plate at zero angle of attack. The whole problem of heat transfer in separated flows has been studied very little and considerable work must be done to establish the actual behavior, but for design purposes the significant fact is that the heat-transfer coefficients are very low compared with those on the lower surface. The rough estimate based on 1/2 the value for a flat plate at zero angle of attack is a conservative one. If the flow should remain attached, the heat-transfer coefficients would be lower still.

The effect of the fuselage bow shock on the wing will require study with the complete model. The actual line of intersection of the shock and the wing will move around as the shock-wave angle changes with the changing Mach number and angle of attack in a flight, and thus local effects at the shock-surface intersections will be spread out. The conditions used in calculating the heat transfer on the rest of the wing behind the shock must include the effect of the fuselage shock.

Another area of high heat transfer is on the dive brakes when they are extended. The specific X-15 configuration has not been tested, but an insight into the method of calculating the heat transfer to the dive brakes can be obtained from the results shown in figure 4, which were obtained on a flare at the rear of a body of revolution at $M = 6.86$. This figure has been taken from reference 11. The heat-transfer data on the forward part of the body follow the laminar curve, but the coefficients rise on the cylinder and indicate that just ahead of the flare the boundary layer is turbulent. In this case the shock was attached at the cylinder-flare juncture. Because the static-pressure rise across the shock is large, the body boundary layer has only a small effect on the flare boundary layer. Therefore, except very near the juncture, the heat transfer can be calculated as though the boundary layer starts at

zero thickness at the juncture. The theoretical curve shown in figure 4 was calculated by using the turbulent flat-plate theory of Van Driest (ref. 7) and the local flow conditions behind the shock wave. It can be seen in this figure that the experimental measurements are in good agreement with values calculated for a flat plate at the conditions behind the shock. A similar approach would appear to be reasonable on the dive brakes of the X-15.

The nose of the fuselage consists of a 6-inch-diameter sphere mounted in a socket which permits rotation. The sphere is instrumented to measure angles of attack and yaw, as described in a subsequent paper by I. Taback and G. M. Truszynski. In flight, the Reynolds number on the sphere will be low enough to permit the assumption of laminar boundary layer.

Figure 5 shows the distribution of the dimensionless heat-transfer parameter $N_{St}\sqrt{R_D}$ around the sphere and on the lower side of the mounting structure at $M = 6.86$. On the sphere, experimental values agree well with the laminar theory of Stine and Wanlass for bodies of revolution. (See ref. 12.) On the stagnation point of the lower lid, however, the heat-transfer rates are very large. Schlieren photographs of this configuration show a shock in the flow just ahead of this point. The problem is being studied further to determine how to reshape the support cone to reduce the heating rates to tolerable values. The heat-transfer values on the upper side of the support cone are very low - too small to show at this scale.

The fuselage of the X-15 is basically a body of revolution with side fairings attached. This is an awkward shape for theoretical calculations. For zero angle of attack, it may be possible to neglect the distortion of the cross section and treat the body, or at least the part of it outside the fairings, as a body of revolution, for which theory and experimental verification are available.

Figure 6 shows preliminary results for a body of revolution similar to the X-15 nose at conditions giving laminar flow. The body was a Karman nose with a fineness ratio of 5, modified by the addition of a tangent 10° half-angle cone in front and followed by a short section of cylinder. This shape is not the X-15 nose shape, but the distribution of heat transfer should be similar.

The circles are $N_{St}\sqrt{R_D}$ plotted on a logarithmic scale from tests at $M = 6.86$ with laminar boundary layer. On the conical tip, the data agree well with the cone theory obtained by applying the Mangler transformation for cones to the flat-plate theory. The experimental data fall off from the cone values as the body shape varies from conical and reach good agreement with the laminar flat-plate theory on the cylinder. The laminar theory of Stine and Wanlass (ref. 12) for this body of revolution

at $M = 6.86$ is shown merging into the curve for the cone at the forward end and meeting the flat-plate calculation at the cylinder, and it is in good agreement with the data over the entire nose.

The squares are values obtained on the same body at $M = 3.69$ in the Langley Unitary Plan wind tunnel at a higher Reynolds number. The values are very close to those for $M = 6.86$, as is the Stine and Wanlass theory for $M = 3.69$, indicating that for laminar boundary layers the Mach number effect over this range is small.

Another series of tests was made on the same model at $M = 3.69$ with roughness applied in a ring near the nose to give a turbulent boundary layer. The preliminary experimental results are shown in figure 7 by circles. Also shown is the turbulent theory for the cone at the nose, calculated by the method of reference 13, and for the flat plate with the use of local flow conditions on the cylinder. The data show roughly the same pattern as was shown for laminar flow, a trend from values near those of the cone at the forward end down to the flat-plate values on the cylinder. There is as yet no turbulent analog of the Stine and Wanlass theory, but experimental data like these can be used to fit an empirical curve for the transition between the cone and flat-plate calculations.

At angles of attack, the prediction of heat transfer to bodies becomes much more uncertain. There is no generally applicable theory such as the Stine and Wanlass theory for zero angle of attack in laminar flow. At small angles of attack, the streamlines around the body should be nearly longitudinal, and an approximation can be made by using cone or flat-plate theory with varying local conditions along the length. At large angles of attack, the body can be approximated by a swept cylinder with varying diameter.

These two kinds of approximation are shown in figure 8 for a turbulent boundary layer. The variation of the nondimensional heat-transfer parameter N_{St} with angle of attack is shown for the lower or windward stagnation line at two stations along the length of the same modified Karman nose discussed earlier at $\alpha = 0$. The curves labeled "longitudinal flow theory" were calculated by using the flat-plate heat-transfer relations for turbulent flow with the local conditions at the two stations.

Local conditions were calculated for each angle of attack by finding the pressure on a cone at zero angle of attack tangent to the lower stagnation line at the nose, and then expanding two-dimensionally along the body to the local body inclination.

The curves labeled "crossflow theory" were computed by assuming that at each station the shock was that appropriate for the tangent cone of the local inclination angle, and then calculating the stagnation-line turbulent heat transfer from the swept-cylinder theory of reference 5, using conditions behind the cone shock.

The experimental points are from tests in the Langley Unitary Plan wind tunnel, with roughness applied in a strip along the lower stagnation line and in a ring at the nose. It can be seen that the data agree fairly well with the crossflow theory at the higher angles and with the longitudinal-flow theory at zero angle of attack, but the experimental points suggest a more rapid increase with angle of attack than is predicted by the longitudinal-flow calculation at small angles and a change in the trend between 14° and 21°. There is need for further work to develop an approach that will be more nearly adequate for moderate angles than either of those described here.

The use of crossflow theory at high angles of attack is further corroborated in figure 9, which shows in polar coordinates the distribution of heat-transfer coefficients around the body at the $X/D = 5.1$ station, where the body is cylindrical. Data are presented for angles of attack of 0°, 7°, 14°, 21°, and 25°. The theoretical curve for $\alpha = 25^O$ was obtained by using the theoretical correlation parameter presented in reference 5 with some unpublished experimental results by the same authors for the distribution of local heat-transfer rates around a swept cylinder with turbulent flow from the stagnation line. At 25° the agreement of theory and experimental values is good.

The data for $\alpha = 14^O$ and $\alpha = 21^O$ fall very nearly on the same curve. This result indicates the need, mentioned before, for further study in this range.

The wind-tunnel results presented in this paper have been compared with available theories to give some indication of how well the theories can be expected to predict the heat transfer to the full-scale airplane. In general, for isolated parts of the airplane which can be approximated by simple shapes, the heat transfer can be satisfactorily predicted by available theories. For regions where there is interference between the flows on adjacent parts - for example, the wing-fuselage juncture, cockpit canopy, and side fairings - more detailed studies are required on the specific configuration, and for this purpose a complete scale model is being prepared by North American Aviation for wind-tunnel tests in the Langley Unitary Plan wind tunnel.

REFERENCES

1. Goodwin, Glen, Creager, Marcus O., and Winkler, Ernest L.: Investigation of Local Heat-Transfer and Pressure Drag Characteristics of a Yawed Circular Cylinder at Supersonic Speeds. NACA RM A55H31, 1956.

2. Eggers, A. J., Jr., Hansen, C. Frederick, and Cunningham, Bernard E.: Theoretical and Experimental Investigation of the Effect of Yaw on Heat Transfer to Circular Cylinders in Hypersonic Flow. NACA RM A55E02, 1955.

3. Beckwith, Ivan E.: Theoretical Investigation of Laminar Heat Transfer on Yawed Infinite Cylinders in Supersonic Flow and a Comparison With Experimental Data. NACA RM L55F09, 1955.

4. Feller, William V.: Investigation of Equilibrium Temperatures and Average Laminar Heat-Transfer Coefficients for the Front Half of Swept Circular Cylinders at a Mach Number of 6.9. NACA RM L55F08a, 1955.

5. Beckwith, Ivan E., and Gallagher, James J.: Experimental Investigation of the Effect of Boundary-Layer Transition on the Average Heat Transfer to a Yawed Cylinder in Supersonic Flow. NACA RM L56E09, 1956.

6. Van Driest, E. R.: Investigation of Laminar Boundary Layer in Compressible Fluids Using the Crocco Method. NACA TN 2597, 1952.

7. Van Driest, E. R.: Turbulent Boundary Layer in Compressible Fluids. Jour. Aero. Sci., vol. 18, no. 3, Mar. 1951, pp. 145-160, 216.

8. Rubesin, M. W., and Johnson, H. A.: A Critical Review of Skin-Friction and Heat-Transfer Solutions of the Laminar Boundary Layer of a Flat Plate. Trans. A.S.M.E., vol. 71, no. 4, May 1949.

9. Crawford, Davis H., and McCauley, William D.: Investigation of the Laminar Aerodynamic Heat-Transfer Characteristics of a Hemisphere-Cylinder in the Langley 11-Inch Hypersonic Tunnel at a Mach Number of 6.8. NACA TN 3706, 1956.

10. Bertram, Mitchel H.: Viscous and Leading-Edge Thickness Effects on the Pressures on the Surface of a Flat Plate in Hypersonic Flow. Jour. Aero. Sci. (Readers' Forum), vol. 21, no. 6, June 1954, pp. 430-431.

11. Becker, John V., and Korycinski, Peter F.: Heat Transfer and Pressure Distribution at a Mach Number of 6.8 on Bodies With Conical Flares and Extensive Flow Separation. NACA RM L56F22, 1956.

12. Stine, Howard A., and Wanlass, Kent: Theoretical and Experimental Investigation of Aerodynamic-Heating and Isothermal Heat-Transfer Parameters on a Hemispherical Nose With Laminar Boundary Layer at Supersonic Mach Numbers. NACA TN 3344, 1954.

13. Van Driest, E. R.: Turbulent Boundary Layer on a Cone in a Supersonic Flow at Zero Angle of Attack. Jour. Aero. Sci., vol. 19, no. 1, Jan. 1952, pp. 55-57, 72.
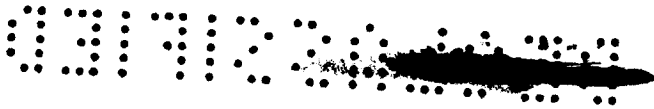
BREAKDOWN OF AIRPLANE FOR HEAT-TRANSFER CALCULATIONS
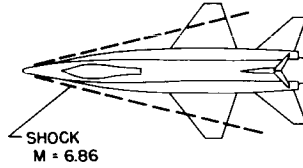
SHOCK
M = 6.86

WING AND TAIL SURFACES
   LEADING EDGE
      FLAT PLATE (WITH AND WITHOUT BOW SHOCK)
      EFFECTS OF FUSELAGE SHOCK

DIVE BRAKE, EXTENDED

FUSELAGE NOSE

FUSELAGE
   ZERO ANGLE OF ATTACK
      LOWER STAGNATION LINE AT ANGLE OF ATTACK
         LONGITUDINAL FLOW
         CROSS FLOW

Figure 1

HEAT TRANSFER TO 60° SWEPT WING
$\alpha = 0°$; $M = 6.86$; $R_D = 0.214 \times 10^6$

--- NEGLECTING BOW SHOCK
— INCLUDING BOW SHOCK

CIRCULAR CYLINDER, 60° SWEEP
LAMINAR

FLAT PLATE, TURBULENT

FLAT PLATE, LAMINAR

$N_{St} \sqrt{R_D}$

STREAMWISE $\frac{X}{D}$
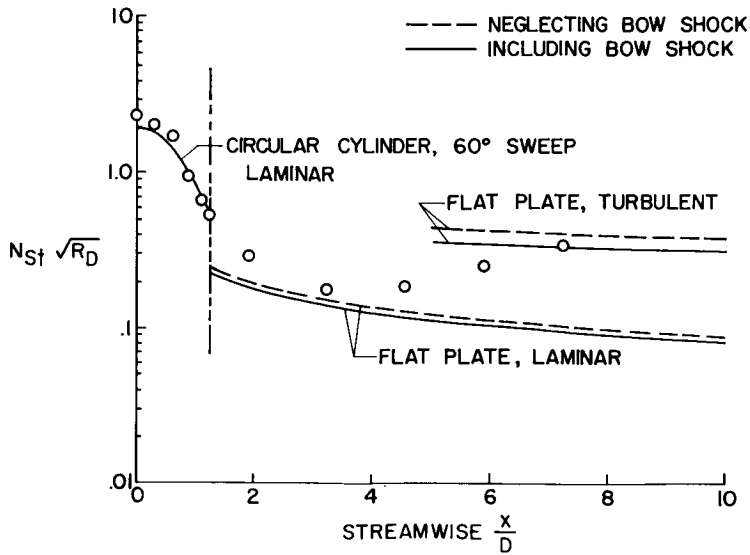
Figure 2

HEAT-TRANSFER COEFFICIENTS ON FLAT-PLATE WING
AT 26° ANGLE OF ATTACK

$\Lambda_{LE} = 36.75°$; M = 6.0; ALT. = 102,000 FT
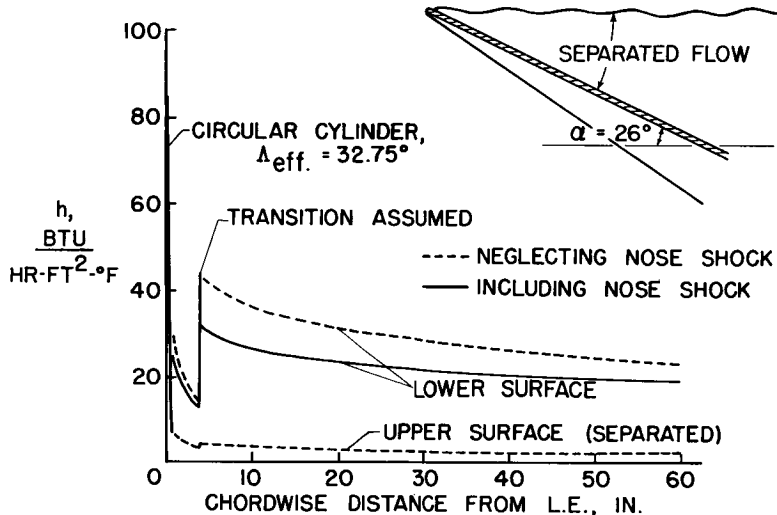
Figure 3

HEAT TRANSFER ON FLARE

$\alpha = 0°$; M = 6.86; $R_D = 0.63 \times 10^6$
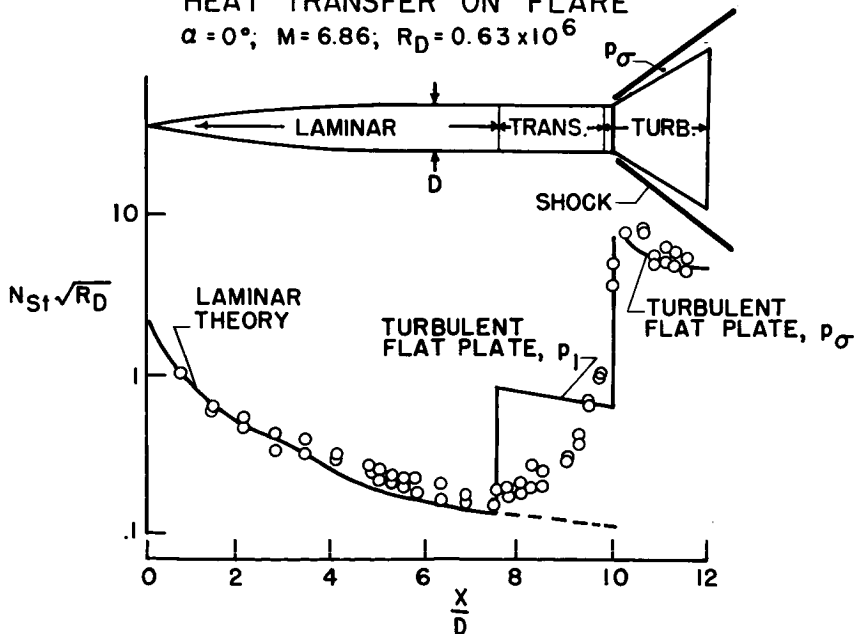
Figure 4

$N_{St}\sqrt{R_D}$ ON FUSELAGE NOSE

$M = 6.86;$ $R_D = 1.3 \times 10^6;$ $\alpha = 24°$
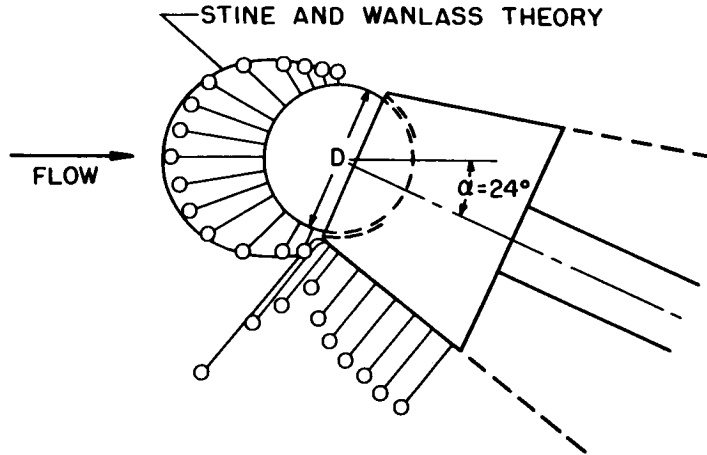
Figure 5

HEAT TRANSFER TO KARMAN NOSE AT ZERO ANGLE OF ATTACK
LAMINAR FLOW
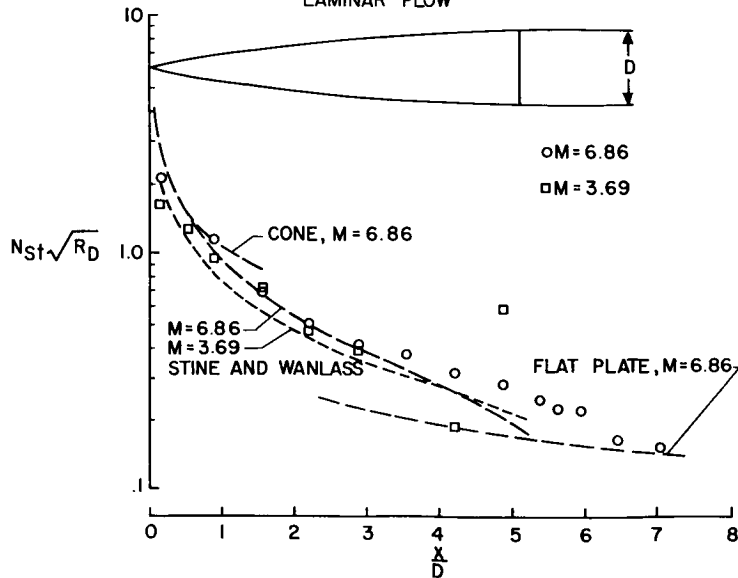
Figure 6

HEAT TRANSFER TO KARMAN NOSE AT ZERO ANGLE OF ATTACK
TURBULENT FLOW

CONE

$\circ$ M=3.69; R_D= 1.25 × 10^6

FLAT PLATE

$N_{St}\sqrt{R_D}$

$\frac{X}{D}$
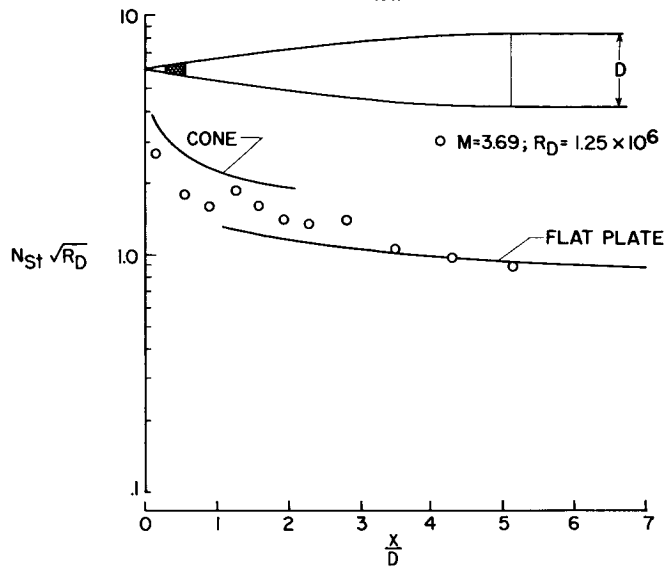
Figure 7

HEAT TRANSFER TO LOWER STAGNATION LINE AT ANGLES OF ATTACK
M = 3.69; R_D = 1.23 × 10^6;   TURBULENT FLOW

ROUGHNESS

$\frac{X}{D}$ = 2.8

$\frac{X}{D}$ = 5.1

8×10^{-3}

CROSSFLOW THEORY

N_{St}

$\circ$ EXP.
M=3.69

LONGITUDINAL
FLOW THEORY

α, DEG

8×10^{-3}

CROSSFLOW THEORY

LONGITUDINAL
FLOW THEORY

α, DEG
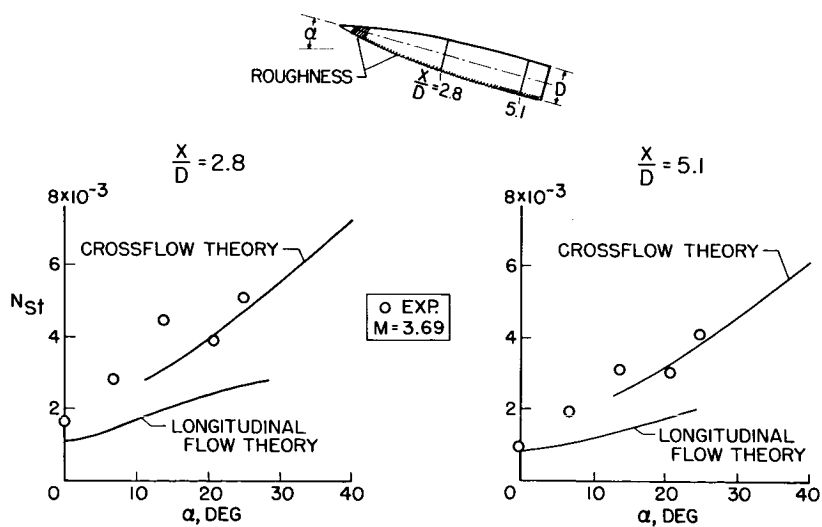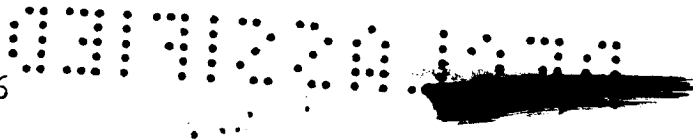
Figure 8

CIRCUMFERENTIAL DISTRIBUTION OF STANTON NUMBER
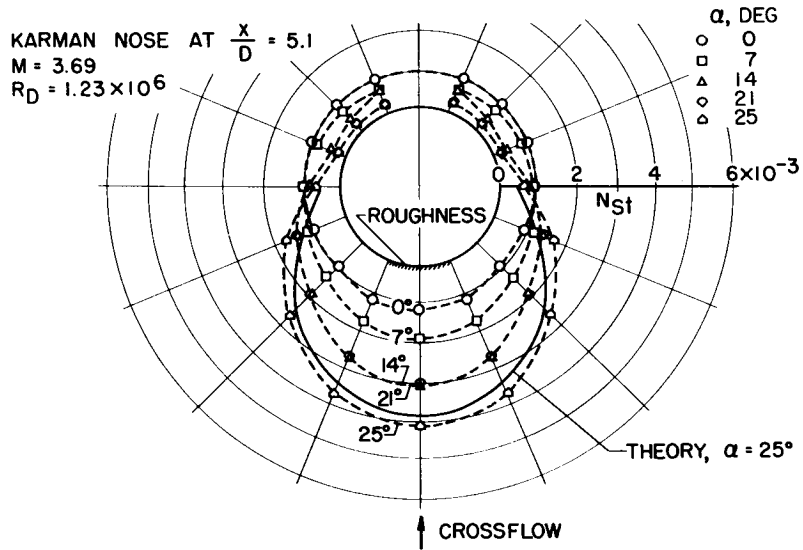
Figure 9

ESTIMATED STRUCTURAL TEMPERATURES FOR THE X-15 AIRPLANE

By Gordon W. Campbell
North American Aviation, Inc.

C. B. Neel
Ames Aeronautical Laboratory

and Martin R. Kinsler
North American Aviation, Inc.

INTRODUCTION

In the paper by William V. Feller, the techniques and theories evolved for predicting aerodynamic-heating input rates to various portions of the airplane have been discussed. Before this information can be put to use by the designer, another link must be inserted, namely, temperature prediction and control. By temperature prediction and control is meant the iterative engineering process of estimating structural temperatures on the basis of an assumed structure and airplane mission, and then reevaluating these parameters until an airplane structure, mission, and temperature consistent with the desired design criteria of the airplane are achieved.

It is the purpose of this paper to present the results of temperature prediction and control studies made by North American Aviation and to point out certain problem areas which still exist.

DISCUSSION

Temperature Definitions

Because of the transient nature of the missions of the X-15 airplane, it is well to examine the time-temperature history of a typical flight. Figure 1 shows certain significant temperatures associated with the speed mission previously described by Charles H. Feltz.

The top curve describes the familiar stagnation temperature encountered during this flight of the X-15. This temperature is seen to maintain a peak value of $3,500^\circ$ F for approximately 1 minute.

The second curve gives the history of the recovery temperature, which, of course, follows the trend of the stagnation temperature and reaches a peak at about 3,300° F.

As John V. Becker indicated in a previous paper, high-temperature skins will lose a considerable amount of heat by radiation. When a surface is at such a temperature that the heat loss by radiation is equal to the heat input from the boundary layer, the surface is said to be at equilibrium temperature.

The third curve describes the equilibrium temperature for a point on the lower surface of the wing, about midspan, and at the 40-percent-chord line. The equilibrium temperature will vary over the airplane as a function of the local heat-transfer characteristics and the local radiation characteristics. Obviously, areas having high heat-transfer coefficients, such as the wing leading edge, would also have higher equilibrium temperatures.

It is interesting to note that the equilibrium temperature does not follow the shape of the recovery-temperature curve because of the variation in heat-transfer coefficient during the mission.

Since the missions of the X-15 are all transient in nature, it is not possible actually to reach the peak value of equilibrium temperature in any structure heated only by aerodynamic heating. As an example, the fourth curve shows the calculated skin temperature for this same point on the wing. A skin gage of 0.064 inch was assumed. Here the skin temperature lags behind the equilibrium temperature and never reaches the peak value of equilibrium temperature. However, if the skin gage were made so thin that essentially no heat sink were available, its transient temperature would, in the limit, coincide with the equilibrium temperature.

Time Relationship - Temperature and Loads

The transient nature of the X-15 flight must also be considered in determining the relationship between structural temperatures and aerodynamic loads. In figure 2 the time-temperature history of a point on the wing skin has been plotted, in addition to the aerodynamic parameters which will determine aerodynamic loads, such as flight dynamic pressure and normal acceleration. Here the wing skin reaches its peak temperature at approximately 190 seconds. This peak temperature results from the 7.33g recovery. The largest dynamic pressures, however, occur at approximately 30 seconds and have dwindled to about one-half of their maximum value by the time peak temperatures have been reached. Loads due to normal forces, on the other hand, occur close to the peak wing skin temperature. As will be shown later, the effects of temperature, temperature gradient, and normal acceleration are additive in this condition and therefore present a definite structural design problem.

Thus, time is important both in predicting peak transient temperatures and in relating these temperatures with the occurrence of other phenomena such as aerodynamic loading.

Wing Skin Temperatures

It should be noted that one of the many research objectives of this airplane is to obtain actual operating experience with high-temperature structures. The structural temperature limit is, of course, established by the high-temperature characteristics of practical structural materials. The use of Inconel X as the basic structural material for this airplane allowed a nominal temperature limit of 1,200° F to be established.

Figure 3 shows the results of the computation of the X-15 wing temperatures for the speed mission. At the top of the figure is a diagram of the wing plan form for the X-15 airplane and directly below it a diagram of the variation of skin gage from the root to the tip of both the upper and lower surfaces. Temperatures at three wing stations and at three chord stations are given for both the upper and lower surfaces.

The temperatures calculated here are thin-skin temperatures; that is, heat conduction to the internal structure has not been considered. Also, as explained by William V. Feller, it was necessary to ignore regions of interference of the fuselage and tip and to assume a completely turbulent boundary layer. The presence of the fuselage was considered, however, in determining the radiation configuration factor.

It will be noted that there is one region near the leading edge and tip of the wing where the calculations show that the nominal 1,200° F design limit has probably been exceeded. It must be remembered, however, that these computations are for an unsupported skin. As will be shown later, the extra heat capacity supplied by the wing spars considerably reduces the skin temperature in close proximity to the spars. At the tip the spars are very closely spaced, and it is believed that further calculations that include this effect will show this local hot spot to fall within the 1,200° F design limit.

In the paper by John V. Becker the prediction was made that the use of Inconel X in the speed range of the X-15 might lead to a structure sized for load rather than limit temperatures. It will be noted that over most of the rest of the wing this condition was found to be true and peak temperatures as low as 480° F are calculated for the upper surface.

Another item always of interest to the designer is the temperature differential or gradient in the structure. In figure 3 it is seen that,

between the upper and lower surfaces of the wing, maximum temperature differentials for the unsupported skin of approximately 400° F exist. These differentials occur near the leading edge at the root of the wing. Minimum differentials occur near the leading edge at the tip and are in the order of 270° F.

The problem of temperature gradients is further illustrated in figure 4, where the chordwise temperature distributions along the wing skin for the upper and lower surfaces are shown for a position near the midspan. A sketch of the wing cross section showing the spar locations is given at the bottom of the figure to aid in visualizing chordwise positions for the temperatures shown. These calculations include the effects of conduction and were performed on an electrical heat-flow analog computer at the Ames Aeronautical Laboratory, which consists of a large network of resistances and capacitances with provision for variable heat-input and radiation functions. The results are for the mission described previously as the high-altitude mission and represent the temperatures attained during the pullout phase of the trajectory. It is seen that the presence of the spars, which act as heat sinks, would cause large depressions in the skin-temperature distribution for the lower surface. These variations in skin temperature were calculated to be as great as 300° F in a chordwise distance of about 2 inches.

Because of the thinner skin on the lower surface and the effect of the high angle of attack, the lower surface would heat more rapidly than the upper surface, which would tend to make the wing warp upward. The maximum temperature difference between upper and lower surfaces was found to be almost 500° F in the forward region of the wing. These temperature differences would occur during pullout of the airplane from high altitude when the normal acceleration and dynamic pressure are highest for this trajectory. Under such conditions, the highest aerodynamic and thermal-stress loads would occur simultaneously and would be additive. This, then, appears to be a critical condition from a design standpoint.

Wing Leading-Edge Temperatures

The leading edges themselves, of course, are subjected to the most severe heating of any part of the wing and have been the subject of a considerable amount of study. Many schemes were conceived in the early thinking about this problem, such as leading edges which would erode away, solid leading edges with high specific heat and thermal conductivity, and leading edges made of materials resistant to ultra-high temperatures, such as ceramics and titanium carbide. As a starting point, however, calculations were made for a leading edge of 1/8-inch-thick Inconel X bent to a 3/8-inch leading-edge radius. This configuration is shown in figure 5. The portion of the leading edge shown in the sketch was broken up into 16 sections and the electrical analog was

written for the system. The results are shown in the accompanying plot by the two solid lines. The top line represents the computed stagnation-point skin temperature. The bottom line shows the corresponding temperature of a point approximately 3 inches back from the stagnation point. A peak temperature of $1,640°$ F and a gradient of $1,390°$ F in 3 inches are indicated. Although this configuration was obviously an undesirable one, it did reveal some unexpected trends. The stagnation-point temperature was much farther from the equilibrium temperatures shown by the asterisks than had been anticipated. The rather large difference between computed stagnation-point and equilibrium temperatures was believed to be due to a more rapid conduction of heat away from the leading edge through the skin than had been assumed. To check this theory, an analog solution was made considering only the segment of the leading edge included in a $60°$ arc. The solution this time showed close agreement with the equilibrium temperatures, proving the importance of the skin rearward of the leading edge as a heat sink.

The question might then be raised as to whether or not the previous analysis of a 4-inch section of the leading edge was too conservative. The leading-edge temperature obtained from an independent calculation in which the entire wing was represented is shown by the dashed curve in figure 5 and is seen to agree well with the temperature calculated for the 4-inch section. This curve was calculated by employing the electrical heat-flow analog computer at the Ames Aeronautical Laboratory. The good agreement indicates that sufficiently accurate calculations of the leading-edge temperature can be obtained for this configuration by considering only a relatively small portion of the wing.

As a result of these studies, a new leading-edge design is being developed at North American Aviation which will result in workable temperatures and temperature gradients. A preliminary estimate indicates that the metal thickness at the stagnation line will be about 1/4 inch, tapering off to the 1/8-inch Inconel skin about 1/2 inch behind the leading edge.

Wing Spar Temperatures

In addition to the temperature of the wing skin, the structural designer is interested in the temperature gradients throughout the main structural members or spars. In figure 6 is shown a typical section of the X-15 wing spar. The surfaces 1 and 7 represent thin skins some distance from the supporting structure. Surfaces 2 and 6 represent skins adjacent to the spar. Points 3 and 5 represent locations on the spar cap adjacent to the web. Point 4 is located at the center of the web.

On the right of the figure are the curves for the variation of temperature with position for this spar and skin assembly. The numbers on

the curves correspond to those on the sketch of the structure. The temperatures shown are those at the time of the 7.33g pullout. The maximum temperature difference for the assembly is seen to be about 820° F. It will be noticed that the greatest gradient occurs in the lower spar cap.

Fuselage Skin Temperatures

Figure 7 shows the skin temperatures that will be reached on the top center line of the fuselage during the speed mission. Here again maximum temperatures occur near the nose of the airplane and are close to the desired value of 1,200° F. Rearward along the top center line of the fuselage the temperatures drop markedly and the skin gages required are again not a function of temperature but are determined by other structural requirements. These temperature estimates were made without considering the effects of the wing, empennage, side fairings, or canopy. However, since the general temperature level of the top center line of the fuselage is so low, no serious design problems are expected to result from slight increases in heat-transfer coefficients caused by local effects.

The bottom of the fuselage presents a more difficult analysis because of the high angle of attack experienced during the pullout maneuver. Initial calculations were based on an analysis in which longitudinal flow was assumed and turbulent flat-plate theory was applied. Under these conditions, the skin gages of the rear part of the fuselage were again determined by loads rather than temperature. However, as the crossflow data described by William V. Feller became available, it became apparent that during the pullout much higher heat-transfer coefficients might be experienced than had been anticipated. Figure 8 presents the calculated time-temperature history for a point on the bottom of the rearward part of the fuselage with a skin gage of 0.062 inch. The calculations are based on an empirical equation derived from the crossflow data on yawed cylinders. The resulting peak temperature, which occurs shortly after pullout, is seen to be approximately 1,300° F. However, the side fairings and wings may considerably alter the crossflow characteristics on the fuselage. Thus, there is a rather wide band of possible temperatures or skin-gage alterations on the bottom of the fuselage.

Model Program

In order to obtain more reliable heat-transfer data for a further analysis of the fuselage problem as well as other problems of the X-15 airplane, a 1/15-scale heat-transfer model is being constructed for wind-tunnel testing. This model is of thin-skin construction and

has approximately 300 thermocouples in the skin, 200 static-pressure taps, and four total-pressure rakes. Measurements of time-temperature histories of the thin skin will permit computation of local heat-transfer coefficients. The local pressure instrumentation will permit the correlation of the heat-transfer coefficients with local aerodynamic parameters.

Figure 9 shows the desired test conditions for the model in relationship to the wind-tunnel operating conditions available. The shaded area indicates the altitude-Mach number band flown by the X-15 for both the speed mission and the high-altitude mission. For a 1/15-scale model it is possible to plot on these coordinates the operating range of existing wind tunnels of the size appropriate to this work. Here are shown the Langley Unitary Plan wind tunnel (4 by 4 feet) and the Arnold Engineering Development Center B minor tunnel which is an interim fixed-nozzle version of the B tunnel.

The critical fuselage-temperature problem at high angle of attack is designated by the solid black area for both the speed and high-altitude missions. It is seen that neither tunnel covers the Mach number range; however, the most important conditions would be well bracketed if tests were conducted in both of these tunnels.

Tests are currently scheduled in the Langley Unitary Plan wind tunnel for February 1957.

CONCLUSION

As was pointed out at the beginning of this paper, temperature prediction and control is an iterative process by which a reasonable combination of structure, mission, and structural temperatures is attained. The information just presented is obviously only an intermediate result of the iterative process and will be refined as further research and analyses are accomplished.

SYS-447L **CHARACTERISTIC TEMPERATURE HISTORIES**
SPEED DESIGN MISSION
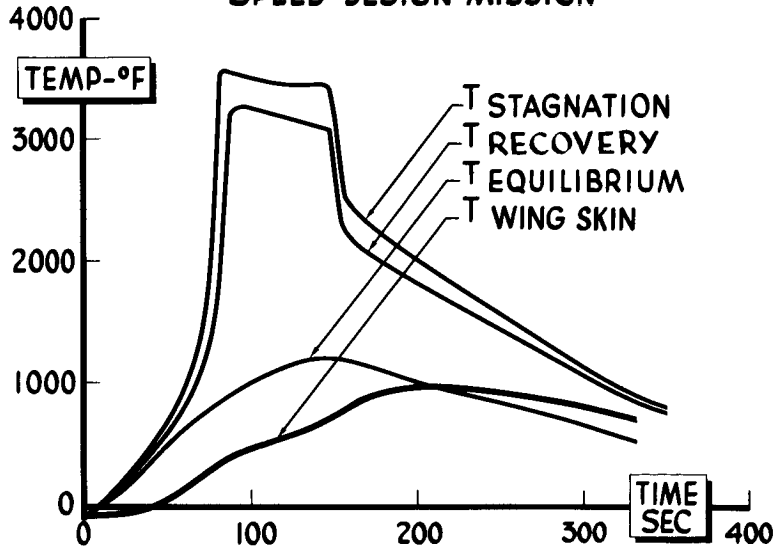
Figure 1

SYS-447L **STRUCTURE TEMP & AERODYNAMIC PARAMETERS VS TIME**
SPEED DESIGN MISSION
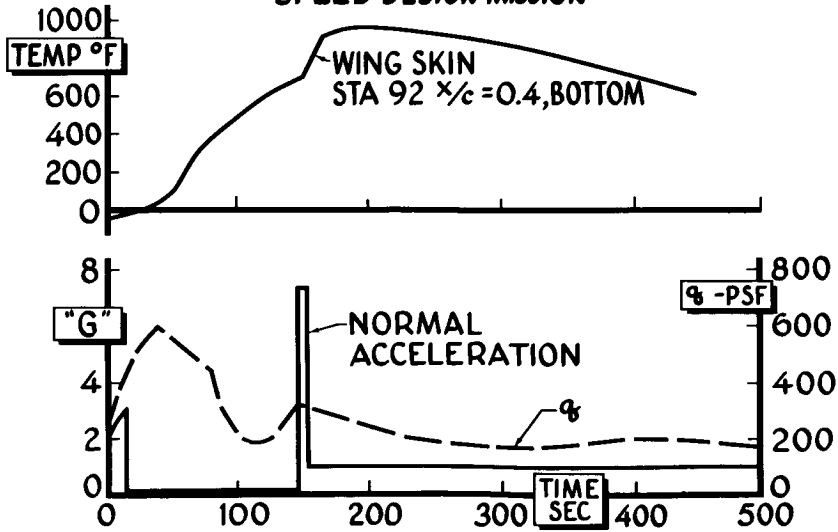
Figure 2

SYS-447L **WING SKIN TEMPERATURES**

x/c = 0.10 — 730 / 1130

840 / 1190

0.40 — 550 / 920

1110 / 1390

650 / 960

870 / 1150

0.75 — 480 / 830

540 / 870

780 / 1050

.125 IN. / .085 IN.

.050 IN. / .045 IN.
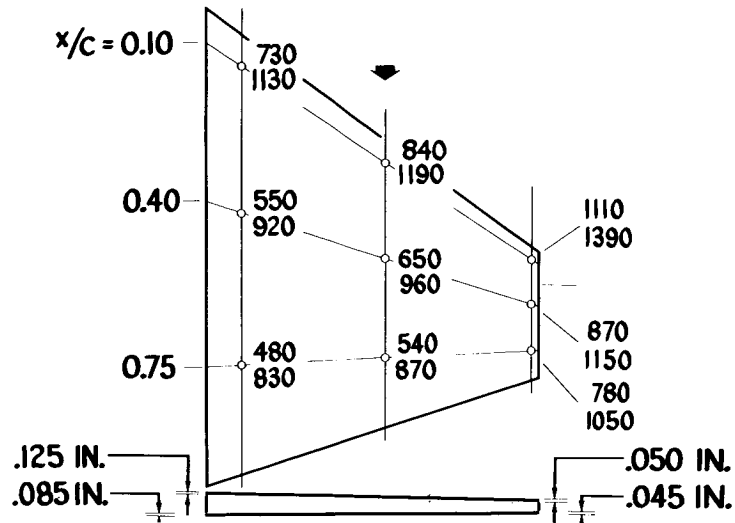
Figure 3

SYS-447L **CHORDWISE WING SKIN TEMPERATURE**
HIGH ALTITUDE MISSION

WING STA 100

TEMP-°F

LOWER

UPPER

X/C

Figure 4

SYS-447L WING LEADING EDGE TEMPERATURES
SPEED DESIGN MISSION

Figure 5

SYS-447L WING SPAR TEMPERATURES
SPEED DESIGN MISSION

Figure 6

SYS-447L
FUSELAGE SKIN TEMPERATURES
SPEED DESIGN MISSION — TOP ₵
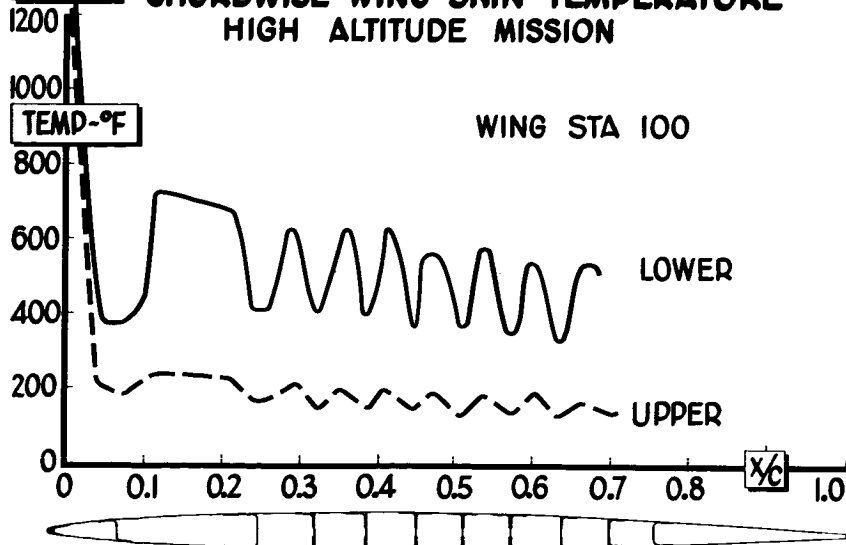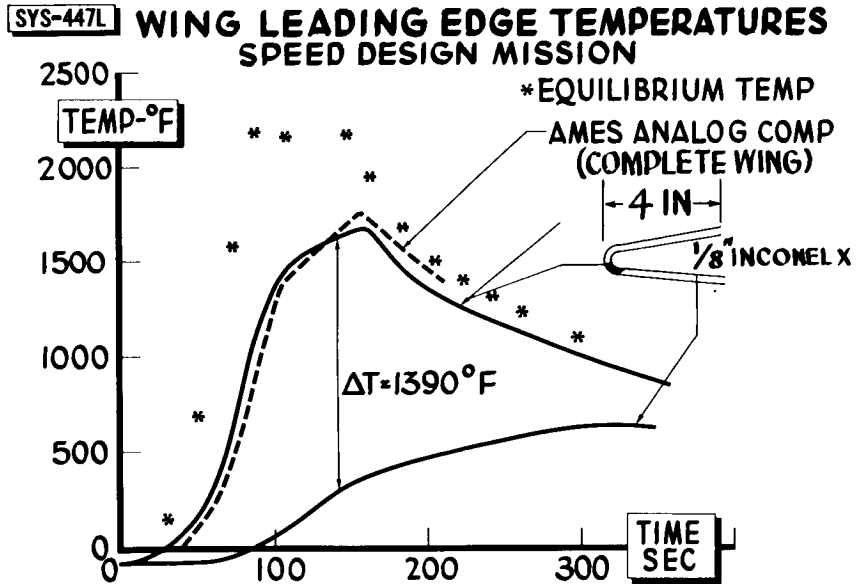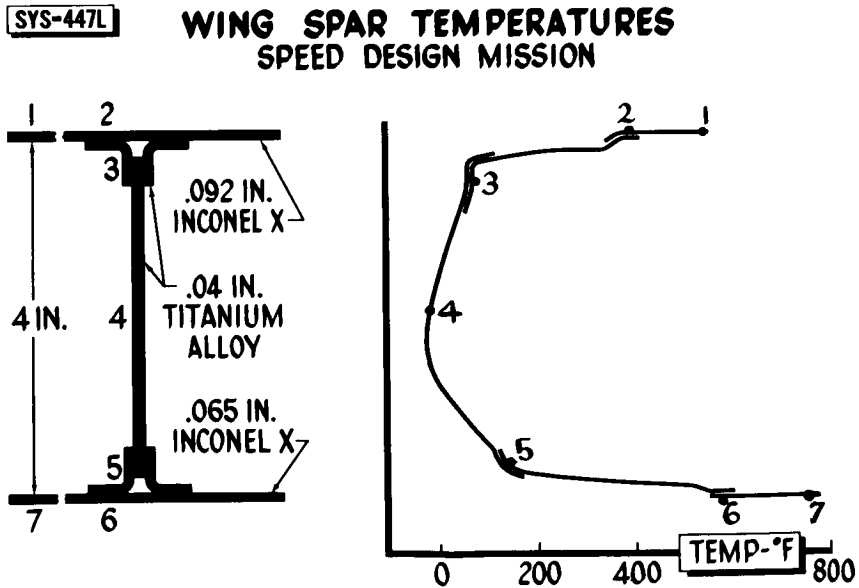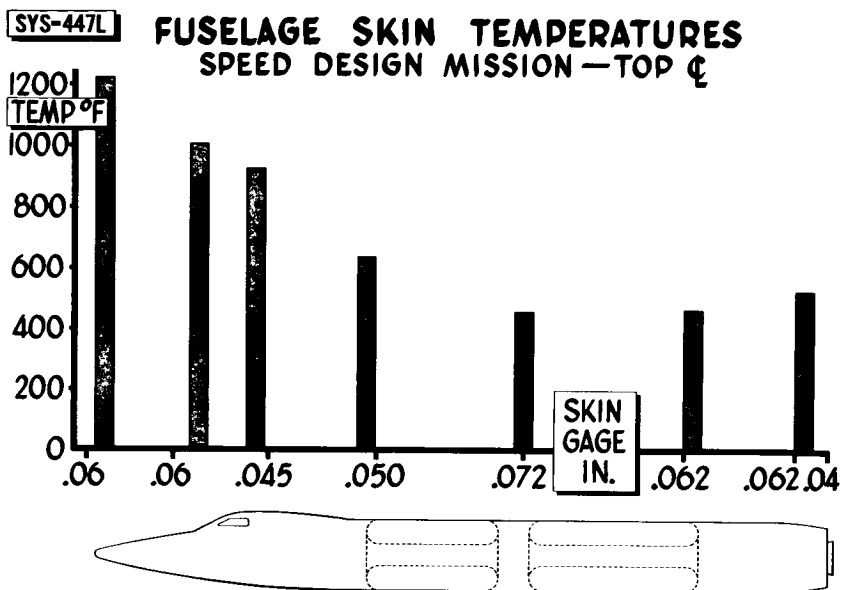
Figure 7

SYS-447L
FUSELAGE SKIN TEMPERATURE HISTORY
SPEED DESIGN MISSION

HIGH α

STA 550
.062 INCONEL X

CROSSFLOW, TURB
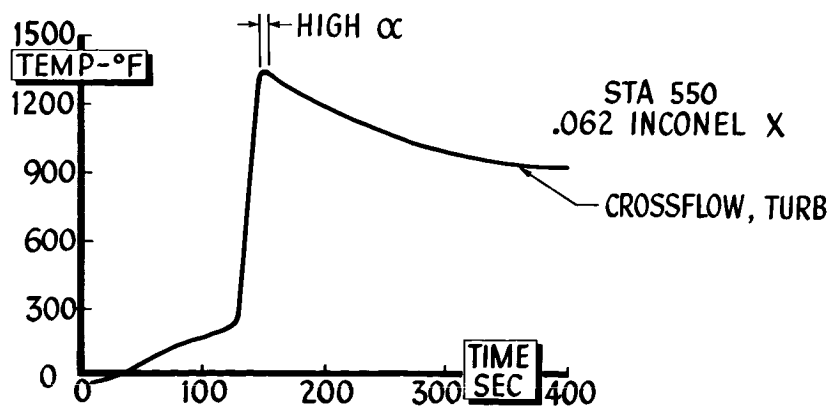
Figure 8

SYS-447L
WIND TUNNEL TESTS
HEAT TRANSFER-1/15 SCALE MODEL

250

ALT-1000 FT

200

150   LANGLEY
       UNITARY
       4 FT X 4 FT

100

50

0
   0   1   2   3   4   5   6   M 7

AEDC
B
MINOR

HIGH α
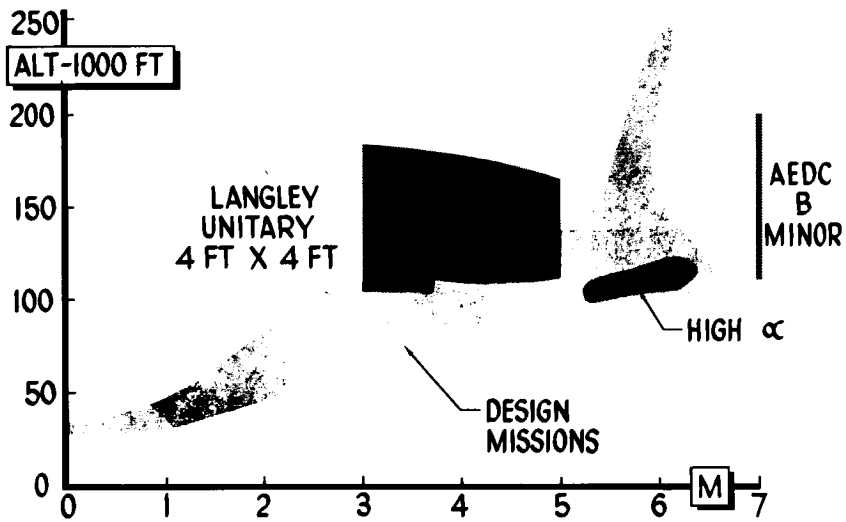
DESIGN
MISSIONS

Figure 9

STRUCTURAL DESIGN OF THE X-15 RESEARCH AIRPLANE

By Richard L. Schleicher

North American Aviation, Inc.

INTRODUCTION

A sketch of the North American X-15 airplane is presented in figure 1. The structure of the X-15 airplane is characterized by several interesting features. For the first time in aeronautical design, environmental conditions which hitherto were associated with the design of missiles have now been assigned to a manned aircraft. Many new problems have arisen - some have been resolved and others remain to be solved. Simplicity has been emphasized wherever possible to aid in the current solution and future analysis of recorded data. In the design of the structure, wherein it is applicable, specification MIL-S-5700 is in effect.

The material presented herein will cover the wing, the fuselage in the region of the propellant tanks, and the empennage.

A list of related papers is presented as a bibliography.

DISCUSSION

Figure 2 shows a typical design mission. From the structural viewpoint, two regions of the flight regime have generated most critical design parameters; namely, (a) launching at a weight of 30,000 pounds, during which drag accelerations are highest but temperatures nominal, and (b) reentry into the atmosphere at a weight of 12,500 pounds, where maximum aerodynamic heating occurs simultaneously with high loads. This figure depicts the maximum wing skin temperatures and acceleration plotted against time during a typical high-speed mission which includes the reentry condition. It will be noted that the maximum loads occur shortly before the maximum temperature has been attained.

Figure 3 presents a sketch of the X-15 wing outer panel. The wing outer panel is a multispar box-beam design with the 25-percent chord swept back 25°. The covering is taper-milled Inconel X sheet because of its strength and favorable creep characteristics at 1,200° F. The internal structure is AMS-4908 titanium-alloy sheet and extrusions. The front and rear spars consist of flat web channel sections. The seven intermediate spars have corrugated webs attached to the skin through scalloped

flanges. Three ribs are employed, being located at the root, midspan, and tip, and their construction is similar to that of the intermediate spars. Leading and trailing structures are of multirib design with panel sizes selected for stiffness. The leading edge consists of a milled bar of Inconel X which acts as a heat sink. The attachments consist of Inconel X and A-286 stainless-steel screws and rivets.

Figure 4 shows the details of the wing-to-fuselage carry-through structure and depicts the nature of the redundancy involved from a combined load and temperature point of view. The outer panel attaches to the side-tunnel structure which contains nine A-shaped frames for this purpose. The two shear panels, shown detached, redistribute the outer panel loads to five A-frames which attach to a like number of fuselage ring frames. Thermal gradients of 400° to 500° F are possible in this area up to burnout time because the temperature of the liquid oxygen is -320° F in the adjoining fuselage structure. A thermoelastic test of this region, simulating all critical effects is being undertaken.

The temperature profiles shown in figure 5 reflect the peak values for the critical thermal mission which occurs during reentry of the vehicle into the atmosphere. The maximum values occur at the stagnation and adjacent points. The temperature differential between the upper and lower surfaces is shown in this figure to be approximately 400° F. The surface gradients existing in the structural box area are of tolerable magnitude. This is the case both spanwise and chordwise.

Profiles of thermal gradients at the critical instant are presented for three typical sections of the wing in figure 6. It is noted that the steepest gradient between the skin and the center of the spar web is 960° F. Laboratory tests reflecting gradients of this magnitude did not indicate any obvious adverse effects. Analysis and tests to determine the true nature of such effects, however, are continuing.

In order to arrive at a near optimum in design, a structural efficiency analysis was made of the X-15 wing at three representative sections - namely, inboard, intermediate, and outboard - at room temperature.

Minimum structural weight is shown in figure 7 as a function of the design variables of bending moment, wing chord, wing depth, and skin-cover thickness. The variables are presented in index form. The points of the X-15 wing plotted in the graph in this figure indicate an essentially optimum balance of the parameters in question as all of the subject points lie close to the maximum efficiency curve.

Figure 8 presents a comparison of the thermally induced skin and spar-cap stresses due to a temperature gradient for two different material combinations. Many other combinations were included in a general study just completed at North American Aviation, Inc. This comparison reveals

the superiority of the Inconel X skin and titanium spar-cap combination to one of all Inconel X. The thermal stresses are definitely lower for the Inconel X skin and titanium combination which is also lighter in weight.

Figure 9 shows a full-scale test box which was subjected to ultimate loads and transient heating conditions equal to those of the X-15 wing. The box is shown with the upper cover removed. The box beam, which is 48 inches by 26 inches by 6.5 inches, was fabricated from Inconel X skins and titanium-alloy spars. The two intermediate spars have corrugated webs attached to scalloped cap angles (two angles on compression surface and one on tension surface). The attachment for the skin to the spar caps consisted of $\frac{3}{16}$ -inch-diameter Inconel X flush screws which were spaced 1 inch on center. No chordwise reinforcements were incorporated.

The purposes of the tests were as follows:

(1) To determine the effects of transient heating, thermal gradients, and biaxial thermal stresses on the buckling and ultimate strength of a box beam.

(2) To determine the magnitude of thermal deformations for varying load levels, temperatures, and gradients.

(3) To determine the influence of thermal stresses on structural attachments.

(4) To ascertain possible creep effects due to repeated loads and heating.

(5) To evaluate importance of steep thermal gradients on flat web spars in the presence of bending stresses.

Figure 10 shows the instrumentation and setup for the wing box test. The box was attached to a rigid jig at one end and a floating jig which was designed for pure bending application was attached at the other end. General Electric T-3 lamps were used as heating elements. Precautions were taken to delete any extraneous influences for the case of thermal loading. This was accomplished by elongating the jig attachment holes in the chordwise direction. Asbestos pads were employed between the box skins and the jig plates to reduce heat losses. Additional heat was concentrated at the ends of the box to minimize gradient differences between adjacent skin elements and to prevent premature buckling and unrealistic thermal stresses in the skin covers. Thermocouples were installed on the inside and outside surfaces of the cover plates. Likewise thermocouples were added on the flanges and webs of the spars. Temperature readings were recorded during each test.

The wing box was subjected to a series of tests designed to demonstrate its strength, thermal effects, and combinations of both. The tests were as follows:

(1) The box was first subjected to heat alone. This was done by simply supporting the four corners and heating the upper surface to 830° F and the lower surface to 990° F. The heating period was 100 seconds. No buckles appeared in the surfaces.

(2) Next, the design ultimate bending moment was applied at room temperature. Sizable compression buckles existed under this condition. Upon removal of the load, all buckles disappeared.

(3) With the upper and lower surfaces heated as in the first test, a moment equivalent to 85-percent limit was applied. Under this combination, the skin buckles had a depth of 3/16 inch. At limit load, the buckle depth remained approximately the same. Figure 11 shows a close facsimile to the observed buckles.

(4) The aforementioned sequence was followed by a variety of load and temperature combinations during which the upper surface reached 450° F and the lower 810° F. This represented the maximum temperature differential. Inspection of the box after the completion of all limit load and temperature tests revealed the fact that all buckles had disappeared.

(5) Finally, with the upper surface at 600° F and the lower at 810° F, the box failed at a moment equal to 116 percent of the calculated strength. The failure ran slightly diagonally across the box, approximately 6 inches from the loading jig. After removal of the load and cooling to room temperature, the unfailed portion of the box had no permanent buckles. At the present time, additional compression panels are being fabricated from the remainder of the box.

One conclusion derived from these tests is that the thermal stresses had very little effect on the ultimate strength of the box.

Wing specimen tests already completed or in progress include the following:

(1) Additional box beams

(2) Leading-edge specimens

(3) Fasteners

(4) Intermediate spars

(5) Stiffness tests of box beams

(6) Combined stresses in Inconel X sheet

(7) Creep buckling

(8) Creep in joints

(9) A-frame details and assemblies

All of these tests involve thermal effects.

Figure 12 presents a diagram of the horizontal stabilizer. The left- and right-hand stabilizers are mounted separately and thus provide both lateral and longitudinal control for the airplane. The structure con- sists of an AM 350 stainless-steel spar located at 57 percent of the chord, an Inconel X front spar located $3\frac{1}{2}$ inches aft of the leading edge, a titanium trailing-edge beam, titanium transverse ribs, and a 0.037-inch Inconel X skin. The surface is all-movable about a spindle which is an integral part of the main spar and which attaches to the fuselage in the region of the side tunnels. For the most efficient design, the main spar is used to carry all normal bending along the entire span. The front spar effectively closes out the torque box which terminates at the root rib. Actuation is by a hydraulic cylinder attached to an arm located in line with the outboard bearing.

Figure 13 shows the maximum skin temperatures on the horizontal tail. These temperatures occur for the high-speed mission at pullout. It also gives the maximum temperature gradient between the skin and the spar caps. The distribution is given for a station at midspan and is typical since the skin gage does not taper spanwise or chordwise, with the exception of the nose skin forward of the leading-edge beam. The temperature of the nose skin is controlled to a maximum value of 1,200° F by varying the skin thickness. The large decrease in temperatures in the area of the beams is due to the large mass of the beam caps with respect to the thin skin. The dashed part of the curve represents the skin temperatures as if there were no internal structure.

Allowable stresses for various materials at 500° F were calculated to determine the optimum spar-cap material and the results are presented in figure 14. At a b/t of 10, AM 350 stainless steel shows an advantage over all other applicable materials. The method used in calculating these allowable stresses has been verified by tests on aluminum specimens. It will be checked further during the present test program.

A study was made in consideration of the problem of whether to per- mit the stabilizer skins to buckle under elevated temperatures. The curves shown in figure 15 give the allowable temperature differential

between the skin and internal structure for initial buckling of Inconel X panels heated to 800° F and include various skin gages and spanwise stiffener spacing with a constant 8-inch rib spacing. It was assumed that the panels were restrained in all directions by virtue of the elastic properties of the skin and stiffeners.

The study indicated that, for even small temperature differences, it is necessary to increase the skin gage and decrease the stiffener spacing in order to eliminate skin buckling. This would impose severe weight penalties. For example, to increase and stiffen the skin to prevent buckling up to limit conditions would add 195 pounds. Consequently, thermal stress buckles are permitted to exist during the brief period of heating at the reentry but no permanent buckles are condoned.

A plot of panel flutter parameters taken from NACA data is shown in figure 16. The flutter parameters include such aerodynamic factors as Mach number and dynamic pressure as well as the physical factors of panel length, width, gage, and Young's modulus. The curve is plotted for zero pressure differential and panels having clamped edges. This curve has been used as a guide to determine rib spacing for thin skin panels when buckled. The lines show the relationship of the panels of the various surfaces with respect to the critical panel flutter boundary. For the main wing box, the points lie completely off the chart. It can be seen that all panels fall outside the critical region.

The curve in figure 17 is a plot of an equation which was suggested by W. G. Howland and P. E. Sandorff in an early article entitled "Permanent Buckling Stress of Thin Sheet Panels Under Compression" (Jour. Aero. Sci., vol. 8, no. 7, May 1941). The curve gives the stress which will cause permanent panel buckling. The allowable stress is plotted against b/t (ratio of panel width to skin gage) for Inconel X sheet at 800° F, and the panel is assumed to be simply supported. As the critical value of buckling stress of the panel decreases, a small increment of bending stress due to the eccentricity caused by the buckles raises the skin stress above its permanent buckling value. Thus, the curve drops for increasing values of b/t; however, at a b/t value of approximately 100, the critical buckling stress has dropped to such an extent that additional stress due to buckle eccentricity becomes less significant and the edge of the panel becomes critical. Therefore, the curve rises rapidly.

The point as plotted for the horizontal tail is representative of the calculated skin stress over the main beam for a typical station. This stress includes the effect of limit bending moment and thermal stresses. The tail is being designed to have no permanent skin buckles for the combined effect of limit stress due to external load and thermal stress. The points as plotted for the wing test box are calculated skin stresses over the spars at the time of box failure. There was no permanent skin buckling at these stresses.

Figure 18 shows the construction of the vertical tail and speed brake. The vertical-tail structure contains two AM 350 stainless-steel beams. One is located just forward of the speed-brake hinge line and one just aft of the vertical-tail hinge line. An Inconel X leading-edge beam is located $3\frac{1}{2}$ inches aft of the leading edge. Titanium ribs are employed together with 0.037-inch Inconel X skin for covering. The two load-carrying beams extend below the root rib and into the fuselage area to form the torque box by which the tail is supported and actuated. The support for the spindle is two bearings spaced $15\frac{1}{2}$ inches on center. A hydraulic cylinder is used as an actuator.

The speed brakes are supported on piano-type hinges which are an integral part of the rear spar cap. The brakes are actuated hydraulically through a bank of eight cylinders, four of which attach to each brake and are linked together to insure symmetrical operation. The brake structure consists of an AM 350 spar, titanium ribs, a 0.050-inch Inconel X skin, and a titanium-alloy trailing-edge section.

The distribution shown in figure 19 gives the maximum skin temperatures at midspan on the vertical tail. These temperatures also occur during pullout from the high-speed mission with speed brakes closed. This is also representative of the maximum temperature differential between the skin and the spar caps. The temperature of the nose skin is controlled to a maximum value of 1,200° F by tapering the skin thickness chordwise. The heat sink due to the spar caps is clearly evident. The dashed portion of the curve represents the skin temperatures as if there were no internal structure. Detail B is also representative of the intermediate beam.

Figure 20 shows the temperatures used for structural design which result from the high-speed reentry condition.

The fuselage consists of an Inconel X shell throughout its length. The forward portion ahead of the propellant tanks is double-walled with spun-glass matting used for insulation. In this region, the inner structure is semimonocoque having an aluminum-alloy inner skin with frames and intercostals of titanium alloy.

The propellant tanks are integral with the outer skin and are not insulated. This feature, therefore, permits a pure monocoque construction which lends itself to a simplified design. High-temperature materials are used and provisions are made to minimize thermal stresses.

Figure 21 shows the weight penalty which must be paid in order to fly under aerodynamic-heating conditions. The curves are based on a given set of loads and diameter of fuselage and are constructed for weldable materials. Although the penalty for operation at high temperature is large, the thickness of the shell required to keep materials

other than Inconel X within their maximum allowable temperatures would
cause the weight of the shell to be greater than when Inconel X is used.

Actually, the choice of optimum material depends on the magnitude
of the applied loads. If the loads are heavy, then the mass of the struc-
ture will easily absorb the heat input with only a small temperature rise.
This would permit use of an efficient low-temperature structure. However,
when the loads are relatively light and the heat input is large, as in
the X-15 airplane, minimum weight is obtained by using a high-temperature
resistant material.

The fuselage structure in the region of the propellant tank is
shown in figure 22. The structure is a circular cylinder of monocoque
design and is dictated by the following considerations:

Heat sink.- For a given heat input and material, there is a minimum
skin thickness which results in a heat rise sufficient to weaken the
material beyond practical use. This would necessitate heavy skins if
semimonocoque construction were used. With only a slight increase in
skin thickness, monocoque construction is possible.

Stresses due to unequal temperatures.- The monocoque design minimizes
stresses due to temperature gradients because all of the material is at
the surface, having an equal opportunity to be heated.

Use of shell as pressure tank.- The circular monocoque structure is
ideal as a pressure vessel.

Additional advantages of this type of structure include the following:

(1) Skin pillowing is eliminated.

(2) The low-stressed material results in greater stiffness.

(3) The uniformity and low-stress level reduce both the fatigue and
creep problems.

(4) The simplicity of construction aids fabrication.

(5) The thick walls will facilitate sealing the propellent tanks
and reduce the possibility of damage through leaks.

Tests now in progress at NACA show that there is a reduction of 10
to 20 percent in the buckling strength of cylinders when the heated out-
side shell is restrained by a cooler internal ring. The cooler ring
induces compression along the circumference of the shell, which in turn
lowers the buckling strength. This influence is further complicated in
the case of the X-15, since many of the frames are semitorus bulkheads

which approach the skin tangentially. In the region of the wing where conventional frames are used, the sides are cool relative to the heated top and bottom areas. Analysis of this problem is continuing. The sides of the fuselage are shrouded by two service tunnels, which offer protection from aerodynamic heating. As a result, the sides of the fuselage do not expand as much as the top and bottom surfaces. If this condition were allowed to prevail, a longitudinal compressive stress would be produced by a temperature differential as low as 300° F. This would be as great as the allowable compressive stress of the cylindrical shell. This condition is eliminated by beading the shrouded skin which in turn introduces problems with respect to pressure loads. Since the side skins can not carry longitudinal tensile loads, the shell bending and tank longitudinal tensile loads must be shunted around this area. Also the hoop tensile loads must be redistributed at the end of each bead.

North American Aviation, Inc., is now conducting a series of compression tests on curved panels representative of the fuselage design.

Figure 23 shows a typical arrangement of the propellant tanks which are integral with the outer shell. The materials chosen had to be compatible in welding for sealing purposes. Each tank is separated into three compartments by torus-shaped frames to maintain balance. In addition, the compartment in each tank farthest from the airplane center of gravity is separated into three sections by slosh baffles.

The construction procedure involves building all the plumbing in one compartment, then sealing that compartment by a torus baffle and proceeding to the next compartment. The heat-treatable portions of the tank structure will be heat-treated prior to assembly. All assembly welding is performed in Inconel which is unaffected by heat-treatment.

The helium-tank storage tube serves to stabilize the torus frames and is also subjected to crushing loads from the tank pressures.

The tank ends were made in the shape of a semitorus in order to accomplish the following:

(1) To produce a nearly "flat" end, so as to provide the maximum useful space for equipment.

(2) By having no material in bending, minimum-weight tank ends are provided.

(3) To allow thermal expansion of the outer shell, thereby reducing the secondary effects of temperature to a minimum.

Negative pressures inside the tanks and the fuel head acting on the semitorus baffles produce compressive stresses in the bulkheads. The

tori thus become critical in buckling. Tests are under way to determine these buckling stresses. The test results will be fitted to a suitable empirical formula.

In order to prove the structure of the outer shell, the side tunnels, the torus frames, and the wing support frames, a full-size test specimen is being constructed and is shown in figure 24. This specimen will be subjected to tank pressures, external loads, and temperature environment. It will also be used to determine leakage rates. The tests will also prove the stiffening effects of the frames on the center tube. A typical wing support frame is also included. This will be loaded through the wing fittings to ultimate loads. The short section of tunnel mounted on the side of the specimen will likewise be loaded during the tests. A series of tests will be performed first at room temperature and later under transient heating conditions. It is felt that these tests will be equally as valuable as a static test of the whole fuselage.
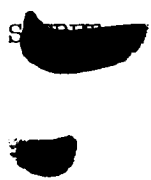
Numerous other structural tests are underway which include

(1) Tests of full-size cylindrical panels in compression

(2) Tests of torus shells in compression

(3) Tests of the inner tank cylinder

(4) Tests of splices, welds, and materials

(5) Tests to determine the effect of transient heating on the ultimate strength of ring frames, and so forth

BIBLIOGRAPHY

1. Rosen, B. Walter: Analysis of the Ultimate Strength and Optimum Proportions of Multiweb Wing Structures. NACA TN 3633, 1956.

2. Sechler, Ernest E., and Dunn, Louis G.: Airplane Structural Analysis and Design. John Wiley & Sons, Inc., 1942.

3. Heldenfels, Richard R.: Some Design Implications of the Effects of Aerodynamic Heating. NACA RM L55F22, 1955.

4. Pride, Richard A.: An Investigation of the Effects of Rapid Skin Heating on Box Beams Loaded in Bending. NACA RM L55B03, 1955.

5. Dukes, W. H., and Schnitt, A.: Structural Design for Aerodynamic Heating. Part I - Design Information. Part II - Analytical Studies. WADC Tech. Rep. 55-305, Pts. I and II (Bell Aircraft Corp., Contract No. AF33(616)-2581), Wright Air Dev. Center, U. S. Air Force, Oct. 1955.

6. Griffith, George E., and Miltonberger, Georgene H.: Some Effects of Joint Conductivity on the Temperatures and Thermal Stresses in Aerodynamically Heated Skin-Stiffener Combinations. NACA TN 3699, 1956.

7. Fraser, Allister F.: Experimental Investigation of the Strength of Multiweb Beams With Corrugated Webs. NACA TN 3801, 1956.

8. Stein, Manuel, and Sanders, J. Lyell, Jr.: A Method for Deflection Analysis of Thin Low-Aspect-Ratio Wings. NACA TN 3640, 1956.

9. Piland, Robert O., and Collie, Katherine A.: Aerodynamic Heating of Rocket-Powered Research Vehicles at Hypersonic Speeds. NACA RM L55E10c, 1955.

10. Vosteen, Louis F., and Fuller, Kenneth E.: Behavior of a Cantilever Plate Under Rapid-Heating Conditions. NACA RM L55E20c, 1955.

11. Gossard, Myron L., Seide, Paul, and Roberts, William M.: Thermal Buckling of Plates. NACA TN 2771, 1952.

12. Heldenfels, Richard R.: A Numerical Method for the Stress Analysis of Stiffened-Shell Structures Under Nonuniform Temperature Distributions. NACA Rep. 1043, 1951. (Supersedes NACA TN 2241.)

13. Timoshenko, S. and Goodier, J. N.: Theory of Elasticity. Second ed., McGraw-Hill Book Co. Inc., 1951.

14. Shaw, F. S.: An Introduction to Relaxation Methods. Dover Publications, Inc., c.1953.

15. Southwell, R. V.: Relaxation Methods in Engineering Science. A Treatise on Approximate Computations. The Clarendon Press (Oxford), 1940.

16. Boley, Bruno A.: The Determination of Temperature, Stresses, and Deflections in Two-Dimensional Thermoelastic Problems. Jour. Aero. Sci., vol. 23, no. 1, Jan. 1956, pp. 67-75.

17. Hoff, N. J.: High Temperature Effects in Aircraft Structures. Appl. Mech. Rev., vol. 8, no. 11, Nov. 1955, pp. 453-456.

18. Goldberg, Martin A.: Investigation of the Temperature Distribution and Thermal Stresses in a Hypersonic Wing Structure. Preprint No. 577, S.M.F. Pub. Fund Preprint, Inst. Aero. Sci., Jan. 1956.

19. Allen, H. F., Brull, M. A., and Wilkie, W. J.: A Study of the Stress-Analysis and Structural-Testing Procedures Applicable to Aircraft Structures at Elevated Temperatures. WADC Tech. Rep. 54-499 (Univ. of Michigan, Contract No. AF 33(038)-12235), Wright Air Dev. Center, U. S. Air Force, Oct. 1954.

20. Gatewood, B. E.: Approximate Procedures for Transient Thermal Stresses in Missile Structures. Preprint No. 578, S.M.F. Pub. Fund Preprint, Inst. Aero. Sci., Jan. 1956.

21. Heldenfels, Richard R., and Roberts, William M.: Experimental and Theoretical Determination of Thermal Stresses in a Flat Plate. NACA TN 2769, 1952.

22. Budiansky, Bernard, and Mayers, J.: Influence of Aerodynamic Heating on the Effective Torsional Stiffness of Thin Wings. Preprint No. 579, S.M.F. Pub. Fund Preprint, Inst. Aero. Sci., Jan. 1956.

23. Howland, W. L. and Sandorff, P. E.: Permanent Buckling Stress of Thin-Sheet Panels Under Compression. Jour. Aero. Sci., vol. 8, no. 7, May 1941, pp. 261-269.

24. Mayers, J., and Budiansky, Bernard: Analysis of Behavior of Simply Supported Flat Plates Compressed Beyond the Buckling Load Into the Plastic Range. NACA TN 3368, 1955.

25. Needham, Robert A.: Permanent Buckling of Sheet-Stringer Panels at Elevated Temperatures. WADC Tech. Rep. 53-209 (Univ. of California, Contract No. AF 33(616)-293), Wright Air Dev. Center, U. S. Air Force, July 1953.

26. Heldenfels, Richard R.: The Effect of Nonuniform Temperature Distributions on the Stresses and Distortions of Stiffened-Shell Structures. NACA TN 2240, 1950.

27. Kromm A., and Marguerre, K.: Behavior of a Plate Strip Under Shear and Compressive Stresses Beyond the Buckling Limit. NACA TM 870, 1938.

28. Sylvester, Maurice A.: Experimental Studies of Flutter of Buckled Rectangular Panels at Mach Numbers From 1.2 to 3.0 Including Effects of Pressure Differential and Panel Width-Length Ratio. NACA RM L55I30, 1955.

29. Timoshenko, S.: Theory of Plates and Shells. McGraw-Hill Book Co., Inc., 1940.

30. Clark, R. A.: On the Theory of Thin Elastic Toroidal Shells. Jour. Math. and Phys., vol. XXIX, no. 3, Oct. 1950, pp. 146-178.

31. Simmons, Ward F., and Cross, Howard C.: Report on the Elevated-Temperature Properties of Selected Super-Strength Alloys. Special Tech. Pub. No. 160, A.S.T.M., 1954.

32. Peterson, James P.: Bending Tests of Ring-Stiffened Circular Cylinders. NACA TN 3735, 1956.

33. Lo, Hsu, Crate, Harold, and Schwartz, Edward B.: Buckling of Thin-Walled Cylinder Under Axial Compression and Internal Pressure. NACA Rep. 1027, 1951. (Supersedes NACA TN 2021.)

CONFIDENTIAL
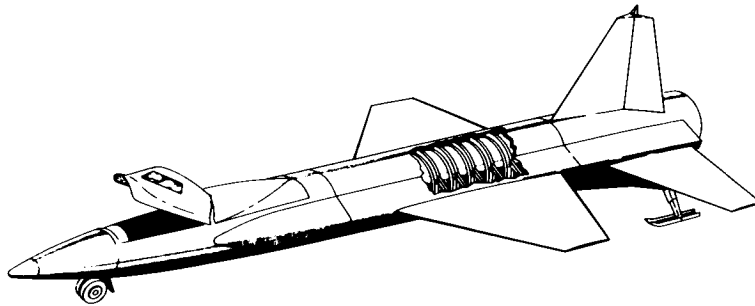
SYS-447L   **X-15**

Figure 1

SYS-447L   **TEMPERATURE VS LOAD**
HIGH SPEED-MISSION

TEMP-°F

ACCEL-n_z

TEMP LOWER COVER

TEMP UPPER COVER

NORMAL ACCELERATION (n_z)

TIME SEC
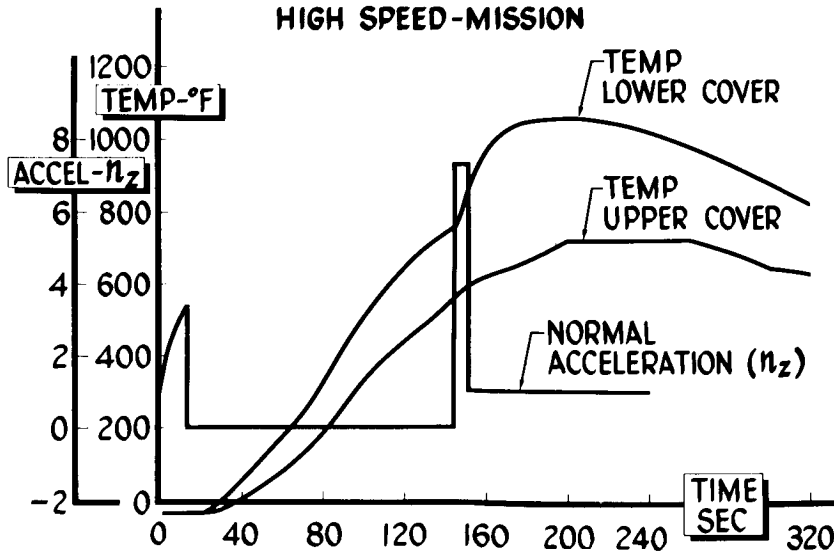
Figure 2

SYS-447L   **X-15 WING**
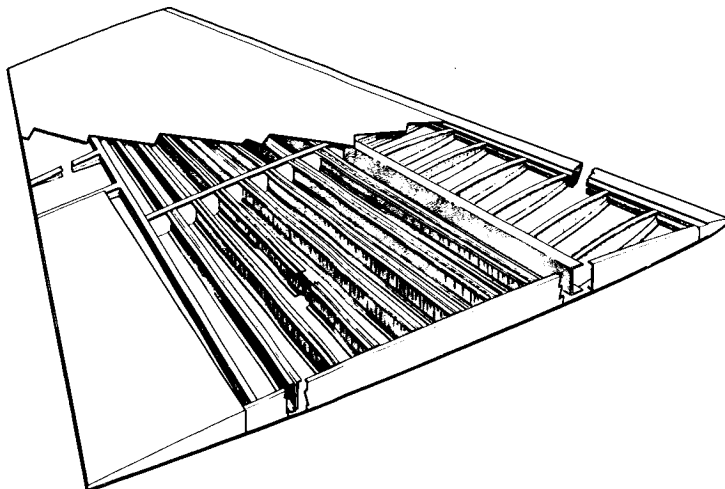
Figure 3

SYS-447L   **WING SUPPORTING STRUCTURE**

Figure 4

154

SYS-447L **WING SKIN TEMPERATURES -°F**

1200° 800°
730° 630° 550° 580° 750°

1130° 920° 830° 850°
1200° 990° 900°

1200° 730°
840° 640°
540° 800° 750°

1200° 960° 870° 960° 870° 850°
1110° 900°
870° 880° 1200° 1190° 1030°
1200° 875°

UP

AFT

OUTB'D

1200° 1150° 1025°
1200° 1180° 1050°
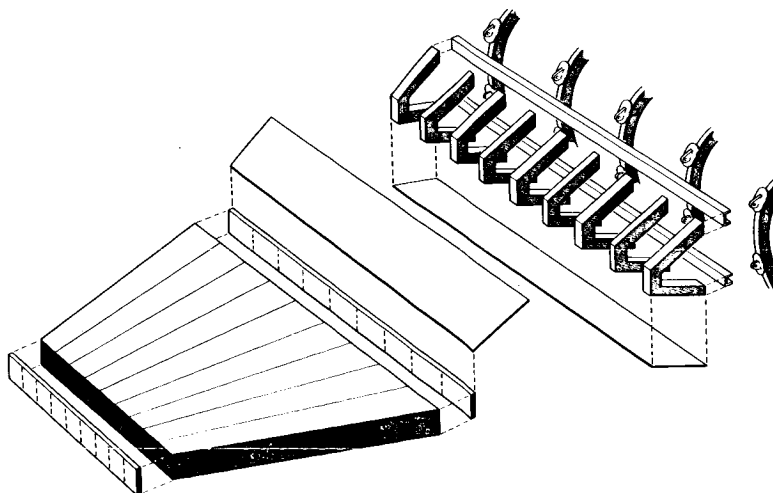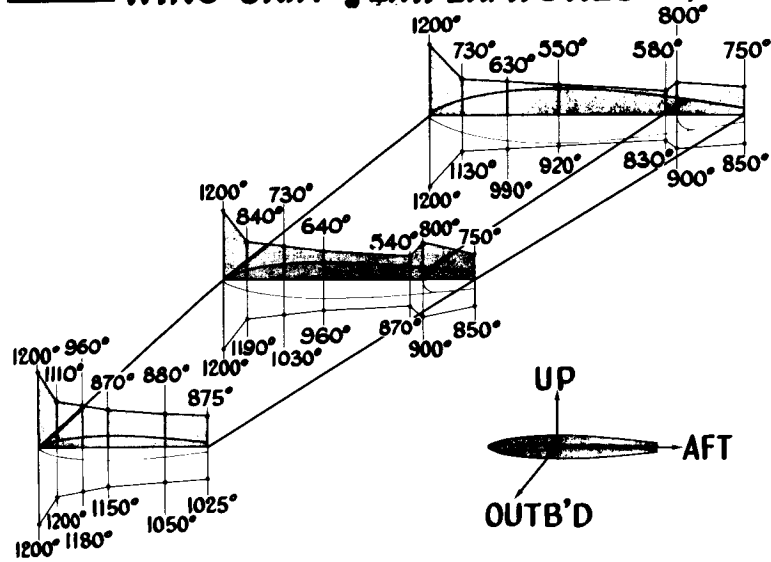
Figure 5

SYS-447L **WING TEMPERATURE GRADIENTS**
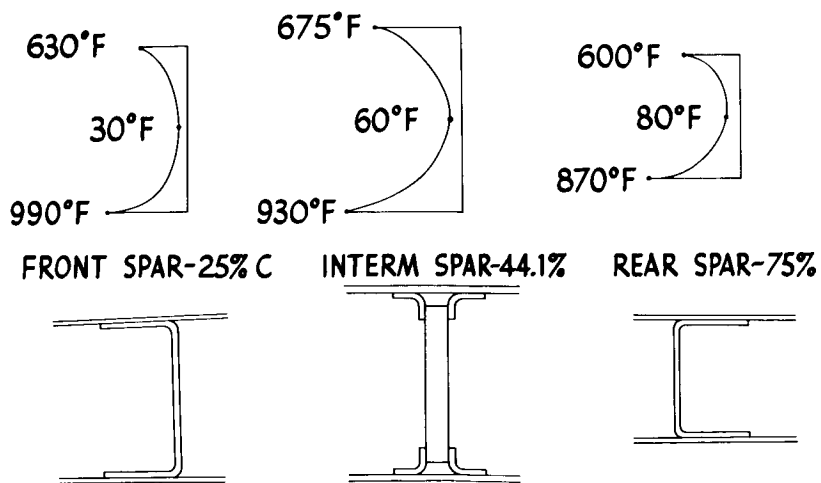
630°F 675°F 600°F

30°F 60°F 80°F

990°F 930°F 870°F

FRONT SPAR-25% C   INTERM SPAR-44.1%   REAR SPAR-75%

Figure 6

SYS-447L

MULTI-SPAR EFFICIENCY

⊕ INBOARD
▣ INTERMEDIATE   X-15 WING
△ OUTBOARD

$\frac{A_i}{H}$ SOLIDITY INDEX

MAX EFFICIENCY ENVELOPE

INCONEL X SKIN

TITANIUM SPARS

$\frac{M_i}{h^2c}$, KSI LOAD INDEX

$\frac{H}{t_s}$

75

10

50

15

150

40

20

25

30

Figure 7

SYS-447L

WING COVER PANEL THERMAL STRESS

$T_{SKIN} = 600°F$

$T_{SPAR\ CAP} = 300°F$

SPAR CAP TENSION

THERMAL STRESS-KSI

1. INCONEL X SKIN & INCONEL X SPAR CAP
2. INCONEL X SKIN & AMS 4908 TITANIUM SPAR CAP

SKIN COMPRESSION

$\frac{A_{SKIN}}{A_{SPAR\ CAP}}$
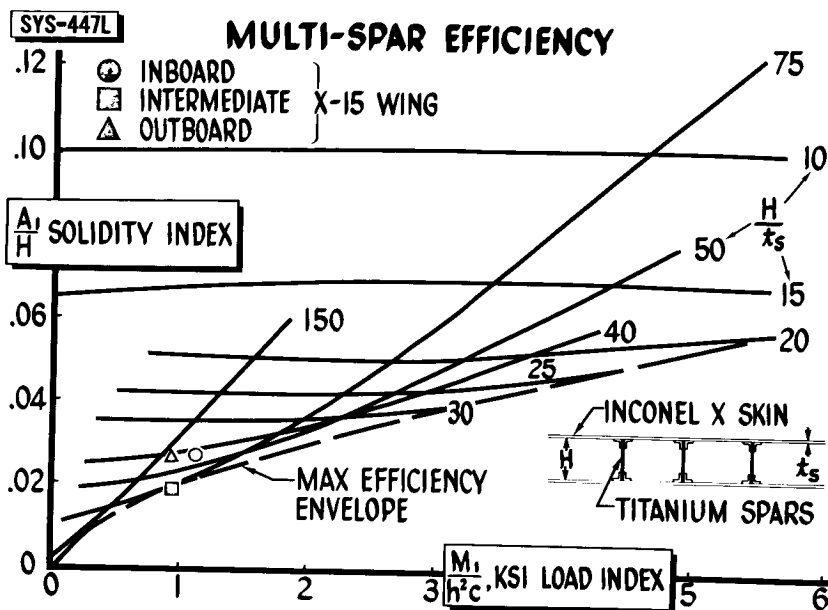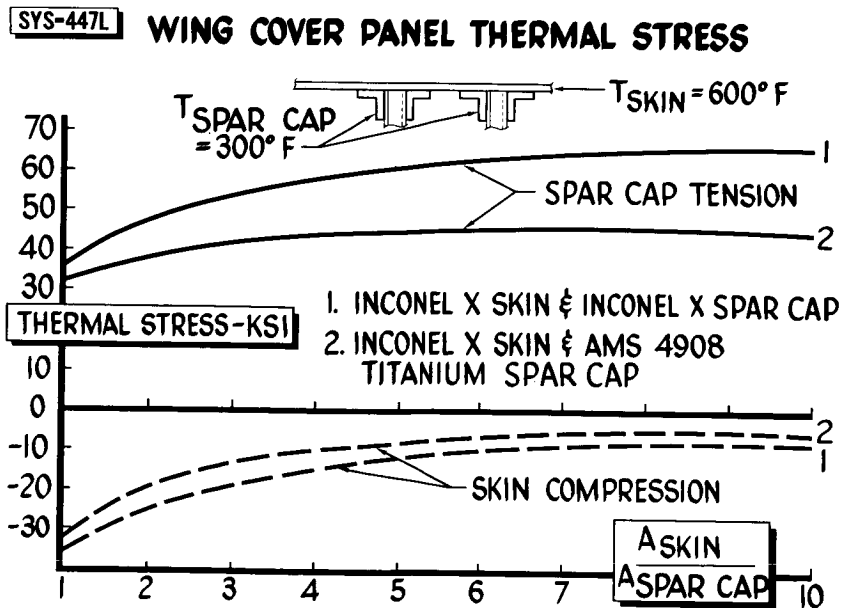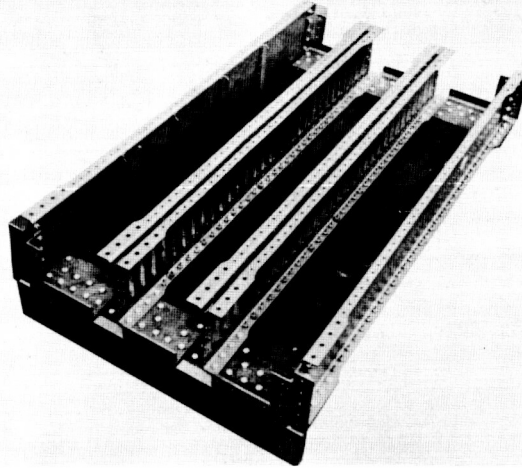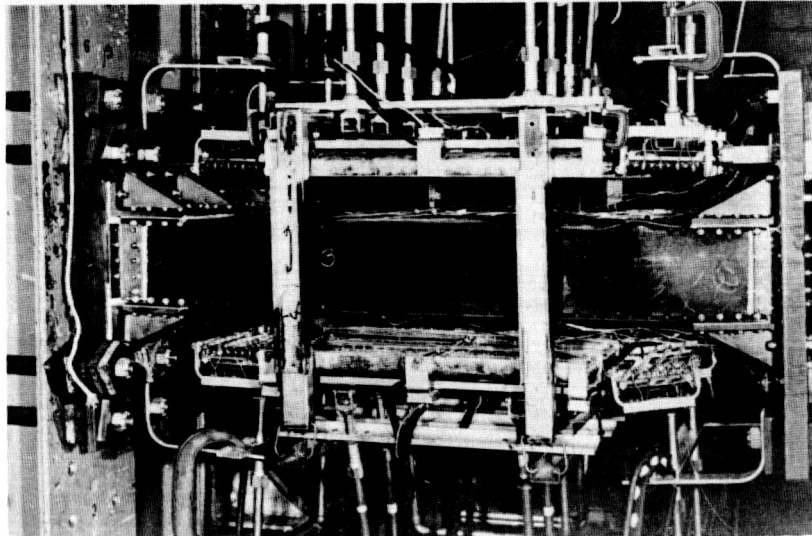
Figure 8

Figure 9

Figure 10

SYS-447L **BUCKLED WING TEST BOX**
SKIN DEFLECTION PATTERN
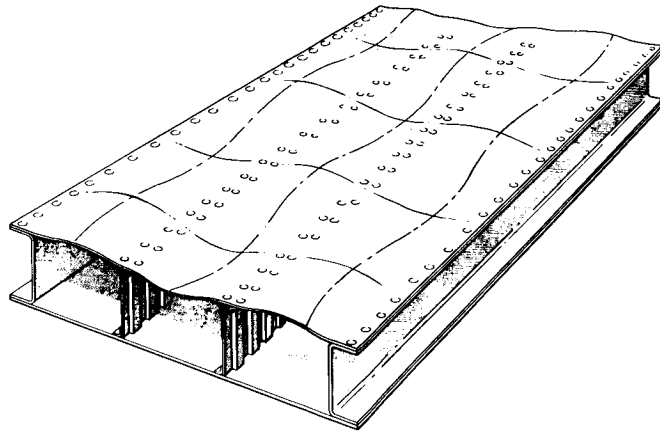
Figure 11

SYS-447L **HORIZONTAL STABILIZER**

DETAIL B-B

DETAIL A-A

DETAIL C-C

Figure 12

158
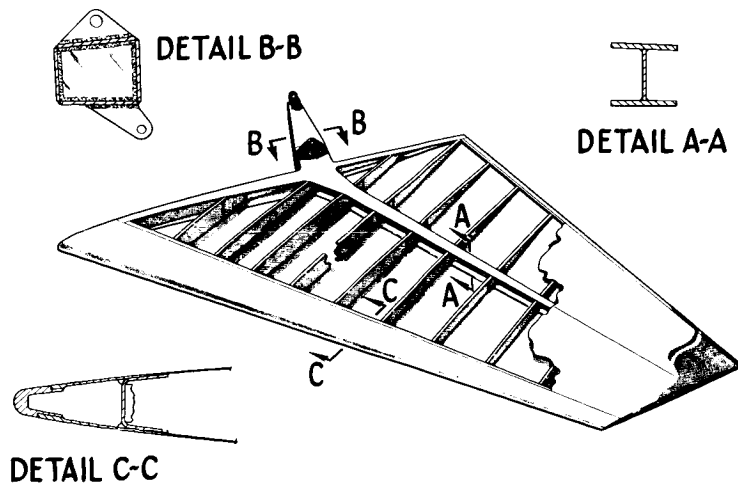
SYS-447L HORIZONTAL STABILIZER TEMPERATURES
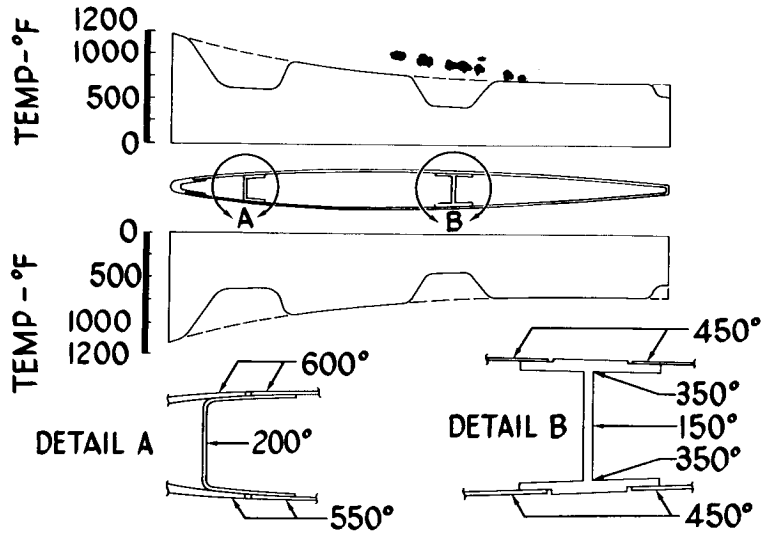
Figure 13

SYS-447L SPAR CAP ALLOWABLES AT 500°F
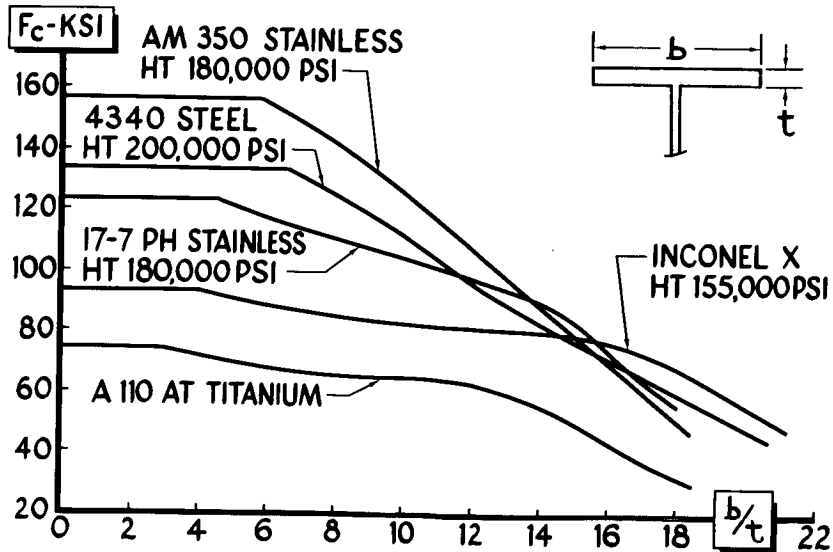
Figure 14

Figure 15

Figure 16

160

PERMANENT PANEL BUCKLING

SYS-447L

Figure 17

INCONEL X SHEET AT 800°F
SIMPLY SUPPORTED PANEL

120
KSI
100
90
80
70
60
50
40
30
20
10
0

0   100   200   300   400   500 b/t 700

WING TEST BOX

HORIZONTAL TAIL
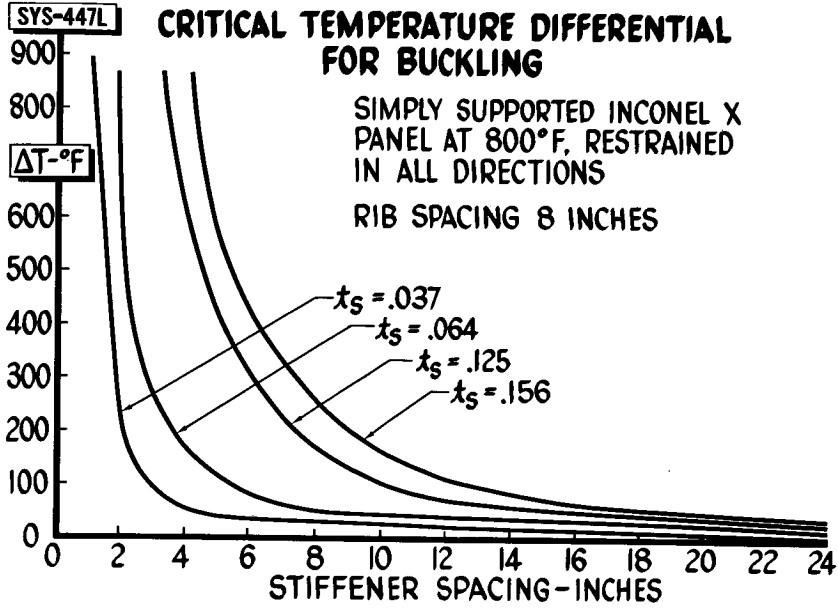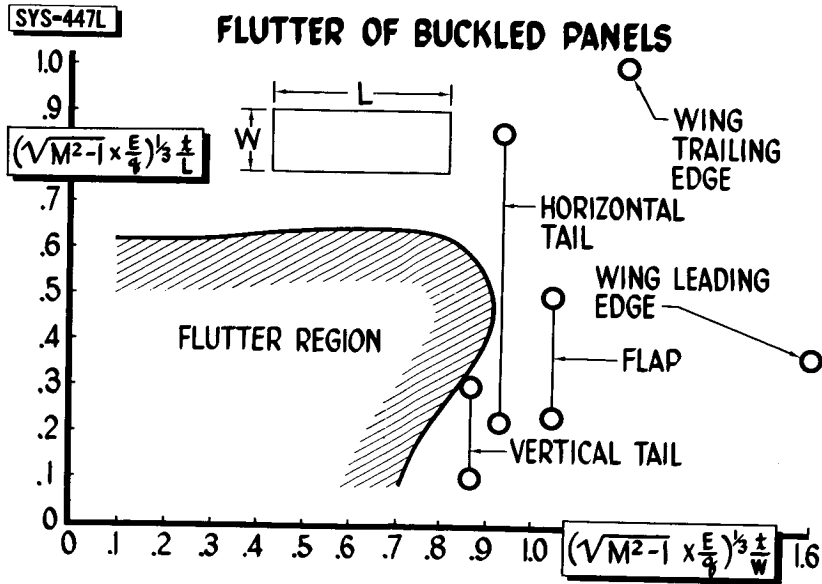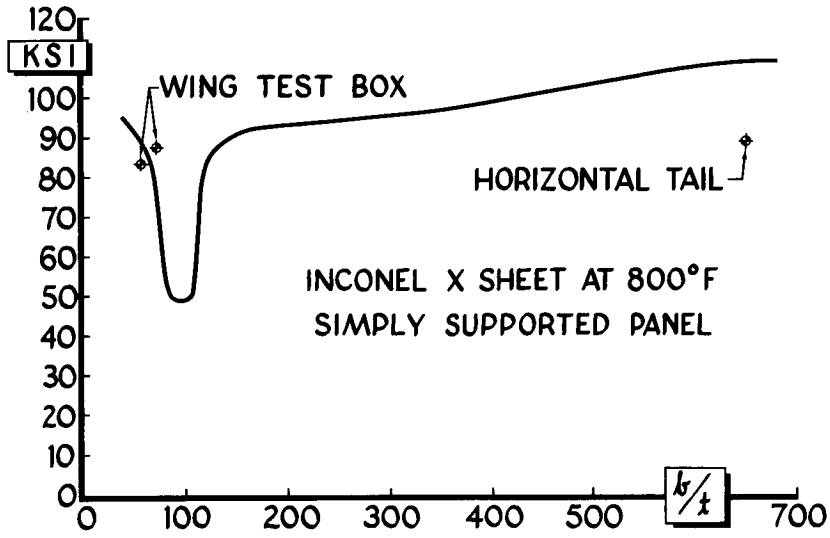
Figure 17

SYS-447L

X-15 VERTICAL STABILIZER
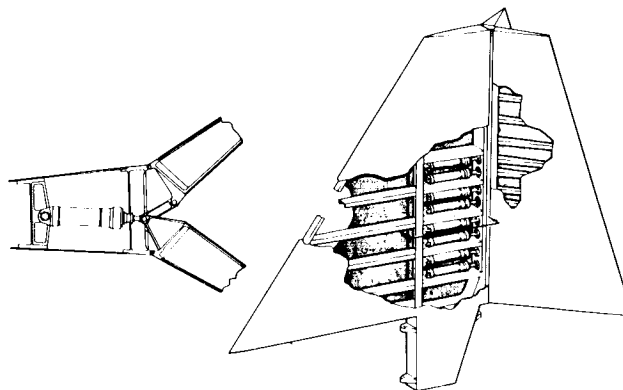
Figure 18

SYS-447L **VERTICAL STABILIZER TEMPERATURE DISTRIBUTION**
TYPICAL CHORDWISE

DETAIL A

325°F → ← 740°F

DETAIL B

700° F ← 350°F → 590°F
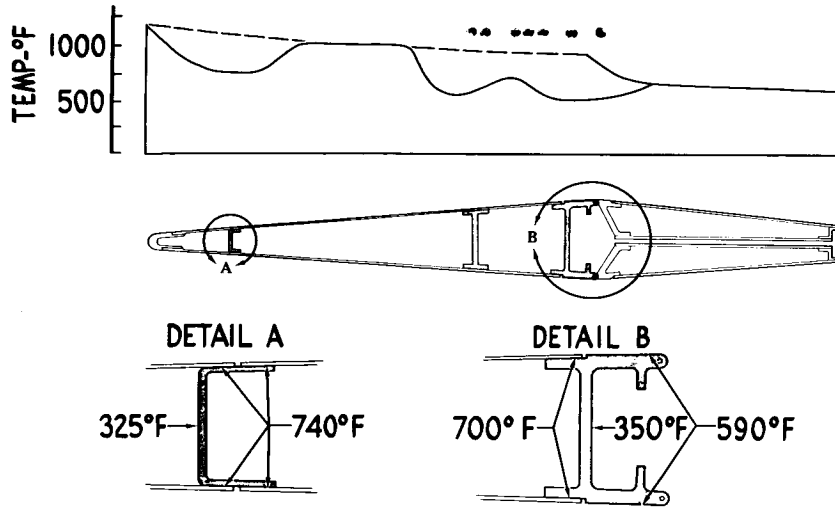
Figure 19

SYS-447L **FUSELAGE DESIGN TEMPERATURES**

1240°F   1230°F   620°F   460°F   470°F   530°F

1240°F   1200°F   1200°F

1200°F   1200°F   1200°F
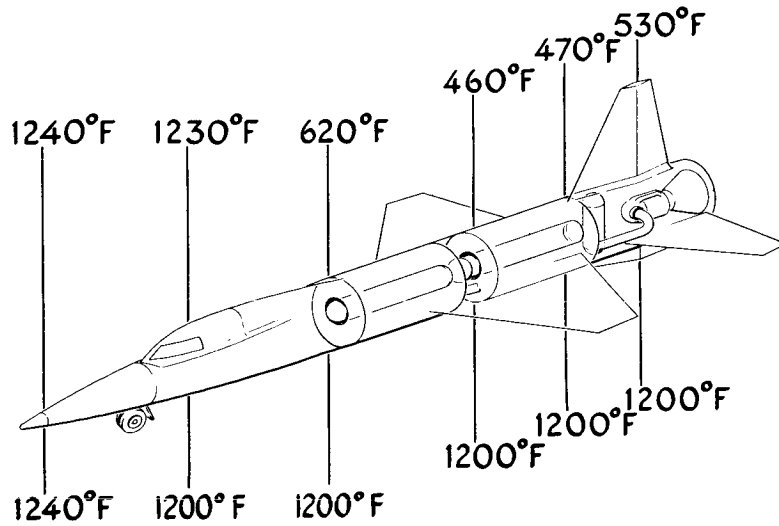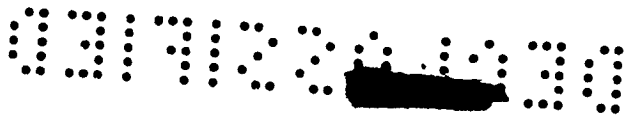
Figure 20

SYS-447L **CYLINDER WEIGHT VS TEMPERATURE**
WELDABLE MATERIALS

LB/IN

BENDING AND
COMPRESSION LOADS

INCONEL X

A110AT
TITANIUM

6061T6
ALCLAD

AZ 31H24
MAGNESIUM

TEMP
(°F)
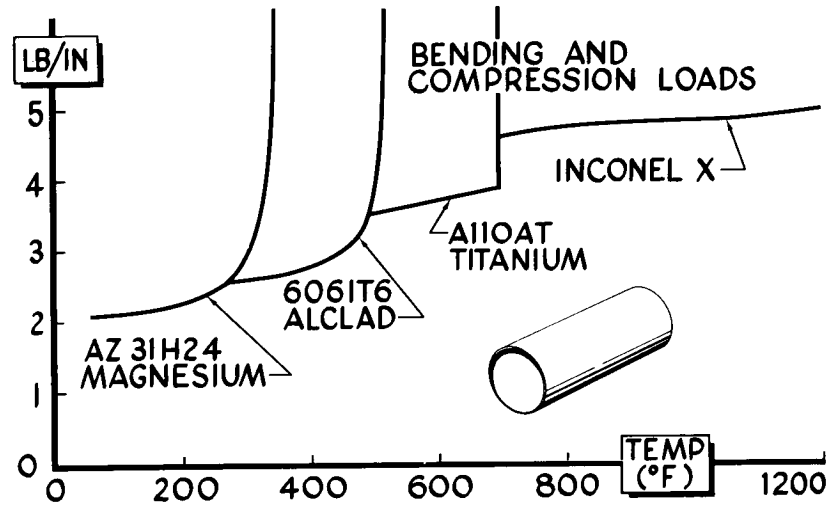
Figure 21

SYS-447L **FUSELAGE MAIN SHELL**

MONOCOQUE
SHELL

TUNNEL
ATTACH
ANGLE

THERMAL
STRAIN
RELIEF
BEADS

WING
SUPPORT
FRAME

WING ATTACH FITTING
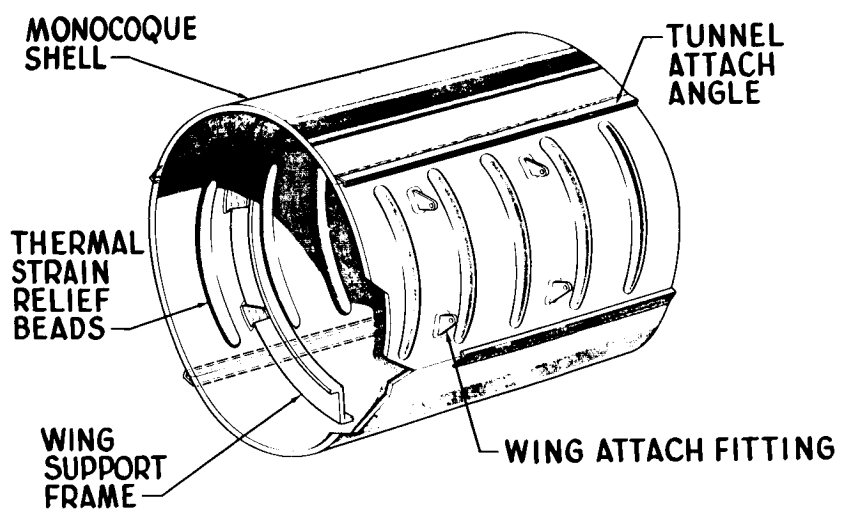
Figure 22

SYS-447L **LIQUID OXYGEN TANKS**

SLOSH BAFFLE — CYL SHELL

BAFFLE TORUS

CENTER TUBE

CLOSE-OUT WELD — STIFFENING RING
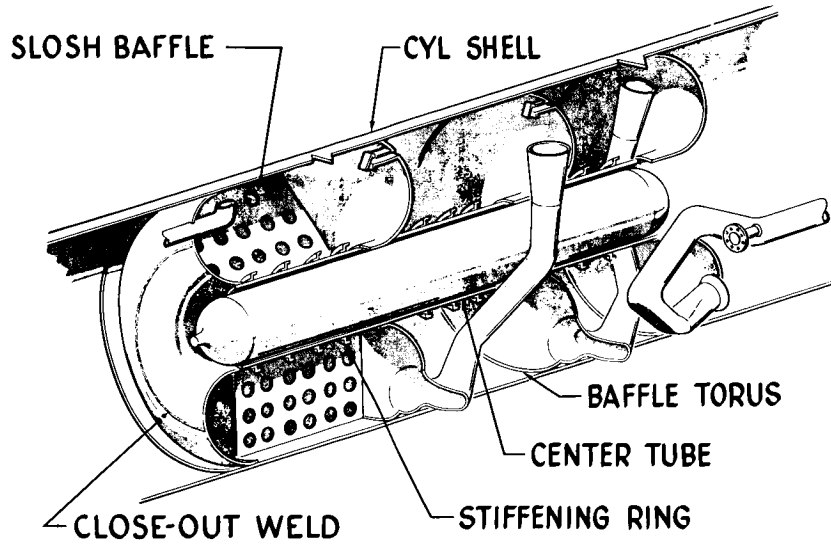
Figure 23

SYS-447L **X-15 FUSELAGE TEST SPECIMEN**

WELDED INCONEL SEMI-TORUS — INCONEL X SHELL HEAT TREATED

SPLICE — SIDE TUNNEL

RIVETED ALUMINUM BAFFLE

WING SUPPORT RING FRAME
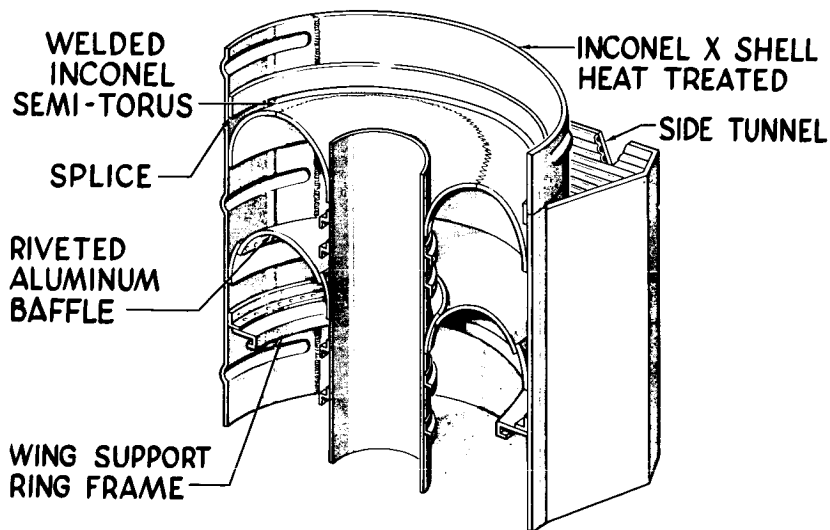
Figure 24
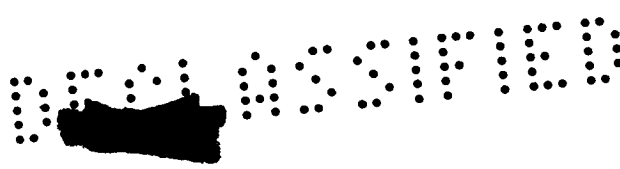
OPERATIONS

SOME EXPERIENCE WITH SIDE CONTROLLERS

By S. A. Sjoberg

Langley Aeronautical Laboratory

INTRODUCTION

With the X-15 airplane, the pilot will be subjected to longitudinal accelerations as large as about 5g. There is some question as to whether or not a pilot will be able to control the airplane by using a conventional control stick when he is subjected to accelerations of this magnitude. In order to alleviate the acceleration effects, it is planned with the X-15 airplane to use a side controller and to restrain the pilot's arm through use of an armrest.

Some problems are anticipated with the use of a side controller. Aside from the different location, which may affect the pilot's controlling ability, the motions of a side controller will be smaller by a factor of about 3 to 6 depending upon the particular design, and thus the mechanical advantage between the stick and the control surface must be reduced. This may cause the side controller to be overly sensitive. Further, the pilot's force capabilities are smaller and this, together with the reduced mechanical advantage, will make the friction forces more important.

Flight tests and ground-simulator studies have been made to study some of these problems and it is the purpose of this paper to present some of the results obtained.

F9F-2

Some flight experience with a side controller has been obtained with one installed in an F9F-2 airplane. Figure 1 is a photograph of this controller. Although this controller is different from that currently proposed for the X-15, the flight experience with it has indicated the feasibility of flying with a side controller and has furnished some information on satisfactory deflection and force gradients.

The F9F-2 controller is simply a short stick (about 4 inches long) which is pivoted at the bottom for both longitudinal and lateral motions. It has been used with electric-power control systems, and the control-valve friction normally present in hydraulic power controls is thus eliminated. The forces required to move this stick are light, with about 4 pounds of force being required for full stick deflection. Since the
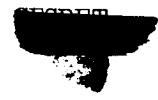
forces are light, the pilots prefer to grip the stick with their fingers and to use finger and wrist motions in moving it rather than arm motions. The friction forces with this controller are between 1/2 and 1 pound and the pilots considered this amount of friction to be within the acceptable range.

Figure 2 shows the stick forces and motions required in steady pull-up maneuvers with the F9F-2 airplane when using the side controller. The upper curve shows the variation of the stick force per g with Mach number, and the lower curve shows the stick motion per g. At Mach numbers between 0.6 and 0.8, where most of the maneuvering was done, the force per g is about $1\frac{1}{2}$ pounds. Most of the pilots were of the opinion that the forces were of about the right magnitude. However, some of the pilots thought they would prefer heavier forces.

The magnitudes of stick motion per g (which at a Mach number of 0.6 is about 0.35 inch) were satisfactory in the pilots' opinions. The stick motions per g are larger with the F9F-2 side controller than those estimated for the X-15 at some flight conditions. At a Mach number of 4.0 and a dynamic pressure of 2,000 pounds per square foot with the X-15, the stick motion per g has been estimated to be about 0.10 inch.

Figure 3 shows the variation of steady rolling velocity with lateral stick motion and lateral stick force with the side controller in the F9F-2 airplane. In this case, full stick throw of almost 2 inches requires a force of about 4 pounds and produces a rolling velocity of about 150 deg/sec. The pilots considered the lateral control characteristics documented here to be satisfactory.

Fourteen pilots have flown the F9F-2 airplane by using the side-located controller. Included in the flying were take-offs, landings, stall approaches, aerobatics, air-to-air tracking, and rough-air flying. All the pilots liked flying with the side controller. They were able to become accustomed to it quickly and found it comfortable and natural to use.

PROPOSED X-15 SIDE CONTROLLER

The design of the side controller for the X-15 has not been definitely established as yet. However, a design now contemplated is shown in figure 4. The solid outline of the controller grip indicates the neutral position and the dashed outlines show the maximum deflections. The controller motion which produces pitching is a pivoting motion about the pilot's wrist. An upward grip motion is required for a pull-up and a downward motion for a push-down. The axis for roll control motions is at the bottom

of the grip and it remains perpendicular to the grip when longitudinal control is applied.

The X-15 controller will be used with a hydraulic power control. This introduces some additional factors which may affect the pilot's ability to control. Some of these factors are being studied by using a ground simulator.

SIMULATOR

Figure 5 is a photograph of the simulator. This simulator duplicates the short-period pitching motion of an aiprlane and the pilot controls the simulator motion through a hydraulic-power control system. The side controller here has motions similar to the one proposed for the X-15.

One of the X-15 flight conditions used in the simulator tests was a Mach number of 4.0 and a dynamic pressure of 2,000 pounds per square foot. For this flight condition the following characteristics were held constant: $\alpha/g = 1.3°$; $\dot{\theta}/g = 0.5$ deg/sec; period, 1.2 seconds; damping ratio, 0.3. The following table lists the control-system characteristics varied in the simulator tests and the effect of the change made.

Variables	Initial value	Changed to -	Effect of change (pilots' opinions)
Valve friction	0	±4.8 lb	Intolerable
Stick friction	±0.5 lb	±3.5 lb	Maximum tolerable
Control sensitivity	$d_s/g = 0.07$ in. $F/g = 2.2$ lb	0.30 in. 0.6 lb	Good control characteristics

The variable labelled "valve friction" is actually the stick force required to overcome the valve friction. The "stick friction" is the friction in the control system other than the valve friction.

With these initial values of 0 valve friction, 1/2 pound of stick friction, a stick motion of 0.07 inch per g, and a stick force of 2.2 pounds per g, the pilot rated the control characteristics as fair. He had no real difficulty in controlling and his only objection was that the control motions were too small.

When the valve friction was increased from essentially 0 to 4.8 pounds (while keeping the initial values of stick friction and control sensitivity) the pilot considered the system to be intolerable and almost unflyable because of pilot-induced oscillations. It should be pointed out that this value of valve friction is quite low. If it were present with a conventional control stick a stick force on the order of 1 pound would be required to overcome it.

With the initial values of valve friction and control sensitivity, the maximum tolerable stick friction (or breakout force) was found to be about 3.5 pounds. This is about the same value that has been found previously with the simulator for a conventional center-located stick. This value of a maximum tolerable stick friction of 3.5 pounds is based on considerations of pilot fatigue and precision control.

When the stick motion per g was increased and the stick force per g was simultaneously reduced to the values shown, while keeping the valve and stick frictions at the initial values, the pilot noted an improvement in the control characteristics mainly because of the larger stick motions. The initial stick motion per g of 0.07 inch is close to that estimated for the X-15 at this flight condition.

As noted previously, the pitching velocity per g is only about 0.5 deg/sec at a Mach number of 4.0. It is the pilot's opinion that the small pitching velocity per g makes controlling easier because he is less likely to induce oscillations. This was checked on the simulator by increasing the pitching velocity per g by 4 times (which corresponds to flight at a Mach number of 1.0). The effect of this was to make the simulator considerably more difficult to control.

TV-2 AND F-102

A controller having motions similar to the proposed X-15 side controller also has been installed in a TV-2 airplane. Figure 6 is a photograph of the controller installation in the TV-2. This controller is also being used with hydraulic-power control system. In an effort to reduce the control-valve friction to an acceptable level, vibrators are mounted on the control valves of the hydraulic actuators.

The flight program with this installation is just getting under way and only a few preliminary flight tests have been made. These preliminary tests have emphasized some of the problems. The presence of some valve friction together with some backlash and flexibility has caused the control system to be unsatisfactory on the initial flights. An effort is being made to eliminate these deficiencies. The pilot who has made these two preliminary flights has commented that the motion required for

longitudinal control (that is, pivoting about the wrist) is not natural to him and his force capabilities are quite limited. With increased experience this may not be too important.

A side controller has recently been installed in an F-102 airplane by Convair. This controller is being used with hydraulic-power control systems. Little information has been published concerning this controller but apparently it has been well received by the pilots.

CONCLUDING REMARKS

The results obtained with the F9F-2 airplane indicate that the pilots basically have no difficulty in flying an airplane using a side controller. However, control-system friction forces, particularly valve friction, must be greatly reduced from the values which are tolerable with conventional center-located sticks.

SIDE CONTROLLER IN F9F-2 AIRPLANE

Figure 1

STEADY PULL-UP CHARACTERISTICS WITH SIDE
CONTROLLER IN F9F-2 AIRPLANE
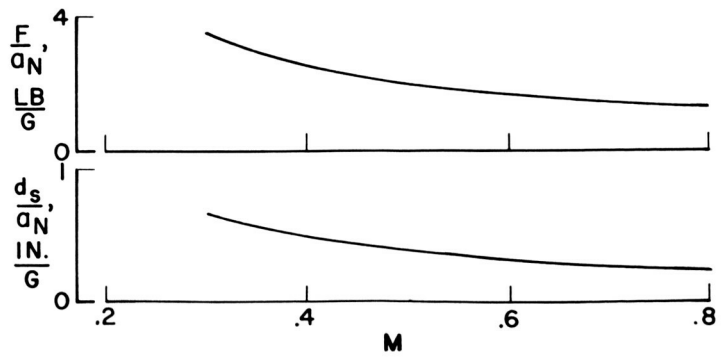
Figure 2

ROLLING CHARACTERISTICS WITH SIDE
CONTROLLER IN F9F-2 AIRPLANE
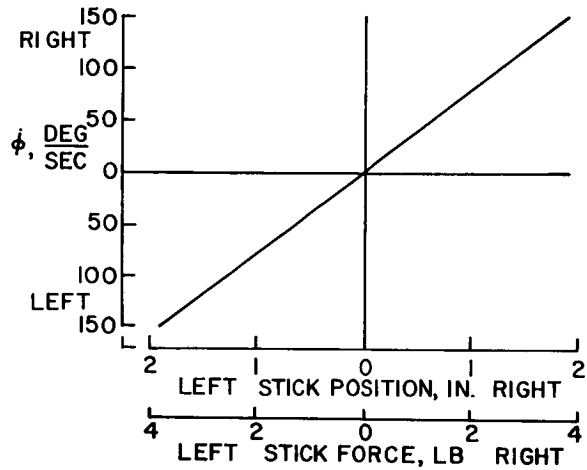
Figure 3

SIDE VIEW OF PROPOSED SIDE CONTROLLER FOR X-15
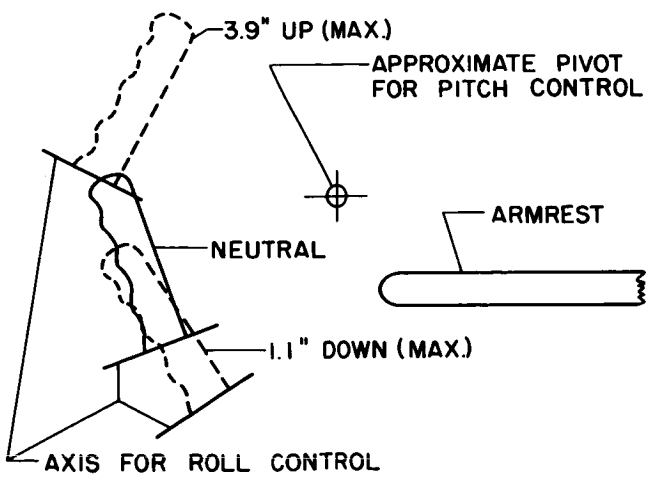
Figure 4

PITCH SIMULATOR WITH SIDE CONTROLLER
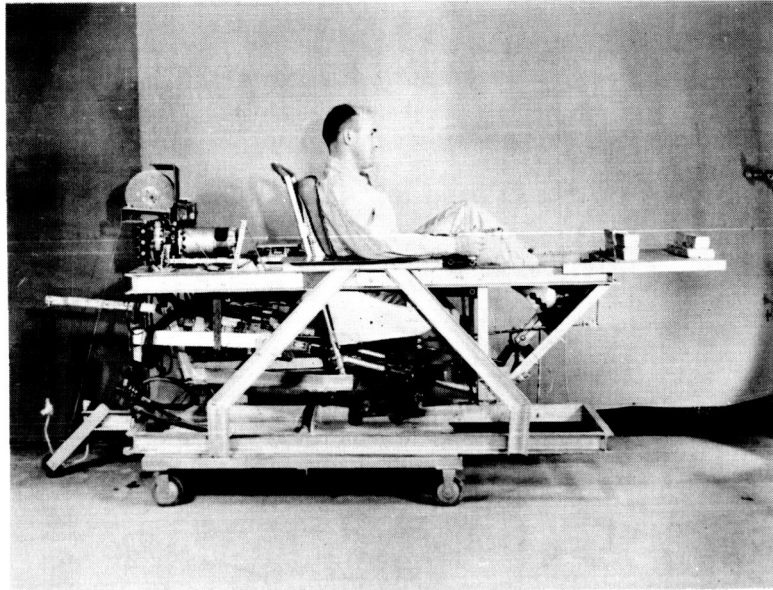
Figure 5

SIDE CONTROLLER IN TV-2 AIRPLANE
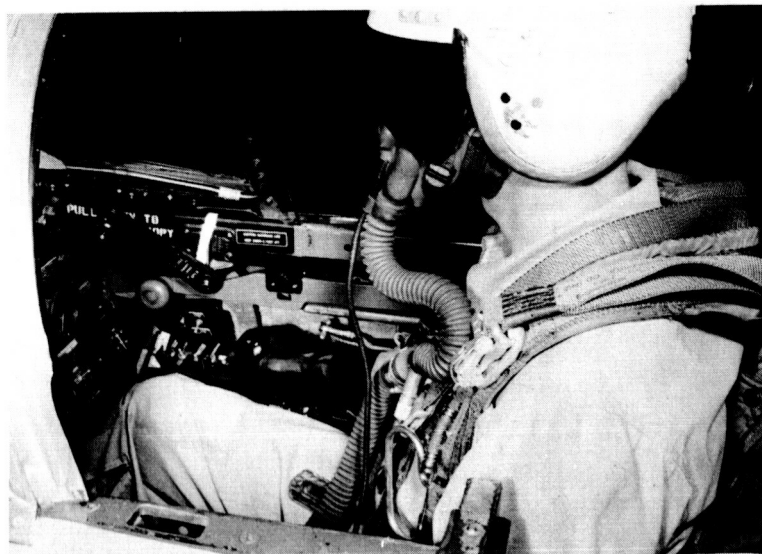
Figure 6

STUDIES OF REACTION CONTROLS

By Wendell H. Stillwell

NACA High-Speed Flight Station

The attitude-control method selected for the North American X-15 for flight at extremely low and zero dynamic pressures utilizes the reaction forces developed by small-rocket units located on the airplane to produce rolling, pitching, and yawing moments. An investigation of reaction controls similar to those selected for the X-15 has shown that unique control problems exist for flight at the low dynamic pressures where this type of control is used. Although the Bell X-1B configuration was utilized for this investigation, a range of variables was covered to determine the significant effects of various factors on flight with reaction controls. It was also of interest to determine fuel requirements for the rocket units. The investigation consisted of analog-computer studies and ground-simulator tests. The significant results of this investigation will be discussed.

The general areas for flight with reaction controls are presented in figure 1 which shows the Mach number and altitude relationship for dynamic pressures q of 2.5 and 10.0 lb/sq ft. Curves showing the performance of the X-1B and X-15 airplanes are also included in figure 1. Other studies have shown that aerodynamic controls will be effective at dynamic pressures greater than about 10.0 lb/sq ft. The shaded region for q, from 2.5 to 10.0 lb/sq ft, is an area where either control may be used. Reaction controls will be required for flight at dynamic pressures less than $q = 2.5$ lb/sq ft. A rather limited region for reaction controls can be explored with the X-1B, but the X-15 will be able to operate over a wide region where reaction controls will be required.

A three-degree-of-freedom analog-computer simulation was initially made for conditions of $q = 0$ in order to eliminate the many additional variables that would be covered if the aerodynamic terms were included.

Figure 2 shows the type of control stick and pilot presentation used. Roll and pitch control were applied by normal hand movement; and yaw control, by a thumb switch. The control stick was not an optimum configuration but after practice pilots became proficient in its use. A small oscilloscope presented roll and pitch angles in a manner similar to the conventional gyro horizon, and a separate instrument needle presented yaw angle.

Simulated flights of 2-minute duration were made in which the airplane was initially disturbed slightly and the pilot was required to stop

motion and maintain steady flight at an attitude of zero for roll, pitch, and yaw. For this 2-minute flight, results were evaluated from pilots' comments and from the impulse.

The investigation was first concerned with the choice of control configuration, or proportioning of control thrust to stick deflection. The variations covered are shown in figure 3. On the left are the proportional controls with a linear variation of control power with stick travel. On the right are the on-off controls which apply full control power or rocket thrust when the control stick reaches a certain position. The proportional control gave trouble because of the difficulty of avoiding small amounts of control application with the stick centered. This problem was eliminated by the addition of a dead spot at the center of the stick to cut off rocket thrust until the stick was moved to approximately 20 percent of travel. It was found that with either of the linear configurations pilots did not use the proportionality features since control inputs consisted predominantly of maximum thrust of short duration. The pilots, in effect, were using the proportional control as an on-off type of control. The pilots reported little difference between the on-off and the proportional control. A relatively short learning period was required to become proficient with either control, and the pilots believed that control was not too difficult. However, they did require almost constant use of the reaction controls to make small trim corrections. The two-step, on-off control was preferred over the one step, but, for simplicity, the one-step control configuration was used for the rest of the investigation.

Since the reaction-control inputs were of a very short duration, it was believed that any time lag of thrust buildup or cutoff at control application might have some effect on control. However, an investigation of time lags up to 0.5 second showed that this lag does not have a significant effect on control.

Early in the investigation, it was found that pilots desired more roll-control power than pitch- or yaw-control power. Therefore, many combinations of control effectiveness were investigated. The results are presented in figure 4 which shows the variation of thrust impulse per second of flight with roll-control effectiveness for various ratios of roll to pitch-control effectiveness or roll to yaw-control effectiveness. Roll-control effectiveness was arbitrarily selected for comparison purposes. Impulse per second is a summation of the reaction-control impulse about all three axes divided by the run duration time. Impulse per second is used not only to show the thrust required but also as an indication of efficiency of the various control combinations. Control effectiveness is expressed in terms of the constant angular acceleration produced by the reaction controls.

The ratio of roll to pitch or yaw control was varied from 1:2 to 8:1. In general, more satisfactory control was obtained at the lower control effectiveness regions. These levels were high enough to allow fairly large disturbances to be controlled and were also satisfactory for trimmed flight conditions requiring small control applications. Increased control effectiveness tended to produce overcontrol and more difficulty in flying and a corresponding increase in impulse.

The pilots preferred ratios of 2:1 to 4:1 and roll-control levels of about $5^\circ/\text{sec}^2$ or $10^\circ/\text{sec}^2$. This is summarized in figure 5 which presents regions of satisfactory and unsatisfactory control for various combinations of roll-control effectiveness and control-effectiveness ratio. The shaded areas indicate the regions investigated. Regions of satisfactory and unsatisfactory control characteristics are shown. The two preferred conditions are indicated by the symbols. Although no data were obtained at lower control-effectiveness levels, the satisfactory area probably extends slightly into this region.

The investigation was next extended to include aerodynamic effects at dynamic pressures up to 10 lb/sq ft. The basic investigation was for the aerodynamic derivatives of the X-1B at a Mach number of 0.5. The pilots' display was modified from the condition at $q = 0$ to provide the pilot with an accurate indication of α and β. Control at low dynamic pressure was more difficult than for $q = 0$ primarily because it was necessary to maintain sideslip angle near zero. If the pilot allowed an appreciable sideslip angle to develop, the dihedral effect produced rolling moments that required considerable roll control to counteract. Therefore, the pilots flew a very precise yaw control.

The effects of changes in directional stability and in effective dihedral were also investigated. The pilots reported a marked increase in ease of control as effective dihedral was decreased, and at $C_{l_\beta} = 0$ control was similar to that at $q = 0$. Reductions in directional stability had less effect on control, and adequate control was maintained even at negative values of directional stability although considerable more pilot's effort was required.

In order to carry the reaction-control studies one step further, a ground simulator was constructed. It was hoped to approximate more closely the pilots' environment and to provide a check for the analog program. Figure 6 shows the simulator in operation. The simulator is pivoted at the supporting strut and is free to rotate around three axes. The center of gravity is at the pivot point, and the pilots' position ahead of the center of gravity is similar to his location on the X-1B airplane. The pilot operates the simulator through a side-arm control stick. The simulator is operated by nitrogen gas which is exhausted out nozzles that simulate the rocket units. Carbon dioxide is shown in the photograph (fig. 6) to illustrate the operation of the simulator.

In general, the simulator tests have verified the analog results as to control-effectiveness levels desired by pilots. It will be further used to evaluate the airplane components for the rocket units and to evaluate pilot presentation and control-stick configurations.

In conclusion, it might be pointed out that, over the range of variables investigated to date, no serious difficulties as to flight at zero dynamic pressure with reaction controls have been evidenced. New pilot's techniques and constant pilot's attention to control will be required. Control at low dynamic pressure will be more difficult primarily because of dihedral effect. It is believed to be important to provide pilots with considerable practice with an analog simulation before flight tests are conducted.

AERODYNAMIC AND REACTION CONTROL REGIONS
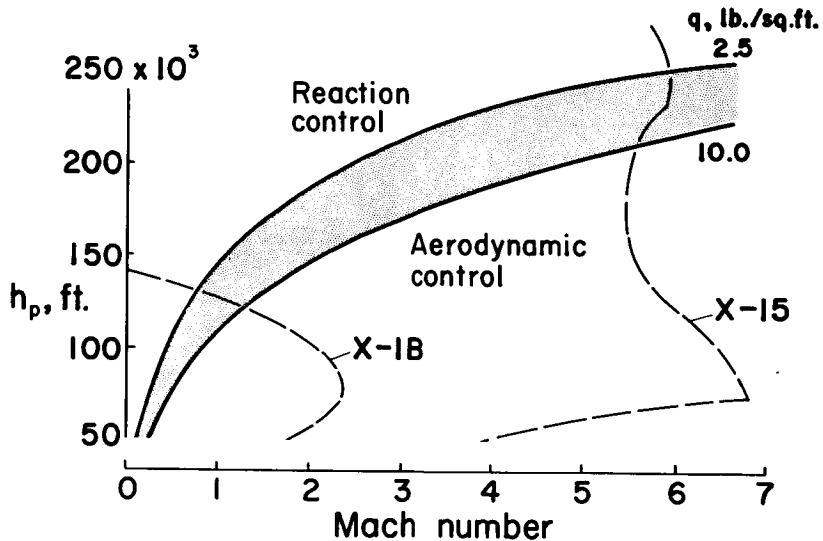
Figure 1

ANALOG CONTROL AND PRESENTATION
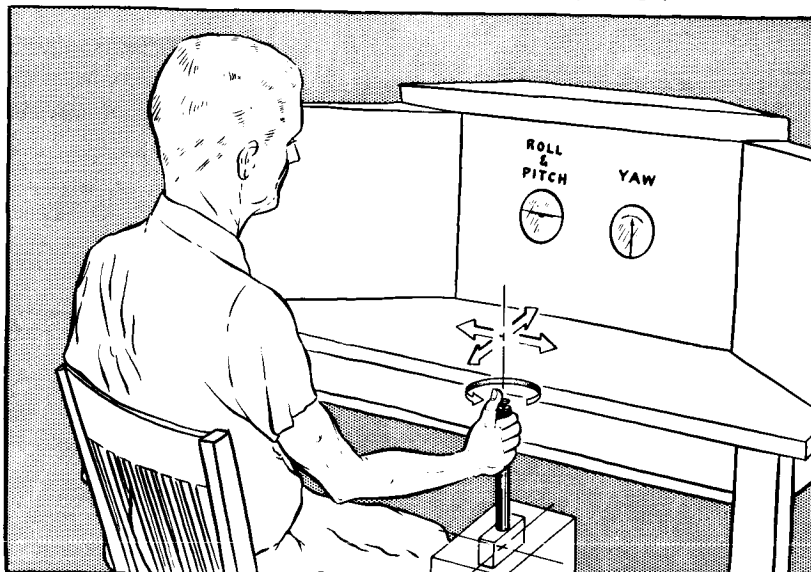
Figure 2

CONTROL CONFIGURATIONS

Proportional   On – Off

100

Control power,
percent   0

Linear

Linear with
deadspot

Two step

One step

100
100   0   100   100   0   100

Control-stick travel, percent
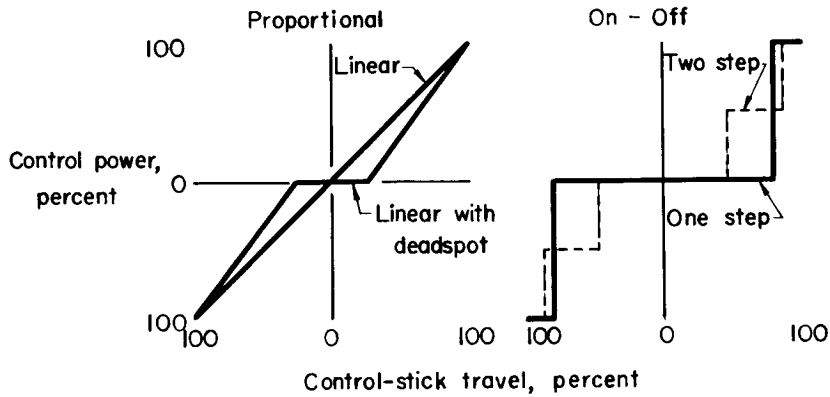
Figure 3

FUEL REQUIREMENTS

Dynamic pressure = 0   ON –OFF Control

20

Impulse per sec,
lb-sec per sec

10

$\dot{p} = \frac{\dot{q}}{2} = \frac{\dot{r}}{2}$

$\dot{p} = \dot{q} = \dot{r}$

$\dot{p} = 2\dot{q} = 2\dot{r}$

$\dot{p} = 4\dot{q} = 4\dot{r}$

0
0   10   20   30

Roll-control effectiveness, $\dot{p}$, deg./sec./sec.
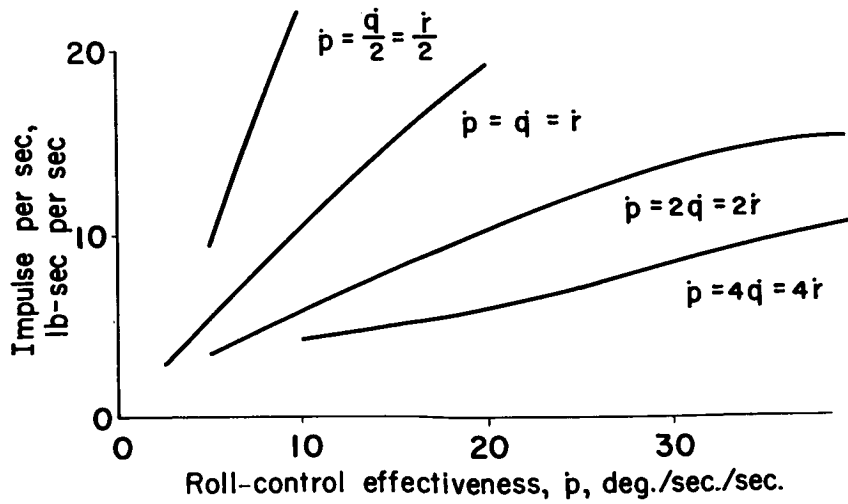
Figure 4

PILOT—OPINION SUMMARY
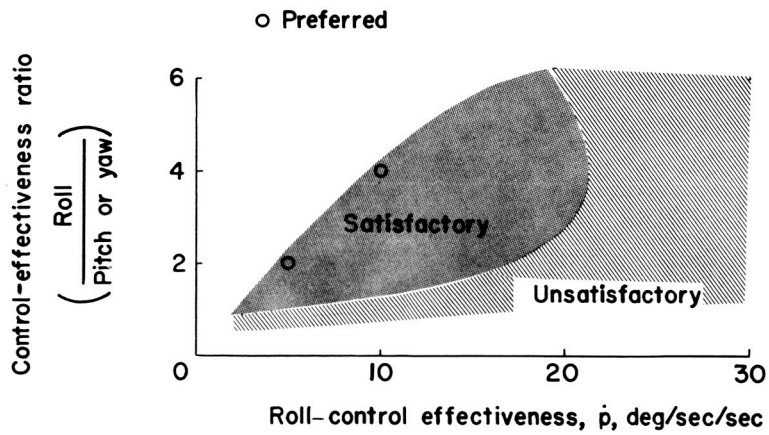
Figure 5

ATTITUDE CONTROL SIMULATOR
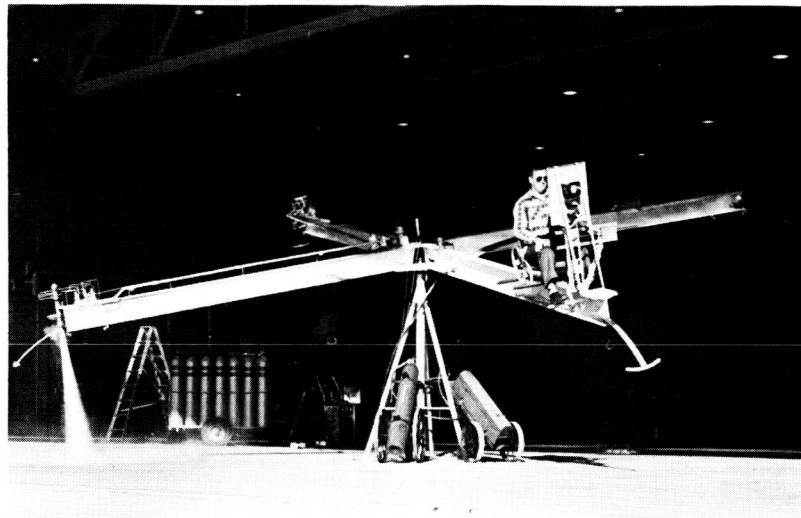
Figure 6

INSTRUMENTATION FOR THE X-15

By I. Taback
Langley Aeronautical Laboratory

and G. M. Truszynski
NACA High-Speed Flight Station

The development of a research airplane which extends manned flight into regions where extremes of temperature and pressure are reached requires the simultaneous development of new instrumentation techniques not only to insure safe operation of the airplane but also to derive a maximum of research data throughout the operational range of the aircraft. The instrumentation required for the North American X-15 airplane project consists of a ground range and its associated equipment and airborne equipment required for pilot's displays and for research measurements.

This paper will outline a plan for a ground range, which is based upon developed equipment already in use, and also will discuss the airborne instrumentation and some of the special airborne devices which are made necessary by the extended performance capabilities of this airplane.

A ground range is required for various reasons, some of these are:

(a) To assist the mother and research aircraft in navigation

(b) To aid the pilot by means of telemetered data and voice communication when necessary

(c) To provide search facilities in the event of an emergency landing

(d) To determine accurately aircraft trajectory for research purposes

The ground range which is required to handle most of the high-speed flight plans covers a distance of about 400 miles in length. Figure 1 indicates the approximate location of the three radar-equipped ground stations which comprise the range facility. These stations, which are near Ely, Nevada, Beatty, Nevada, and at the NACA High-Speed Flight Station at Edwards, Calif., are located along a selected flight path and are appropriately spaced, so that adequate overlapping of tracking is secured. Also indicated in this figure are the locations of lake beds which may be used as emergency landing areas.

The tracking equipment will consist of radars similar to those now being used at the Air Force Missile Test Center in Cocoa, Florida. Figure 2 indicates the flow of information to and from each of the ground stations. The information coming from the airplane consists of vehicle

range, elevation and azimuth data as secured by the tracking radar, telemetered engine and aerodynamic data, and voice communication. Received from an up-range station are timing signals, voice communication, and radar acquisition data. Recorded at each station on magnetic tape or on film are the precision radar data, the telemetered information, timing, and the voice channels. The telemetered quantities which must be monitored are also directly displayed. The outgoing information consists of station-to-station and ground-to-air voice, timing, and radar acquisition data. The radar information when received at a down-range station is corrected for parallax and earth curvature, and these data are then used to train the down-range radar on the target. The timing signals emanate from a timing system at Edwards and are relayed to each of the stations.

The detail design and fabrication of this range are being undertaken by the Electronic Engineering Co., Los Angeles, California, and it is estimated that the range will be ready for use sometime in 1958.

The airborne equipment required for piloting aids and research measurements will now be considered. Figure 3 gives a side view of the airplane showing the instrument compartments. A small compartment near the nose permits installation of a pressure recorder. The tubing leading to this recorder will be short so that reasonable lags are encountered at low absolute pressures. The main instrument compartment is immediately behind the pilot. The midsection of this compartment consists of a removal rack which can be placed on a convenient surface outside the airplane. Removal of this rack allows access to the remainder of the instruments which are mounted on shelving surrounding the rack well. Another compartment adjacent to the center of gravity is used for center-of-gravity accelerometers and some other small sensing elements. All of the compartments will be pressure and temperature controlled.

The measurements which are required for the X-15 are: accelerations; attitude angles; angular velocities; control positions; engine pressures and temperatures; structural strains, temperatures, and deformations; velocity; altitude; air temperature; Mach number; and air-flow angles. At moderate speeds and altitudes these quantities will be sensed by conventional means, recorded on NACA developed recorders, and indicated to the pilot, as necessary, by standard panel instruments. No difficulty is forseen at high Mach numbers with the instrumentation which can be protected within the airplane. These are the devices which will record accelerations, attitude angles, angular velocities, control positions, engine pressures, and engine temperatures. Structural strains, temperatures, and deformations will have to be measured in order to study heat transfer and to determine the effect of high temperatures on the structure. It is estimated that approximately 500 measurements of various strains and temperatures will be required. A method of making accurate strain measurements at the temperatures which this airplane will ultimately reach is

not yet known; however, some development work is underway at the Langley Laboratory as well as at many other agencies in regard to this problem.

It is planned to secure the structural temperature measurements with thermocouples which are spot welded to the structure. This technique provides good heat transfer to the thermocouple and results in a minimum of mass connected to the aircraft skin. A good measurement of local skin temperature can thereby be secured, as changes in the heat capacity of the skin are minimized. The thermocouples have been tested with leads supported 3 to 5 inches away from the junction, at temperatures up to 1400° F, and under intense vibration, with satisfactory results. A severe data workup problem exists if many local temperatures and strains are to be measured and analyzed in detail. At present, work is being done to reduce this problem. A laboratory setup is now under test which would enable this mass of data to be sampled and recorded on magnetic tape. This technique will be used if satisfactory results are secured. It is also possible that commercial equipment suitable for recording low-level signals on magnetic tape will become available for use on the airplane.

Structural deformations of the wings and tail surfaces will be viewed by cameras which will be enclosed in pressure- and temperature-controlled compartments.

Present techniques for measuring velocity, altitude, and Mach number depend upon an accurate determination of static pressure. It will be extremely difficult to sense static pressure accurately at high speeds because of the conditions which are indicated in figure 4. Plotted against Mach number is the ratio of impact pressure behind a normal shock to the stream static pressure and the stagnation temperature in increments of 100° R. The values are based on an ambient temperature of 400° R and real gas properties. One of the difficulties in sensing static pressure is caused by the fact that the ratio of impact pressure behind a normal shock to the stream pressure increases rapidly as the Mach number increases, varying from about 1 at sonic speeds to over 60 at a Mach number of 7. A static-pressure probe with a 1-percent impact-pressure error could sense static pressure to 1 percent at sonic speeds. At a Mach number of 7, however, if the same percentage of impact pressure leaks into the static-pressure measurement, an error of over 60 percent in static pressure would result.

The second difficulty encountered is that the temperature rise encountered at high speeds greatly limits the probe configurations which should be used to minimize pressure errors. The thermal problem has been sufficiently discussed with respect to the airplane. Similar structural problems exist in the design of a probe and are aggravated by the high heat-transfer coefficients which would exist on the nose and along the length of a probe of reasonable diameter. In order to extend the measurement of velocity and altitude to high speeds, a stable platform-integrating accelerometer system will be used instead of pressure methods. Equipment

similar to that proposed is already available for navigational purposes. This equipment is in general heavy and of large size because of extreme navigational accuracy requirements. Also, only horizontal velocities and displacements are measured, since altitude is usually determined by pressure methods.

A three-axis system is being proposed for use in the X-15. Specifications for the platform and computing elements have been prepared which are based on current manufacturing capabilities, and manufacturers' proposals are now being reviewed.

The proposed platform system is a three-gyro assembly which is oriented tangent to the earth and along a planned great-circle path. Three accelerometers are borne by the platform. These measure accelerations in the coordinate system which is indicated in figure 5. The coordinate axes are: any selected great-circle path, an axis perpendicular to this path, and local vertical. The outputs of the 3 accelerometers are inserted into computing networks which apply corrections for earth rotation and curvature and Coriolis accelerations. The accelerations are then integrated and summed with proper initial conditions to produce horizontal and vertical velocities. The velocities are vectorially summed to provide total velocity which is furnished to a pilot's indicator. Vertical velocity is available from the vertical integrator and is again integrated to secure altitude. Pitch, yaw, and roll angles are available from pickoffs on the platform gimbals and will be supplied to a pilot's indicator and recorded for research purposes. It is believed that this apparatus will be extremely valuable for the control and investigation of hypersonic aircraft.

The measurement of air temperature from the airplane is difficult. In order to secure accurate measurements, it is necessary to design the temperature probe so that full stagnation temperature is reached by the sensing element, and yet the probe supports and radiation shields must retain adequate strength under high pressure and acceleration loads. Some high-temperature probes have been designed for measuring exhaust jet temperatures; however, no apparatus is available which is suitable for the X-15 airplane. It is planned at present to secure air temperature from a radiosonde survey. These data, in combination with data secured from the airplane, can be used to compute Mach number and also stagnation temperature. It is unfortunate that balloon-sounding techniques are at present limited to altitudes of about 100,000 feet and therefore these derived quantities will be similarly limited.

A device which will be suitable for the determination of angle of attack and sideslip is now being investigated. Although these flow angles are not normally considered basic to the control of an airplane, the X-15 is faced with unusual problems of flight-path control, both on leaving the effective atmosphere and also upon reentry after ballistic flight.

There are various criteria for the design of this sensing element. The sensing element must

(a) Be forward of aircraft flow disturbances

(b) Be structurally sound at elevated temperatures

(c) Operate with reasonable accuracy at extremely low pressures to provide angle information well before reentry

(d) Introduce a minimum flow disturbance so that heat-transfer phenomena on the forward portion of the aircraft can be studied.

These criteria lead to the consideration of the null-balance sensing device shown in figure 6. The sensing element is a sphere located in the nose of the airplane. It is on appropriate gimbals and is servo driven in two planes. The sphere has 5 orifices, one at the stagnation point and pairs of orifices at about 30° or 40° from the stagnation point in the pitch and yaw planes. Each pair of orifices produces a pressure difference which is proportional to the misalinement of the sphere with the relative air flow. The pressure differences are sensed and guide the servos to realine the sphere into the relative wind. Computations have been made which indicate that a 6-inch-diameter spherical nose, constructed of Inconel, can be made of reasonable thickness so that its surface temperature will not exceed $1,200^{\circ}$ F under the proposed flight plans. When based upon sphere pressure distributions and the sensitivity of an available differential pressure sensor, the resolution of the device is estimated to be about 0.6° at 200,000 feet for a typical flight plan. This resolution would increase by about a factor of 10 for each 50,000 feet decrease of altitude. These computations indicate that sufficient accuracy is available to allow making successful reentry into the atmosphere upon completion of ballistic flight.

No static source is available on this configuration. In order to provide indicated airspeed to the pilot during the landing condition, an alternate pitot-static source will be provided, which will be calibrated for use at landing speeds. At the present time, various sphere-cone configurations are being tested to determine heat-transfer characteristics along the fuselage and at the lip and some of the pressure characteristics of the sphere at high angles of attack. Some of the heat-transfer data have been presented by William V. Feller in a previous paper, and these data indicate that there are severe thermal problems to be overcome in the design of the external configuration. Many technical difficulties will also be encountered in designing the mechanism which drives this device; however, it is felt that a workable unit can be made available for the X-15 airplane.

This paper has described the ground range and airborne equipment which is to be used with the X-15 airplane. Some of the instruments

required are now in use. However, as has been pointed out, new measure-
ment problems introduced by the increased performance characteristics
of the airplane will require novel approaches. Means of obtaining these
new measurements have been decided upon; however, much further development
work is necessary before suitable apparatus can be made available.

LOCATION OF X-15 GROUND RANGE

Figure 1

INFORMATION FLOW ON X-15 RANGE

RECORDED { RADAR DATA   TELEMETER
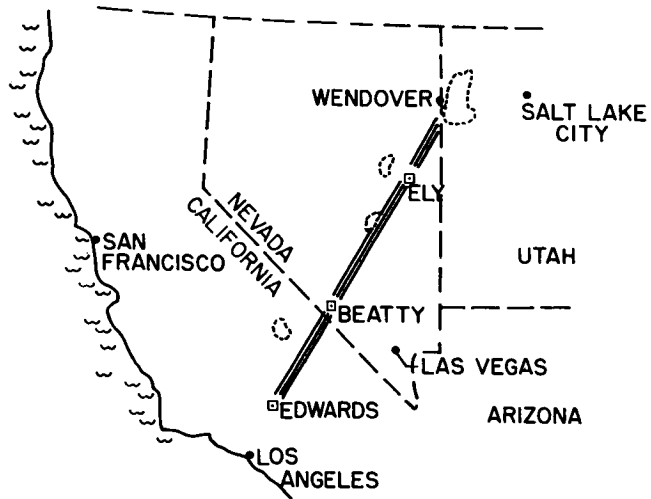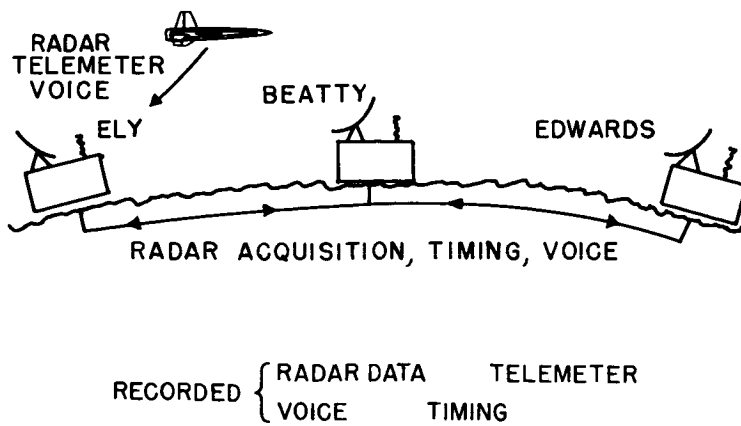   VOICE   TIMING

Figure 2

INSTRUMENT COMPARTMENTS IN X-15 AIRPLANE
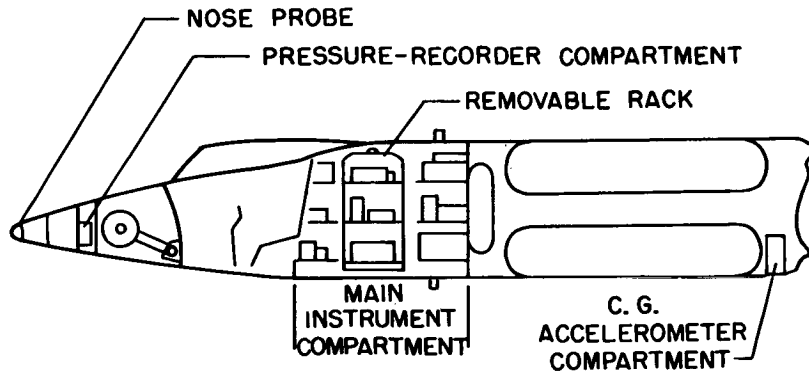

Figure 3

PRESSURE RATIO AND STAGNATION
TEMPERATURE VS. MACH NUMBER
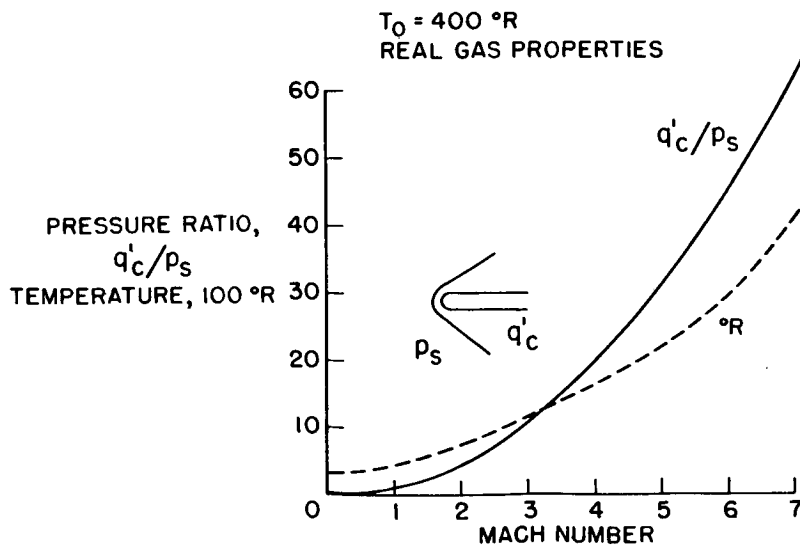
Figure 4

STABLE-PLATFORM SYSTEM FOR X-I5 AIRPLANE
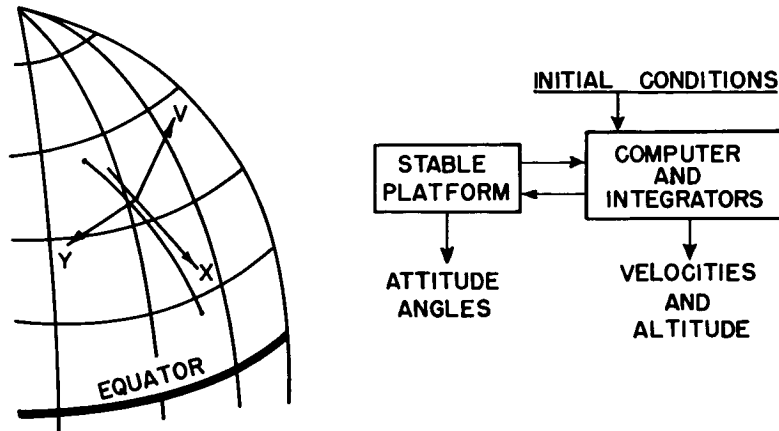
Figure 5

ANGLE-OF-ATTACK AND YAW SENSOR FOR X-I5
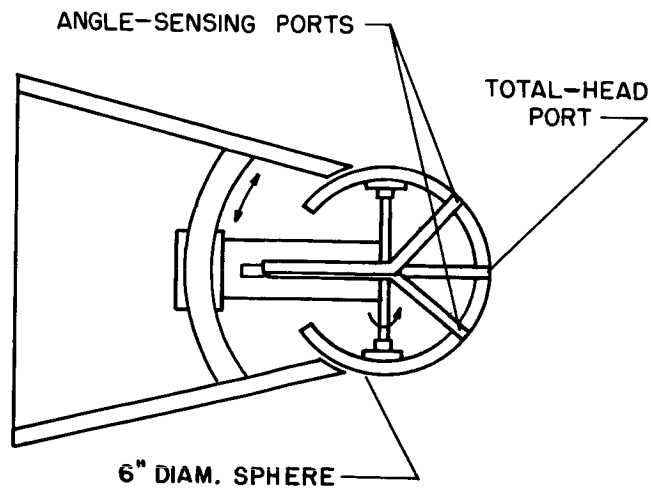
Figure 6

X-15 CREW PROVISIONS AND ESCAPE

By A. Scott Crossfield

North American Aviation, Inc.

INTRODUCTION

This paper will cover several subjects of immediate concern to the pilot including emergencies, pilot furnishings, cockpit arrangement, accelerations, and landing characteristics.

EMERGENCIES AND ESCAPE

Basic in the X-15 concept is that it is to be manned. Since it is manned, modern practice dictates that prime consideration be given to escape in the airplane design. In setting about the determination of an escape system, two predominant ideas were strictly adhered to: (1) the most suitable escape system compatible with this airplane would be selected and (2) no approach would be attempted that would not be developed within the airplane development time and hence leave the pilot with no escape capability at all, as has happened in the past.

An exhaustive study has been made on the X-15 escape system along the following lines. First, of course, an intensive search of available literature on the several approaches to escape was made. Analysis for X-15 application was made of four types of internal cockpit capsules, five types of nose capsules, a canopy shielded seat, a stable seat-full pressure suit combination, and a stable seat-suit combination with a "skip flow" generator shielding device.

First, an elaborate comparison of escape systems was made assuming 100-percent pilot and mechanical reliability covering the protective capabilities in all phases of emergencies and escape. A balance sheet was made with careful analysis of the foregoing as applied to the X-15.

The next part of the study was a detailed analysis of X-15 accident potential based upon the airplane's missions and previous rocket airplane records of malfunctions that could cause critical emergency. Maintenance and flight experience records of rocket airplanes were analyzed. The airplane time spent in each segment of its design envelope was weighted by the malfunctions that typically occurred in each phase of flight. Figure 1 summarizes the results of the first of three studies. The envelope shown encompasses the design altitude and Mach number regime of the X-15. The numbers indicate the accident potential within the areas

15

enclosed by the boundaries and the arcs. This chart then indicates that 98 percent of the accident potential occurs below a Mach number of 4. The low 2 percent for the rest of the envelope is because of no fire or explosion hazard and low aerodynamic loads. Therefore, it is intended to build an escape system which will assure escape up to a Mach number of 4 and dynamic pressure q of 1,500 lb/sq ft. Structurally, the system would be good for q = 2,500 and every effort will be extended to raise the system capability to q = 2,500 for escape with reversible physiological effects on the pilot.

Next, escape systems were analyzed and divided into assemblies and evaluated from the standpoint of complexity. A complexity index was determined and an analytical probability of reliability applied. As the complexity of the system rose, the reliability dropped rapidly as is, of course, expected.

Escape systems were evaluated on the basis of performance penalty imposed upon the airplane due to size and/or weight increase.

The foregoing is a very brief review of the investigation which has been compiled in reference 1. On the basis of this thoroughgoing investigation, it was concluded that a modern ejection seat and a full pressure suit designed for the X-15 was the most suitable system for the airplane. The U. S. Air Force and NACA concurred in this conclusion.

Figure 2 shows a modern version of the ejection seat as befits the X-15. A rocket-type ejection gun is used to conteract initial tumbling. Upon ejection, the stabilizing fins at the shoulders erect the seat to a mean angle of attack of 120° so that the seat bucket and back take the blast, heating, and acceleration loads. The alternate version with the skip-flow generator allows a reduction in weight because of lesser drag and some alleviation of blast, temperature, and stability problems. Although not necessary, the advantages will be used but largely for reasons of weight reduction. A skip-flow generator is a leading deflector that causes flow separation so that the pilot is immersed in a separated, turbulent, low velocity region.

The escape envelope capabilities for the X-15 system are illustrated for the level flight case in figure 3. Lines of constant altitude indicate the expected g levels due to drag imposed upon the pilot as a function of Mach number for supersonic ejection. Critical areas are the right boundary at a Mach number of 4 because of aerodynamic heating since the low deceleration causes extended times at high speed and the upper boundary because of g. The 32g limit at high q is acceptable because of the seat attitude, the mechanically forced positioning of the pilot, and its transient nature. Use of the skip-flow generator can reduce the severity of the g loads or raise the escape limit q whichever is determined more critical.

This escape envelope is reduced if escape is required during ascent on an altitude mission. Figure 4 shows post-separation time histories of altitude and Mach number for the escape systems for separations during the ascent. Above 80,000 feet, drag coefficient has little effect upon the peak altitude attained and the durations of sustained speeds. The numbered ticks indicate the altitude and speed of separation. For example, cases 2 and 3 are escapes at about 85,000 feet with low and high drag devices, respectively. In each case, peak altitude is about 118,000 feet and the Mach number time traces similar.

Post-separation time histories were summarized and are shown on figure 5. Here is shown the peak altitude to which an escape system will coast if separation occurs during the ascent trajectory. Drag has little effect upon the peak altitude attained by the escape system. "Low drag" is typical of the airplane; "high drag" is typical of large drag devices, chutes, and so forth. Most escape systems will roughly fall in the high drag half of the area shown. For example, if ejection occurs on ascent trajectory at 100,000 feet, the system will coast to between 140,000 and 145,000 feet peak altitude. Extended durations at high speeds in these trajectories cause temperature limitations. A soak boundary-layer temperature of $300°$ F is considered limiting for the seat and restricts escape to below 100,000 feet on ascent. The best salvation lies with staying with the airplane above this altitude for the ascent case. The temperature problem increases logarithmically with increase in ejection altitude because of the speed and trajectory time increase. The converse of this argument is an increase in the escape envelope during the descent phase of the flight and g is the limiting factor.

Choosing a supersonic ejection with the seat at $q = 1,500$ lb/sq ft, a motion study is shown in figure 6. The variation of g due to drag is shown by the solid line. The dashed line is the total resultant at the pilot's head due to drag plus rotational motions. The dash-dot trace is the total resultant at the pilot's head with one version of a skip-flow generator. In the lower chart, the direction of the resultant g at the pilot's head is shown for the dashed case in the top chart. The momentary peak of 38g and the subsequent oscillation of 4 cycles per second may be critical. Amplitude and frequency are reduced by the skip-flow generator as is shown by the dash-dot trace. This is due to a greater reduction in drag than weight and to increased moments of inertia. Except for the momentary peaks these g's are within Air Force specifications.

The pilot's equipment will be based upon a full pressure suit incorporating ventilation and anti-g protection, as shown in figure 7. The methods applied here are typical of those already developed in several versions under manufacture for the Armed Services. The isolated and controlled pilot environment removes exposure to ozone. There is, incidentally, no evident cause for concern about exposure to cosmic radiation.

The suit garment raises two questions. First, upon ejection, severe pressure surges due to blast may occur within the suit as illustrated in figure 8 which shows an ejection phase time history of a suit pressure variation in a 1,200 q stream. When the canopy leaves, there is a suit pressure drop. On ejection, an abrupt rise occurs at about 0.23 second. The short-duration surge of possibly 9 lb/sq in. requires investigation but is not felt to be critical. The lagging surge which will occur within the helmet may become critical because of the large unbalanced pressures possible which yield a pressure shock to the ears and lungs.

Ejection at high speed and hence temperature raise a question of structural integrity of suit materials. Though calculations indicate very small temperature rises for exposure durations, tests were run of representative suit materials under typical stress in a high q, high-temperature blast. Figure 9 shows the endurance time to incipient failure of the material as a function of temperature and dynamic pressure. The test results indicated, for example, that the material would withstand a blast of 1,500 fps behind the normal shock, 1,800 lb/sq ft dynamic pressure and 490° F stagnation temperature for 30 seconds before any sign of failure while under stress. The velocity is, of course, well above any flight possibility. The X-15 escape conditions lie beneath the lower curve in this figure.

The suit requires a control system. The system used is a scheduled control regulator assembly mounted on the pilot's back, as shown in figure 10. The emergency pressure and breathing supply for 20 minutes is mounted on the back pan as is the anti-g control valve which utilizes the same gas source. The X-15 oxygen system shown in figure 11 is mounted on the seat for normal use and for emergency pressure and breathing upon escape until separation from the seat. The only connection to the airplane is for B-36 breathing and ventilating supply use before launch. Suit pressure and breathing supply are furnished by the X-15 in flight except in the case of separation. The suit is scheduled for 35,000 feet and uses cabin air source, X-15 oxygen, or emergency oxygen for pressure source in that order as emergency develops.

The seat, in one version, is shown in figure 12. The pilot is shielded on all sides except in front and is restrained at the head, shoulders, hips, and feet. The action of the ejection handles restrains his arms with no effort required by the pilot. Stabilized free fall is provided by the seat or as a backup the man may separate positively by use of a reefed personal chute and free fall with the reefed chute to safe altitude where the chute is disreefed. Alternately, he may stay with the seat to low altitude and separate with simultaneous release and opening of his main canopy.

The X-15 system then can, with well supported and improved methods, accomplish escape in a range to 120,000 feet and up to a Mach number of 4 within the X-15 flight spectrum, which area includes 98 percent of the airplanes accident potential.

THE COCKPIT ENVIRONMENT

Although it cannot be denied that escape is important, the X-15 has a mission and a purpose. That purpose is, in part, best served by designing for the pilot a good working area and reasonable environmental conditions compatible with the airplane design.

The cockpit and instrument bay are a double-wall insulated conditioned compartment near the nose of the airplane schematically shown in figure 13. Liquid nitrogen stored aft of the instrument bay has a closed circuit pressurizing loop. The pressure buildup forces the liquid nitrogen through a distribution manifold. In the equipment bay pneumatically actuated thermally controlled valves spray liquid nitrogen into distribution ducts downstream of compartment air circulating fans. The vaporizing nitrogen forms a cool mixture which is distributed to the instrument shelves. Either of the two distribution systems can handle the expected loads. Environmental limits in the compartment are determined by the electronic equipment. The pilot, however, has secondary control available with the use of nitrogen ventilation gas flow through the suit governed by comfort requirements. Additional gas flow, always sufficient to maintain cabin pressure, is distributed through a manifold over the windshield for cooling and defogging. An emergency ram air gate and valve are provided for cockpit decontamination below critical altitudes and speeds.

Figure 14 indicates the trends with time of cabin pressure, nitrogen supply requirements, and temperatures. The cabin pressure is maintained for a 35,000-foot cabin altitude during the flight. The suit is scheduled for 35,000 feet should cabin pressure fail. With this arrangement, the pilot has no pressure variations during the critical portion of the flight nor can he be subjected to explosive decompression. The nitrogen atmosphere affords inert gas fire protection during the critical phases of the flight.

On the high-temperature mission, the cockpit temperature may rise to about 150° F which is the equipment limit. It should be noted that about 80 times the cooling capacity is required by the equipment than required by pilot. About 95 percent of the thermal inertia of the flow charged to the pilot is rejected to the cabin to warm the ventilating nitrogen. The pilot, by selection of ventilation rates, is at any desired temperature. Radiation from the hot windshield to the pilot's face is attenuated by a filtered visor lens.

THE COCKPIT WORKING AREA

The pilot's tools are, of course, the information presentation and the controls. Figure 15 shows a single point perspective of the cockpit somewhat as viewed by the pilot. Comfort is problematical but will at least be better than present rocket planes. All operations and gages

are forward of the pilot's forearms. All controls, switches, and so forth, are located to minimize cross reaching and the number of simultaneous actions required of either hand. Further, location of various operations has been given consideration of the g forces involved when such operations are necessary.

The airplane system displays are located to minimize divided attention during the various phases of the flight as areas of attention change. The system gages are laid out in logical sequence to afford the best diagnosis of abnormal operation. System controls and warning lights are arranged near the related gages and in a sequence to insure proper operation. Visibility from the X-15 is excellent in all flight phases where there is anything to see. Effects of distortion that may come from the hot windshield are as yet unknown.

Going around the cockpit from left to right figure 15 shows: the left arm rest in the outboard position and the ballistic control handle that moves on three axes and governs the thrust of the space attitude control rockets as the pilot requires. The flap and suit ventilation controls are just beneath on the console. On this airplane the speed brakes are considered a primary control and the brake positioning handles are given a priority position on the console. Just inboard on the seat console are the breathing oxygen control panel and gage. Forward on the left console is the throttle. Inboard motion starts the engine and thrust is varied by fore-and-aft motion. The propulsion-system control valves for pressurizing and jettison control are mounted on the outboard wall above the throttle. The throttle is stowed outboard when not in use. On the forward quarter panel are the landing-gear release handle and indicators.

On the left main panel are the engine controls, warning lights, and gages, as well as the engine bay fire warning and extinguishing system.

In the center of the main panel are the flight instruments. Standby conventional altitude and airspeed are on the left of this area. Vertical plane attitude indicators - that is, speed, normal g, angle of attack, altitude, and artificial horizon - are mounted horizontally. Horizontal plane or directional instruments - that is, sideslip angle, turn and slip, the compass, and homing zero reader - are mounted vertically in a line. Mach number, true speed, altitude, and attitude presentations come from a stable platform inertia integrating and attitude system proposed by NACA. Sideslip and angle-of-attack information are from a pressure sensing, servo-operated, null seeking hypersonic nose proposed by NACA.

To the right of the flight instruments are the a-c electrical and APU control panel and monitoring system. Below these are the cabin pressure and temperature system gages and controls. On the right quarter

panel are the test circuit and accessory switches and the emergency canopy jettison handle. The lower center pedestal contains the NACA flight recording instrument controls and circuit breakers and the stability augmentation gain controls available to either hand.

On the right console are the radio and homer control panels. The cockpit circuit breakers are located aft on the console. Above the console are the right arm rest and the console-mounted aerodynamic control. In the center is a conventional stick which will probably be eliminated. The elimination of the center stick throws the burden of control on the console stick. Its reasons for being are many.

Design criteria at North American dictate that the X-15 will be stable without augmentation over the speed range within practical possibility. Therefore, aerodynamically, the pilot will be provided with reasonable longitudinal stability and control power and the airplane will have some measure of directional stability, and roll-to-yaw ratios will approach zero and coupled motions from control inputs will approach zero.

Simulator tests confirm, as has been documented for years, that trends in these directions result in significant improvements in handling qualities. Also, as experience has proven, the present investigations show that small changes in the pilot-airplane control loop can have unexpectedly large effects upon handling qualities. Therefore, each isolated system in the loop is being carefully analyzed and will be carefully matched to the complete loop to achieve handling qualities which will not require a superlative exhibition of pilot capability to fly. Then, given the aforementioned stability, major improvements in handling qualities can rely upon control-system accuracy and pilot-positioning accuracy. These in turn are a function of control-system friction and energy storage, pilot-sensed control-stick friction, and inadvertent pilot-induced control inputs.

The console stick is devised with the foregoing in mind and is shown in figure 16. The wrist is restrained in this version by pressure against the arm rest against acceleration forces. Pitch and roll control are by motions in the conventional directions but by wrist movement only. Control system friction effects are to be minimized by the use of a master cylinder to do the pilot's work and located as near to the stick as possible to overpower system loads. The stability of the system between the master cylinder and the surface actuators will give problems. Stick friction and preloads are minimized by virtue of having little or no work to be accomplished by the stick motions. Inadvertent pilot inputs are thought to be virtually eliminated by the wrist rigidity.

The motions shown in the figure are those of the currently proposed control. The pitch axis goes through the center of the wrist and the roll axis lies below the forearm but rotates with pitch motion to maintain

a fixed angle with the stick grip. The center view illustrates the total arc of travel in pitch and that arc within which motion with a fixed wrist position can be obtained. This amount of control encompasses that required during the accelerated phases of the flight.

The present envelope of roll and pitch motion of the reference point is shown on the left and is subject to change as control harmony dictates. The use of console controls of several forms have been tested for some years with favorable results. As indicated in a previous paper by S. A. Sjoberg, the Langley Aeronautical Laboratory has done some tests on a similar stick for the X-15. Centrifuge, simulator, and variable stability airplane flight tests are in initiation stages. The elimination of the center stick rests upon these tests and a break with tradition.

FLIGHT ACCELERATIONS

Accelerations during the X-15 missions may pose control problems if not physiological problems. First and incidently, there is no evidence that zero g flight for X-15 durations poses serious problems. The longitudinal acceleration, however, during the power phase of an exit trajectory has levels and durations which give rise to requirements for arm restraint as longitudinal g varies from about 2 to 5 during a burning time of 88 seconds. During reentry, the control and physiological problems are more severe. Figure 17 illustrates the time variation of the worst expected accelerations along three axes selected for centrifuge tests for a reentry and recovery trajectory without augmented damping. Tests will be made at several mean levels. While the angle-of-attack oscillation damps, the normal accelerations n_z diverge as long as q is increasing rapidly. The same is true of yaw disturbances resulting in side loads n_y. The normal and lateral oscillations add to the control problem during a phase of flight where accurate control is required. The mean levels of g are about 7 normal and 5 longitudinal with a maximum of ±2g superimposed on the normal case. The normal g is severe from loads on the pilot. The oscillatory g superimposed upon the normal and lateral case poses control problems due to inadvertent inputs by the pilot. The sustained negative longitudinal acceleration n_x is very probably critical physiologically as well as from a restraint standpoint.

LANDING

Another acceleration investigation was made as a result of the landing conditions imposed by the X-15 configuration. Figure 18 shows the landing design limit conditions of $6°$ angle of attack, 164 knots and 9 fps rate of descent. Upon contact, the airplane essentially becomes pin-jointed

to the ground at the tail; the rotational velocity increases to yield a rate of descent of about 23 fps· at the cockpit. This velocity is arrested in 18 inches of stroke on the nose gear. The resulting g's peak at about 6 as shown in the time history of figure 19. At nose gear contact the g rises at about 300°/sec rate of onset to a peak of 6g and then falls off in about 0.2 second. Near simulations were run in the laboratory typical of the dashed curves shown. Subjects were run repeatedly to from 5g to 11g peaks with no adverse effects other than comments on the severity of the jolts.

LANDING-GEAR STABILITY

The unusual gear of the X-15 was selected among other reasons because it was stable during the post contact runout. That it was well within stable limits was determined by tests of a dynamically similar model which was launched on a runway at speeds up to an equivalent 150 knots. The effects of systematically varying the following were recorded:

Fore-and-aft skid location
Strut stiffness
Skid friction
Asymmetric skid friction
Nose-wheel friction
Nose-gear castering friction
Nose-gear castering damping
Vertical and horizontal center-of-gravity location
Corotating wheels
Independently rotating wheels
Effects of cross winds with varied location of side-force resultant

These tests were run with initial yaw angles varying from 0° to 30° and cross winds up to 90°. Compilation of these data indicates that the X-15 design conditions are very stable. An incidental observation was that because the skids have little or no tracking ability side loads govern the airplane path. Therefore, if the pilot applies right rudder, the airplane path would deviate to the left.

CONCLUDING REMARKS

Of the various areas of immediate concern to the pilot treated in this paper, two areas because of their particular importance to the pilot require special attention. First, adequate presentation and control of the airplane systems must be afforded to allow the pilot to most effectively use the airplane mechanisms. And second, given a reasonably stable and controllable aerodynamic configuration, adequate flight information along

with control accuracy and harmony are to be provided so that the pilot can control the X-15 to serve its useful purpose of systematic data accumulation.

REFERENCE

1. Anon.: X-15 Research Airplane - Ejection Seat and Capsule Study. Rep. No. NA-56-686, North American Aviation, Inc., 1956.

SYS-447L ANALYSIS OF X-15 ACCIDENT POTENTIAL

ALT 1000 FT

260
200
160
120
80
40
0

0.5%
25
50
$q=100$
B.O.
1.5%
6%
$q=1500$
92%
2500
EXPECTED FLIGHT LIMITS
DESIGN LIMITS
M

0   1.0   2.0   3.0   4.0   5.0   6.0   7.0
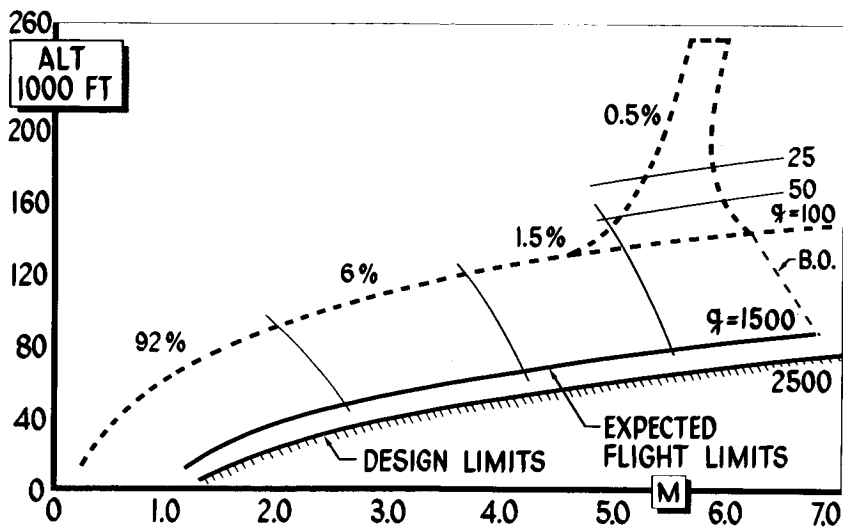
Figure 1

SYS-447L DETAIL ESCAPE SYSTEM STUDY X-15 SEAT

V

EJECTION   WT 460 LB
FIN AREA   2 SQ FT

ALTERNATE
WT 390 LB
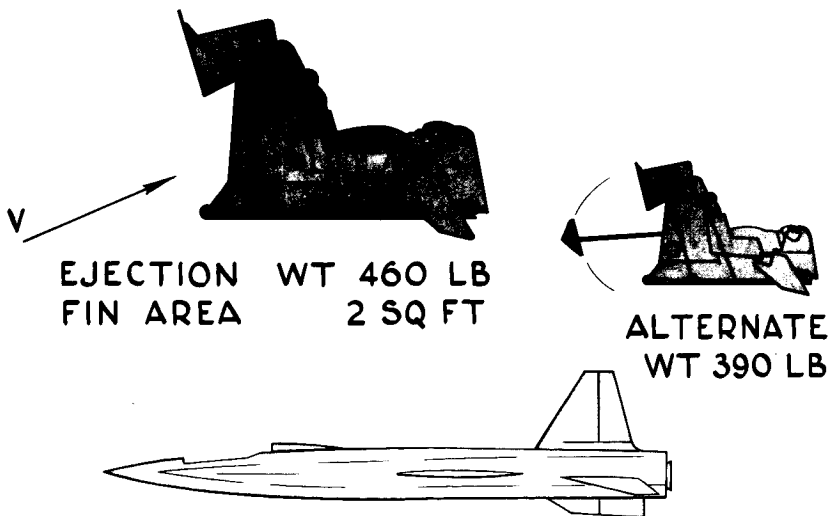
Figure 2

SYS-447L LEVEL FLIGHT X-15 ESCAPE CONDITIONS
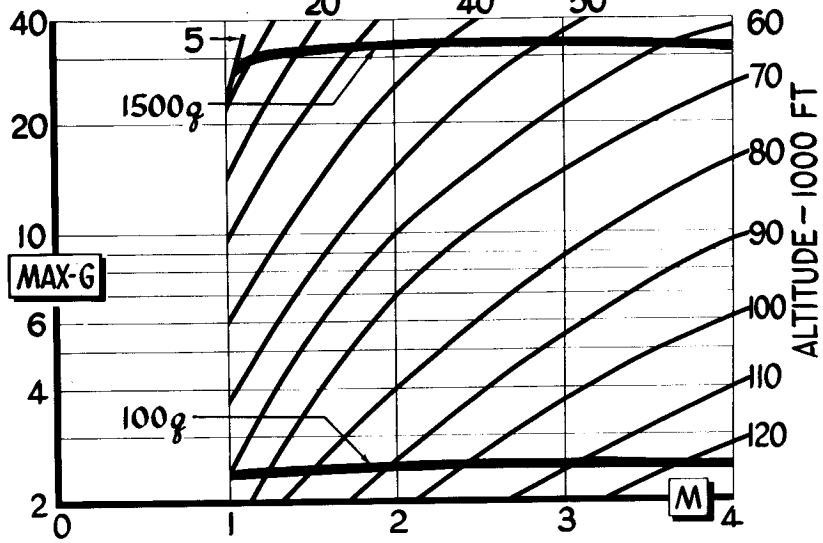
Figure 3

SYS-447L REPRESENTATIVE ESCAPE TRAJECTORIES ON ASCENT

Figure 4

REPRESENTATIVE PEAK ESCAPE ALTITUDES ON ASCENT
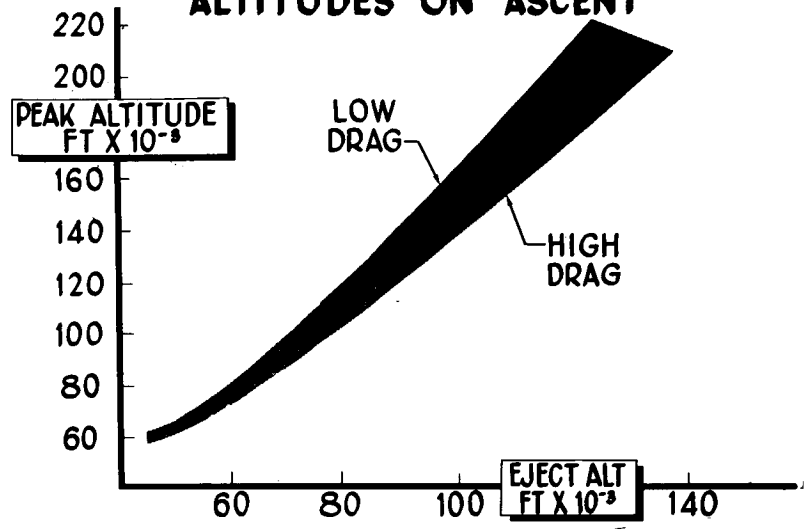
SYS-447L

Figure 5

X-15 SEAT MOTION STUDY
q = 1500 PSF
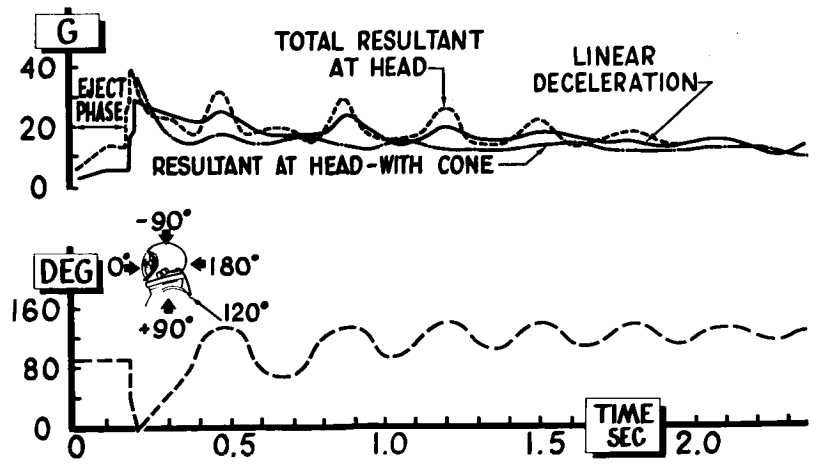
SYS-447L

Figure 6

SYS-447L **BASIC PRESSURE SUIT**

HEADPIECE

OUTER GARMENT — VENT LINER

VENTILATION FLOW

OXYGEN IN 70 PSI — REG

OCULAR CAVITY

ORAL-NASAL CAVITY

EXHAUST TO SUIT

ANTI G BLADDER (TYPICAL)

PRESSURE SUIT INTERNAL SYSTEM
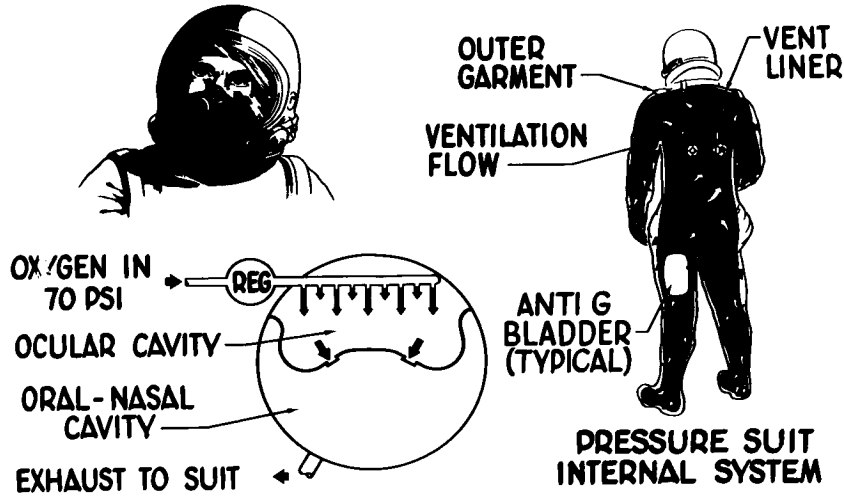
Figure 7

SYS-447L **COCKPIT & SUIT PRESSURE VARIATION ON ESCAPE**

PRESSURE (PSIG)

12
10
6
4
2
0
-2
-4
-6

CANOPY EJECTION   TIME DELAY   SEAT EJECTION   DRAG FORCES BEGIN TO STABILIZE

SUIT PRESSURE

$V \cong 600 + KN$
$q \cong 1200 \ PSF$

COCKPIT PRESSURE

TIME SEC

0   .04   .08   .12   .16   .20   .24   .28   .40
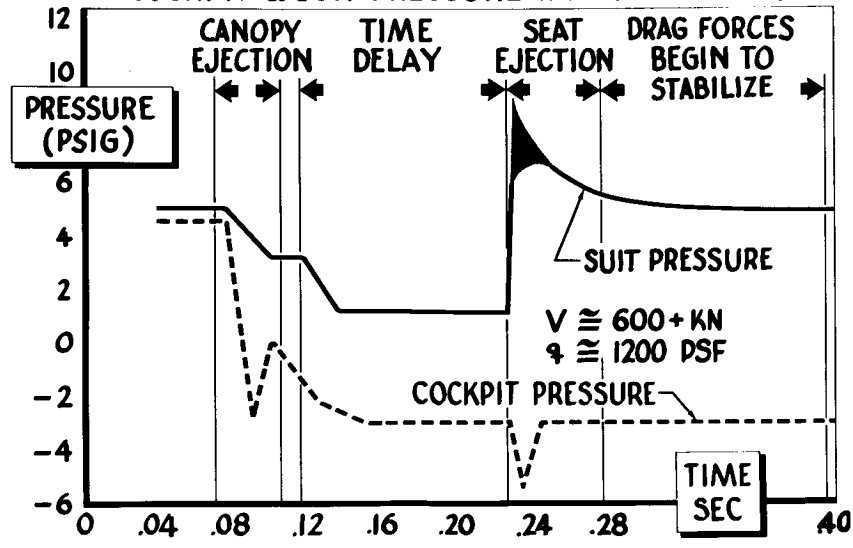
Figure 8

SYS-447L
SUIT FABRIC TEST TRENDS
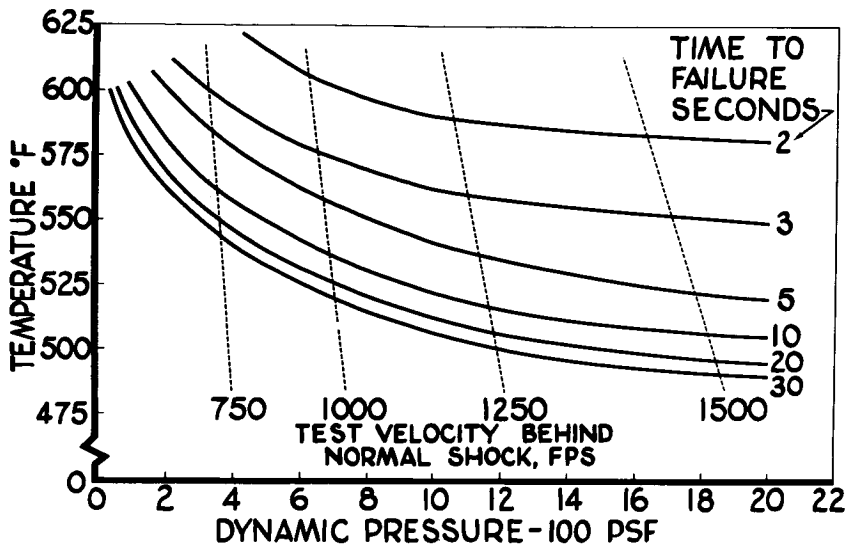
Figure 9

SYS-447L
PRESSURE SUIT CONTROL SYSTEM
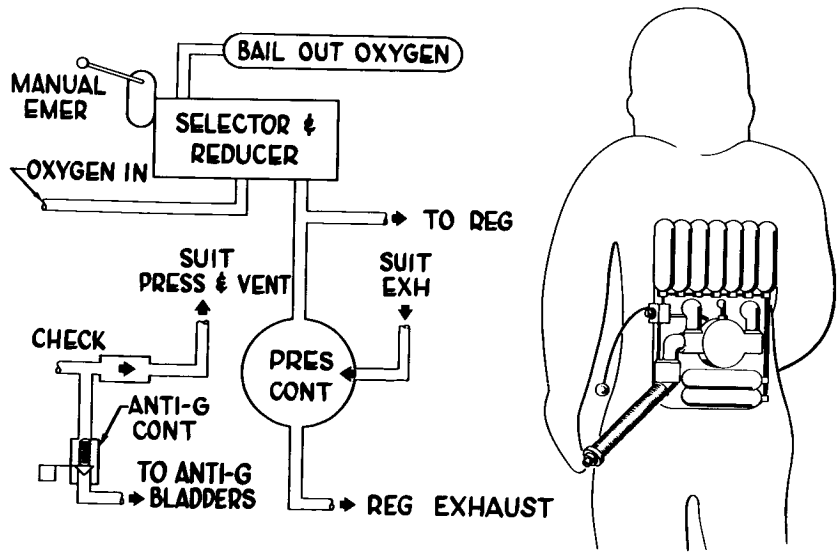
Figure 10
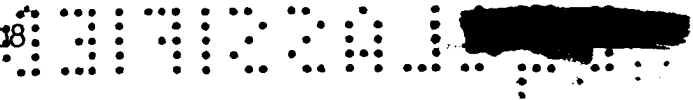
SYS-447L SEAT MOUNTED OXYGEN SYSTEM

OXYGEN INPUT
FROM B-36
(50-70 PSI)

X-15 OXYGEN
SUPPLY

OXYGEN FILLER

REDUCER

70
1800

SELECTOR

GAGE

DISCONNECT
BLOCK

X-15 OXYGEN
TO BACKPAN
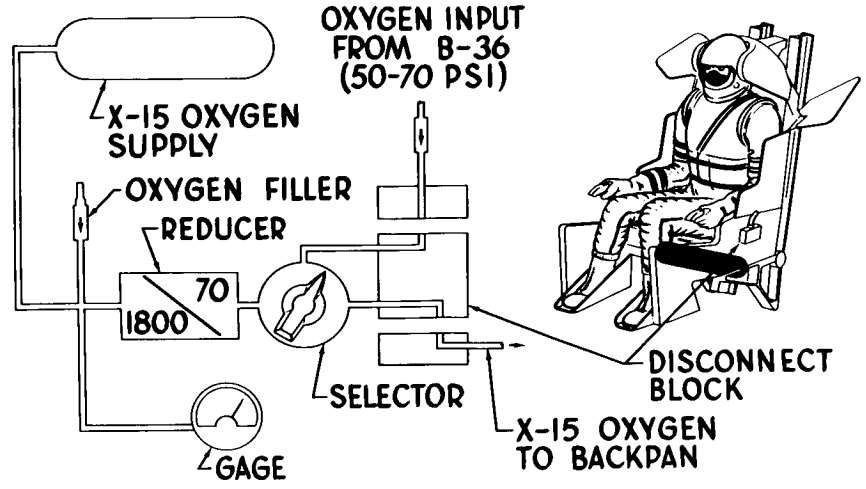
Figure 11

SYS-447L EJECTION SEAT RELEASE SYSTEM

AUTOMATIC
SEPARATION

PILOT IS RESTRAINED
IN THE EJECTION SEAT:
AT THE HIPS
AT THE SHOULDERS
AT THE FEET
AT THE HEAD
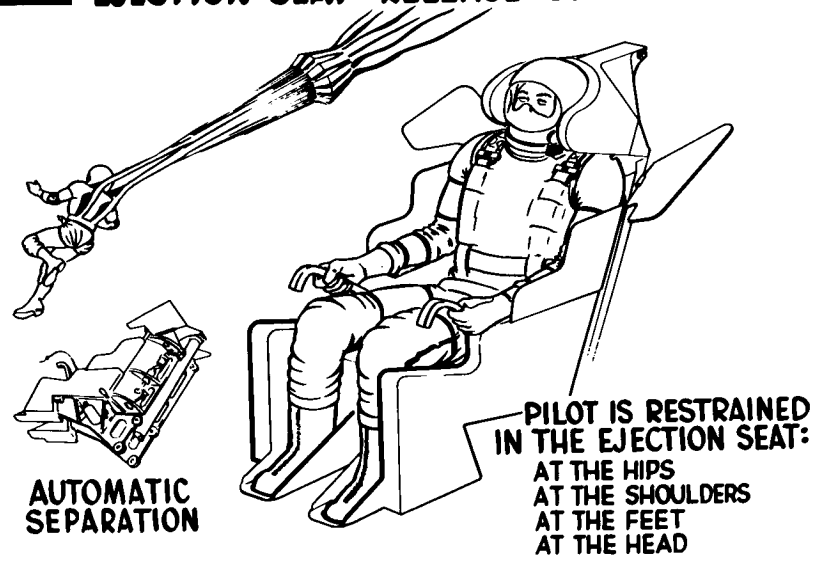
Figure 12

SYS-447L | **HEAT AND VENT**

DOUBLE WALL CONSTRUCTION — PRESSURE REGULATOR — LN₂ TANK

APU

— RAM AIR

— RAM AIR GATE

— SUIT VENT CONTROL

— BLOWERS

— SYSTEM SHUT-OFF —
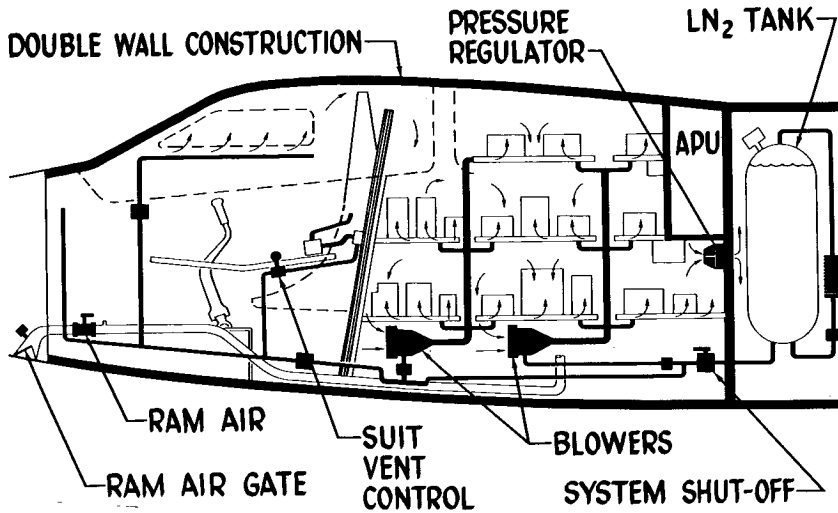
Figure 13

SYS-447L | **CREW COMPARTMENT ENVIRONMENT**

15
COMPARTMENT-PSIA
5
0

4
LIQUID NITROGEN FLOW-LB/MIN
2
1
0

— COMPARTMENT AND EQUIPMENT

PILOT VENTILATION —

TEMPERATURE-°F

COMPARTMENT —   — PILOT

150
100
50
0

— LAUNCH

TIME MIN

-4 -2 0 2 4 6 8 10 12 14 16 18 20 22 24   30
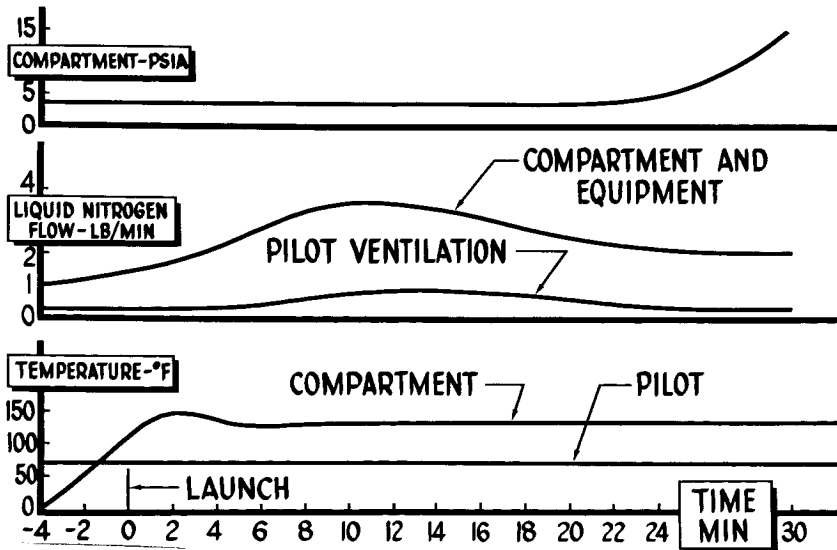
Figure 14

SYS-447L

X-15 COCKPIT

ENGINE

FLIGHT

ENG CONTROLS

APU & ELEC

SPACE ATTITUDE CONTROL

CONSOLE AERO CONTROL
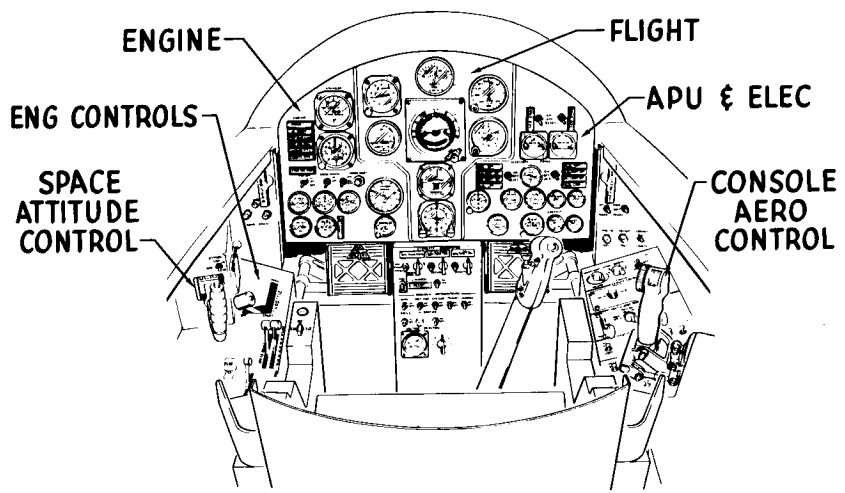
Figure 15

SYS-447L **CONSOLE AERODYNAMIC CONTROL**

PITCH THROW
WRIST RESTRAINED
$\delta_s = 10°$ TO $-35°$

STICK REF POINT
PITCH AND ROLL
ENVELOPE OF
MOTION

ROLL AXIS

NOSE DOWN LIMIT
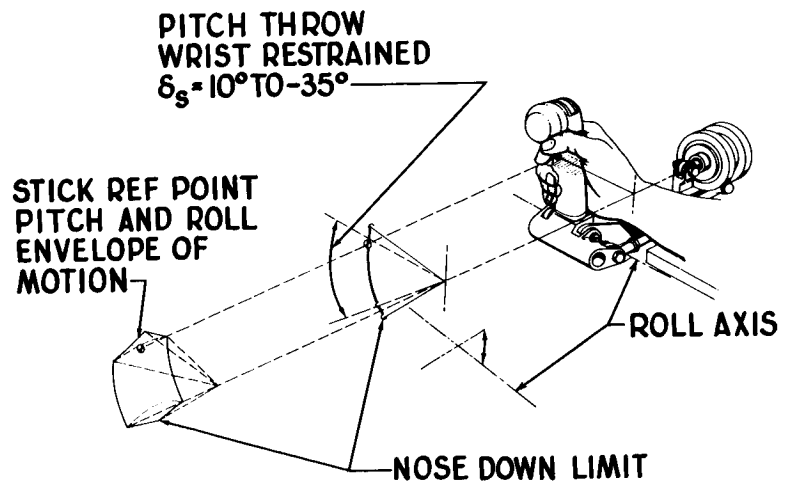
Figure 16

SYS-447L

RE-ENTRY ACCELERATIONS
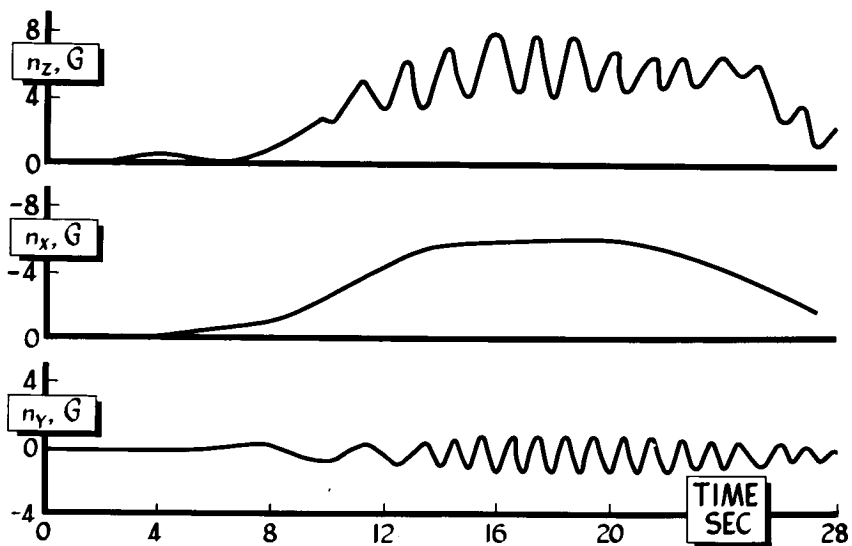
Figure 17

SYS-447L

DESIGN LANDING

TOUCH-DOWN ATTITUDE

$6°$

STATIC POSITION

R/D = 9 FPS
α = 6°
V_L = 164 KNOTS

Figure 18

SYS-447L **PILOT LANDING LOAD FACTORS**
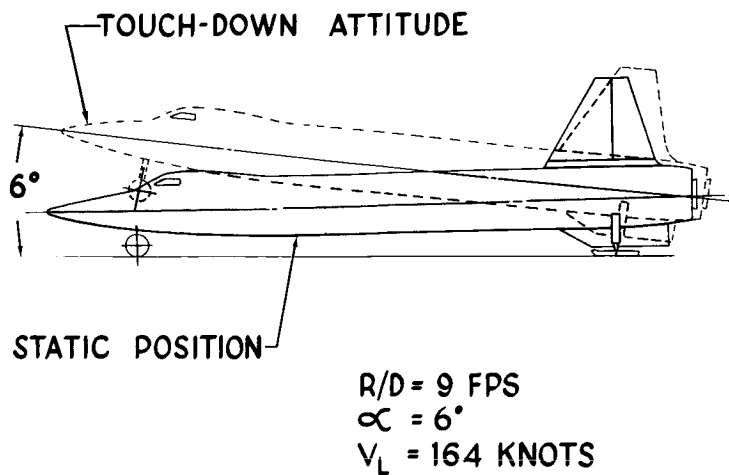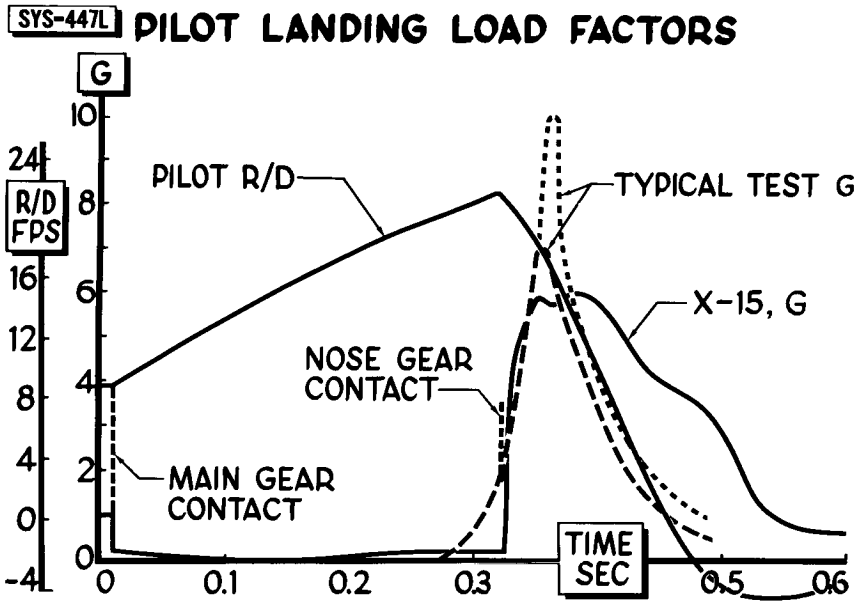
Figure 19

PROPULSION

XLR99-RM-1 ROCKET ENGINE FOR THE X-15

By William P. Munger and Robert Seaman

Reaction Motors, Inc.

This paper contains a discussion of the XLR99-RM-1 rocket engine, which is to be used to power the X-15 airplane. Some of the philosophy and problems underlying the design of this engine are presented.

The specifications for the engine are as follows:

Engine Specifications (40,000 feet)

Thrust:
  19,200 to 57,200 lb

Propellants:
  Anhydrous ammonia
  Liquid oxygen
  90 percent hydrogen peroxide

Weight:
  Dry, 618 lb
  Wet, 748 lb

Specific Impulse:
  256 seconds at minimum thrust
  276 seconds at maximum thrust

Installation Envelope:
  43.2-inch diameter by 71.7-inch length

The general arrangement of the engine is illustrated in figure 1 by a side view of a mock-up. It features a single thrust chamber and turbo-pump with thrust recovery of the turbine exhaust. Propellant valves are visible below the turbopump.

Figure 2 is a forward end view of the engine mock-up. Beginning at the top right-hand corner and progressing counterclockwise, it shows the control box, the H_2O_2 throttle valve, the H_2O_2 gas generator, the turbine, the fuel pump, the main propellant valves, the igniter, the lox pump, the igniter propellant accumulator, and the purge valve system. The turbopump consists of a two-stage impulse turbine driving a dual inlet fuel pump and a single axial inlet oxidizer pump. The oxidizer pump incorporates a

16

directly driven inducer to obtain high suction specific speeds. Propellants for the igniter start are contained in two tanks in the assembly. Sequencing control is accomplished by means of pressure switch and timer components. Thrust control is achieved indirectly by regulation of pump speed accomplished with a speed-governing unit with setting adjustment incorporated into the pilot's throttle.

The major engine operating requirements for the X-15 are as follows:

(1) Safety

(2) Reliability

(3) Throttleability

(4) Environmental capabilities

(5) Restart capability

Since the X-15 is a manned vehicle, the first two items on the list, engine system safety and reliability, are very important requirements. The method for meeting these requirements will be discussed subsequently when engine operation and the engine schematic diagram are discussed.

The third item listed as a requirement for this engine is the ability to throttle continuously the single thrust chamber over a thrust range from 30 percent of rated thrust to maximum rated thrust, which is from 15,000 pounds to 50,000 pounds at sea-level conditions.

Figure 3 shows the estimated engine-thrust envelope as a function of altitude; this estimate shows thrust to extend from a minimum thrust of 15,000 pounds at sea level to a maximum thrust of 59,000 pounds at infinite altitude. This variable-thrust feature is necessary in order to provide proper power level for specific missions required of the X-15 vehicle.

Figure 4 presents some typical flight conditions. The top curve is for a high-temperature mission requiring operation at maximum thrust from start to propellant exhaustion. The middle curve is for an intermittent maximum-thrust mission during which the engine is operated at maximum thrust level for a short period, stopped, and restarted several times. The bottom curve is for an intermittent low-thrust mission during which the engine is operated at less than maximum thrust level for a short period, stopped, and restarted several times. This thrust variation of the engine is accomplished by controlling the shaft speed of the turbopump unit based upon the relationship of the turbopump speed to thrust. This method was selected as a result of studies concerning the safety of the engine system. The reason for the selection of turbopump-speed

monitoring instead of thrust-chamber-pressure monitoring or discharge-pressure monitoring was the fact that sudden loss of load on the pump, such as cavitation of the pump, would be compensated for in a proper direction by the speed monitoring system; whereas a correction in the wrong direction, calling for more power instead of less, would be necessary in the event of unloading of the pump in a system in which either discharge pressure or thrust chamber pressure was utilized as the bases for pump power.

The variable-thrust feature occasions a number of problems with regard to the thrust chamber. Reaction Motors, Inc., has chosen to utilize a thrust-chamber propellant injector providing constant injection port area over the thrust range. A ratio of injection pressure drop to chamber pressure of approximately 0.25 is maintained for stability purposes at the minimum thrust level; this condition, of course, results in a high ratio of injector pressure drop to chamber pressure of approximately 0.85 at maximum thrust. This method was selected as opposed to a variable-port-area injector that would have required complicated mechanisms for port-area restriction, propellant seals, and throttle control.

The regenerative cooling of the thrust chamber with the coolant flow proportional to thrust chamber level requires that the regenerative section of the chamber must be designed to cool with the velocity conditions available at any thrust condition. Of course, the higher the coolant velocity at minimum thrust, the higher the coolant pressure drop at maximum thrust. The design, therefore, requires the balancing of velocity at minimum thrust with pressure drop at maximum thrust.

Item (4) on the list of requirements is illustrated by figure 5, which is a plot of engine-compartment temperature against time for the three flight conditions previously presented. As may be seen, the environmental temperature conditions for this engine are extreme, with the upper end of the environmental range at 400° F, considerably above the normally required +160° F. In order to compensate for this high temperature condition, the engine design places components which are critical with regard to this temperature in areas adjacent to the large heat sinks represented by the propellant lines for the oxidizer and fuel. In the event that the temperature conditioning of the components by means of the heat capacity of the propellants is insufficient, since the primary source is radiant transfer from the walls of the vehicle, radiation shielding will be provided in the critical areas.

Figure 5, together with figure 4, illustrates the fifth requirement, which is concerned with restarting the rocket engine at very high altitudes without servicing, but by utilizing only controls available to the pilot. This restart requirement dictates that the thrust chamber and system must be properly conditioned at the end of each operation so that a restart may be safely accomplished. A discussion of the restarting system is included in the description of the engine system and its operation that follows.
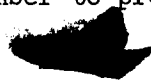
A diagram of the basic engine system is shown in figure 6. Primary sections of the engine system are: the pumping assembly indicated in the upper left of the illustration, the thrust chamber with igniter system to the right, a start and shutdown propellant supply system consisting of gaseous oxygen tank, ammonia tank and oxidizer, and ammonia accumulators. A purging system assembly which is utilized for clearing the thrust chamber and igniter at shutdown in preparation for restart is omitted from the diagram for the sake of clarity. Pilot controls for the engine have also been omitted. These controls consist of an arm switch for energizing of engine controls system, a priming switch for propellant-system priming control, and a throttle lever operating from start through the thrust range. There is also a reset switch for resetting the electrical system after a malfunction shutoff.

Briefly, the sequence of engine operation is as follows. An arm switch energizes the engine control system. Priming of the pump system is initiated by a prime switch. Priming of the pumps is required to cool them down to the point where the oxygen and ammonia in these pumps will exist in liquefied state. When the priming function is complete, the first stage of the igniter is fired, this stage receiving gaseous oxygen from the igniter start tank and fuel from the igniter fuel start tank, both of which are regulated to a pressure that is slightly below minimum-thrust propellant-supply pressure to the chamber. A pressure switch senses satisfactory operation of the first stage of the igniter and starts the turbopump unit by initiating peroxide flow to the hydrogen peroxide gas generator. At the same time the second-stage igniter propellant valves are opened. Propellants for the second stage of the igniter are supplied from the turbopump. Satisfactory operation of the second-stage igniter is also sensed by a pressure switch and when satisfactory operation has been established, the main propellant valves for the thrust chamber are opened and ignition of the thrust chamber is achieved by means of the second-stage igniter flame. During this starting period, a system of timers monitors the time required for the first stage, then for the second stage, and finally for the thrust chamber to arrive at satisfactory operating pressures. In the event that excessive time is required in any of these three steps, shutoff of the system results. Also, during the starting sequence, as the pump discharge pressures rise above the pressure supplied from the igniter start tanks to the first-stage igniter, a switch-over to propellant supply from the pump system is automatically accomplished, the oxidizer for the first stage igniter being passed through a heat exchanger in the turbine exhaust in order to provide gaseous oxygen to the first stage of the igniter. Also during this period, the oxidizer and ammonia accumulators are filled as the pump discharge pressures rise, the accumulated volume and pressure being consistent with level of thrust operation. Maintenance of thrust level is accomplished by means of the turbopump governing system, which is referenced against the pilot's throttle setting. Shutdown is accomplished in reverse order from the start.

The cornerstone on which the whole safety system rests is the principle that nowhere in the engine is accumulation of unburned propellants permitted to reach an amount so great that if this accumulation of propellants were intimately mixed and ignited, the resulting pressure surge would exceed the failure limits of the structure. This principle is adhered to even in the event of a single malfunction. The system operates in the following way. The igniter is a two-stage unit. During a start, the first stage is ignited by a spark and operates on gaseous oxygen and ammonia. The body of the igniter is designed to withstand the pressure which can be generated by the maximum accumulation of propellants that can occur and that is limited by the fact that the oxidizer is in gaseous form. Operation of the first-stage igniter triggers the propellant valves on the second-stage igniter, which operates on liquid oxygen and liquid ammonia. Safety of the second stage of the igniter is achieved by the energy release obtained from the first-stage igniter. This energy release and its distribution throughout the second-stage-igniter injection area prevents the accumulation of a critical quantity of propellants by vaporizing and igniting them. Safety of the thrust chamber is achieved in exactly the same manner as that of the second-stage igniter. The igniter-energy release prevents the accumulation of a critical quantity of propellants within the thrust chamber. Each stage of the igniter is designed so that its operation will not be affected by malfunction of downstream combustion units. The igniters operate continuously during engine operation and continue to operate during a shutdown cycle with propellants supplied by the igniter oxidizer and fuel accumulators. Safety is achieved during either a normal or malfunction shutdown by purging the residual propellants from the thrust-chamber injector into the thrust chamber and by vaporizing and burning them with the igniter. After shutdown of the thrust chamber occurs, the second-stage igniter is shut down and purged, and the first stage continues to run on propellants from the accumulators and finally from the start tanks. The energy release of the first-stage igniter performs the same function on the second-stage igniter as the complete igniter performs on the thrust chamber. Shutdown of the first stage does not require purge since a critical quantity of propellants cannot accumulate because gaseous oxygen is used as the oxidizer.

Inasmuch as the engine system is designed to react in a safe manner in the event of any single malfunction, paralleling of components is required in several areas. The purge system is an example of this. In this system parallel valves are used to control purge flow so that, in the event of failure of a single valve to open, the system can still be purged.

During periods when the propellant tanks are pressurized but when the engine is not operating there exists the possibility that a propellant valve might leak. Therefore, a continuous inert gas-bleed system is provided for the injection heads of the first-stage igniter, second-stage igniter, and thrust chamber to prevent propellants from reentering

the injection head sections and causing injector explosions on a subsequent start. This possible accumulation of unburned propellants in the wrong place at the wrong time has given rocket designers a difficult time over the years. The use of two volatile propellants, namely liquid oxygen and liquid ammonia, which boil away and leave no residue is a definite safety factor.

In closing, it is fitting to emphasize that the development of a variable-thrust rocket engine with a maximum sea-level thrust of 50,000 pounds capable of being stopped and restarted in flight at extreme temperature and altitude conditions is a difficult task and will represent a major advance in the field of rocketry. Research aircraft such as the X-15 and the operational aircraft which will eventually follow it can never be achieved without safe and reliable rocket power plants of the type under discussion.

SIDE VIEW XLR99-RM-I ENGINE MOCK-UP

Figure 1
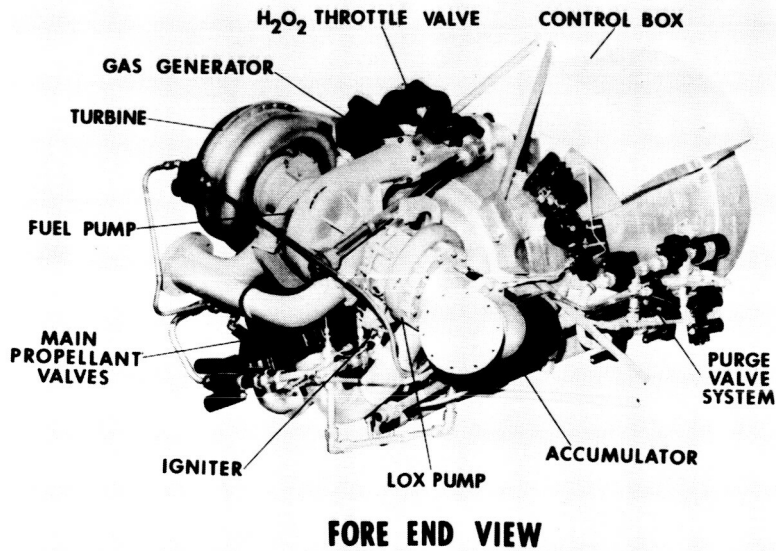
FORE END VIEW

XLR99-RM-1 ENGINE MOCK-UP

Figure 2

ENGINE THRUST ENVELOPE

Figure 3
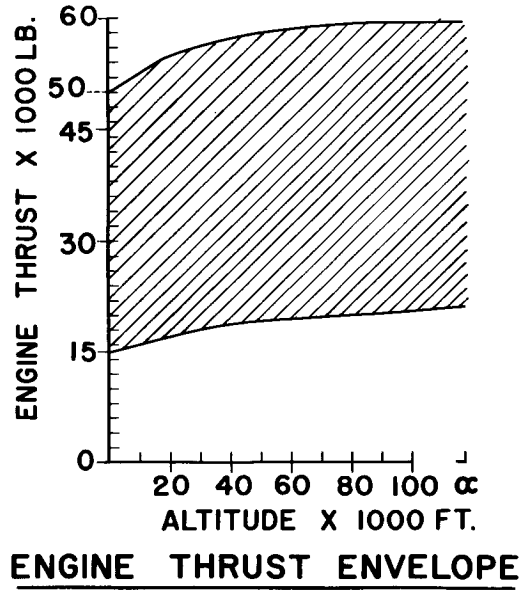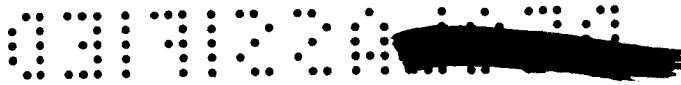
TYPICAL FLIGHT CONDITIONS
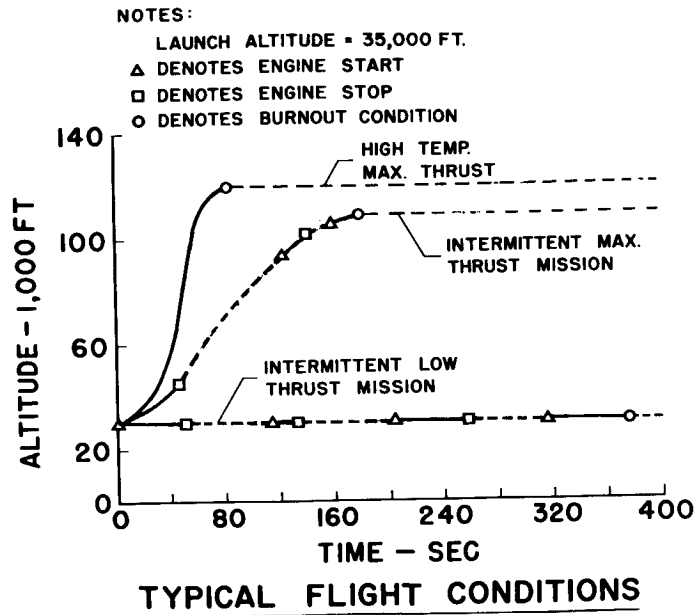
Figure 4

NOTES:
LAUNCH ALTITUDE = 35,000 FT.
△ DENOTES ENGINE START
□ DENOTES ENGINE STOP
○ DENOTES BURNOUT CONDITION

HIGH TEMP.
MAX. THRUST

INTERMITTENT LOW
THRUST MISSION

INTERMITTENT MAX.
THRUST MISSION

COMPARTMENT AIR TEMPERATURE – °F

TIME – SEC

TYPICAL FLIGHT CONDITIONS

Figure 5

TURBINE THRUST
RECOVERY

LOX PRIME
VALVE

MAIN LOX
PROPELLANT VALVE

NH₃

LOX

LOX
ACCUMULATOR

H₂O₂ GAS
GENERATOR

(GOX)

IGNITER START
SYSTEM

IGNITER

THRUST
CHAMBER

POWER CONTROL

(NH₃)

NH₃
ACCUMULATOR

NH₃ PRIME VALVE

MAIN NH₃
PROPELLANT VALVE

2nd STAGE IGNITER
PROPELLANT VALVE

BASIC ENGINE SCHEMATIC

Figure 6

X-15 AIRPLANE ENGINE INSTALLATION

By Bruce O. Wagner

North American Aviation, Inc.

INTRODUCTION

The engine installation in the North American X-15 airplane and the propellant-feed system are now considered, the rocket-engine assembly having been described by William P. Munger and Robert Seaman in a previous paper. Major elements of the total propulsion system are shown within the outline of the airplane profile in figure 1. It is to be noted that the main propellant tanks for liquid oxygen (designated Lox herein) and ammonia are placed so that they straddle the airplane center of gravity, the Lox tank having a volume of approximately 1,000 gallons and the ammonia tank, approximately 1,400 gallons. A 75-gallon hydrogen peroxide tank immediately behind the ammonia tank supplies monopropellant for the engine-propellant-pump turbine. The rocket-engine assembly, including the propellant turbopump, the igniter system, electrical controls, and so forth, is mounted in a rear engine compartment. Seven cubic feet of helium gas under a pressure of 3,600 pounds per squre inch is stored within a cylindrical bottle mounted concentrically within a structural core tube passing through the Lox tank. This detail is shown in the fuselage cross-section view of figure 1. The high-pressure gas contained in this bottle provides expulsion pressure for the Lox and ammonia tanks. An additional 4 cubic feet of helium under a pressure of 3,600 pounds per square inch is stored at a higher temperature in a bottle located between the main propellant tanks for monopropellant expulsion pressure. This supply also provides gas for the engine purge and for the pneumatic valving operation in both the engine and the propellant feed system.

17

PROPELLANT-FEED SYSTEM

For a more detailed examination of the propellant-feed system, figure 2 shows a simplified schematic flow diagram of the installation within the North American X-15 airplane and, in addition, the Lox "top-off" system installed in the B-36 type carrier airplane. If the system is followed through from left to right, it may be seen that the Lox "top-off" bulk of approximately 1,000 gallons is valved intermittently down into a sump tank during carried flight. This arrangement promotes boil-off cooling of the X-15 Lox load under minimum liquid head pressure, the cooler Lox being of considerable advantage relative to the rocket-engine

pump suction feed characteristics. A common Lox vent outlet for both the X-15 and the B-36 airplanes is carried out through the B-36 airplane.

For clarity, the main propellant section of the total system is now shown separately in figure 3. The Lox tank and also the ammonia tank are divided into three compartments to permit forcing both propellants toward the center of gravity of the airplane during expulsion. This arrangement is necessary for maintaining airplane balance during both powered flight and emergency jettison. During powered flight, longitudinal acceleration forces of 2g to $4\frac{1}{2}$ g will tend to force all propellant toward the rearward ends of tanks and tank compartments. The angle of slope for intercompartment transfer tubes is different in the Lox and ammonia tanks. This difference is the result of a design compromise between effective filling during servicing, the control of reverse transfer due to decelerations during intermittent thrust, and also the effort to minimize the quantity of any remaining propellant after engine feed or jettison. Intercompartment transfer tests completed on a simulated full-scale compartment have proven to be very satisfactory when water was used as the test liquid.

In the case of the liquid-ammonia fuel tank shown in figure 3, no "top-off" system is provided. It has been determined that a propellant temperature rise of no more than 10° F will occur in a sealed tank during the time between X-15 servicing and the launching. The tank will therefore be closed after servicing to prevent altitude "boil-off" during carried flight. The tank volume allows for the added increment required for reduced propellant density resulting from this rise in propellant temperature. A significant condition, which is favorable to this design arrangement, is the fact that the rocket-engine pump-section requirements are less critical for an increase in fuel temperature than for an increase in oxidizer temperature.

Both propellants are carried back to the engine in 6-inch-diameter low-velocity lines to minimize the pressure required for the acceleration of the mass flow on starting. Tank shutoff valves immediately forward of the engine firewall isolate the propellant system. Jettison valves in this same area will permit a bypass of the engine compartment for emergency jettison.

The long helium bottle below the Lox tank shown in figure 3, although it is actually surrounded by the Lox tank, will be charged to 3,600 pounds per square inch with the gas at -300° F. This low-temperature high-density-gas condition requires less bottle volume and weight and also provides an expulsion gas which will not be chilled to a greater density on entering the cold propellant tanks. The expulsion pressure for the Lox and ammonia tanks will be regulated to 48 pounds per square inch gage. Selection of

a suitable material for the pressure vessel and the control-valve development for this extreme-low-temperature gas condition will still require much time.

Figure 4 shows the monopropellant and engine-purge section of the total system. The second helium bottle appears on the left-hand side of figure 4 and is a sphere in the environment of the ammonia tank which has a temperature of approximately -30° F. It will supply gas pressure to the higher temperature end items: the hydrogen peroxide tank, the pneumatic-operated valves, and the engine purge. The source pressure of 3,600 pounds per square inch gage is reduced to 550 pounds per square inch gage in this supply system. All propellant-system valving is pneumatically operated whereas direct mechanical linkage will be used between the cockpit control and the system main selector pilot valve.

The hydrogen peroxide tank is cylindrical in the vertical direction and has domed ends. An internal swing-spout outlet fitting (not shown) will be used in the lower end of the tank. Such an outlet will maintain satisfactory uninterrupted flow under the longitudinal acceleration forces experienced by this airplane during on-off engine operation and with the instantaneous quantity of propellant remaining at such times. For safety reasons the tank will be insulated to maintain the temperature of the hydrogen peroxide within the limits of 20° F to 160° F at all times.

ANALYTICAL CONSIDERATIONS

Some of the analytical considerations for the feed-system design are now considered; figure 5 presents the variation of the inlet pressure in pounds per square inch absolute with time in seconds for both the Lox and ammonia pumps for a typical continuous high-thrust flight mission. The curves of "pressure required" have a slight rise with time. These curves depict the conventional pump inlet requirement in terms of a certain increment above vapor pressure and also show a slight rise due to the increase in propellant temperature as a result of aerodynamic heating of the tank shells. The pressure at start (solid symbols) is shown with a normal margin above the pump inlet requirement; the pressure at full thrust (open symbols) rises to a value that is considerably higher as a result of the acceleration force developed by this thrust value. With the reduction in the weight of the airplane due to propellant usage, pump inlet pressure is seen to rise continually as a result of the ever-increasing longitudinal-acceleration force developing at a constant-thrust condition. From this condition it is apparent that the selected tank pressure is dictated by the engine starting conditions and that excess supply pressures exist during high-thrust operation. These increments above the pump-design inlet-pressure requirement have been referred to the engine manufacturer for consideration when the engine

is being adjusted for optimum performance. The most involved analytical area pertaining to the propellant system is the thermodynamic calculation of propellant temperatures for the transient conditions starting with initial ground servicing and continuing through carried flight and free flight up to engine burnout. Such conditions may cover a period of possibly 6 hours. The heat exchange between various temperature zones of the aircraft and the extremes of the transient operating environment makes this analysis complex. Many individual airplane design details and functioning characteristics, such as exact tank volumes for all propellants and high-pressure gas, the entire top-off system, and the vent-system detail design, are dictated by these data. The quantity of the unusable propellants and numerous lesser design points are also in this category. Much of this work has been done on the analog computing machines in support of the design to date. Recalculations will be made periodically as warranted by later refinements in the definition of such items as the airplane mission profiles, airplane preflight servicing procedure, and other items which influence the thermodynamic processes.

ENGINE INSTALLATION

Figure 6 shows an exploded perspective view of the engine compartment section from the firewall (station 521) and rearward. This structure area is classified as primary structure forward of station 565, the attachment point for the engine-mount truss. Three large structural access doors occur between the empennage root locations. The design is suitable for ground operation of the engine with these doors removed; thus closed circuit "T.V." observation of the engine in operation is facilitated. The removable rearward fairing between stations 565 and 588 is designed to explode open at a pressure below the rating of the forward structure in order to provide engine-compartment explosion relief. The engine-mount truss which joins the thrust chamber at three locations may be seen to mate with three fittings on the fuselage frame structure at points where there is a fore-and-aft intercostal structure.

During ground operation of the rocket engine, rearward-extending tension links are attached to these mount points to react the engine thrust. Provisions to restrain the airplane by connection to fittings in the forward fuselage area would involve an unacceptable weight increase in the adjacent fuselage structure. Similar engine-mount locations will also be used for attachment of an engine ground-handling dolly to facilitate installation and removal of the total engine assembly after the rearward fairing is removed.

A rigid-type engine mount is being designed at the present time, no effort being made toward vibration attenuation, and a study of the

anticipated engine vibration characteristics is in process. An exact criteria for structural design relative to the engine forcing vibrations will be established from instrumented tests of a prototype engine assembly mounted in a typical rear airframe structure. No thermal insulation of the engine compartment is intended, and a structure very nearly airtight except for a specific breathing opening at the forward end of the compartment will be designed. Hot- or cold-boundary-air infiltration will be minimized. The engine-compartment shell structure has been calculated to reach a maximum of 260° F during engine operation. After burnout, variation of maximum temperature over the engine-compartment surface will range between 580° F and 1,200° F. Successful engine functioning should be accomplished with a minimum of special temperature-conditioning provisions by taking full advantage of the favorable thermal inertia characteristics and also of the flow of cold propellants.

ENGINE ALINEMENT

The engine mount has been described as having three attachment fittings, the top fitting being the main pivot point for the mount. The two lower points are adjustable fore and aft to accomplish angular adjustment of the engine installation. This adjustment will provide for accurate alinement of the thrust vector with the airplane center of gravity. Relative to this engine-alinement adjustment, figure 7 depicts the thrust-vector tolerance requirement as stated to the engine manufacturer. Suitable-location points are to be supplied on the thrust chamber for an index to the nominal total thrust line. This nominal thrust line includes chamber thrust and turbine exhaust thrust and is to be determined from firing tests of each engine. For conditions of variable thrust and for the service life of the thrust chamber, the actual thrust vector is required not to fall outside the tubular envelope that extends to a point "A" that approximates the airplane center of gravity. (See fig. 7.)

The tubular form of envelope was selected as a simple and practical definition of the tolerance field for any combination of offset and angular deviation of the thrust vector which might occur in the engine and still pass within the required proximity of the airplane center of gravity. Lateral offset variation of the thrust vector is expected to be very small. If the assumption of no offset for an actual thrust vector because of its intersection with the nominal thrust line at point "B" within the thrust chamber is made, the maximum angular variation falling within this envelope would be only an arc of 20'.

It is estimated that the accuracy of the determination of actual airplane center-of-gravity location and its excursion during flight can

be held within a target area equal to the $2\frac{1}{4}$ - inch diameter of the tubular engine tolerance field. If perfect alinement of these two tolerance fields on engine installation is assumed, the possible thrust vector to the actual center-of-gravity misalinement has a value double that considered acceptable from the airplane aerodynamic analysis to date. The foregoing case describes a problem which must be resolved on the basis of the establishment of any possible engine-thrust-vector excursion by engine firing tests. In addition, this problem will require a more detailed study of the directional instability promoted by variations in aerodynamic trim for engine-on or engine-off conditions. This study will give consideration to the summation of all engine-alinement variables. Tolerances permitted in each of the variable areas at this date are felt to be as small as is practical to consider on the basis of presently available design or test data.
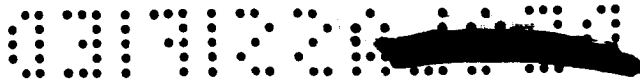
COCKPIT CONTROLS

Associated with the foregoing description of the complete propulsion system are the cockpit controls and instrument arrangement which are shown in figure 8. The instrument-panel display is expected to be subject to change during the development period of the engine and also throughout design evolution and proof-testing of the propellant-feed system. The throttle control is located on the side console and an engine prime switch button is located in the throttle-control knob. A three-position propellant-tank-pressure control shown on the vertical console panel permits selection of tanks depressurized and vented, pressurized for engine feed, or pressurized for jettison. The supplementary "Stop Jettison" switch will permit override cutoff of either or both Lox and ammonia. This arrangement allows for individual jettison of each propellant if hydrogen peroxide, the third propellant, is jettisoned first. Such a procedure is expected to be used for safety reasons on the ground or in the carrier airplane. It also permits interruption or cutoff of emergency jettison while in flight if flow rates outside of design limits are causing critical airplane unbalance. At the top of the instrument panel, six rectangular indicator lights are allocated to engine starting, malfunction indications, and fire warning. The electrical switches shown are for engine-master, engine-arm, and fire-extinguisher functions. Five dual indicators give pressure values at selected points in the system for each propellant. In addition to a thrust-chamber-pressure indicator, a totalizing impulse indicator will be used to determine the remaining engine power much in the manner that conventional fuel quantity indicators are used. The criteria which have established the present controls arrangement are to provide pilot-actuated controls specifically associated with a well-defined airplane operational parameter and procedure rather than for a wide diversity of flight operations. The indicator arrangement is intended to give the maximum practical display that would

allow the pilot to make in-flight evaluation of both normal and abnormal operation of the total propulsion system. This arrangement is not intended to replace any need for automatic safety or reliability features in the propulsion system; it is intended to expedite early satisfactory operation. It should also assist in attainment of maximum performance from the total propulsion system, since it will facilitate the monitoring of the performance of the various elements which are in a development category typical for a research vehicle of this type.

SYS-447L **PROPULSION-SYSTEM ARRANGEMENT**

LOX TANK NH₃ TANK H₂O₂ TANK

CG

FUSELAGE
CROSS SECTION

He TANKS

PROPELLANT
FEED LINES

ROCKET ENGINE
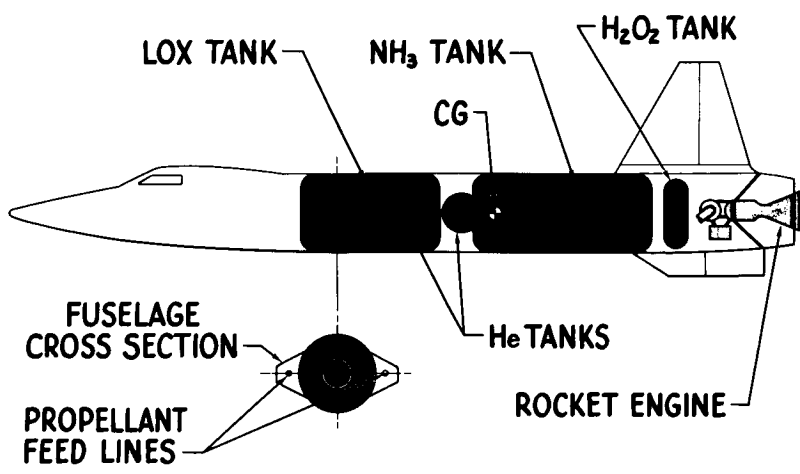
Figure 1

SYS-447L **PROPELLANT—FEED SYSTEM**

⊗ SHUT-OFF VALVE

◪ PRESSURE
   REGULATOR

B-36
AIRPLANE

ROCKET ENGINE

He

NH₃

H

PURGE

H₂

PNEUMATIC VALVES
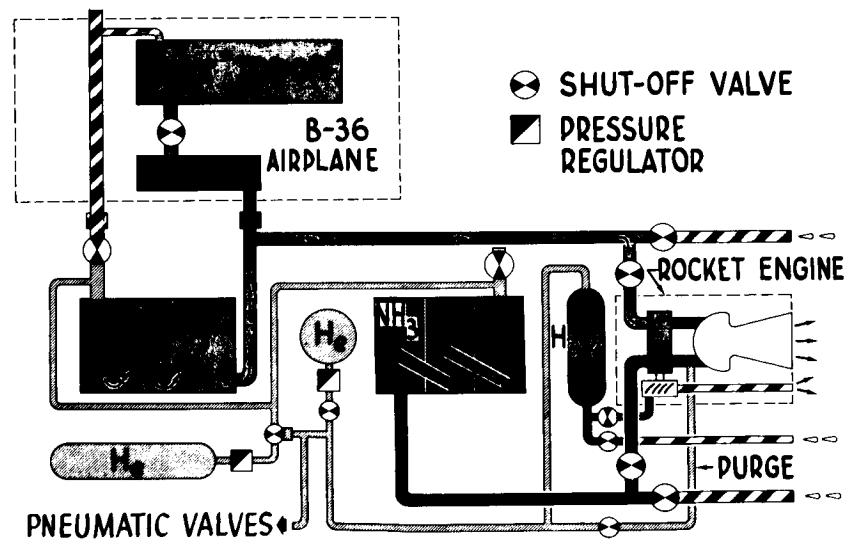
Figure 2

SYS-447L

LOX & NH₃ SYSTEM

⊖ SHUT-OFF VALVE
◩ PRESSURE REGULATOR

VENT "TOP-OFF"

FILL JETTISON

H₂

ROCKET
ENGINE
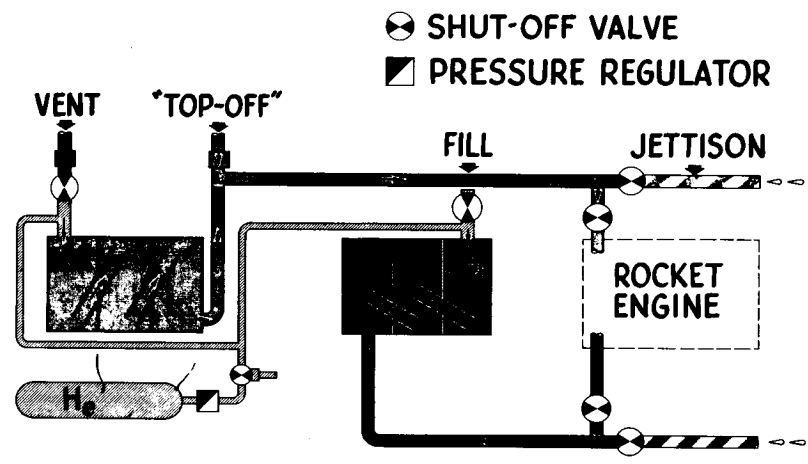
Figure 3

SYS-447L

H₂O₂ & PURGE SYSTEM

⊖ SHUT-OFF VALVE
◩ PRESSURE REGULATOR

3600 PSIG

H₂

ROCKET
ENGINE

550 PSIG

PNEUMATIC
VALVES

JETTISON
PURGE

Figure 4

PROPELLANT-SYSTEM-FEED PERFORMANCE

SYS-447L

Figure 5

SYS-447L ROCKET-ENGINE INSTALLATION

521
565 —ENGINE MOUNT
565   588

ACCESS DOORS —

AFT FAIRING —

Figure 6

DE_____SIFIED
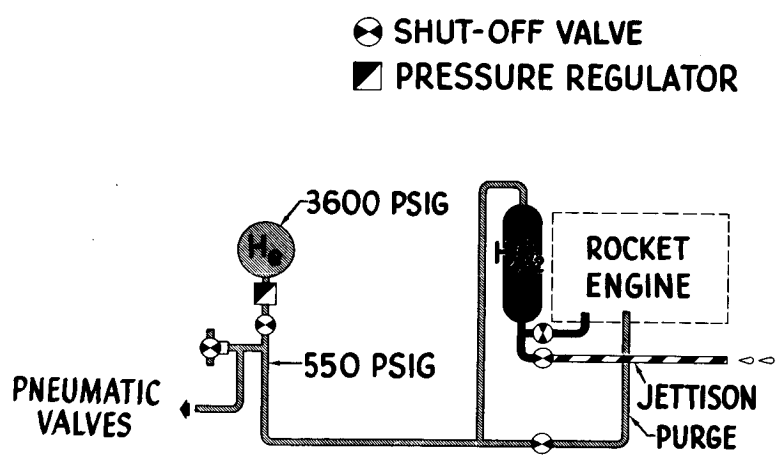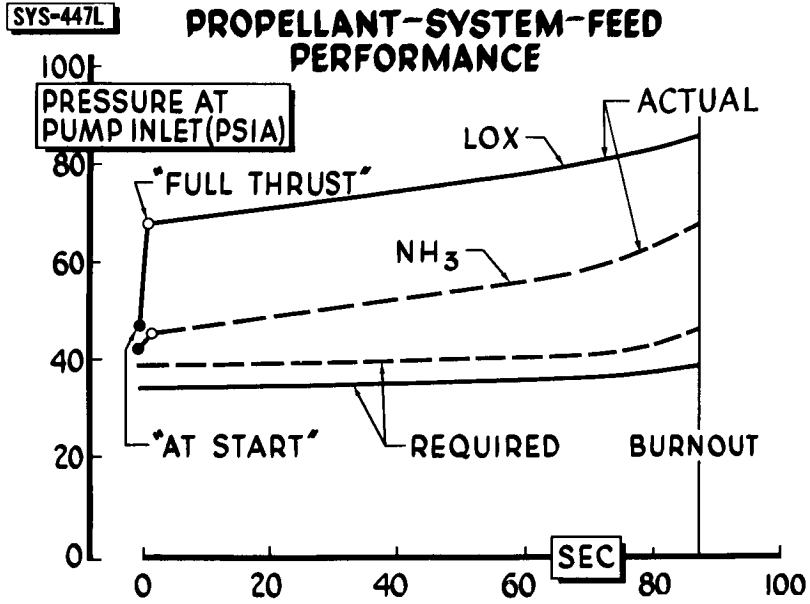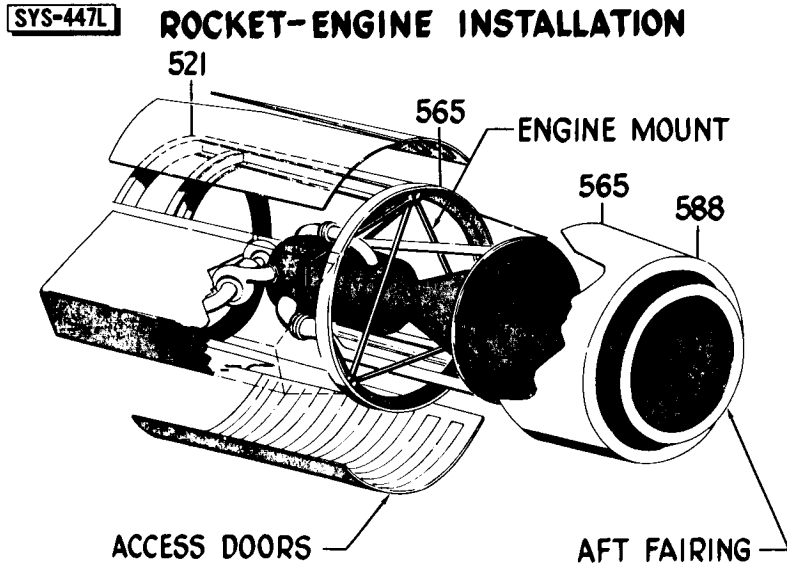
SYS-447L **ENGINE THRUST ALINEMENT**

◄ FORWARD

ENGINE REF PLANE

PUMP
TURBINE
EXHAUST

POINT "B"

POINT "A"

2.25 IN. DIA

ACTUAL
THRUST
VECTOR

←∿200 INCHES∿→

NOMINAL
TOTAL
THRUST
LINE

THRUST CHAMBER
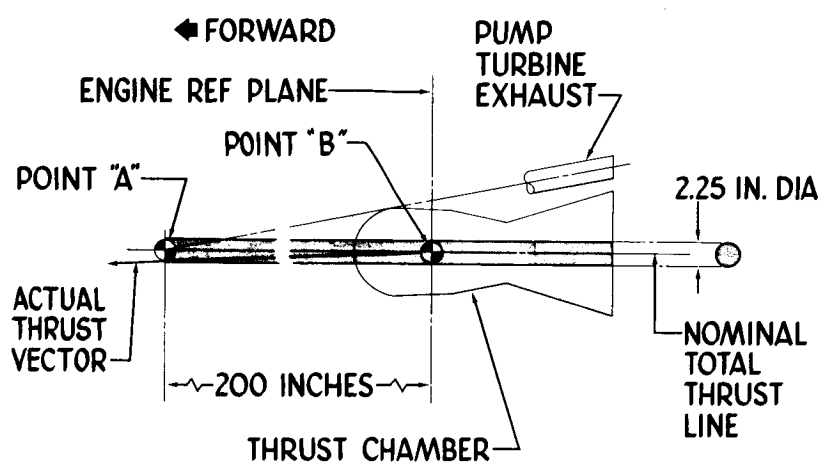
Figure 7

SYS-447L **PROPULSION-SYSTEM PILOT CONTROLS**

INSTRUMENT PANEL

TANK PRESSURE &
JETTISON CONTROLS

ENGINE INDICATOR
LIGHTS

ENGINE CONTROL
SWITCHES

STOP JETT.

BOTH LOX
NH₃

PRESS. JETT.
VENT

CHAMBER
PRESSURE

TOTAL
IMPULSE
REMAINING

MAX.
OFF START

THROTTLE

PROPELLANT-SYSTEM &
PURGE-SYSTEM PRESSURES

Figure 8

SUMMARY OF PERTINENT PROBLEMS AND CURRENT

STATUS OF THE X-15 AIRPLANE

By Lawrence P. Greene

North American Aviation, Inc.

Upon consideration of the wealth of information which has been presented at this symposium, it is quite evident that a summary would be highly desirable. However, it would be extremely presumptive to assume that one could, in the short space of time available to the writer, present a complete compilation of the information. It is, however, the intent of this paper to present, as c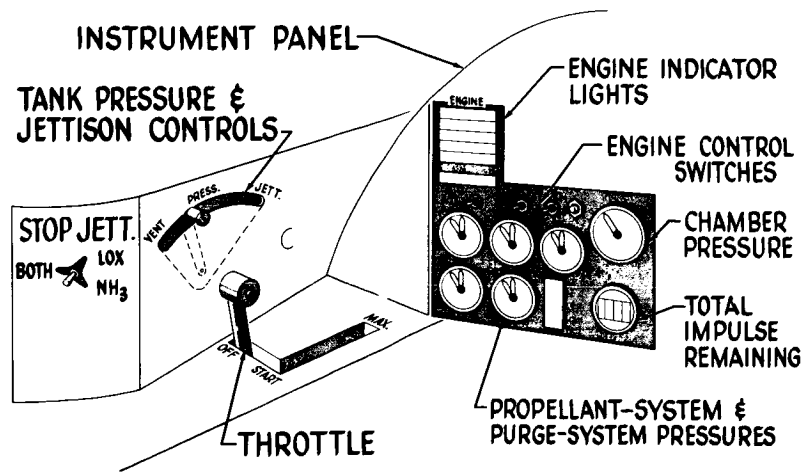learly as possible, the most important factors concerning the design of the X-15 airplane (fig. 1), particularly those factors which have been discussed at this symposium. In addition, certain problem areas in the design and construction of the airplane, not discussed previously, will be presented to provide an overall picture of the progress which has been made to date from the designer's viewpoint.

One realizes that some of the research effort reported in this symposium is directly applicable and some is indirectly applicable to the airplane and there are various research interests involved. One speaker has said that the airplane is primarily designed to obtain stability and control characteristics. Another speaker has said that it is primarily designed to determine heat-transfer characteristics and flow conditions. In reality, each is right, for one of the primary reasons for the project is to stimulate research.

At the risk of being repetitive, it is expedient to reexamine a figure in John Becker's paper, which is shown here as figure 2. In consideration of the research effort required to investigate regions of flight anticipated for aircraft such as the space rocket or even the satellite vehicle, the NACA had concluded that an airplane could be designed and built to provide research data and flight experience in the regions desired. It was expected that determination of the problem areas and the character of these problems could be obtained with this type of vehicle. Furthermore, it was expected that this could be accomplished within a reasonable time period. The result of this study has been the instigation of the X-15 program. The X-15's performance curve can be seen to represent generally the altitude considerations of primary importance.

The X-15 airplane therefore is being designed as a vehicle for the procurement of research data in the fields of endeavor pertinent to high-altitude flight including the following five items:

(1) The study and experimental determination of the character of aerodynamic heating, having sufficient flexibility of operation that significant variations can be considered

(2) The effect of aerodynamic heating on structural design up to a nominal temperature of $1,200°$ F, the purpose being to evaluate thermal distortions and stresses which may be experienced in the structure

(3) The high Mach number characteristics of the aerodynamic configuration, particularly investigations considering exit and reentry characteristics

(4) The investigation of space controls or reaction controls for that portion of the flight out of the influence of the atmosphere

(5) The high-altitude evaluation of physiological and psychological effect on the pilot of weightless flight

The job of designing the X-15 airplane is, therefore, a tremendously stimulating project which is clearly brought to mind by the fact that

(1) It is to be a piloted airplane capable of a speed range from zero to a Mach number of 6.5

(2) It will have an altitude range from sea level to nearly 700,000 feet, if necessary

(3) It is being designed for the usual normal acceleration of 7.33g and -3g but, in addition, for axial accelerations of approximately ±5g

(4) It will be able to fly through an environmental stagnation temperature of about $3,500°$ F

With these general goals in mind, it is no wonder that this project has stimulated considerable effort within the NACA in the form of research and development program interest and in the contractor's activity in the form of interest in the design. It is fairly evident that the NACA has a role in the design and operation of the X-15 - they are both the instigators and the advisors as well as the ultimate recipients or users of the vehicle. The contractor's role, therefore, is primarily to provide a physical means of producing the particular vehicle and to accomplish the job of putting together a vehicle which can be expected to accomplish the intent of the project.

The attempt in this paper is to point up this effort. Before specifically recapping items of interest that have been brought up in this conference, consideration is first given to an item of particular importance but on which there are not sufficient data available, to date, to present in this conference.

RECAPITULATION

Several new and vitally important flutter problems have arisen in the development of the X-15. At the present time, basic research has not progressed to the point where answers to these problems can be provided to aid in the design of the X-15. These flutter problems can be divided into two rather broad fields: the aero-thermal-elastic problem and the general problem of flutter at hypersonic Mach numbers.

As shown in figure 3, the trend of flutter speeds at hypersonic Mach numbers can be reasonably determined by flutter model tests. Present flutter trend data extend only to a Mach number of 3.0 and most of these data are for plan forms different from those on the X-15. Within the limits of these data, transonic speeds are most critical. However, these limited data do show an indication that effects of plan form, center-of-gravity location of the surface, temperature, and thickness may result in higher Mach numbers that may be more critical. In order to determine flutter trends at hypersonic Mach numbers and the effects of these parameters for a particular configuration, some model testing at these speeds is required.

The aero-thermal-elastic problems of the X-15 may be very difficult to solve satisfactorily. It is possible to scale the aeroelastic problem for model testing, but no adequate way of scaling the aero-thermal-elastic problem appears possible. For this reason, as shown in figure 4, some full-scale rocket vehicle testing of the horizontals and verticals with the speed brakes must be done to determine the adequacy of the design in the speed range where this problem becomes important. These tests are scheduled for the mid 1958 prior to North American's flight testing program.

In order to provide some information on the thermal problem at a sufficiently early date to be useful in the initial design, vibration tests of the wing structural boxes and the full-scale horizontal tail will be made at high temperatures and high heating rates. These tests will provide information on the magnitude of the loss of stiffness arising from thermal stress as compared to the loss of material properties at elevated temperatures for the construction used.

Installation of the speed brakes on the vertical stabilizer is a very desirable aerodynamic configuration. Such a configuration produces several potential problems, and model tests of the vertical-stabilizer speed-brake assembly at transonic and supersonic speeds in the Langley flutter tunnels are required to establish the required rotational stiffness for the speed brake and stabilizer.

Experience has indicated that local flexibility at the root of a spindle surface can be vitally important. It is difficult to scale such flexibilities adequately for model tests, so it is necessary for experimental verification to resort to full-scale sled tests at transonic speeds.

Actual full-scale horizontal and vertical tails with their actuation and back-up structure will be used to ensure a satisfactory installation of the spindle surfaces and the speed brakes.

One of the most serious unknowns in the design of the X-15 today has to do with aerodynamic heating. William V. Feller provided the means for an analysis of the local heating problem. However, rather meager heat-transfer data are available today at hypersonic speeds and much of the data presented are wind-tunnel data on smooth flat plates, swept cylinders, and axisymmetric bodies. Investigations by the Langley Pilotless Aircraft Research Division also have been made for simple smooth bodies, at much higher Reynolds numbers than those of the wind-tunnel tests.

The test programs which have been formulated to provide the necessary design information in support of the estimates provided in the paper by Gordon W. Campbell, C. B. Neel, and Martin R. Kinsler include the simple symmetrical body tests which were reported on in Feller's paper and are shown in figure 5. Further testing of this model may be conducted with model modifications to simulate the X-15 side fairings. The specific X-15 configuration will be tested in the Langley Unitary Plan wind tunnel, the tests starting approximately January of 1957. This model will be a 1/15-scale model with provisions for procurement of heat-transfer coefficients as well as static and total pressure-distribution surveys. Testing will be made for fuselage and side-fairing data with first priority, speed brakes with second priority, and wing and empennage surfaces with third priority. Approximately 1/15-scale rocket models will be tested by the Langley Pilotless Aircraft Research Division with two models mounted at angle of attack upon a three-stage rocket test vehicle. This vehicle will obtain a limited amount of heat-transfer data under full-scale flight Reynolds numbers conditions.

The problems of determination of transition Reynolds number are well known. Model testing can investigate some of the characteristics of transition conditions and those of fully turbulent conditions by use of roughness. However, the designer will have to take into account the influence of skin joints and panel deformations under load and heating conditions. The present state of aerodynamic-heating calculations for the X-15 assumes laminar conditions for wing and empennage leading edges and conservative turbulent conditions for the remainder of the airplane. Crossflow conditions are being analyzed for the fuselage and side fairings based on the available data as presented in this briefing.

According to the current calculations, the X-15 can be expected to be flown in conditions of stagnation temperatures of about 3,500° F, where the skin temperatures are expected to be of the order of 1,000° to 1,300°. Use of Inconel X with moderate skin gages results in a wing which should not be critical to the temperature variations along the chord. The wing and empennage leading-edge radii need not be as large

as the 1/2 to 1-inch radius which was originally contemplated. It is now known that the required volume of the heat sink material, at the leading-edge radii, can be obtained by conventional fabrication techniques. Although consideration of estimated local temperatures alone would have permitted changing the skins from Inconel X to, say, titanium, this has not been considered because Inconel X provides greater utilization of the airplane from a research standpoint, allowing the technique, as Mr. Feller pointed out, of tripping the boundary layer for heat-transfer investigations.

The structure of the lower wing surface, for instance, will be constructed of large panels of unjointed skin, which will allow for the possibility of a long laminar boundary-layer condition being obtained.

The materials to be used in the fabrication of this airplane were briefly described by Richard L. Schleicher, but a brief review of some of the problems will be of interest. First, Inconel X is a relatively new structural material and its welding and subsequent heat treatment have created some problems. Inconel X has been welded under laboratory conditions. However, production welding will have to be evaluated and machining and heat treatment of this material will also require additional effort. To accomplish this, large processing jigs have already been constructed and fabrication development begun.

From consideration of the necessity for seals of the cockpit, wheel wells, and equipment bays, flexible materials by their very nature have poor high-temperature resistance. It is quite possible that silicone rubbers will provide the best solution. Mechanical seals for the ammonia and lox tanks present a difficult material and design problem since large temperature differentials occur as the fuel is transferred for control of center of gravity.

In the paper presented by A. Scott Crossfield discussing the pilot's environment and problems of the control system, it was indicated that the construction of the cockpit enclosure would include double pressure walls. A satisfactory method of insulation of the area has been developed for preventing the cockpit and instrumentation compartments from over-heating as a result of high skin temperatures. This insulation consists of an inorganic fiber batt material and reflective metal-foil radiation shield, which will be installed between the metal skins of the double-walled structure.

In the paper on the structural design of the X-15, Mr. Schleicher has given a rather complete picture of the analysis being conducted on the airplane. In summary, only the method and techniques employed on all phases of the program will be illustrated. The aerodynamic loads on a specific surface are calculated in the usual manner. The effects of elevated temperature are then added to this on the basis of the aerodynamic

heating expected to be encountered in the operating conditions. Additional loads induced by thermal stresses are therefore developed out of these temperature conditions. The combination of these loads results then in the total stress. A test box will then be constructed to simulate a portion of the item in question. Some solutions of the basic thermal-elastic problems associated with the wing outer panel are already complete or nearing completion. Numerous tests applicable to the problem areas of the design are also in various stages of completion.

Figure 6 shows a portion of the test box of the horizontal tail. The test program includes a study of the behavior of the structure at high temperatures, both with and without external loads applied. The high-temperature condition without the application of external loads has been completed. The skins in this particular case were buckled under the temperature distributions shown in the figure. After cooling to room temperature, however, all the buckles disappeared and left no evidence of permanent set. These tests are continuing at the present time. The conclusion to date is that some minor changes in the structural members may be indicated as a result of the thermal stresses.

Foremost among the areas of concern in the design of the X-15, primarily because of the far reaching aspects of it, are the effects of the aerodynamic characteristics. As shown in figure 7, which is the first one from the paper by Herbert W. Ridyard, Robert W. Dunning, and E. W. Johnston, the static longitudinal stability has been found to be generally satisfactory for the configuration as originally proposed. However, the increase in fuselage diameter from 53 to 56 inches and the incorporation of a more blunt fuselage forebody, including the extension of the side fairings, has caused a loss in static stability margin of approximately 15 percent M.A.C. at $M = 6.86$. These changes were brought about by changes in requirements after the design had started. Elimination of the fuselage side fairings ahead of the pilot's compartment and relocation of certain internal equipment items is estimated to compensate for this loss to achieve an acceptable static stability margin. The 1/50-scale model of the X-15 is being modified currently to check these estimates.

An important aspect of the analysis of longitudinal-control data is the fact that the airplane will be capable of trimming to approximately a lift coefficient C_L of 1.0 throughout the Mach number range by using a stabilizer deflection of no more than 35°. The limit of deflection provided in the airplane is 45°. This longitudinal-control power is considered to be completely satisfactory for the intended maneuvering capabilities of the airplane. There therefore appears to be no danger of obviating the possibility of achieving the desired missions.

In figure 8 is shown the variation of static directional stability derivative C_{n_β} and the lateral stability derivative C_{l_β} as a function of Mach number. Although these characteristics are shown for the zero angle-of-attack condition, they are fairly representative of the trend of the characteristics with Mach number, even for increased angle of attack. Furthermore, Ridyard, Dunning, and Johnston presented rather complete data showing that the loss in directional stability, particularly with increase in angle of attack, was severe at the higher Mach numbers.

These characteristics have been considered to be satisfactory in the overall picture, since including the influence of speed brakes results in a very desirable increase in the stability derivatives, especially at high angles of attack in the critical speed range. Ridyard, Dunning, and Johnston showed similar characteristics in their paper. Referring also to the effect of speed brakes on C_{l_β} indicates a large increase in this parameter.

In the combination of the increase in C_{l_β} and the variation of C_{n_β} with angle of attack, Martin T. Moul presented some indication that the results could be satisfactory even with low values of C_{n_β}. Howard F. Matthews and George B. Merrick, in the paper on the reentry conditions, indicated, however, that an increase in C_{l_β} was adverse to the characteristics. In contrast to this, experiments reported in the paper by Windsor L. Sherman, Stanley Faber, and James B. Whitten indicated that with the inverted T type of presentation to the pilot, the variations in C_{l_β} were not particularly important.

Recognizing that these separate programs may not be examining exactly the same condition and furthermore that the design is in a preliminary stage, both of these things must be kept in mind in examination of the future changes to airplane. There is, however, a serious disadvantage to using the speed brakes to provide the required levels of stability, since as obviously intended, they increase the drag an excessive amount. If they are used, therefore, to provide stability increase, they would probably eliminate the necessity of obtaining that stability increment by reason of restricting the airplane to a lower Mach number. Consequently, considerable attention has been directed toward achieving the proper characteristics in the clean configuration.

It is to be further emphasized that the attainment of proper aerodynamic characteristics, both static and dynamic, is undergoing considerable investigation. Numerous dynamic-stability analyses have been conducted for various phases of the high-altitude mission. These analyses are being conducted both by North American and by the NACA laboratories. Investigations have already reported the airplane characteristics for a wide range of Mach numbers, dynamic pressures, and altitude and for varying types of

aerodynamic data representative of the current configuration, with and without speed-brake deflections. Additional programs with more complete mechanization are under way.

As an example of the general range of damping parameters that can be expected of this type of vehicle, figure 9 shows the relative position of the X-15 with reference to the stability-specification requirements and also compares it to a conventional airplane of the current period. It would be uneconomical to provide aerodynamic damping to make these characteristics for the X-15 satisfactory through aerodynamic means alone, particularly when consideration is given the tremendous importance of weight in this airplane. Therefore, dampers are definitely desired and, as Matthews and Merrick have shown, the effect is very important to the reentry conditions.

In compiling the results of these analyses, it is apparent that, at least in the contractor's opinion,

(1) The directional stability $\left(C_{n_\beta}\right)$ should be a finite positive value at the maximum Mach number for a flexible heated airplane and for speed brakes in their basic retracted position.

(2) In the interest of simplicity and absolute reliability, obtaining a positive value of C_{n_β} should not rely on pilot actuation or actuation by any program function such as Mach number.

(3) Deflection of the speed brakes to provide additional stability increments should only be used as desired for research investigations.

(4) Zero directional control power $\left(C_{n_{\delta_V}}\right)$ at high angles of attack is unacceptable regardless of the Mach number at which it occurs, and this must be overcome.

(5) The roll due to yaw $\left(C_{l_\beta}\right)$ has been found to be excessive and should be corrected.

(6) The roll due to yaw control $\left(C_{l_{\delta_V}}\right)$ also has been found to be excessive and is in fact connected with the previous item.

These last two items are primarily caused by the asymmetric vertical tail of the original configuration.

On the basis of the information presented at this conference, North American is studying a revised configuration as shown in figure 10. It is to be noted that

(1) The side fairings ahead of the pilot's compartment have been eliminated for improvements in longitudinal stability as previously discussed. This particular point was brought up in connection with the characteristics shown by John W. Paulson in low-speed flight results in which a pitch-up at high angle of attack was encountered as well as was a loss in directional stability. It is anticipated that the side fairing will make improvements in both of these characteristics.

(2) In order to increase C_{n_β}, the vertical-tail area has been increased from 50 to 80 square feet. In accordance with this change and also to reduce C_{l_β} and $C_{l_{\delta_V}}$, the vertical empennage has been made more symmetrical.

This specific configuration will not necessarily eliminate all problems associated with static and dynamic stability but at least it is indicated to be in the right direction in many cases. The investigation will continue to use all means of determining proper levels of values. The lower vertical tail has been made movable to provide directional control at high angles of attack. The lower portion would be jettisonable for landing.

In order to avoid unknown weight penalties for the flutter-free requirements, studies of alternate speed-brake locations are being made at the present time. Preliminary tests of brakes located in the most rearward portion of the fuselage side fairings have not proved completely satisfactory. The latest consideration is to leave the brakes on the vertical tail, both upper and lower surfaces.

Since the basic concept of the airplane incorporated a human pilot as the sole means of recovery, special attention will be given to his control capabilities, as indicated by Crossfield in his paper. From consideration of the results of the papers presented by Sherman, Stillwell, and Matthews, the complete altitude mission shown in figure 11 is reexamined to assess briefly the pertinent areas of concern. In the exit phase the pilot is subjected to a varying longitudinal acceleration up to 4g in addition to attempting to pull approximately 4g normal acceleration during the initial portion of the burnout and subsequently holding the airplane at a steady zero-g condition throughout the major portion of the power-on phase. As has previously been discussed the problems associated with thrust misalinement in this region are important. At the top of the arc in the coasting region, reaction controls, as discussed by Stillwell, begin to provide the main means of control and problems associated with the match of this control and the aerodynamic control and the transition

between the two are currently being studied by NACA and by North American. The problems associated with aerodynamic stability in the reentry phase were presented in the paper by Matthews and Merrick. As mentioned previously, provision for satisfactory aerodynamic characteristics is expected in all regions of flight to be experienced.

In order to examine further the considerations being made of this problem and the associated pilot control, it shall be first assumed that the stability of the modified configuration will be satisfactory.

In figure 12 are shown the altitude and dynamic-pressure variations with time for recoveries from 250,000-foot-altitude missions for various entry conditions into a pull-out. Use of a lift coefficient of approximately 0.2 results in a pull-out altitude of approximately 68,000 feet for the limit dynamic pressure of 2,500 pounds per square foot. The highest possible recovery altitude for the C_L of 1.0 recovery is 110,000 feet. The variation of dynamic pressure with time shown on the right-hand side of figure 12 presents the fact that in recoveries with small airplane angles of attack at the lower altitudes, very careful angle-of-attack flight programming would be required. In attempting a flight at a dynamic pressure of 2,500 pounds per square foot, an angle of attack of 8° would be programmed. However, if the angle actually is only 4° a dynamic pressure in excess of 3,000 pounds per square foot would be experienced. The angle-of-attack accuracy of the hypersonic angle-of-attack system has been quoted to be 6° at 250,000 feet and 0.6° around 150,000 feet. This accuracy should be adequate provided that the null-seeking servosystem does not introduce abnormal lags on the readings. I. Taback and G. M. Truszynski in their paper have given assurance that the results should be satisfactory.

Figure 13 shows a plot in a little different manner of the same general results, that is insofar as angle of attack and C_L plotted against peak dynamic pressure are concerned. In addition, this figure shows the variation of normal acceleration as a function of the peak dynamic pressure involved. The nominal angles of attack for these recoveries are denoted on the upper curve. Establishing a 25° angle of attack at 250,000 feet would result in a dynamic pressure of approximately 300 pounds per square foot. In this recovery the pilot would experience a normal acceleration of 4g and an axial deceleration of 2g so that limiting the recovery to 2,500 lb/sq ft would require an angle of attack of approximately 8°. The resulting normal acceleration would be 7.1g with axial acceleration of approximately 2g. Either of these two types of reentries could be accomplished easily by the pilot. Matthews and Merrick presented a slightly different approach to the optional reentry by holding constant space attitude. This possibility is seriously considered although it may be limited due to high α.

The upper curve in figure 14 represents the peak dynamic pressure obtained in a 7.33g pull-out initiated at the various altitudes shown on the left scale. This pull-out is preceded by a zero-lift, speed-brakes-closed reentry from the altitude mission. As was discussed in the paper by Taback and Truszynski on instrumentation, the stable platform can give accumulated errors in the altitude readings, as is shown in the bottom curve. For the design-altitude mission the pull-out occurs in approximately 300 seconds. An error of approximately 3,000 feet can have accumulated by this time. If, in a predetermined flight plan, a dynamic pressure of 1,500 lb/sq ft were desired, a 3,000-foot altitude error reading would result in either a 1,300 or 1,900 lb/sq ft pull-out. The pull-out altitude, rather than being 98,500 feet, may be either 101,500 or 95,500 feet; likewise, an intended 2,500 lb/sq ft pull-out might end up at 3,000 lb/sq ft by attaining an indicated altitude of 92,000 feet when actually conditions at 89,000 feet altitude were being experienced. By virtue of the altitude-error possibility and pilot lag, it is unlikely that any reentry plan would intentionally be scheduled to approach dynamic pressures of 2,500 lb/sq ft.

It is shown therefore that there is quite an altitude region in which safe satisfactory pull-outs can be made although it does point out that any attempt to achieve a specific pinpoint condition will require that the pilot have extremely good control characteristics and an extremely accurate presentation. As Mr. Crossfield has pointed out and as has been presented in other papers on dynamic stability the problems associated with pilot control are not new. In the extensive investigations which are now in progress, both at the North American and at the NACA laboratories, consideration of all of the factors involved in pilot orientation and pilot control are being considered. The complete program is too lengthy to discuss here but it is definitely designed to evaluate completely the pilot's ability successfully to accomplish the intended purposes of the program without undue hazard. It will investigate variations in pilot-control sensitivity, pilot-information presentation, instrumentation accuracy, and all other aspects of the program indicated to be important. Furthermore, it is expected that the equipment developed to investigate the problems will also be available for pilot training. Although this seems to be an exhaustive program to embark upon, it is not, however, unusual. This same approach and many of the same problems exist in current designs. One should not get the impression that the pilot is a limiting factor in this airplane. He is in fact a very efficient, dependable, and extremely flexible computer which takes only a fraction of the space, weight, cooling, and development time of an electronic one.

In conclusion the design fabrication and test program schedule of the North American X-15 airplane is presented in figure 15. The program actually began in early December of 1955. Within a little more than a month and a half, aerodynamic data were being obtained on this specific

configuration. The basic drawing development has begun and will continue
until basic release occurs a year from now, approximately in December
of 1957. The mock-up is scheduled for early December of 1956. The crit-
ical aerodynamic, structural, flutter, and heat-transfer data will be
obtained during 1956 and early 1957 to allow for the full engineering
release of major components of the airplane as scheduled.

Data which will be obtained subsequent to engineering release will
be concerned with less critical items and will also provide information
to define the complete operating flight envelope of the airplane.

Tooling for the airplane will be made from February 1957 through
the middle of 1958. Fabrication of three airplanes will follow a similar
schedule, the last airplane being finished approximately in March of 1959.

The B-36 carrier airplane will be modified from the middle of 1957
to the point of being ready for ground check-outs by approximately October
of 1958. The Reaction Motors, Inc., engines are scheduled for ground
check and installation in the airplane during the latter part of 1958
and early 1959. North American flight testing of the three airplanes
is expected to be conducted from February through October of 1959, after
which the Air Force and the NACA will continue the program.

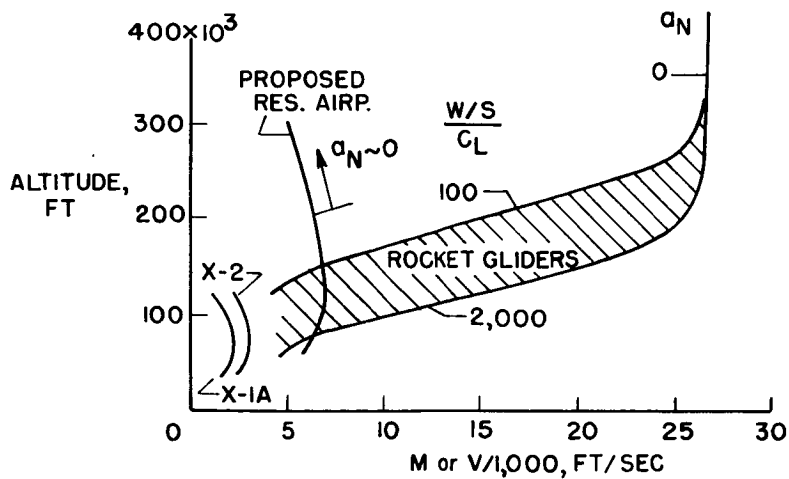SYS-447L **NORTH AMERICAN X-15 RESEARCH AIRPLANE**
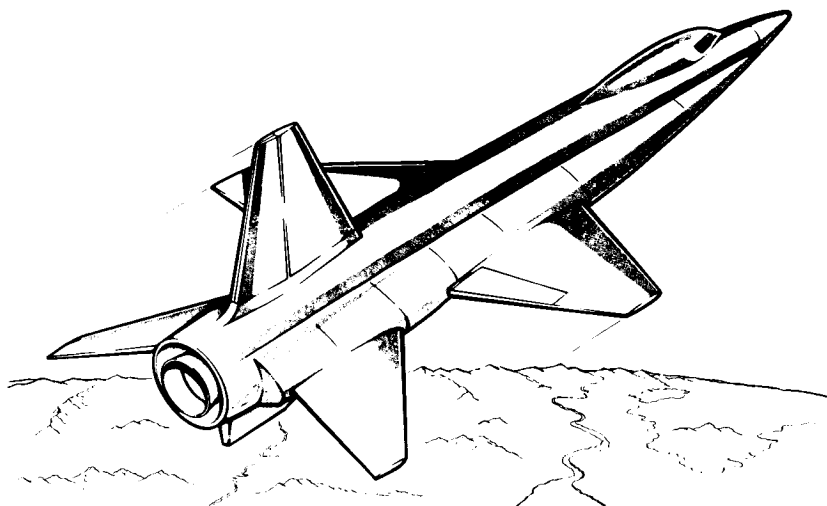
Figure 1

FLIGHT REGIMES
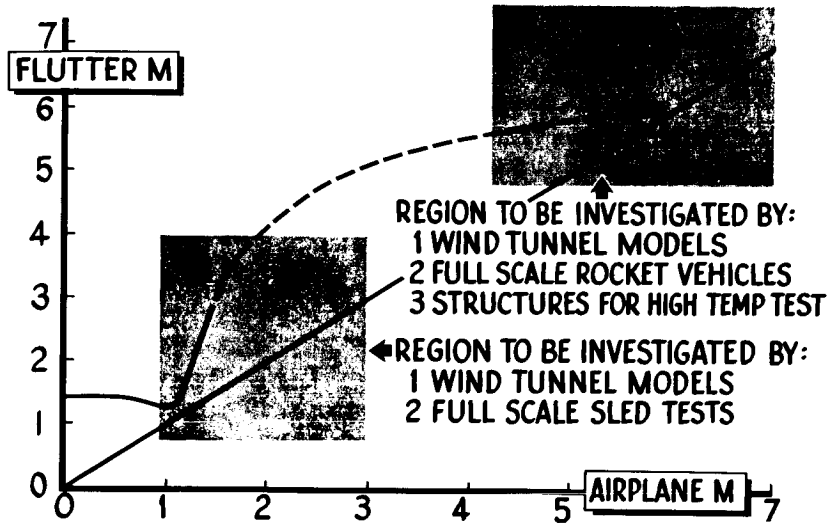

Figure 2

SYS-447L **FLUTTER CONSIDERATIONS**

FLUTTER M

REGION TO BE INVESTIGATED BY:
1 WIND TUNNEL MODELS
2 FULL SCALE ROCKET VEHICLES
3 STRUCTURES FOR HIGH TEMP TEST

REGION TO BE INVESTIGATED BY:
1 WIND TUNNEL MODELS
2 FULL SCALE SLED TESTS

AIRPLANE M

Figure 3

SYS-447L **VIBRATION AND FLUTTER TEST PROGRAM**

* INDICATES TEST DATE

SURFACE	MACH NO. RANGE	SCALE	TEST FACILITY	1956	1957	1958
HORIZONTAL STABILIZER	5-8	1/10	A.E.D.C. E-2 WIND TUNNEL			
	.9-1.2	FULL	INYOKERN SNORT SLED			
	0-6.5	FULL	P.A.R.D., LANGLEY FIELD			
VERTICAL STABILIZER AND SPEED BRAKES	.85-1.3	1/10	26 IN. LANGLEY BLOWDOWN WIND TUNNEL			
	1.3-4	1/10	9 IN. X 18 IN. LANGLEY SUPER-SONIC FLUTTER TUNNEL			
	.9-1.2	FULL	INYOKERN SNORT SLED			
	0-6.5	FULL	P.A.R.D., LANGLEY FIELD			
STATIC HEATING TESTS WING BOX	——	——	N.A.C.A. STRUCTURES LAB HEATING FACILITY, LANGLEY FIELD			
HORIZONTAL STABILIZER	——	FULL	N.A.C.A. STRUCTURES LAB HEATING FACILITY, LANGLEY FIELD			

Figure 4

SYS-447L

AERODYNAMIC HEATING
TEST PROGRAMS

• PRELIMINARY BODY

20° α
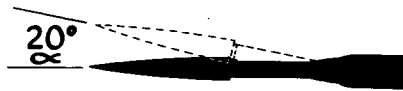
LANGLEY UNITARY 4 FT X 4 FT
CURRENT

• X-15 SPECIFIC
CONFIGURATION
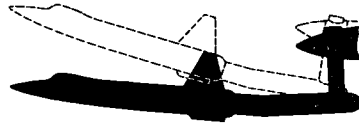
LANGLEY UNITARY
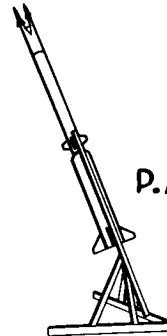JAN, 1957

• X-15 SPECIFIC
CONFIGURATION

P.A.R.D.

Figure 5
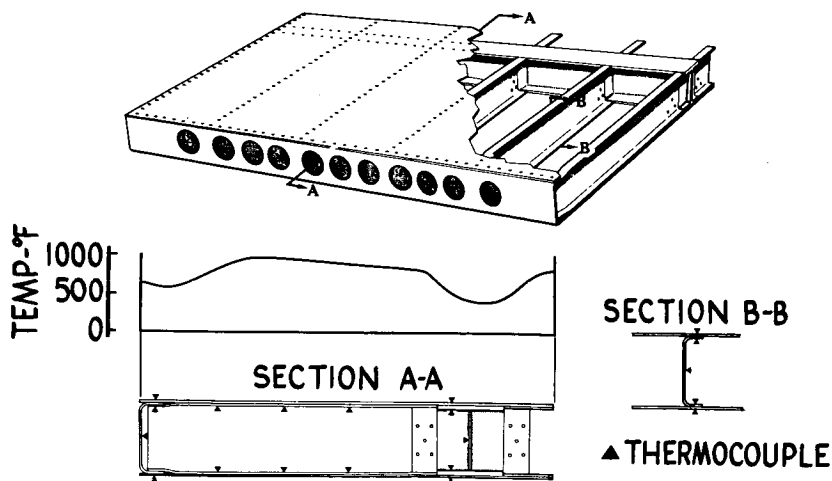
SYS-447L

HORIZONTAL TAIL TEST BOX

TEMP-°F

1000
500
0

SECTION A-A

SECTION B-B

▲ THERMOCOUPLE

Figure 6

LONGITUDINAL STABILITY AT $C_L = 0$

C.G. IS AT $\bar{c}/4$

$\dfrac{dC_m}{dC_L}$

CONFIGURATION

○ 1
● 2

M
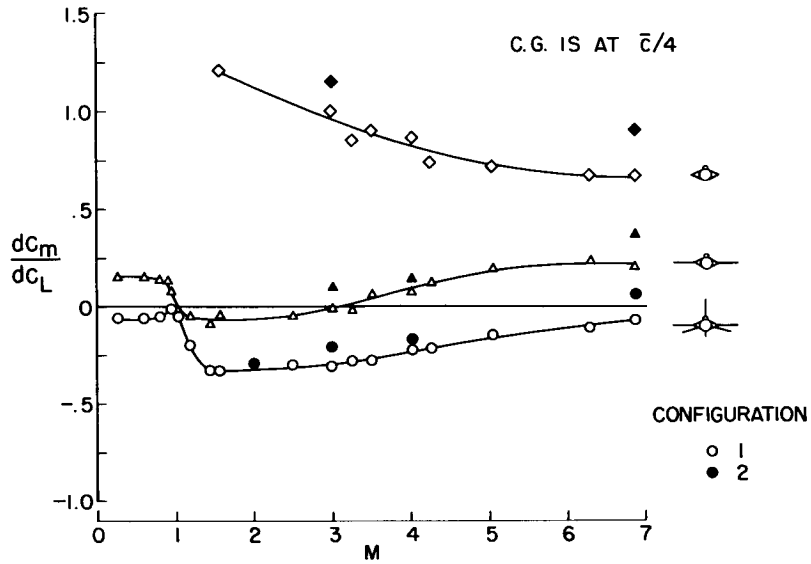
Figure 7

SYS-447L **STATIC LATERAL-DIRECTIONAL STABILITY**

$C_{n_{\beta^\circ}}$

.012

.008

.004

0

SPEED BRAKES FULL OPEN

FULL WEDGE

DOUBLE WEDGE

M

$C_{\ell_{\beta^\circ}}$

0

-.001

-.002

-.003

M

DOUBLE WEDGE

SPEED BRAKES FULL OPEN
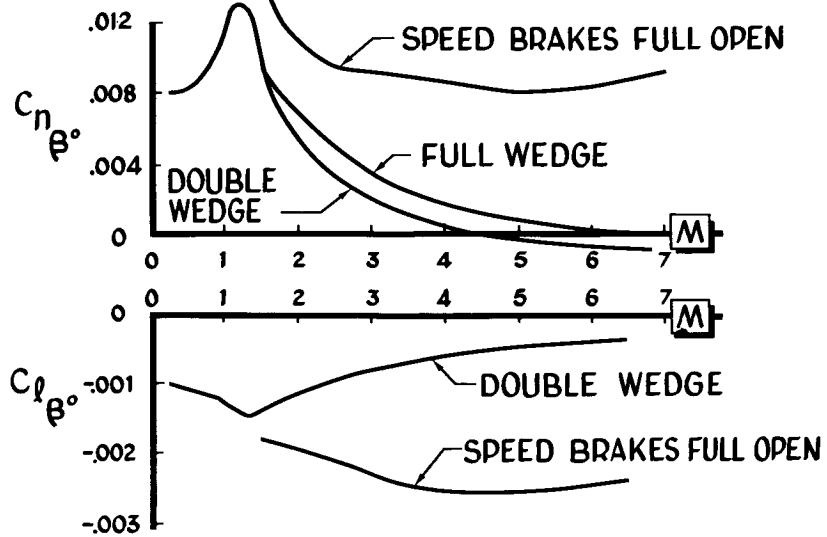
Figure 8

COMPARISON OF LONGITUDINAL SHORT—PERIOD
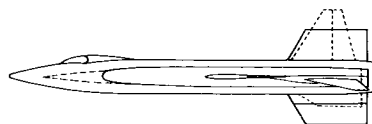CHARACTERISTICS WITH FLYING QUALITIES SPECIFICATIONS
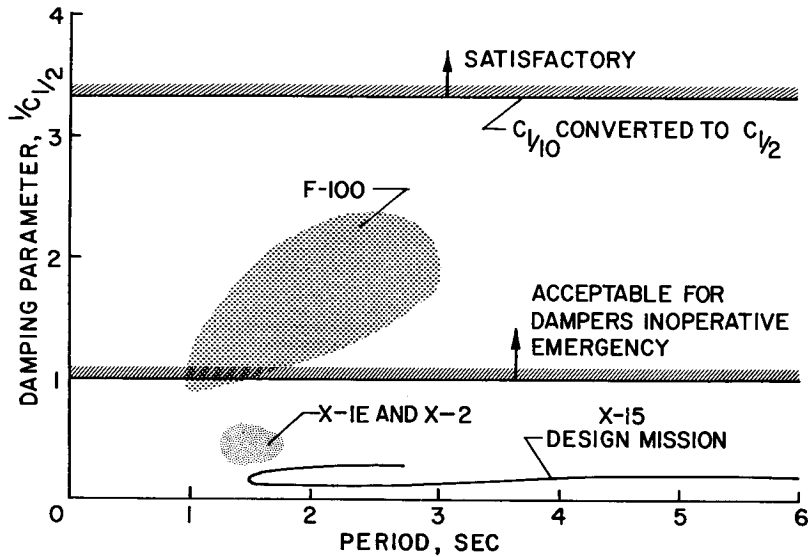
Figure 9

SYS-447L **REVISED CONFIGURATION**
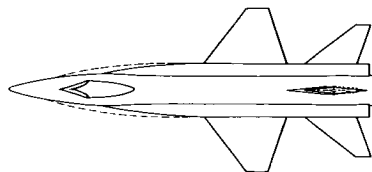
- **LONGITUDINAL**

  SHORTEN SIDE FAIRINGS
  MOVE EQUIP. FORWARD

- **LATERAL- DIRECTIONAL**

  VERTICAL AREA INCREASED
  AND MADE SYMMETRICAL

  SPEED BRAKES RELOCATED
  MADE SYMMETRICAL AND
  SMALLER

  LOWER VERTICAL TAIL
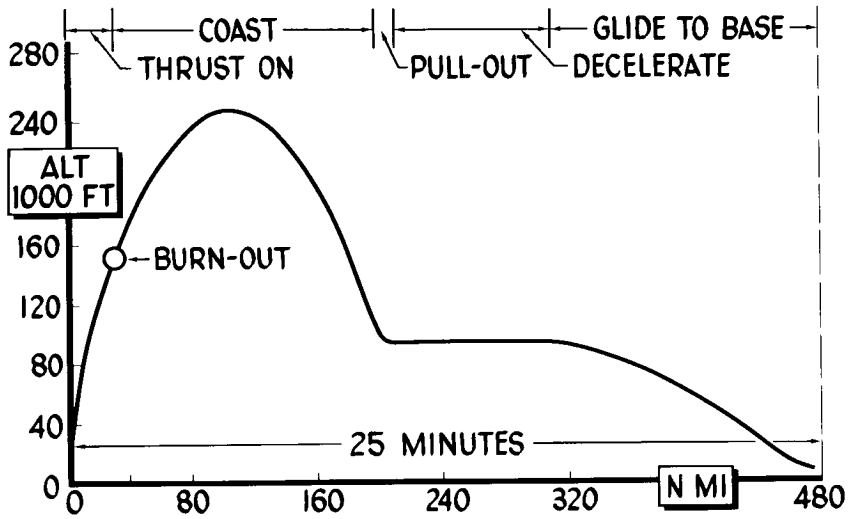 MADE MOVABLE

Figure 10

SYS-447L **COMPLETE ALTITUDE MISSION**

COAST — THRUST ON — PULL-OUT — DECELERATE — GLIDE TO BASE

ALT 1000 FT

○ — BURN-OUT

25 MINUTES

N MI

Figure 11

SYS-447L **RECOVERY FROM ALTITUDE MISSION**
SPEED BRAKES CLOSED

ALT-1000 FT

$C_L = 1.0$
$C_L = .40$
$C_L = .20$
$C_L = .10$

TIME SEC

DYN PRESS. q-PSF

$C_L = .10$ ($\alpha = 4°$)
$C_L = .20$ ($\alpha = 8°$)
$C_L = .40$ ($\alpha = 16°$)
$C_L = 1.0$ ($\alpha = 34°$)

TIME SEC

Figure 12

RECOVERY FROM ALTITUDE MISSION
SPEED BRAKES CLOSED

SYS-447L

Figure 13

EFFECT OF ALTITUDE ACCURACY
RECOVERY FROM ALTITUDE MISSION

SYS-447L

Figure 14

DECLASSIFIED
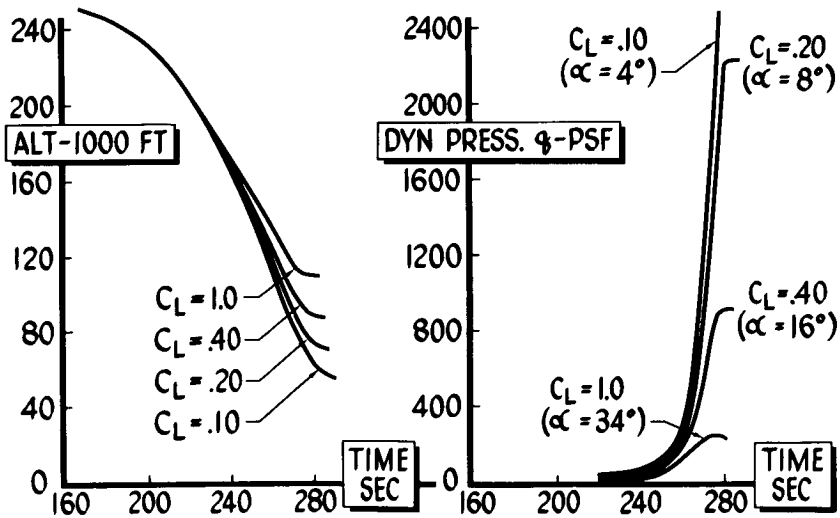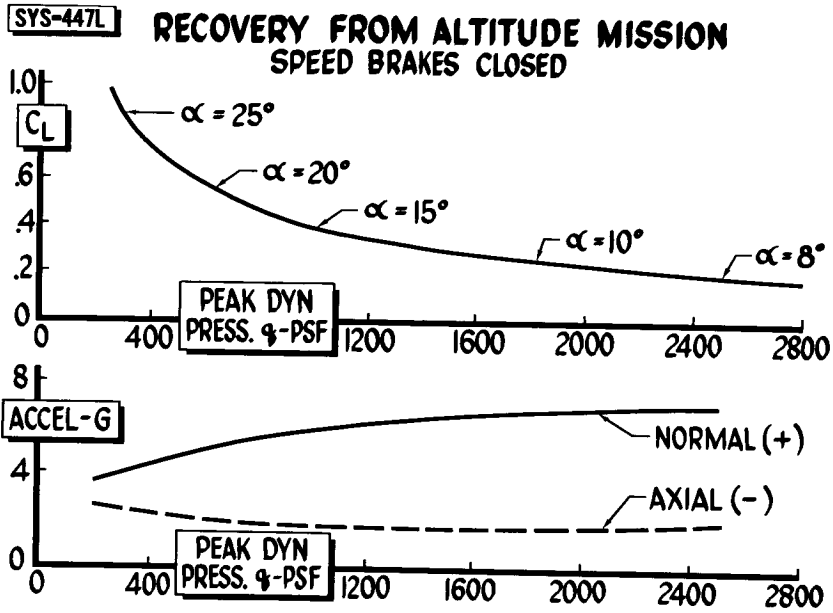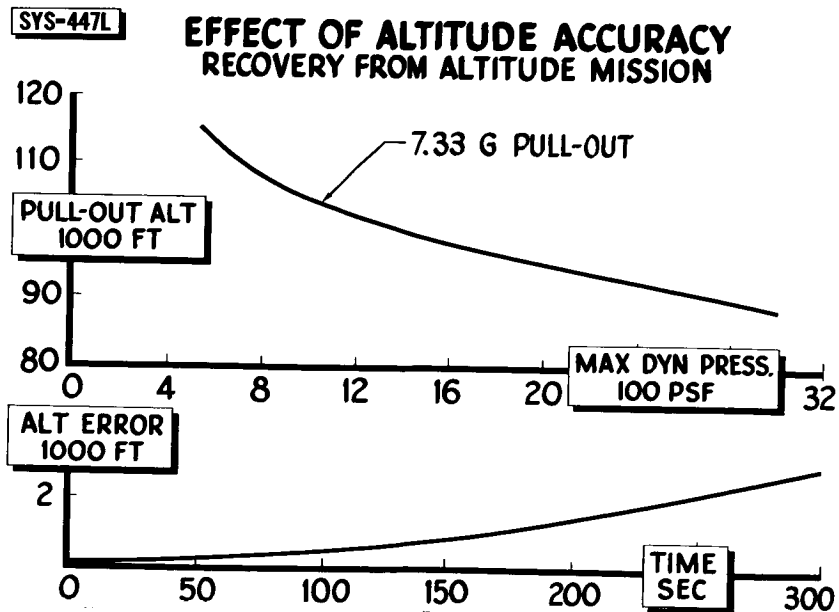
MASTER PHASING PROGRAM

SYS-447L

BASIC DWG RELEASE
MOCK-UP
AERODYNAMIC DATA
STRUCTURAL DATA
FLUTTER DATA
HEAT TRANS. DATA
TOOLING
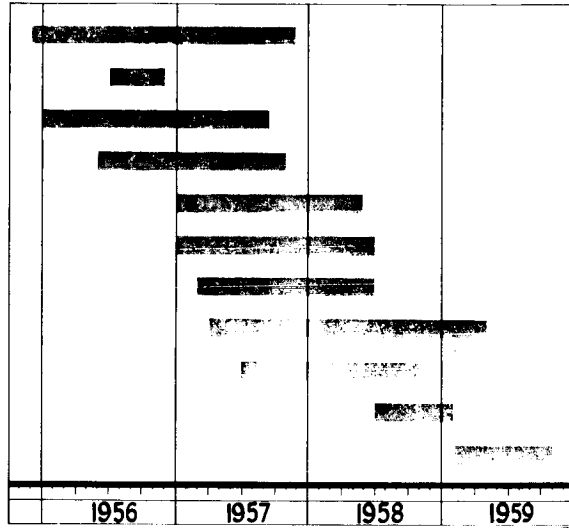A/P FABRICATION
B-36 CARRIER MOD
GFAC (ENGINE)
FLT TEST & DELIVERY

1956   1957   1958   1959

Figure 15